



The author of the doctoral dissertation: mgr inż. Aleksandra Kuplińska
Scientific discipline: Chemical Sciences

DOCTORAL DISSERTATION

Title of doctoral dissertation: Enzymes of the L-methionine biosynthesis pathway in *Candida albicans* as potential novel targets for antifungal chemotherapy.

Title of doctoral dissertation (in Polish): Enzymy szlaku biosyntezy L-metioniny z *Candida albicans* jako potencjalne nowe cele molekularne dla chemoterapii przeciwgrzybowej.

Supervisor	Auxiliary supervisor
<i>signature</i>	<i>signature</i>
Prof. Sławomir Milewski, PhD, DSc, Eng.	Kamila Rząd, PhD, Eng.





STATEMENT

The author of the doctoral dissertation: mgr inż. Aleksandra Kuplińska

I, the undersigned, declare that I am aware that in accordance with the provisions of Art. 27 (1) and (2) of the Act of 4th February 1994 on Copyright and Related Rights (Journal of Laws of 2021, item 1062), the university may use my doctoral dissertation entitled: *'Enzymes of the L-methionine biosynthesis pathway in Candida albicans as potential novel targets for antifungal chemotherapy'* for scientific or didactic purposes.¹

Gdańsk,.....

.....
signature of the PhD student

Aware of criminal liability for violations of the Act of 4th February 1994 on Copyright and Related Rights and disciplinary actions set out in the Law on Higher Education and Science (Journal of Laws 2021, item 478), as well as civil liability, I declare, that the submitted doctoral dissertation is my own work.

I declare, that the submitted doctoral dissertation is my own work performed under and in cooperation with the supervision of Prof. Sławomir Milewski, PhD, DSc, Eng., and the auxiliary supervision of Kamila Rząd, PhD, Eng.

This submitted doctoral dissertation has never before been the basis of an official procedure associated with the awarding of a PhD degree.

All the information contained in the above thesis which is derived from written and electronic sources is documented in a list of relevant literature in accordance with Art. 34 of the Copyright and Related Rights Act.

I confirm that this doctoral dissertation is identical to the attached electronic version.

Gdańsk,.....

.....
signature of the PhD student

I, the undersigned, agree to include an electronic version of the above doctoral dissertation in the open, institutional, digital repository of Gdańsk University of Technology.

Gdańsk,.....

.....
signature of the PhD student

¹ Art 27. 1. Educational institutions and entities referred to in art. 7 sec. 1 points 1, 2 and 4–8 of the Act of 20 July 2018 – Law on Higher Education and Science, may use the disseminated works in the original and in translation for the purposes of illustrating the content provided for didactic purposes or in order to conduct research activities, and to reproduce for this purpose disseminated minor works or fragments of larger works.

2. If the works are made available to the public in such a way that everyone can have access to them at the place and time selected by them, as referred to in para. 1, is allowed only for a limited group of people learning, teaching or conducting research, identified by the entities listed in paragraph 1.





DESCRIPTION OF DOCTORAL DISSERTATION

The Author of the doctoral dissertation: Aleksandra Kuplińska

Title of doctoral dissertation: Enzymes of the L-methionine biosynthesis pathway in *Candida albicans* as potential novel targets for antifungal chemotherapy.

Title of doctoral dissertation in Polish: Enzymy szlaku biosyntezy L-metioniny z *Candida albicans* jako potencjalne nowe cele molekularne dla chemoterapii przeciwgrzybowej.

Language of doctoral dissertation: English

Supervisor: Prof. Sławomir Milewski, PhD, DSc, Eng.

Auxiliary supervisor: Kamila Rząd, PhD, Eng.

Date of doctoral defense:

Keywords of doctoral dissertation in English: *Candida albicans*, L-methionine biosynthesis pathway, antifungal compounds, enzyme inhibitors.

Keywords of doctoral dissertation in Polish: *Candida albicans*, szlak biosyntezy L-metioniny, związki przeciwgrzybowe, inhibitory enzymów.

Summary of doctoral dissertation in English:

Fungal pathways of essential amino acids biosynthesis provide an abundant source of molecular targets for new antifungal compounds, among which the L-methionine biosynthesis pathway (MBP) may be promising. In this dissertation I characterized three *C. albicans* enzymes involved in MBP: homoserine *O*-acetyltransferase (CaMet2p), *O*-acetyl-L-homoserine sulfhydrylase (CaMet15p), and cystathionine- γ -synthase (CaStr2p). I performed crystallization trials of analyzed proteins, which led to the formation of a CaMet15p crystal of 7 Å resolution. Additionally, I proved that the inhibition of CaMet2p, CaMet15p, and CaStr2p induces fungal growth deficiency dependent on L-methionine (L-Met) presence. Among variety of examined potential inhibitors, I selected L-penicillamine (L-PEN) as the most effective against CaMet2p enzyme, and β -(5-Oxo-3-isoxazolin-2-yl)-L-alanine as an inhibitor of CaMet15p and CaStr2p. Moreover, I have assessed antifungal effect induced by combination of inhibitors, which showed a synergistic effect between L-PEN and other selected potential inhibitors of MBP. I discovered that the growth of fungal cells treated with L-PEN could be rescued by the supplementation of media with L-Met concentration 10-fold higher than that found in human serum. Presented results confirm the significance of MBP in the development of novel antifungal compounds.



Summary of doctoral dissertation in Polish:

Źródła poszukiwań potencjalnych celów molekularnych dla nowych terapii przeciwgrzybiczych stanowią m.in. szlaki biosyntezy aminokwasów egzogennych, spośród których szlak biosyntezy L-metioniny (MBP) wydają się być najbardziej obiecujący. W ramach pracy doktorskiej scharakteryzowałam trzy enzymy uczestniczące w MBP w komórkach *C. albicans*: transacetylazę homoserynową (CaMet2p), sulfhydrylazę O-acetylo-L-homoserynową (CaMet15p) oraz syntazę- γ -cystationiny (CaStr2p). Przeprowadziłam próby krystalizacji badanych białek i otrzymałam kryształ białka CaMet15p o rozdzielczości 7 Å. Dodatkowo, wykazałam, że inhibicja badanych enzymów powoduje zahamowanie wzrostu komórek grzybowych, zależne od obecności L-metioniny (L-Met). Wytypowałam L-penicilaminę (L-PEN) jako najbardziej skuteczny inhibitor CaMet2p, oraz β -(5-Oxo-3-isoxazolin-2-yl)-L-alaninę jako inhibitor CaMet15p i CaStr2p. Wykonałam badania wpływu kombinacji inhibitorów na wzrost komórek grzybowych i wykazywałam, że L-PEN wykazuje działanie synergistycznie z innymi, badanymi inhibitorami MBP. Udowodniłam, że zahamowanie wzrostu komórek grzybowych traktowanych L-PEN może być odwrócone przez dodanie do pożywki L-Met o stężeniu dziesięciokrotnie przewyższającym to w ludzkiej surowicy krwi. Przedstawione wyniki potwierdzają znaczenie MBP w poszukiwaniu nowych związków o działaniu przeciwgrzybowym.



I would like to express my gratitude to Professor Sławomir Milewski for allowing me to conduct research under his supervision and for his guidance throughout all the years of my PhD studies.

I sincerely thank my auxiliary supervisor Dr. Kamila Rząd for introducing me to essential skills that enriched my experience, and for providing invaluable support.

I would also like to thank Professor Iwona Gabriel for her openness and assistance, which helped me overcome obstacles in my research project.

Furthermore, I am grateful to all the members of the Department of Pharmaceutical Technology and Biochemistry for their everyday kindness, supporting environment, and all the good memories.

Finally, I would like to extend my deepest gratitude to my family and friends for their unwavering support during the challenging moments. Your encouragement has been invaluable.





TABLE OF CONTENTS

LIST OF SYMBOLS AND ABBREVIATIONS	12
1. INTRODUCTION	14
1.1. Fungal diseases – an increasing global health concern	14
1.2. <i>Candida albicans</i> – an enemy or an ally?	16
1.3. Antifungal chemotherapeutics applied in clinical practice	17
1.4. Essential amino acids biosynthetic pathways in the fight against fungal infections	19
1.5. Fungal L-methionine biosynthesis pathway	21
1.6. Enzymes of the L-methionine biosynthesis pathway as potential molecular targets	22
1.7. Homoserine <i>O</i> -acetyltransferase (Met2p)	24
1.8. <i>O</i> -Acetyl-L-homoserine sulfhydrylase (Met15p)	25
1.9. Cystathionine- γ -synthase (Str2p)	26
1.10. Inhibitors targeting the L-methionine biosynthesis pathway	28
2. RESEARCH AIM AND OBJECTIVES	31
3. MATERIALS AND METHODS	32
3.1. Materials	32
3.1.1. Laboratory equipment	32
3.1.2. Software	33
3.1.3. Mass markers	33
3.1.4. Culture media	33
3.1.5. Bacterial and yeast strains	34
3.1.7. DNA	35
3.1.8. Restriction enzymes	38
3.1.9. Enzymes substrates and coenzymes	38
3.1.10. Tested potential inhibitors	39
3.2. Methods	39
3.2.1. Bioinformatical analysis	39
3.2.2. Microorganisms culture conditions	39
3.2.3. DNA purification	40
3.2.4. Agarose electrophoresis	40
3.2.5. Amplification of MET2, MET15 and STR2 genes	40
3.2.6. Cloning of PCR product to pET101/D-TOPO or pLATE vectors	41

3.2.7.	<i>Transformation to E. coli competent cells</i>	42
3.2.8.	<i>Restriction digest analysis</i>	43
3.2.9.	<i>Mutagenesis</i>	43
3.2.10.	<i>Polyacrylamide SDS-PAGE electrophoresis</i>	44
3.2.11.	<i>Western Blot analysis</i>	45
3.2.12.	<i>Preparation of E. coli competent cells</i>	45
3.2.13.	<i>Optimization of overproduction of recombinant proteins in the Tabor-Studier system</i>	45
3.2.14.	<i>Preparation of cell-free extract</i>	46
3.2.15.	<i>Purification of recombinant oligoHis-tagged proteins using metal-affinity chromatography</i>	46
3.2.16.	<i>Purification of native proteins using anion exchange chromatography</i>	46
3.2.17.	<i>Purification of proteins using size exclusion chromatography</i>	47
3.2.18.	<i>Determination of protein concentration using the Bradford method</i>	47
3.2.19.	<i>Densitometric analysis</i>	48
3.2.20.	<i>Concentration of recombinant protein solutions</i>	48
3.2.21.	<i>Protein solution buffer exchange</i>	48
3.2.22.	<i>Determination of the protein molecular mass and oligomeric structures</i>	48
3.2.23.	<i>Crystallization trials</i>	49
3.2.24.	<i>Activity assay</i>	50
a)	<i>Homoserine O-acetyltransferase (Met2p) activity assay</i>	50
b)	<i>O-acetyl-L-homoserine sulfhydrylase (Met15p) activity assay</i>	50
c)	<i>Cystathionine-γ-synthase (Str2p) activity assay</i>	50
3.2.25.	<i>Determination of enzyme inhibitory potential</i>	51
3.2.26.	<i>Determination of the Minimum Inhibitory Concentration</i>	51
3.2.27.	<i>Checkerboard dilution test for determination of drug interaction</i>	51
4.	RESULTS AND DISCUSSION	53
4.1.	Identification of genes encoding putative CaMet2p, CaMet15p and CaStr2p	53
4.1.1.	<i>Nucleotide sequences</i>	53
4.1.3.	<i>Amino acid sequences</i>	54
4.2.	Construction of expression systems and isolation of putative CaMet2p, CaMet15p and CaStr2p	55
4.2.1.	<i>Construction of expression plasmids encoding CaMet2p, CaMet15p and CaStr2p</i>	55
4.2.2.	<i>Production of recombinant proteins in E. coli host cells</i>	56
4.2.3.	<i>Purification of recombinant proteins</i>	61
4.3.	Characterizations of recombinant CaMet2p, CaMet15p and CaStr2p	66
4.3.1.	<i>Determination of molecular mass and oligomeric structure</i>	66
4.3.2.	<i>Enzymatic activity of CaMet2p, CaMet2NHp, and CaMet2CHp.</i>	71
4.3.3.	<i>Enzymatic activity of CaMet15NHp and CaMet15CHp</i>	75

4.3.4.	<i>Enzymatic activity of CaStr2NHp and CaStr2CHp</i>	79
4.4.	Searching for inhibitors of CaMet2p, CaMet15p and CaStr2p	83
4.4.1.	<i>Inhibitory assay</i>	84
4.4.2.	<i>Antifungal activity of selected inhibitors</i>	87
4.4.3.	<i>Assessment of the CaMet2p, CaMet15p and CaStr2p inhibitors interactions in combinations</i>	93
4.5.	Preliminary crystallization trials	97
4.5.1.	<i>Bioinformatical prediction of crystallization success</i>	98
4.5.2.	<i>Optimization of crystallization conditions</i>	100
5.	CONCLUSIONS	104
	ACKNOWLEDGMENTS	106
	SCIENTIFIC ACHIEVEMENTS	107
	REFERENCES	109
	LIST OF FIGURES	124
	LIST OF TABLES	129
	LIST OF SUPPLEMENTARY FIGURES	131
	SUPPLEMENTARY FIGURES	132

LIST OF SYMBOLS AND ABBREVIATIONS

Index	Definition
5-OXO	(2S)-2-Amino-5-oxohexanoic acid
6-OXO	(2S)-2-Amino-6-oxoheptanoic acid
5-FU	5-Fluorouracil
AcCoA	Acetyl coenzyme A
AC	Affinity chromatography
Ac-DAB	L-4-Acetamide-2-aminobutanoic acid
AEX	Anion exchange chromatography
A-FBA	2-Amino-4-fluorobutanoic acid hydrochloride
AmB	Amphotericin B
AS	Ammonium sulfate
BSA	Bovine serum albumin
CaMet15CHp	<i>Candida albicans</i> O-acetyl-L-homoserine sulfhydrylase with 6xHisTag C-terminal domain
CaMet15NHp	<i>C. albicans</i> O-acetyl-L-homoserine sulfhydrylase with 6xHisTag N-terminal domain
CaMet15p	<i>C. albicans</i> O-acetyl-L-homoserine sulfhydrylase
CaMet2CHp	<i>C. albicans</i> homoserine O-acetyltransferase with 6xHisTag C-terminal domain
CaMet2NHp	<i>C. albicans</i> homoserine O-acetyltransferase with 6xHisTag N-terminal domain
CaMet2p	<i>C. albicans</i> homoserine O-acetyltransferase
CaStr2CHp	<i>C. albicans</i> cystathionine- γ -synthase with 6xHisTag C-terminal domain
CaStr2NHp	<i>C. albicans</i> cystathionine- γ -synthase with 6xHisTag N-terminal domain
CaStr2p	<i>C. albicans</i> cystathionine- γ -synthase
CV	Column volume
Cys3p	Cystathionine- γ -lyase
Cys4p	Cystathionine- β -synthase
DAD	Diode array detector
DL-ALG	DL-2-Allylglycine
DL-GLUF	DL-Glufosinate
D-PEN	D-Penicillamine
DTNB	5,5-dithio-bis-(2-nitrobenzoic acid)
FICI	Fractional inhibitory concentration index
FLU	Fluconazole
FPLC	Fast protein liquid chromatography
HPLC	High pressure liquid chromatography
IPTG	Isopropyl- β -D-thiogalactoside
ISOX	β -(5-Oxo-3-isoxazolin-2-yl)-L-alanine
k_{CAT}	Turnover number
k_{CAT}/K_M	Kinetic efficiency
K_i	Inhibition constant
K_M	Michaelis constant
L-AAA	L-2-Aminoadipic acid

LB	Luria-Bertani medium
L-CAR	<i>N</i> -acetyl-L-carnitine
L-CAV	L-Canavanine
L-CTT	L-Cystathionine
L-DBA	L-2,4-Diaminobutanoic acid dihydrochloride
L-HCT	L-Homocysteine
L-HMP	L-Homoserine methyl <i>O</i> -phosphonate
L-HOM	L-Homoserine
L-MES	L-Methionine sulfoximine
L-OAH	<i>O</i> -Acetyl-L-homoserine
L-OAS	<i>O</i> -Acetyl-L-serine
L-PEN	L-Penicillamine
L-SMP	L-Serine methyl <i>O</i> -phosphonate
MBP	L-Methionine biosynthesis pathway
Met15p	<i>O</i> -Acetyl-L-homoserine sulfhydrylase
Met17p	Bifunctional <i>O</i> -acetyl-L-homoserine/ <i>O</i> -acetyl-L-serine sulfhydrylase
Met2p	Homoserine <i>O</i> -acetyltransferase
Met6p	Methionine synthase
MIC ₅₀	Minimal inhibitory concentration causing 50 % growth inhibition
MIC ₉₀	Minimal inhibitory concentration causing 90 % growth inhibition
MS	Mass spectrometry
OD ₆₀₀	Optical density measured at 600 nm
PCR	Polymerase chain reaction
PDB	Protein Data Bank
PLP	Pyridoxal 5'-phosphate
RP	Reverse phase
SEC	Size exclusion chromatography
SG	Sodium glutamate
Str2p	Cystathionine- γ -synthase
Str3p	Cystathionine- β -lyase
T-ALA	3-(2-Thienyl)- L-alanine
TMB	3,3',5,5'-Tetramethylbenzidine
V _{MAX}	Maximum velocity
YNB	Yeast Nitrogen Base medium

1. INTRODUCTION

1.1. Fungal diseases – an increasing global health concern

Infectious diseases caused by fungal microorganisms are commonly known as unwanted but not very dangerous superficial mycoses like thrush, ringworm, or athlete's foot infection. The reason standing after this is high the frequency of skin and nail mycoses that affect approximately 25% of people globally (Havlickova et al., 2008) However fungal infections can be more dangerous than one might suppose. Each year, life-threatening invasive fungal infections affect over 300 million people, and in effect kill over 1.5 million individuals globally (Bongomin et al., 2017). These estimates are accumulating each year, but the exact numbers remain elusive due to insufficient attention and resources for gathering data on fungal infection incidence (Stop neglecting fungi, 2017; Denning, 2024).

The emergence of invasive fungal infections is partly due to the development of modern medicine and increased availability of treatment, causing the at-risk population to expand. Invasive fungal mycoses are most dangerous for immunocompromised patients, including transplant recipients and individuals suffering from HIV, tuberculosis, cancer, and diabetes. According to estimates, invasive aspergillosis is the cause of death of over 50% of lung-transplant recipients, and *Cryptococcus meningitis* is the second, after tuberculosis, cause of death of patients suffering from HIV (Rajasingham et al., 2017; Fisher and Denning, 2023). Invasive fungal infections have been also associated with COVID-19 patients and survivors (Kuchi Bhotla et al., 2021; Raut and Huy, 2021; Rayens et al., 2022). Reported COVID-19-associated pulmonary aspergillosis cases are estimated with a 40% mortality rate (Hoenigl et al., 2022).

Another emerging global health concern is the rising resistance of fungal organisms to currently available chemotherapeutics. Frequent use of antifungals in agriculture or during supporting therapy with fluconazole of immunocompromised patients promotes both specific and multidrug resistance (Azevedo et al., 2015). The frequency of fluconazole-resistant *Candida albicans* strains ranges from 1% to 30%, reaching 26% in the case of the azole-resistant *Aspergillus fumigatus* strains (Skrodenienė et al., 2006; Gualco et al., 2007; Jafari-Nodoushan et al., 2008; van Paassen et al., 2016). Moreover, the world-threatening outbreak of *Candida auris* pathogen is an emerging major problem, as this microorganisms exhibits intrinsic 90% resistance to Fluconazole, 'the golden standard' amphotericin B and other available antifungal chemotherapeutics (Wiederhold, 2017). *C. auris* is also difficult to identify among other *Candida* strains with conventional techniques. This brings up another problem of diagnosis and identification of fungal pathogens. There are various methods of fungal infection diagnosis, however, the methods for identification of a pathogen remain unsatisfactory (Mendonça et al., 2022). In many cases, prolonged time of fungal infection identification leads to the application of an antifungal agent before the arrival of the test results (Keighley et al.).

Identification of fungal species and their resistance is crucial for selection of the adequate chemotherapy which should be applied immediately to increase the patient's chance of survival. The current method for the identification of fungal pathogens requires development in the area of automation, time of analysis, and globalization (Mendonça et al., 2022).

Recently, the World Health Organization (WHO) launched the first fungal priority pathogens list, categorizing 19 fungal pathogens, that pose the greatest threat to public health, into three groups – critical, high, and medium (World Health Organization, 2022). The first, critical group is associated with the highest incidence of mortality and morbidity and consists of *Candida albicans*, *Candida auris*, *Aspergillus fumigatus*, and *Cryptococcus neoformans*. The WHO's first fungal priority pathogen list not only brings the world's attention to fungal infections but also calls for surveillance on research, monitoring, and diagnostics.




















Critical group	High group	Medium group
 <i>Cryptococcus neoformans</i>	 <i>Nakaseomyces glabrata</i> (<i>Candida glabrata</i>)	 <i>Scedosporium</i> spp.
 <i>Candida auris</i>	 <i>Histoplasma</i> spp.	 <i>Lomentospora prolificans</i>
 <i>Aspergillus fumigatus</i>	 Eumycetoma causative agents	 <i>Coccidioides</i> spp.
 <i>Candida albicans</i>	 Mucorales	 <i>Pichia kudriavzevii</i> (<i>Candida krusei</i>)
	 <i>Fusarium</i> spp.	 <i>Cryptococcus gattii</i>
	 <i>Candida tropicalis</i>	 <i>Talaromyces marneffei</i>
	 <i>Candida parapsilosis</i>	 <i>Pneumocystis jirovecii</i>
		 <i>Paracoccidioides</i> spp.

Fig. 1. The WHO fungal priority pathogens list. Adapted from (World Health Organization, 2022).

1.2. *Candida albicans* – an enemy or an ally?

C. albicans is a natural component of the human microbiome, that is composed of bacteria, protists, and fungi. The human microbiome plays an important role in human physiology as it is involved in digestion and metabolism, regulation of the immune system, and protection from diseases (Pflughoefl and Versalovic, 2012). Only less than 0.1% of the human microbiota are fungal organisms, however, with a 100-fold larger genome than bacteria, fungal cells represent a significant biomass with versatile functions (Musumeci et al., 2022). The presence of *C. albicans* in the human microbiome seems to be important from the day of birth; more than 30% of infants' fecal microbiota was found to be composed mainly of *C. albicans*, whereas the gastrointestinal microbiome of preterm infants was discovered to be colonized by a single species of yeast with *Candida* spp. being the most common (James et al., 2020; Kondori et al., 2021). The exact role of *C. albicans* in human microbiota is still poorly understood however evidence determining its beneficial role in human microbiome includes protection against pathogen infections induced by *A. fumigatus*, *Staphylococcus aureus*, *Pseudomonas difficile*, or even *Clostridium difficile* (Musumeci et al., 2022).

Regardless of its role in the human microbiome, under certain circumstances, *C. albicans* stops being a commensal participant of the microbiota and promotes infections, that can range from commonly known superficial cutaneous and mucosal infections to life-threatening systemic candidiasis. The latter involves multi-organ inflammation including the heart, central nervous system, bones, and blood, affecting mostly the immunocompromised patients (World Health Organization, 2022). Among all fungal infections, *C. albicans* is responsible for approximately 70% of them, among which systemic infections constitute more than 400 thousand cases, however in 2017 a total of ~700 000 systemic *C. albicans* infections were recorded (Morad et al., 2018; Ho et al., 2021). The mortality rate associated with invasive *C. albicans* infections ranges between 46% and 75%, which is as high as the mortality rate attributed to aggressive bacterial sepsis (Brown et al., 2012). Moreover, hospitalized invasive *Candida* infections are costly for patients and healthcare providers due to prolonged, even up to two months, hospital stays that are estimated to cost between \$6 thousand and \$29 thousand (Morgan et al., 2005; World Health Organization, 2022). Systemic *C. albicans* infections are problematic to diagnose and difficult to cure, mainly because of the limited number of available drugs. Moreover, an observable increase in the resistance of pathogens to existing antifungal chemotherapy causes a severe clinical problem. For these reasons, there is an urgent need for the development of novel antifungal agents.

1.3. Antifungal chemotherapeutics applied in clinical practice

Currently applied methods for fighting systemic fungal infections are not sufficiently effective. To begin with, the limited set of existing antifungal classes consisting of azoles, echinocandins, polyenes, and flucytosine (Tab. 1), that were discovered and developed during the past century are characterized by a unique profile and spectrum of activity (Johnson, 2021; Ajetunmobi et al., 2023). The close relatedness of fungal and human cells contributes to the shortage in antifungal arsenal that in consequence limits the possibilities of selective molecular targets for new antifungal compounds. Existing classes of antifungal compounds in the majority target the components of the fungal cell membrane enzymes participating in biosynthesis of the membrane and cell wall or interfere with DNA biosynthesis (Perfect, 2017).

The first and the oldest class are the polyenes, represented by amphotericin B (AmB), which was the first antifungal agent approved by the FDA in 1958 and used in the treatment of invasive fungal infections (Cavassin et al., 2021). AmB targets fungal cell membrane by extraction of ergosterol from the cell membrane that in consequence leads to pore formation and leakage of cells (Ajetunmobi et al., 2023). Commonly it is referred to as 'the gold standard' as it is lifesaving and most widely used in the treatment of serious systemic infections. AmB displays excellent efficacy against a broad spectrum of fungal infections, including candidiasis, and a relatively low resistance rate. However, its high toxicity can lead to severe adverse effects like nephrotoxicity, especially when combined with other drugs (Cavassin et al., 2021).

The next class of antifungal drugs are 'azoles', which block the synthesis of ergosterol, leading to the disintegration of the cell membrane (Pianalto and Alspaugh, 2016). The azoles are the largest class of antifungal agents represented among others by fluconazole, the first in-line drug used in the treatment of invasive candidiasis with improved safety over AmB, but with developing resistance (Ajetunmobi et al., 2023).

The echinocandins are the compounds that target fungal cell wall via inhibiting 1,3- β -D-glucan synthase, an enzyme generating glucan crucial for the construction of the cell wall (Denning, 2002). The echinocandins display activity against various fungal strains including most isolates of *Candida* spp., but their spectrum is significantly narrower compared to AmB or azoles. It is characterized by a low toxicity that is related to a lack of molecular target counterpart found in human cells, and improved pharmacokinetics limiting the number of dosages (Denning, 2002). Unfortunately, the emerging resistance of fungal strains, especially *Candida* spp. to echinocandins points out a great concern (Wiederhold, 2022).

The last class of antimetabolites consists of flucytosine (5-fluorocytosine), an analog of pyrimidine, which is an inhibitor of DNA and RNA synthesis. The mechanism of action involves its deamination to 5-fluorouracil (5-FU) by cytosine deaminase present in fungal but not mammalian cells. Product of the of 5-FU inhibits thymidylate synthase and is incorporated into RNA, leading to malfunctioning protein biosynthesis and cell division (Pianalto and Alspaugh, 2016). Due to the related cytostatic effect

and developing resistance of fungal strains, flucytosine is rarely used in the form of monotherapy. However, high efficacy against cryptococcal meningitis has been reported for the combinatory treatment of flucytosine and AmB (Pianalto and Alspaugh, 2016).

Tab. 1. Clinically applied antifungal drugs for the treatment of invasive fungal infections. Created on the base of (Pianalto and Alspaugh, 2016; Johnson, 2021)

Antifungal drug	Indication	Molecular target	Adverse effects
Echinocandins			
Caspofungin	Fungicidal: <i>Candida spp.</i> Fungistatic: <i>aspergillus spp.</i> Not active against <i>Cryptococcus spp.</i>	Cell wall: (1,3)- β -D-glucan synthase	Elevations in liver enzymes, Gastrointestinal disturbances, Hypokalemia, Fever, Infusion-related reactions
Micafungin			
Anidulafungin			
Azoles			
Fluconazole	<i>Candida spp.</i> <i>Cryptococcus spp.</i>	Cell membrane: Ergosterol biosynthesis, (CYP-dependent 14a-demethylase (CYP51))	Hepatotoxicity, Alopecia, Peripheral neuropathy, Hormone-related effects, Teratogenicity
Itraconazole	<i>Aspergillois, Blastomycosis, Histoplasmosis</i>		
Voriconazole	<i>Aspergillois, Non-neutropenic Candidiasis</i>		
Isavuconazole	Invasive yeasts and molds		
Posaconazole	Prevention of invasive fungal infections in neutropenic or transplant recipients		
Polyene macrolides			
Amphotericin B	<i>Candida spp., Rhodotorula spp., Cryptococcus spp., Aspergillus spp., Rhizopus spp., Mucor spp., Rhizomucor spp., Histoplasma spp., Coccidioides spp. Blastomyces spp</i>	Cell membrane: Ergosterol interference	Infusion-related reactions, Nephrotoxicity, Electrolyte disturbances
Flucytosine	<i>Cryptococcus spp., Aspergillus spp., Candida spp., (except C. krusei)</i>	Nucleic acid synthesis	Gastrointestinal effects Hepatic disturbances, Bone marrow suppression

Despite the effectiveness in treatment invasive fungal infections, there are many challenges of currently available drugs that are related to the activity spectrum, pharmacokinetic properties, and adverse effects. Available chemotherapies are associated with a majority of adverse effects (Tab. 1), prolonged therapy, and drug-drug interactions (Lamoth et al., 2022). Another concern is the increasing antifungal resistance to current chemotherapeutics, including a recent outbreak of *C. auris* developing resistance to multiple antifungal agents (Lyman et al., 2023). The above reasons, together with an increase in the frequency of invasive

fungal infections, provide an urgent need for the development of novel antifungal chemotherapies. However, the similarity between fungal and mammalian cells makes the development of an antifungal agent extremely difficult. Unfortunately, over the last decades, the research and development on novel antifungal drugs received little attention in comparison to antibacterial or antiviral drugs (Ajetunmobi et al., 2023). Nevertheless, several potential agents are in the clinical pipeline of clinical trials including rezafungin and ibrexafungerp in phase 3 (Johnson, 2021). These two compounds are new (1,3)- β -D-glucan synthase' inhibitors with enhanced efficacy and safety, but are not regarded as alternative chemotherapy due to comparable to echinocandins antifungal spectrum (Lamoth et al., 2022). Currently applied candidates for new antifungal drugs are developed via the improvement of existing antifungal agents, but novel molecular targets are frequently being introduced, e.g. calcineurin signaling or the inhibition of the heat shock protein 90 (Scorzoni et al., 2017). Another source of possible molecular targets for novel antifungal agents characterized by an alternative mechanism of action may be the essential amino acid biosynthesis pathways that are present in fungal cells, but not in humans (Kuplińska and Rząd, 2021).

1.4. Essential amino acids biosynthetic pathways in the fight against fungal infections

Many of the presently used antifungal chemotherapeutics are associated with serious side effects such as nephrotoxicity because the molecular target for the drug is also found in the host cell. Thus, novel molecular targets should be crucial for the virulence of fungal cells but simultaneously absent in mammalian cells. Therefore, an abundant source of new potential molecular targets for novel antifungal chemotherapy may be found within the human essential amino acid biosynthesis pathways.

There are nine essential amino acids: histidine, isoleucine, leucine, lysine, methionine, phenylalanine, threonine, tryptophan, and valine. These amino acids are essential for human cells but because there are no pathways of their biosynthesis in human cells, humans must introduce these amino acids in their diet. (Fig. 2). Fungal cells, on the other hand, possess routes and enzymes that allow them to synthesize these nine amino acids. In consequence, most of the enzymes involved in the essential amino acids biosynthesis pathways are unique for fungal cells and may serve as a great source of molecular targets for novel potential drugs.



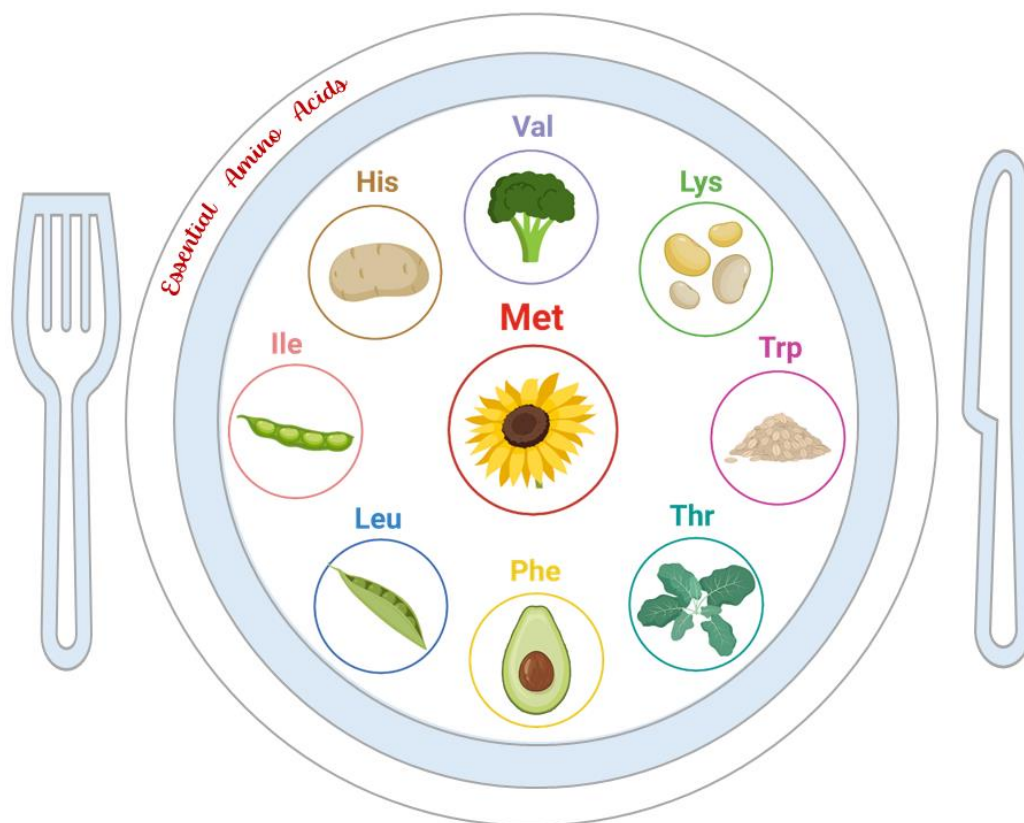


Fig. 2. Examples of essential amino acid food sources. Created on the base of (Munro, 1970).

The development of an enzyme inhibitor targeting enzymes involved in essential amino acid biosynthesis appears to be a great starting point for the discovery of a novel antifungal agent. Although it might seem ambiguous whether blocking the biosynthesis of human essential amino acids in fungal cells would make a successful antifungal at all, since the requirement for a specific amino acid may be satisfied by the exogenous supply of amino acids in human serum. For example, enzymes of the L-lysine biosynthesis pathway have been intensively investigated, however, studies performed on fungal mutant cells, deprived of genes encoding enzymes involved in L-lysine biosynthesis brought ambiguous results. Several studies reported that mutations in L-lysine biosynthesis genes caused auxotrophy for lysine and attenuated virulence, whereas others stated that the same genes are not essential for virulence (Liebmann et al., 2004; Kur et al., 2010; Schöbel et al., 2010). What is more, the usefulness of the lysine pathway as a source of potential molecular targets might seem questionable, because of the relatively high concentration of this amino acid in human serum (Schmidt et al., 2016; Han et al., 2018).

From this perspective, fungal enzymes involved in the L-methionine biosynthesis pathway (MBP) might serve as an attractive source of novel molecular targets for antifungal chemotherapy because the human serum level of L-methionine (L-Met) is particularly too low to prevent the rescue of the drop in L-Met concentration induced by the inhibition of its biosynthetic pathway in fungal cells (Han et al., 2018).

Moreover, L-Met is a crucial amino acid needed for the proper functioning of each cell, most of all it is needed for protein biosynthesis as it plays the role of its initiator. L-Met also participates in various metabolic processes and acts as a precursor for the synthesis of S-adenosyl methionine (SAM), which is required for the methylation of DNA or phospholipids (Gophna et al., 2005). Several study reports suggested that enzymes involved in MBP can be regarded as a promising source of targets for new antifungal drugs (Aoki et al., 1995; Pascon et al., 2004).

1.5. Fungal L-methionine biosynthesis pathway

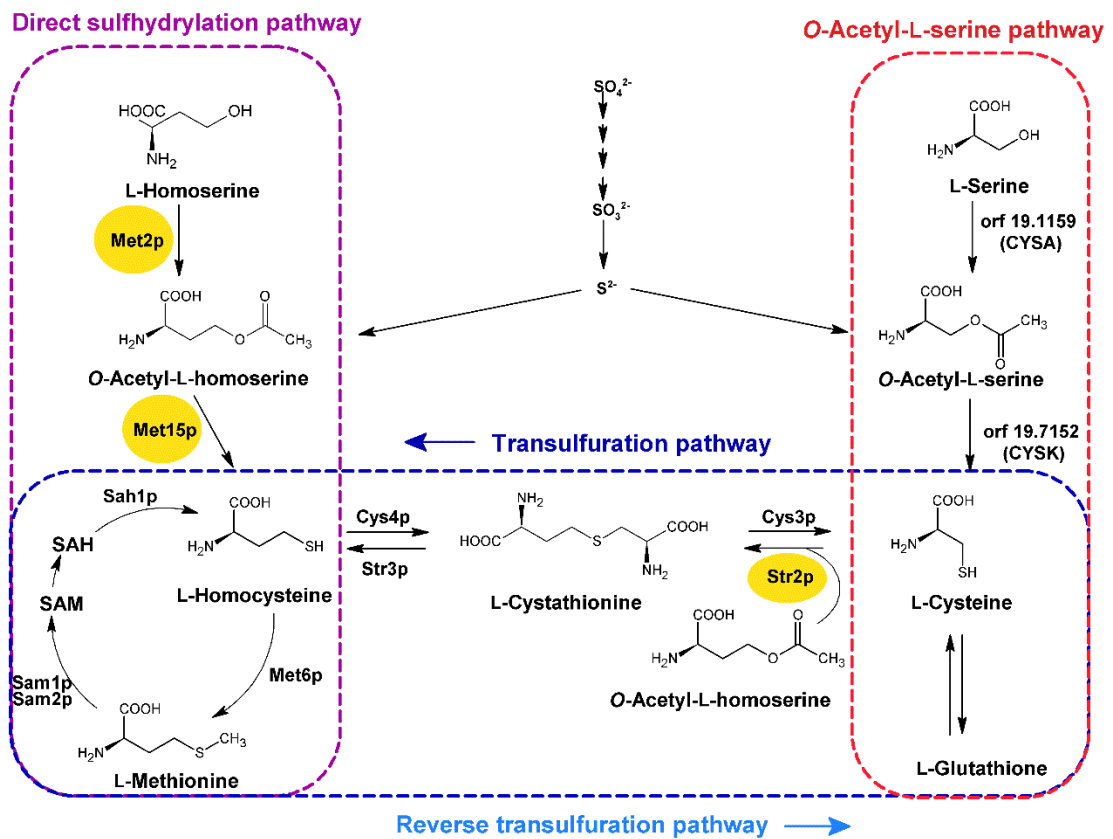


Fig. 3. The putative *C. albicans* MBP. Enzymes explored in this dissertation are marked with yellow circles i.e. Met2p EC 2.3.1.31 homoserine *O*-acetyltransferase; Met15p EC 2.5.1.49 *O*-acetyl-L-homoserine sulphydrylase; Str2p EC 2.5.1.48 cystathionine- γ -synthase. Other enzymes: Cys3p EC 4.4.1.1 cystathionine- γ -lyase; Cys4p EC 4.2.1.22 cystathionine- β -synthase; Met6p EC 2.1.1.13 methionine synthase; Sah1p EC 3.3.1.1 adenosylhomocysteinase; Sam1p, Sam2p EC 2.5.1.6 methionine adenosyltransferase; Str3p EC 4.4.1.8 cystathionine- β -lyase; CYSK orf 19.7152 putative *O*-acetyl-L-serine sulphydrylase homolog from *Aspergillus*; CYSA orf 19.1159 putative L-serine *O*-transacetylase analog of *Aspergillus nidulans*. Figure adapted from (Kuplińska et al., 2022).

L-Met is biosynthesized by fungal, bacterial and plant organisms and the respective pathway starts from L-homoserine (L-HOM) precursor, but subsequent reactions within pathways present in different organisms are not the same (Gophna et al., 2005). In the first step, in fungal cells L-HOM is *O*-acetylated by homoserine *O*-acetyltransferase (Met2p) to *O*-acetyl-L-homoserine (L-OAH), in plant cells L-HOM is *O*-phosphorylated, however, bacterial cells yield *O*-succinyl-L-homoserine at this step. Next, a sulfur atom

is incorporated into the amino acid chain, either from inorganic sulfide through the direct sulfhydrylation pathway (Fig. 3) or from L-cysteine *via* the transsulfuration pathway (Hébert et al., 2011; Kulikova et al., 2019). The process of direct sulfhydrylation involves *O*-acetyl-L-homoserine sulfhydrylase (Met15p), free sulfide, and L-OAH to produce L-homocysteine (L-HCT). Interestingly, some fungal microorganisms catalyze this reaction by bifunctional *O*-acetyl-L-homoserine/*O*-acetyl-L-serine sulfhydrylase (Met17p) (Brzywczy and Paszewski, 1993). On the other hand, the transsulfurylation pathway requires two enzymes: cystathionine- γ -synthase (Str2p) and cystathionine- β -lyase (Str3p). The first one utilizes L-OAH and L-Cys to produce L-cystathionine (L-CTT) and the next reaction catalyzed by Str3p yields L-HCT. Many organisms also possess the so-called reverse transsulfuration pathway that involves L-HCT transformation to L-CTT by cystathionine- β -synthase (Cys4p) and conversion of L-CTT to L-Cys catalyzed by cystathionine- γ -lyase (Cys3p) (Hébert et al., 2011). Thus, the incorporation of inorganic sulfur into L-Cys via an assimilatory mechanism can be also performed through the two alternative ways, that are not equally present within all fungal species. In many fungal cells, the main pathway leading to L-Cys biosynthesis is the *O*-acetyl-L-serine pathway, which starts from L-serine, followed by the condensation of sulfide with *O*-acetyl-L-serine. The second available route is the described above direct sulfhydrylation pathway, yielding L-HCT, which is then converted upon the reverse transsulfuration pathway into L-CTT and L-Cys. Many yeasts including *C. albicans* and various filamentous fungi such as *Neurospora crassa* and *Aspergillus nidulans* can synthesize L-Cys through both *O*-acetyl-L-serine and reverse transsulfuration pathway, however *C. glabrata* and *S. cerevisiae* are deprived of the *O*-acetyl-L-serine pathway, and thus have only one possible way for L-Cys biosynthesis (Cherest and Surdin-Kerjan, 1992; Hébert et al., 2011). The last reaction of the MPB leading to L-Met biosynthesis is catalyzed by methionine synthase (Met6p).

1.6. Enzymes of the L-methionine biosynthesis pathway as potential molecular targets

The first-in-line enzyme of the MBP, homoserine *O*-acetyltransferase (Met2p), is regarded as a promising target for novel antifungal agents because it was proven to be required for the virulence of *C. neoformans* in a mouse inhalation model (Nazi et al., 2007). Other studies performed on *S. cerevisiae*, *C. albicans*, and *C. guilliermondii* reported that *MET2* gene-depleted mutant cells display auxotrophy for methionine (Singh and Sherman, 1974; Kingsbury and McCusker, 2010c; Obando Montoya et al., 2014). It was suggested that the active site of Met2p is “highly druggable” (Chaton et al., 2019).

Another enzyme involved in MBP is *O*-acetyl-L-homoserine sulfhydrylase (Met15p). A study revealed that *C. glabrata* and *S. cerevisiae* mutants deficient in Met15p activity were auxotrophic towards methionine or sulfur (Singh and Sherman, 1974; Yadav et al.,

2011). This result indicates that *C. glabrata* and *S. cerevisiae* produce L-Cys only through the transsulfuration pathway (Hébert et al., 2011). In addition, it was discovered that *S. cerevisiae* cells lacking the Met15p activity were more sensitive to sulfometuron methyl agents causing starvation for isoleucine and valine, amino acids belonging together with L-Met to the aspartate family (Bae et al., 2017). In another study, *C. guilliermondii* mutants depleted in Met15p appeared to be prototrophic even in the absence of methionine (Obando Montoya et al., 2014). Prototrophic character was also observed in *C. albicans* cells disrupted in Met15p encoding genes however it led to a severe defect of growth on sulfate-containing media (Viaene et al., 2000).

The *MET6* gene encodes the enzyme catalyzing the last step of the L-Met biosynthesis pathway, i.e. methionine synthase (Met6p). It is worth noting that this enzyme is also present in mammalian cells, however, it is structurally different from the fungal version (Ubhi et al., 2014). A fungal enzyme is cobalamin independent while mammalian methionine synthase uses cobalamin as a cofactor, thus there are mechanistic differences between both enzyme versions. Inhibition of methionine synthase causes the accumulation of toxic intermediates involved in L-Met biosynthesis, L-HCT, and L-HOM, which simultaneously disrupts ergosterol biosynthesis (Pascon et al., 2004; Kingsbury and McCusker, 2010b, 2010a, 2010c). It was discovered that Met6p is essential for fungal growth and full virulence in a mouse infection model of *C. albicans* double deletion *MET6* mutant cells (Aoki et al., 1995; Suliman et al., 2007). Moreover, in *Aspergillus fumigatus*, a filamentous fungus, the methionine synthase encoding gene, is essential *in vivo* and required for the infection of the host cell (Amich et al., 2016). Interestingly, a study revealed different localizations of Met6p in various organisms, in *C. albicans* and *P. pastoris* Met6p is localized in the nucleus but in *S. cerevisiae* cells it is a cytoplasmic protein. It was concluded that nuclear localization of Met6p is a unique feature of respiratory yeasts like *C. albicans* and *P. pastoris*, and is crucial for the stability and function of the enzyme (Sahu et al., 2017).

The transsulfuration pathway involves two enzymes: cystathionine- γ -synthase and cystathionine- β -lyase encoded by *STR2* and *STR3* genes, respectively, and utilizes L-Cys to produce L-HCT. Str2p catalyzes the first step of the transsulfuration pathway using L-Cys and OAH as substrates to produce L-CTT. Upon the action of Str3p, L-CTT is transformed to L-HCT. Study results revealed that *S. cerevisiae* cells depleted in both *STR2* and *STR3* genes were unable to grow in a medium containing glutathione as the sole sulfur source, however, only *STR3*-depleted mutants were unable to grow in a medium containing L-CTT as the sole sulfur source (Hansen and Johannesen, 2000). It should be noted that L-Cys metabolism is important, since an excess of L-Cys may induce a toxic effect (Kumar et al., 2006). According to the study results, Str2p was proven to play an important role in regulating various processes including vegetative differentiation of cells in *Botrytis cinerea* cells, where cells deprived of the *STR2* gene were unable to grow in a minimal medium (Shao et al., 2016). Moreover, *B. cinerea* deletion mutant cells exhibited decreased conidiation and increased sensitivity

to osmotic, oxidative, and thermal stresses and most importantly were avirulent on host plant tissue.

The above results indicate that Str2p, Met15p, and Met2p should be considered as potential targets for novel antifungal agents, especially because of the fact that mammalian cells lack MBP thus there are no targets of potential inhibitors in human cells.

1.7. Homoserine *O*-acetyltransferase (Met2p)

The homoserine *O*-acetyltransferase EC 2.3.1.31 (Met2p), which is encoded by the *MET2* gene, is one of the key enzymes of the fungal MBP. It is reported to be found in all fungal and some bacterial strains including *Haemophilus influenzae* and *Mycobacterium tuberculosis* (Nazi and Wright, 2005). Met2p utilizes L-HOM and AcCoA as substrates (Fig. 4) and carries out the acetylation of the L-HOM hydroxyl group via a covalent acyl-enzyme intermediate to produce OHS via the double displacement (ping-pong) mechanism (Mirza et al., 2005).

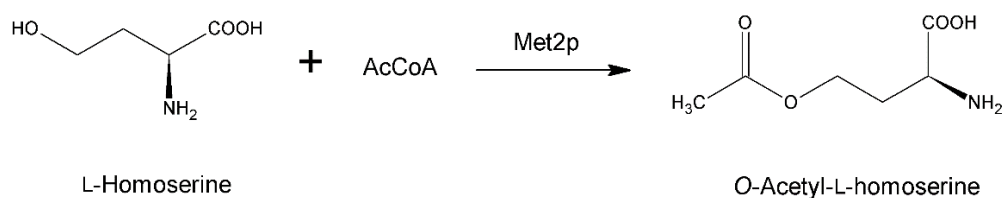


Fig. 4. Reaction catalyzed by *C. albicans* Met2p.

Met2p represents an α/β hydrolase fold superfamily, which is distinguished by eight β -sheets joined together by α -helices (Mindrebo et al., 2016). Structures of the Met2p enzyme from the *Ascomycetes* group show a similar overall fold, represented by the emergence of two distinct domains: a main core domain, and a lid domain contributing to the dimerization of the enzyme (Sagong et al., 2019). The active site of an enzyme is found in a deep cavity enabling the contribution of both domains to the active site. The active site contains a highly conserved catalytic triad composed of serine, histidine, and aspartic acid residues that are located at the base of a narrow tunnel forming an active site. The lid domain mainly constitutes the AcCoA and L-HOM binding site, however, the core domain also takes part in substrate binding. The probable structure of the *C. albicans* Met2p enzyme is similar, as shown by our research group (Kuplińska et al., 2022) reporting a putative 3D model of the *C. albicans* enzyme built on the template of the *M. smegmatis* enzyme (PDB code: 6IOH). It was revealed that six out of 10 catalytic residues forming the intramolecular tunnel between the two residues are conserved in the *C. albicans* enzyme. The catalytic triad is composed of Ser152, His345, and Asp315 in *M. smegmatis* enzyme, and in *C. albicans* is formed by Ser154, Asp360, and His389.

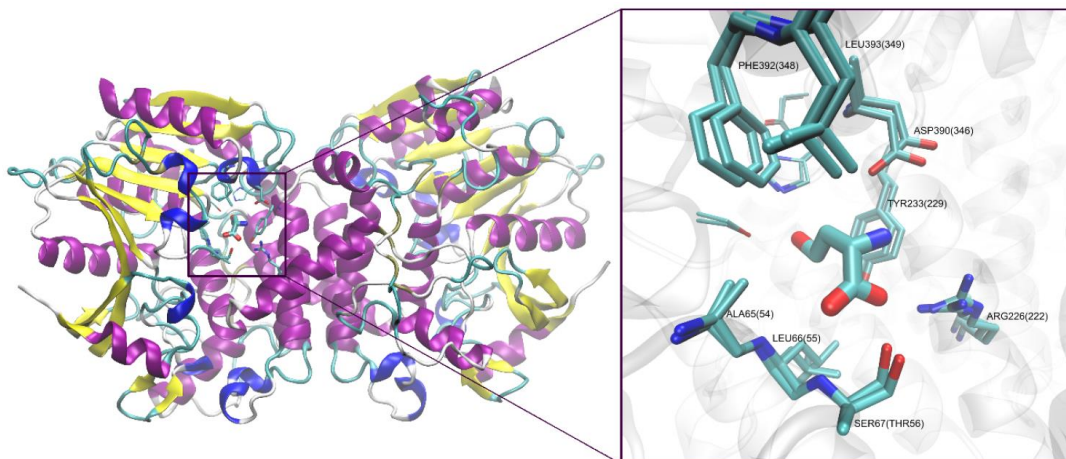


Fig. 5. Model of a putative structure of the *C. albicans* Met2p, built on the template of *M. smegmatis* Met2p (PDB: 6IOH) and AlphaFold. L-HOM placed in the center of the active site, neighboring catalytic residues are presented as sticks and labeled according to the *C. albicans* amino acid sequence (residue number for *M. smegmatis* is given in parentheses). Figure generated by Marek Wojciechowski (Kuplińska et al., 2022).

1.8. *O*-Acetyl-L-homoserine sulfhydrylase (Met15p)

O-Acetyl-L-homoserine sulfhydrylase (EC 2.5.1.49) (Met15p) is a PLP-dependent enzyme, utilizing L-OAH and a sulfide ion to catalyze L-HCT synthesis (Fig. 6), the reaction involved in the direct sulfhydrylation pathway of the MBP. There is, however, some evidence for the existence in some fungi of a bi-functional enzyme, capable of L-Cys biosynthesis from the *O*-acetyl-L-serine (L-OAS) via transulfuration pathway (Fig. 3) (Yamagata, 1989; Brzywczy and Paszewski, 1993). To distinguish the monofunctional enzyme from the bifunctional one, the latter is also known as *O*-acetyl-L-homoserine/*O*-acetyl-L-serine sulfhydrylase and referred to as Met17p (EC 2.5.1.49, EC 2.5.1.47) (Morzycka and Paszewski, 1982; Yamagata, 1984; Cherest and Surdin-Kerjan, 1992). This enzyme was found in cells of *S. cerevisiae*, *Kluyveromyces lactis*, *Yarrowia lipolytica*, *Schizosaccharomyces pombe*, and *Aspergillus nidulans* (Brzywczy and Paszewski, 1993)

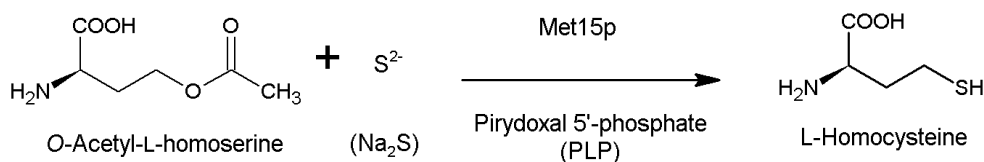


Fig. 6. Reaction catalyzed by fungal Met15p.

Analysis of the crystal structure of the bacterial Met15p from *Wolinella succinogenes*, revealed that this enzyme belongs to the PLP-dependent Cys/Met family characterizing enzymes capable of carrying a variety of β -eliminations, γ -eliminations, and γ -replacements reactions. However, the *W. succinogenes* enzyme was assigned to the γ -elimination subclass of the above family, as it was found to be able to catalyze

only this type of reaction (Tran et al., 2011). The biological unit of Met15p forms a homotetrameric structure (Fig. 7) (Brzywczy and Paszewski, 1993; Tran et al., 2011). The monomer consists of two domains: a small C-terminal domain and a large domain responsible for the PLP binding together with flanking N-terminal loop. The highly conserved catalytic residues of *W. succinogenes* Met15p are: Tyr53, Arg55, Gly83, Glu152, Asp180, Phe108, Thr182, Ser202, Thr204, Lys205, and Arg387. The mechanism of catalysis involves the formation of covalent bonds between the PLP cofactor and L-OHS (Du and Ryan, 2019). Three major catalytic residues Phe108, Thr182, and Ser202 interact with the PLP pyridine ring through van der Waals interactions and sandwich the cofactor in the active site (Tran et al., 2011).

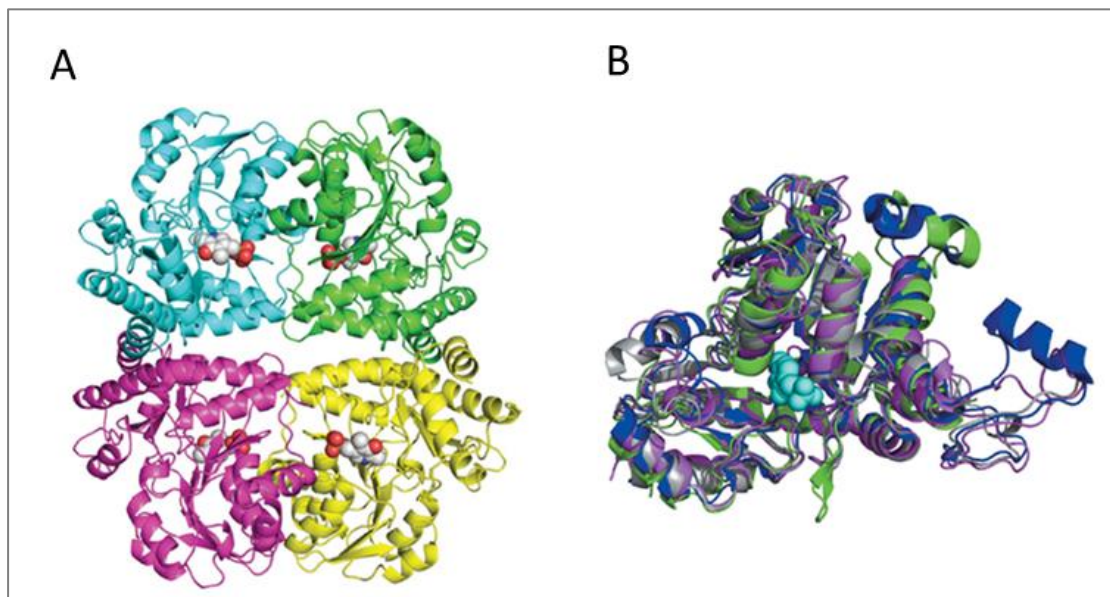


Fig. 7. Structure of *W. succinogenes* Met15p. **A.** Structure of the biological tetramer with PLP represented as spheres; **B.** Superposition of homologous Met15p enzymes with PLP in the center (cyan). PDB codes: 2cb1 (green), 1n8p (blue), 2o7c (gray). Adapted from (Tran et al., 2011).

1.9. Cystathionine- γ -synthase (Str2p)

The cystathionine- γ -synthase EC 2.5.1.48 (Str2p), is the first enzyme of the transsulfuration pathway, the alternative way for incorporation of a sulfur atom into MBP from L-Cys (Fig. 3). In this process, the PLP-dependent Str2p enzyme catalyzes the production of L-cystathionine (L-CTT) via the γ -replacement reaction from L-Cys and an activated form of L-homoserine, which is the *O*-acetyl-L-homoserine (L-OAH) in fungal cells, *O*-succinyl-L-homoserine and L-OAH in bacterial cells and *O*-phospho-L-homoserine in plants (Kerr and Flavin, 1970; Steegborn et al., 1999, 2001). The γ -replacement reaction catalyzed by the fungal Str2p is presented in (Fig. 8).

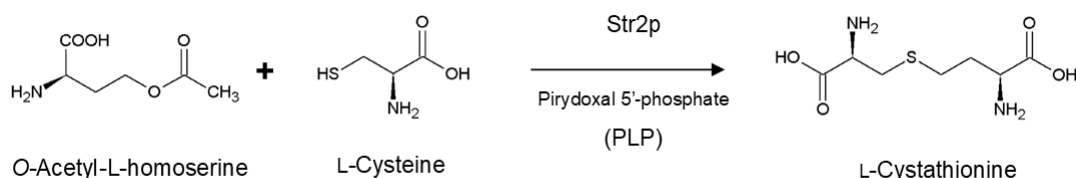


Fig. 8. Reaction catalyzed by fungal Str2p.

The Str2p was classified into the γ -family of the PLP-dependent enzymes (Alexander et al., 1994; Wahl et al., 1997). The catalyzed reaction follows a double displacement (ping-pong) mechanism, engaging the formation of the aldimine linkage between the PLP cofactor and L-OAH, followed by the detachment of the α - and β - proton (Kreft et al., 1994; Steegborn et al., 2001). After the release of an activated residue, the α -imino- β - γ -unsaturated pyridoxamine derivative is formed, which is later attacked by the sulfur atom of L-Cys (Brzovic et al., 1990; Steegborn et al., 1999, 2001). Similarly to Met15p and other PLP-dependent enzymes, Str2p comprises the large PLP-binding domain, the small C-terminal domain, and an extended N-terminal loop domain, that in the case of the *E. coli* enzyme consists of 51 amino acid residues (Clausen et al., 1998). The large PLP-binding domain emerges from seven-stranded β -sheet, located at the center with surrounding seven α -helices, that sandwich the cofactor binding site. The *E. coli* Str2p forms a covalent Schiff base linkage between PLP and Lys198, one of the most conserved catalytic residues. The majority of the other residues involved in enzyme catalysis are also located in the PLP-binding domain (Clausen et al., 1998; Sagong and Kim, 2017). The C-terminal domain is similar in structure to the PLP binding domain but comprises four or five-stranded β -sheet, respectively for *Corynebacterium glutamicum*, and *E. coli* enzyme, and six covering α -helices. The extended N-terminal loop domain is composed of one α -helix and an extended N-terminal loop that together with the C-terminal domain is responsible for binding of L-OHS. In the *E. coli* enzyme, it is not only the Lys198 that contributes to the binding of the PLP cofactor, also Gly76, Met77, Ser195, and Thr197 residues interact with the cofactor's phosphate group. Asp173 and Arg361 are largely conserved and structurally important; Asp173 contributes to the formation of a strong hydrogen bond and a salt bridge to the pyridine nitrogen of the PLP increasing its electrophilic character, whereas Arg361 together with Ser326, and Asn148 takes part in the binding of the incoming substrate, respectively (Clausen et al., 1998). Reports concerning the oligomeric structure of the Str2p enzyme provide evidence for a homotetrameric structure that is formed via the association of two dimers (Wahl et al., 1997; Clausen et al., 1998; Sagong and Kim, 2017).

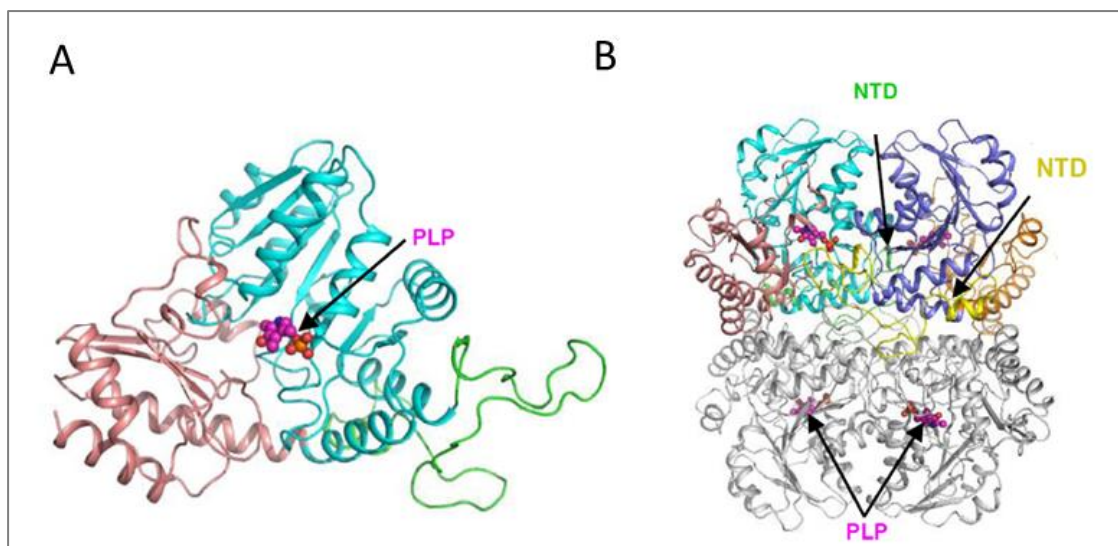


Fig. 9. Structure of *C. glutamicum* Str2p. **A.** Single monomer with bound PLP cofactor; **B.** Tetrameric structure with bound PLP cofactor, one of the active dimers is highlighted, with separate color coding for distinct monomers, the N-terminal loop domain of two monomers is shown with arrows. Color coding of domains found in single monomer: the large PLP-binding domain (cyan/blue), the small C-terminal domain (pink/orange), and an extended N-terminal loop domain (green/yellow). Adapted from (Sagong et al., 2019).

1.10. Inhibitors targeting the L-methionine biosynthesis pathway

The absence of the MBP in human cells, as well as low concentration of L-Met in human serum, create an encouraging opportunity for searching for new compounds targeting enzymes involved in this pathway. An additional motivating aspect is provided by the importance of enzymes of the MBP on fungal viability, described in section 1.6. Throughout the years, several inhibitors targeting the microbial MBP have been reported, but none of them has advanced to clinical use (Jastrzębowska and Gabriel, 2015; Kuplińska and Rząd, 2021).

Nazi et al., performed a high-throughput screening of small compounds inhibiting protein kinases, that gave rise to the CTCQC inhibitor (Fig. 10 A) (Nazi et al., 2007). CTCQC appeared to be an effective inhibitor of *C. neoformans* Met2p, competitive to AcCoA, characterized by an IC_{50} value of 4.5 μ M. Despite a relatively good inhibitory effect, the CTCQC displayed a disproportionately modest antifungal activity against *C. neoformans*, with MIC_{90} estimated to be 128 μ g mL^{-1} in a minimal medium. This low antifungal activity was assumed to be caused by inefficient transport into the cell, or inadequate metabolism of a compound to an active form (Nazi et al., 2007).

Azoxybacillyn (Fig. 10 B), is a natural compound isolated from *Bacillus cereus*, with a broad spectrum of antifungal activity (Fujiu et al., 1994; Aoki et al., 1996). It was found to display antifungal activity against various fungal strains including those belonging to the genus of *Aspergillus*, *Candida*, *Microsporum*, *Trichophyton*, and *Absidia* in the range between 0.017 μ g mL^{-1} and 9.8 μ g mL^{-1} , but not against *C. neoformans* (Fujiu et al., 1994). Azoxybacillin was then assumed to be an inhibitor targeting one of the enzymes involved in the MPB, as the inhibitory effect was decreased by the addition



of L-Met to the minimal media. Only later, it was deduced that the antifungal activity displayed by Azoxybacillin is due to the inhibition of expression of genes encoding enzymes associated with sulfate assimilation, including Met15p (Aoki et al., 1996). However, the inhibitor displayed moderate inhibitory activity towards Met15p ($IC_{50} = 100 \mu\text{g mL}^{-1}$), followed by even lower activity in the animal infection model (Aoki et al., 1996).

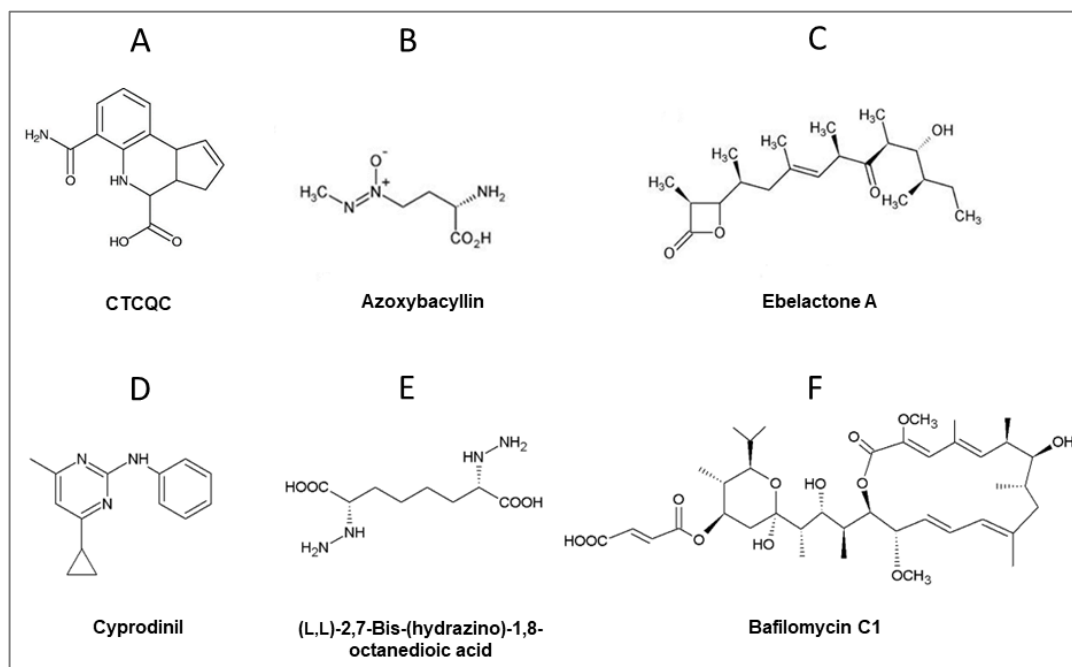


Fig. 10. Inhibitors of enzymes from the L-methionine biosynthetic pathway. **A.** CTCQC; **B.** Azoxybacillin; **C.** Ebelactone A; **D.** Cyprodinil; **E.** (L, L)-2,7-Bis-(hydrazino)-1,8-octanedioic acid; **F.** Bafilomycin C1. Adapted from (Jastrzębowska and Gabriel, 2015; Kuplińska and Rząd, 2021).

Inhibitors belonging to the β -lactam group such as penicillin or cephalosporin, inhibit enzymes by covalently modifying the catalytic serine residue (Robinson et al., 2019). Met2p also contains the catalytic triad consisting of serine, histidine, and aspartic acid residues, thus it was assumed that a similar mode of action could be applied towards inhibition of the Met2p enzyme with β -lactones derivatives (De Pascale et al., 2011). A series of β -lactones derivatives containing acyl chains were tested as potential inhibitors capable of binding to the *H. influenzae* Met2p active site, including ebelactone A (Fig. 10 C), a natural product of *Streptomyces spp.* and a known strong inhibitor of esterases (De Pascale et al., 2011). Ebelactone A and its two other synthetic derivatives displayed antifungal activity against *C. albicans* (MIC_{90} between $64 \mu\text{g mL}^{-1}$ and $8 \mu\text{g mL}^{-1}$) in contrast to *H. influenzae*. Further studies displayed the relationship between the length of the alkyl chain and inhibitory potential i.e. shorter alkyl chain facilitates inhibitory effect by increasing the availability to fit inside the narrow active site (De Pascale et al., 2011). Despite promising results, there are no reports of further application of ebelactone A or its derivatives, leaving a possibility for exploitation of new inhibitors.

Few reports introduced inhibitors targeting enzymes involved in the transsulfuration and reverse transsulfuration pathway: cystathionine- γ -synthase (Str2p), cystathionine- β -lyase (Str3p), cystathionine- γ -lyase (Cys3p), cystathionine- β -synthase (Cys4p) (McCune et al., 2016; Hou et al., 2018; Tu et al., 2018). Cyprodinil (Fig. 10 D), an anilinopyrimidine fungicide derivative, was proposed as a new inhibitor targeting the fungal transsulfuration pathway (Hou et al., 2018). Cyprodinil was proved to be effective against *Sclerotinia sclerotiorum* with an EC₅₀ value of 0.19 $\mu\text{g mL}^{-1}$. The growth inhibition could be decreased by supplementing L-Met or L-Cys, which provoked the assumption that either Str2p or Str3p are the molecular targets for cyprodinil. However, conducted sequence alignment revealed no differences in the amino acid composition of Str2p and Str3p, between the sensitive strains and cyprodinil-resistant mutants (Hou et al., 2018). In another study, a new compound (L, L)-2,7-bis(hydrazino)-1,8-octanedioic acid (Fig. 10 E), was designed via a structure-based approach, as a potential inhibitor of the reverse transsulfuration pathway by targeting *S. cerevisiae* Cys4p enzyme (Tu et al., 2018). There is no data regarding the antifungal activity of this inhibitor, however, it was proven to inhibit the activity of Cys4p, yielding a K_i value of 48 μM in an animal neuroblastoma model, while it was regarded as a potential treatment against stroke (McCune et al., 2016). Since then, there has been no evidence for development of a potent inhibitor of a fungal Str2p or any other enzyme involved in the fungal transsulfuration or reverse transsulfuration pathway.

Methionine synthase (Met6p) is the last enzyme of the MBP. It is cobalamin-independent, thus different structurally from the mammalian cobalamin-dependent counterpart (Ubhi et al., 2014). Another natural compound, bafilomycin C1 (Fig. 10 F), a macrolide antibiotic produced by *Streptomyces albolongus*, was assumed as potential inhibitor of fungal Met6p (Ding et al., 2016). Bafilomycin C1 is effective against a broad range of microorganisms; it exhibits antibacterial activity against *B. subtilis* and *Staphylococcus aureus* (MIC₉₀ 12.5 $\mu\text{g mL}^{-1}$), and antifungal activity towards *Candida sp.* and *C. neoformans* (MIC₉₀ 1.56 $\mu\text{g mL}^{-1}$) and *Aspergillus fumigatus* (MIC₉₀ 16 $\mu\text{g mL}^{-1}$) (Frändberg et al., 2000; Ding et al., 2016). The following research concerning bafilomycin C1 brought insight into the molecular target of this compound. Significant downregulation of the expression of *C. albicans* genes related to ergosterol biosynthesis was correlated with bafilomycin activity. (Su et al., 2018) Notably, the *MET6* gene expressing the *C. albicans* Met6p enzyme was also downregulated. Inhibition of the Met6p enzyme can lead to a dual effect; auxotrophy for L-Met and consequent sterol biosynthesis inhibition caused by the accumulation of L-HCT (Newell et al., 1988). Despite this dual feature, and open search for compounds targeting Met6p, no successful inhibitors have been proposed.

2. RESEARCH AIM AND OBJECTIVES

The main aim of my doctoral project has been identification and characterization of enzymes exhibiting activities of the homoserine *O*-acetyltransferase EC 2.3.1.31 (Met2p), *O*-acetyl-L-homoserine sulfhydrylase EC 2.5.1.49 (Met15p) and cystathionine- γ -synthase EC 2.5.1.48 (Str2p) in *Candida albicans*. The results obtained have been expected to enhance the comprehension of the fungal L-methionine biosynthesis pathway, and offer insights into the hypothesis, determining whether enzymes involved in *C. albicans* L-methionine biosynthesis pathway may be considered as novel potential targets for antifungal chemotherapy.

The objectives of the research project involved:

- ★ Identification and cloning of genes encoding enzymes of the *C. albicans* L-methionine biosynthetic pathway: homoserine *O*-acetyltransferase (Met2p), *O*-acetyl-L-homoserine sulfhydrylase (Met15p), and cystathionine- γ -synthase (Str2p),
- ★ Isolation and biochemical characterization of CaMet2p, CaMet15p and CaStr2p as wild type or recombinant proteins
- ★ Searching for potential inhibitors of *C. albicans* Met2p, Met15p, and Str2p as candidates for antifungal agents
- ★ Protein crystallization trials.

3. MATERIALS AND METHODS

3.1. Materials

3.1.1. Laboratory equipment

Tab. 2. Laboratory equipment used in research.

Agarose electrophoresis apparatus DELFIN (DNA Gdańsk)
ÄKTA Fast protein liquid chromatography (FPLC) System with Frac-950 Fraction Collector (Amersham Biosciences)
ÄKTA pure™ 25 chromatography system (Cytiva)
Amicon™ Ultra Centrifugal Filter Units (Merck Millipore)
Basic power supply PowerPac™ Basic (BIO-RAD)
BioSpec-nano (SHIMADZU BIOTECH)
Centrifuge MPW-380R (MPW MED. INSTRUMENTS)
Dry block heater QBD2 (Grant)
Dry block thermostat BioTDB-100 (Biosan)
Eppendorf® centrifuge mini spin® (Eppendorf)
Eppendorf® refrigerated centrifuge 5415R (Eppendorf)
Eppendorf® Mastercycler nexus GX (Eppendorf)
GEL DOC XR+ (BIO-RAD)
HisTrap™ Fast Flow (Cytiva)
HiTrap™ Desalting column (Cytiva)
HPLC-DAD 1200 Quaternary DAD HPLC System (Agilent)
HPLC-DAD 1260 Infinity II 6470 (Agilent)
HPLC-MS Triple Quad LC/MS (Agilent)
IR Autoflow Water-Jacketed CO ₂ incubator NUAIRE™ NU-2700 (NuAire)
Laboratory incubator shaker Unitron (INFORS HT)
MSC-Advantage™ Class II Biological Safety Cabinets (Thermo Scientific)
Multi-reax test tube shaker (Heidolph)
Non-electric magnetic stirrer (WABEL)
NuPAGE® electrophoresis system (Invitrogen)
pH-meter CPI-505 (Elemetron)
Polyacrylamide electrophoresis apparatus BlueStar nr Blue 01C (DNA Gdańsk)
Refrigerated bench centrifuge 6515 (Sigma laboratory centrifuges)
Resource™ Q column (Cytiva)
Rocking Platform Shaker KL-942 Shaker OKAP (JW ELECTRONIC)
Scale As/110/C/2 (Radwag)
Scale WPS 720/C/2 (Radwag)
Scale AS.R2 (Radwag)
Sonifier digital W-250 (Branson)
Spark® 10M micro plate reader (TECAN)
Spectrofotometer BioSpec-nano (SHIMADZU BIOTECH)
Spectrophotometer Genesys 20 (Thermo Spectronic)
Superdex™ 200 10/300 Increase column (Cytiva)
Superdex™ 200 16/600 GL column (Cytiva)
Thermocycler Mastercycler gradient (Eppendorf)
Ultrasonic waterbath P-5033 (Polsonic)
Vortex REAX top (Heidolph instruments)
Water bath MLL 547 (AJL Electronics)
Zorbax Eclipse C18 column 5 µm, 250 mm x 4.6 mm (Agilent)

3.1.2. Software

Tab. 3. Software used in research.

Vector NTI Advance	Version 11.5.4, 2014, Invitrogen
SnapGene Viewer	Version 5.1.5
BioEdit Sequence alignment editor	Version 7.0.5.3, 2005
Oligo Calc: Oligonucleotide Properties Calculator	Version 3.27, 2015
Gel analyzer	Version 19.1
GraphPad Prism	Version 8.0.0 for Windows, GraphPad Software
Combenefit	Version 2.021, Cancer Research UK Cambridge Institute
XtalPred	Version 2007

3.1.3. Mass markers

Tab. 4. Mass markers used in research.

Name	Band mass	Application
PageRuler Plus Prestained Protein Ladder (Thermo Scientific)	250; 130; 95; 72; 55; 36; 28; 17; 10 kDa	SDS-PAGE electrophoresis (proteins)
GeneRuler 1 kb Plus DNA Ladder (Thermo Scientific)	20 000; 10 000; 7000; 5000; 4000; 3000; 2000; 1500; 1000; 700; 500; 400; 300; 200; 75 bp	Agarose electrophoresis (DNA)
Native MARK™ Unstained Protein Standard (Thermo Scientific)	11236; 1048; 720; 480; 242; 146; 66; 20 kDa	NATIVE-PAGE electrophoresis (proteins)
Gel Filtration Markers Kit for Protein Molecular Weights 29.000-700.000 Da (Sigma-Aldrich)	669; 200; 150; 66; 29 kDa	Size exclusion chromatography (proteins)

3.1.4. Culture media

Tab. 5. Solid media for bacterial and yeast cultures.

Name	Components
YPG	glucose 20 g L ⁻¹ ; peptone 10 g L ⁻¹ ; yeast extract 10 g L ⁻¹ ; bacteriological agar 25 g L ⁻¹
LA	sodium chloride 10 g L ⁻¹ ; yeast extract 5 g L ⁻¹ ; peptone 10 g L ⁻¹ ; bacteriological agar 15 g L ⁻¹
Supplements	ampicillin 100 µg mL ⁻¹ ; chloramphenicol 34 µg mL ⁻¹ ; tetracycline 5 µg mL ⁻¹

Tab. 6. Liquid media for bacteria and yeast culture.

Name	Components
YPG	glucose 20 g L ⁻¹ ; peptone 10 g L ⁻¹ ; yeast extract 10 g L ⁻¹
LB	sodium chloride 10 g L ⁻¹ ; yeast extract 5 L ⁻¹ ; peptone 10 g L ⁻¹
SOC	sodium chloride 10 g L ⁻¹ ; yeast extract 5 g L ⁻¹ ; peptone 10 g L ⁻¹ ; tryptone 20 g L ⁻¹ ; MgSO ₄ 2.44 g L ⁻¹
Supplements	ampicillin 100 µg mL ⁻¹ ; chloramphenicol 100 µg mL ⁻¹ ; tetracycline 5 µg mL ⁻¹ 1% glucose; 4% glycerol; 3% EtOH; 0.5 M sorbitol

Tab. 7. Liquid media for MIC and synergism assay.

Name	Components
RPMI-1640	glucose 18 g L ⁻¹ ; RPMI-1640 with L-glutamine 10.4 g L ⁻¹ ; MOPS 34.5 g L ⁻¹ ; pH 7 adjusted with NaOH
YNB AS L-Met	glucose 20 g L ⁻¹ ; YNB without amino acids with ammonium sulfate 1.7 g L ⁻¹ ; L-methionine 1.5 g L ⁻¹
YNB AS	glucose 20 g L ⁻¹ ; YNB without amino acids and ammonium sulfate 1.7 g L ⁻¹
YNB SG L-Met	glucose 20 g L ⁻¹ ; YNB without amino acids and ammonium sulfate 1.7 g L ⁻¹ ; sodium L-glutamate 1.2 g L ⁻¹ ; L-methionine 1.5 g L ⁻¹
YNB SG	glucose 20 g L ⁻¹ ; YNB without amino acids and ammonium sulfate 1.7 g L ⁻¹ ; sodium L-glutamate 1.2 g L ⁻¹

3.1.5. Bacterial and yeast strains

Tab. 8. Bacterial and yeast strains used in research.

Name	Source	Application
<i>Candida albicans</i> SC5314	Department of Pharmaceutical Technology and Biochemistry (DPTB)	Isolation of genomic DNA
<i>Escherichia coli</i> One Shot™ TOP10	Invitrogen	Multiplication of constructed plasmid, verification of correct cloning
<i>E. coli</i> TOP10F'	DPTB	Multiplication of constructed plasmid, verification of correct cloning, characterization of the plasmid, propagation, and maintenance
<i>E. coli</i> One Shot™ BL21 Star™ (DE3)	Invitrogen	Expression strains, overexpression of recombinant genes <i>MET2</i> , <i>MET15</i> , <i>STR2</i> , in Tabor-Studier system
<i>E. coli</i> BL21 (DE3) pLysS	Invitrogen	
<i>E. coli</i> Rosetta (DE3) pLysS	Novagen	
<i>E. coli</i> Rosetta (DE3) pLacI	Novagen	
<i>E. coli</i> BL21 Star™ (DE3) pLysS	Invitrogen	
<i>Escherichia coli</i> Origami (DE3) pLysS	Novagen	
<i>E. coli</i> BL21 ER2566	New England Biolabs	
<i>E. coli</i> BL21(DE3)/MAGIC	Creative Biolabs	
<i>E. coli</i> Lemo21 (DE3)	New England Biolabs	

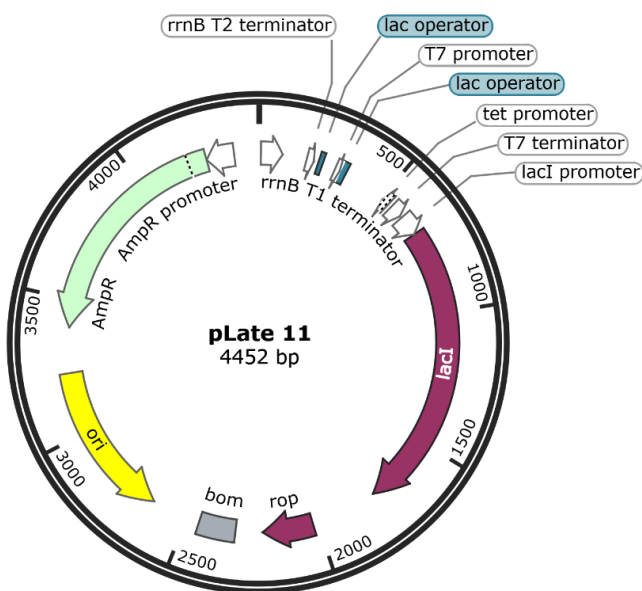
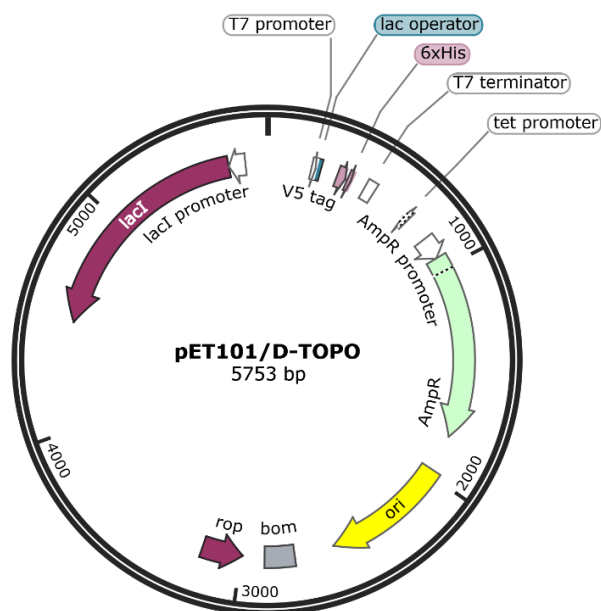
3.1.7. DNA

a) Plasmids

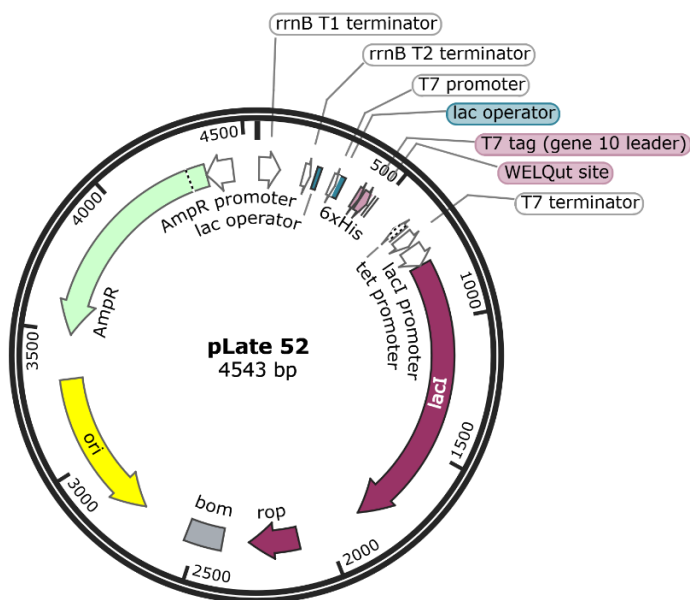
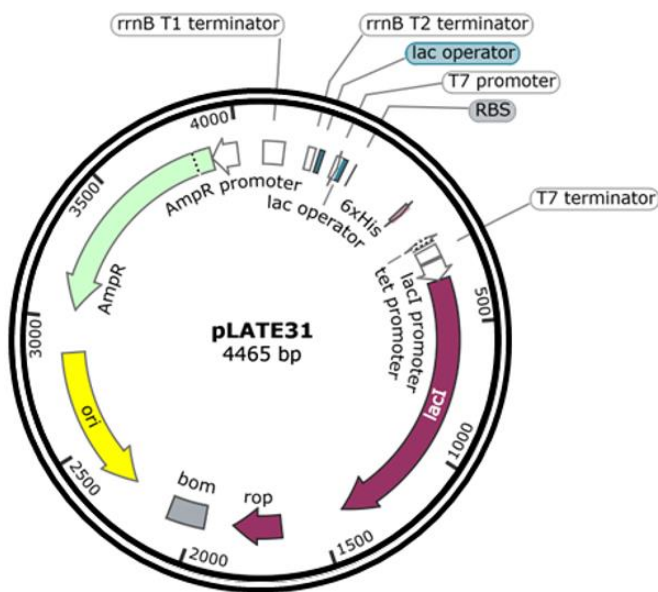
Tab. 9 describes plasmids that were used for cloning, figures Fig. S1 - Fig. S3 depict constructed plasmids with inserted *C. albicans* *MET2*, *MET15*, and *STR2* genes.

Tab. 9. Maps of plasmids used for cloning experiments.

Name	Size	Source	Application and characteristics
pET101/D-TOPO®	5753 bp	Invitrogen	<p>Enables high-level protein production in <i>E. coli</i> host strains. System based on the Tabor-Studier method (Tabor, 1990; Studier, 1991).</p> <p>Features:</p> <ul style="list-style-type: none"> • T7 promoter from ϕ 10 phage T7 • <i>lac</i> operator of the lactose operon • TOPO Cloning site (directional) • <i>AmpR</i> ampicillin resistance gene • pBR322 origin of replication • ROP ORF encoding rop protein participating in replication • <i>lacI</i> ORF encoding repressor protein of the lacO <p>Used for construction of plasmids: pET101/D-TOPO+<i>MET2</i> pET101/D-TOPO+<i>MET2CH</i> pET101/D-TOPO+<i>MET2NH</i></p>
pLATE11	4452 bp	Thermo Scientific™	<p>Enables high-level protein production of untagged proteins in <i>E. coli</i> host strains. System based on the Tabor-Studier method (Tabor, 1990; Studier, 1991).</p> <p>Features:</p> <ul style="list-style-type: none"> • T7 promoter from ϕ 10 phage T7 • <i>rrnBT1-T2</i> transcription terminator • <i>Tet</i> promoter flanking the T7 promoter • <i>lac</i> operators upstream and downstream of the T7 promoter • <i>AmpR</i> ampicillin resistance gene • <i>ROP</i> ORF encoding rop protein participating in replication • <i>lacI</i> repressor of lac <p>Used for construction of plasmids: pLATE11+<i>MET15</i> pLATE11+<i>STR2</i></p>



Name	Size	Source	Application and characteristics
pLATE31	4465 bp	Thermo Scientific™	<p>Enables high-level production of proteins with C-terminal 6xHisTag in <i>E. coli</i> host strains. System based on the Tabor-Studier method (Tabor, 1990; Studier, 1991).</p> <p>Features:</p> <ul style="list-style-type: none"> • T7 promoter from ϕ 10 phage T7 • T7 transcription termination region • <i>rrnBT1-T2</i> transcription terminator • <i>Tet</i> promoter flanking the T7 promoter • <i>lac</i> operators upstream and downstream of the T7 promoter • <i>AmpR</i> ampicillin resistance gene • <i>ROP</i> ORF encoding <i>rop</i> protein participating in replication • <i>lacI</i> repressor of <i>lac</i> • C-terminal 6xHisTag <p>Used for construction of plasmids: pLATE11+MET15CH pLATE11+STR2CH</p>
pLATE52	4543 bp	Thermo Scientific™	<p>Enables high-level production of proteins with N-terminal 6xHisTag and WELQut Protease cleavage site in <i>E. coli</i> host strains. System based on the Tabor-Studier method (Tabor, 1990; Studier, 1991).</p> <p>Features:</p> <ul style="list-style-type: none"> • T7 promoter from ϕ 10 phage T7 • T7 transcription termination region • <i>rrnBT1-T2</i> transcription terminator • <i>Tet</i> promoter flanking the T7 promoter • <i>lac</i> operators upstream and downstream of the T7 promoter • <i>AmpR</i> ampicillin resistance gene • <i>ROP</i> ORF encoding <i>rop</i> protein participating in replication • <i>lacI</i> repressor of <i>lac</i> • N-terminal 6xHisTag • WellQut protease recognition sequence <p>Used for construction of plasmids: pLATE11+MET15NH pLATE11+STR2NH</p>



b) Oligonucleotides

Tab. 10. Oligonucleotides used in research for PCR reaction.

Name	Sequence	Characteristics
Primers for cloning of <i>C. albicans</i> MET2 gene into pET101/D-TOPO vector		
MET2_f (forward primer)	5' CACCATG ACATACAAAGACGTGACA3'	Amplification of <i>MET2</i> gene (cloning) ■ Part complementary to the sequence of <i>C. albicans</i> <i>MET2</i> gene ■ Sequence required for directional cloning to the pET101/D-TOPO vector ■ Start codon ■ Stop codon ■ Sequence coding for 6xHisTag domain
MET2_r (reverse primer)	5' GATTATTC AATTATTCAAAAACTAGTGATGAAAC3'	
MET2_rCH (reverse primer inserting 6xHisTag domain)	5' TCAATGATGATGATGATGATGAT TATTCAAAAACTAGT3'	
MET2_fNH (forward primer inserting 6xHisTag domain)	5' CACCATG CATCATCATCATCATCA TACATACAAAGACGT 3'	
MET2_r2 (reverse primer)	5' TGTCATCC TTGATTATTC AATTA TTCAAAAACTAGTGATG3'	
Primers for cloning of <i>C. albicans</i> MET15 gene into pLATE11, pLATE31 and pLATE52 vectors		
Met15_LIC_f1 (forward primer - pLATE11)	5' AGAAGGAGATATAACTATG CCCTTCTCACTTTGATACT3'	Amplification of <i>MET15</i> gene (cloning) ■ Part complementary to the sequence of <i>C. albicans</i> <i>MET15</i> gene ■ Sequence required for directional cloning to the pLATE11 and pLATE31 vector ■ Sequence required for directional cloning to pLATE52 vector and for WELQut protease recognition ■ Start codon ■ Stop codon ■ Sequence coding for 6xHisTag domain
Met15_LIC_r1 (reverse primer - pLATE11, pLATE52)	5' GGAGATGGGAAGTCATTA GTTGTATATAACCTT3'	
Met15_LIC_fNH (forward primer – pLATE52)	5' GGTTGGGAATTGCAA CCCTTCTCACTTTG3'	
Met15_LIC_f2 (forward primer – pLATE31)	5' AGAAGGAGATATAACTATG CCCTTCTCACTTTGATACTCTTCAATT3'	
Met15_LIC_rCH1 (reverse primer – pLATE31 inserting 6xHisTag domain)	5' GTGATGATGATGATGATGATG CCCGTTGTTATAAACCTTCT3'	
Primers for cloning of <i>C. albicans</i> STR2 gene into pLATE11, pLATE31 and pLATE52 vectors		
Str2_LIC_f2 (forward primer - pLATE11, pLATE31)	5' AGAAGGAGATATAACTATG CCCTTCAACAAGAAATAGGGAT3'	Amplification of <i>STR2</i> gene (cloning) ■ Part complementary to the sequence of <i>C. albicans</i> <i>STR2</i> gene ■ Sequence required for directional cloning to the pLATE11 and pLATE31 vector ■ Sequence required for directional cloning to pLATE52 vector and for WELQut protease recognition ■ Start codon ■ Stop codon ■ Sequence coding for 6xHisTag domain
Str2_LIC_r2 (reverse primer - pLATE11, pLATE52)	5' GGAGATGGGAAGTCATTA TATAC TTTCATCTAAACTTTTTTGC3'	
Str2_LIC_fNH3 (forward primer – pLATE52)	5' GGTTGGGAATTGCAA CCCTCACAAGAAATAGGGATG3'	
Str2_LIC_rCH2 (reverse primer – pLATE31 inserting 6xHisTag domain)	5' GTGATGATGATGATGATGATG CCCTACTTTTCATCTAAACTTTTTTGC3'	

Primers used for mutagenesis of the <i>MET2</i> gene		
MET2mut_f2 (forward primer for directional mutagenesis)	5'P-GCATTAGAATAC ^{TC} GGCAATT TACAACAATA3'	Mutagenesis of <i>MET2</i> gene ■ Part complementary to the sequence of <i>C. albicans MET2</i> gene ■ Place of mutation insertion P Phosphorylated N-terminus (forward primer) and C-terminus (reverse primer)
MET2mut_r (reverse primer for directional mutagenesis)	5'P-CATTCCCCCATGGATCCTCC A3'	
Primers used for sequencing analysis of constructed plasmids		
pET101seq_N (forward primer)	5'GATGCGTCCGCGTAGAGG3'	Sequencing of plasmids based on pET101/D-TOPO vectors
pET101seq_C (reverse primer)	5'AGCCGGATCAAACCTCAATGGTG3'	
LIC_seq_f (forward primer)	5'TAATACGACTCACTATAGGG3'	Sequencing of plasmids based on pLATE vectors
LIC_seq_r (reverse primer)	5'GAGCGGATAACAATTCACACAG G3'	

*I designed all cloning and mutagenesis primers with the help of Vector NTI software. Sequences of primers required for sequencing were given by vector manufacturers.

3.1.8. Restriction enzymes

Tab. 11. Restriction enzymes used in research.

Name	Source	Site of cleavage	Application
<i>Bam</i> HI	Thermo Scientific™	5' G A ^{m6} ↓ T C 3' 3' C T ↑ A ^{m6} G 5'	Digestion of STR2 and <i>MET15</i> containing plasmids
<i>Dpn</i> I	Thermo Scientific™	5' G A ^{m6} ↓ T C 3' 3' C T ↑ A ^{m6} G 5'	Mutagenesis
<i>Eco</i> RI	Thermo Scientific™	5' G ↓ A A T T C 3' 3' C T T A A ↑ G 5'	Digestion of <i>MET2</i> containing plasmids
<i>Bcu</i> I (<i>Spe</i> I)	Thermo Scientific™	5' A ↓ C T A G T 3' 3' T G A T C ↑ A 5'	Digestion of <i>MET2</i> containing plasmids
<i>Sac</i> I	Thermo Scientific™	5' G A G C T ↓ C 3' 3' C ↑ T C G A G 5'	Digestion of STR2 and <i>MET15</i> containing plasmids

3.1.9. Enzymes substrates and coenzymes

Tab. 12. Substrates and a cofactor of CaMet2p, CaMe15p, and CaStr2p enzymes.

Name	Index	Enzyme	Source	
L-Homoserine	L-HOM	Met2p	Commercial (Sigma-Aldrich)	
Acetyl-coenzyme A lithium salt	Ac-CoA			
Pyridoxal 5'-phosphate	PLP			Met15p and Str2p
L-Cysteine	L-CYS			Str2p
Sodium sulfide	Na ₂ S	Met15p	Commercial (Chemat)	
O-Acetyl-L-homoserine	L-OAH	Met15p and Str2p	Synthesized (Department of Organic Chemistry)	

3.1.10. Tested potential inhibitors

Tab. 13. Potential inhibitors of CaMet2p, CaStr2p, and CaMe15p enzymes.

Name	Index	Source
Acetyl-L-carnitine	L-CAR	Commercial (Sigma-Aldrich)
D-Penicillamine	D-PEN	
L-Penicillamine	L-PEN	
3-(2-Thienyl)-L-alanine	T-ALA	
L-Methionine sulfoximine	L-MES	
DL-Glufosinate	DL-GLUF	
L-2,4-Diaminobutyric acid dihydrochloride	L-DBA	
DL-2-Allylglycine	DL-ALG	
L-Canavanine	L-CAV	
L-2-Aminoadipic acid	L-AAA	
L-Methionine	L-MET	
2-Amino-4-fluorobutanoic acid hydrochloride	A-FBA	
L-Homoserine methyl phosphonate	L-HMP	
L-Serine methyl <i>O</i> -phosphonate	L-SMP	
L-4-Acetamide-2-aminobutyric acid	Ac-DAB	
β -(5-Oxo-3-isoxazolin-2-yl)-L-alanine	ISOX	
(2S)-2-Amino-5-oxohexanoic acid	5-OXO	
(2S)-2-Amino-6-oxoheptanoic acid	6-OXO	
		Synthesized (Department of Organic Chemistry)

3.2. Methods

3.2.1. Bioinformatical analysis

Genes encoding *C. albicans* Met2p, Met15p, and Str2p were retrieved from the *Candida* Genome Database (Skrzypek et al., 2017). The nucleotide and amino acid sequences were analyzed with the help of available programs that are listed in Tab. 14.

Tab. 14. Programs used in bioinformatical analysis.

Software	Application
BLAST(Altschul et al., 1990)	Multiple sequence alignment
ESPrtr 3.x(Robert and Gouet, 2014)	Rendering of aligned sequence similarities
InterPro Scan(Jones et al., 2014)	Identification of characteristics domains
ProtParam(Gasteiger et al., 2005)	Primary structure analysis
Expasy Translate(Gasteiger et al., 2003)	Primary structure determination

3.2.2. Microorganisms culture conditions

a) Bacterial culture

Bacterial strains were cultured on solid LA and liquid media. Strains were first cultured at 37 °C for 24 h on a solid medium, then transferred to liquid medium. Inoculated liquid cultures were incubated in a laboratory shaker for 24 h at 37 °C, 180 rpm. Solid cultures were stored at 4 °C and used for inoculation of liquid medium.



b) Yeast culture

Yeast strains were cultured on solid and liquid YPG media. Strains were first cultured at 30 °C for 24 h on a solid medium, then transferred to liquid medium. Inoculated liquid cultures were incubated in a laboratory shaker for 24 h at 30 °C, 180 rpm. Solid cultures were stored at 4 °C and used for inoculation of liquid medium.

3.2.3. DNA purification

a) Isolation of plasmid DNA

Isolation of plasmid DNA was conducted with the use of a Plasmid Mini AX kit (A&A Biotechnology).

b) Isolation of genomic DNA

Isolations of genomic DNA were conducted with the use of a Genomic Mini AX Yeast kit (A&A Biotechnology).

c) Gel-out

Genomic DNA was subjected to gel electrophoresis in 0.7% agarose gel, 80 V cm⁻¹ (3.2.4). Next, a band of the correct size was cut from the gel. Isolation of the DNA from the gel fragment was performed using GenElute™ Gel Extraction Kit (Sigma-Aldrich).

3.2.4. Agarose electrophoresis

The electrophoresis of DNA was carried in 0.7-1% agarose gel and electrophoresis buffer 1xTAE for 80V cm⁻¹. The results of the analysis were documented with the help of the Gel Doc XR+ Gel Documentation System (BioRad).

Solutions: Agarose gel: 1% agarose gel: 0.5 g agarose; 50 mL TAE x1; 4 µL ethidium bromide aqueous solution 10 mg mL⁻¹ (Sigma). Electrophoresis Buffer: TAE50: 2 M Tris-HCl pH 7.5; 0.5 M EDTA; H₂O.

3.2.5. Amplification of MET2, MET15 and STR2 genes

Amplification of genes was carried out on the *C. albicans* SC5314 matrix with the use of polymerase chain reaction (PCR). Primers were designed with Vector NTI software and sequences retrieved from the Candida Genome Database (Skrzypek et al., 2017) according to instructions given by pET101/D-TOPO (Invitrogen) or pLATE (Thermo Scientific) vectors manufacturers. A list of primers used for PCR amplification is given in Tab. 10. Amplification of genes was performed according to the protocol described below. A reaction mixture for PCR was set up according to the recipe given in Tab. 15.

Tab. 15. Reaction mixture components for the PCR reaction

Component	Volume [μL]
Phusion High-Fidelity PCR Master Mix with HF Buffer (Thermo Scientific)	5.00
Starter forward	1.25
Starter reverse	1.25
Matrix 1:10	1.00
H ₂ O	1.50

Reaction mixtures for *STR2*, *STR2CH*, and *STR2NH* require the addition of 3% DMSO.

PCR was conducted in the temperature gradient of starters annealing. The temperature-time profile of the reaction is given in Tab. 16.

Tab. 16. The temperature-time profile of the PCR reaction.

Initial denaturation	98°C	10 s	} 30 cycles
Denaturation	98°C	1 s	
Starter annealing	X °C	5 s	
Elongation	72°C	30 s	
Elongation	72°C	60 s	
Cooldown	4°C	∞	

X -temperature selected for each gene individually: *MET2* 58°C; *MET2CH* 60°C; *MET2NH* 68°C; *MET15*, *MET15CH* 60°C; *MET15NH* 56°C; *STR2* 65°C; *STR2CH*, *STR2NH* 55°C.

The correctness of PCR products was checked by agarose gel electrophoresis (3.2.4). Obtained PCR products were next purified with GeneJET Gel Extraction and DNA Cleanup Micro Kit (Thermo Scientific) according to the given protocol.

3.2.6. Cloning of PCR product to pET101/D-TOPO or pLATE vectors

a) Cloning to pET101/D-TOPO™ vector

The cloning reaction mixture (Tab. 17) was prepared with the use of Champion™ pET101 Directional TOPO™ Expression Kit (Invitrogen) and incubated for 30 minutes at room temperature. The mixture was next subjected to the transformation of *E. coli* One Shot™ TOP10 (Invitrogen) competent cells according to procedure (3.2.7). Obtained plasmids were verified by nucleotide sequencing.

Tab. 17. Components of the pET101/D-TOPO vector cloning mixture.

Component	Volume [μL]
PCR product	2.5
Salt Solution	1.0
H ₂ O	2.0
Vector pET101/D-TOPO	0.5

b) Cloning to pLATE vectors

PCR products were cloned into pLATE11, pLATE52, and pLATE31 vectors, respectively for the native, NH-his-tagged, and CH-his-tagged variants, using a Thermo Scientific aLICator™ LIC Cloning and Expression System (Thermo Scientific). Cloning of pLATE vectors (LIC cloning) was performed according to the instructions given by the manufacturer. In the first step, obtained PCR products were mixed with 5xLIC buffer and T4 DNA Polymerase to generate the necessary 5' and 3' overhangs. Components of the LIC mixture are given in Tab. 18.

Tab. 18. Components of the pLATE vectors LIC cloning mixture.

Component	Volume [μL]
PCR product	3.0
5x LIC buffer	2.0
H ₂ O	4.0
T4 DNA Polymerase, (1u μL^{-1})	1.0

The mixture was then incubated at room temperature for 5 minutes, followed by the addition of 0.6 μL 0.5 M EDTA which stopped the reaction. In the next step, the annealing reaction was set according to Tab. 19.

Tab. 19. Components of the annealing reaction.

Component	Volume [μL]
PCR product treated with T4 DNA Polymerase (from step 1)	10.0
pLATE, LIC- ready vector (60 ng, 0.02 pmol DNA)	1.0

pLATE LIC-ready vectors: pLATE11 used for CaMet15p and CaStr2p; pLATE31 used for CaMet15CHp and CaStr2CHp; pLATE52 used for CaMet15NHp and CaStr2NHp.

The annealing mixture was incubated at room temperature for 5 minutes after which it was ready for transformation to *E. coli* TOP10F' competent cells according to procedure (2.2.7). Obtained plasmids were verified by nucleotide sequencing. The mixture was next subjected to the transformation of *E. coli* One Shot™ TOP10 (Invitrogen) competent cells according to procedure (2.2.7). Obtained plasmids were verified by nucleotide sequencing.

3.2.7. Transformation to *E. coli* competent cells

For transformation, 3 μL of cloning mixture (3.2.6), 1 μL of plasmid, or 25 μL of ligation mixture was added to *E. coli* competent cells and incubated for 30 minutes on ice (2 hours for the ligation mixture). The cells were next heat-shocked at 42 °C for 30 s and then put on ice for 2 minutes. In the next step, 250 μL of S.O.C medium (Invitrogen) or LB medium was added to the mixture and incubated for 1 h at 37 °C, 180 rpm. After incubation, the cells were spread on a solid LA pLATE supplemented with ampicillin (3.1.4). PLATEs were incubated for 24 h at 37 °C, and stored at 4 °C.

3.2.8. Restriction digest analysis

Digestion of plasmids with restriction enzymes was performed by obtaining the reaction mixture according to the table below. Used restriction enzymes are given in Tab. 11.

Tab. 20. Restriction digest reaction mixture components.

Component	Volume [μL]
Buffer Green fast Digest x10 (Thermo Scientific)	2.0
DNA	10.0
Restriction enzyme 1	0.5
Restriction enzyme 2	0.5
H ₂ O	7.0

The reaction mixture was incubated for 30 minutes at 37 °C. After incubation 0.1% (per volume) of SDS was added to the reaction mixture and incubated at 65 °C for 10 minutes followed by cooling on ice and centrifugation for 30 s 13 000 rpm. Products of digestion analysis were subjected to agarose gel electrophoresis (3.2.4).

3.2.9. Mutagenesis

Direct mutagenesis was carried out in the case of the plasmids containing the *MET2* gene, since this gene contains a CTG codon at a position +490 to +493 that is translated differently in bacteria and yeast cells; in *C. albicans* it encodes for L-serine, whereas in *E. coli* cells it is read as L-leucine (White et al., 1995). For the mutagenesis reaction, constructed pET101/D-TOPO + *MET2*, pET101/D-TOPO + *MET2CH*, and pET101/D-TOPO + *MET2NH* plasmids were used to insert mutation resulting in a change of the CTG to TCG nucleotide triplet encoding L-serine in *E. coli* cells. To conduct a mutation, a PCR reaction was performed using designed mutagenesis starters listed in Tab. 10, which poses phosphorylated 5' termini, enabling further ligation of obtained products. The mutagenesis reaction mixture was prepared according to the Tab. 21.

Tab. 21. Mutagenesis reaction mixture components.

Component	Volume [μL]
Phusion High-Fidelity PCR Master Mix with HF Buffer (Thermo Scientific)	25.00
Starter forward	6.25
Starter reverse	6.25
DNA matrix 1:10	1.00
H ₂ O	11.50

The reaction mixture was subjected to PCR with a temperature gradient. The profile of the PCR reaction is given in the Tab. 22.

Tab. 22. Mutagenesis PCR temperature gradient profile.

Initial denaturation	98 °C	10 s	} 30 cycles
Denaturation	98 °C	1 s	
Starter annealing	59 °C	5 s	
Elongation	72 °C	320 s	
Elongation	72 °C	60 s	
Cooldown	4 °C	∞	

Obtained PCR products were digested with the *DpnI* restriction enzyme at 37 °C for 30 minutes. The components of the mixture are given in Tab. 23.

Tab. 23. *DpnI* restriction enzyme digestion reaction mixture components.

Component	Volume [μL]
Buffer fast digest (x10) (Thermo Scientific)	5.0
<i>DpnI</i> Fast Digest (Thermo Scientific)	1.0
PCR product	40.0
H ₂ O	4.0

To identify plasmids with inserted mutations, gel electrophoresis was carried out in 0.7% gel (3.2.10). Gel fragments containing bands of the required size were cut out (undigested: 7000 bp). Afterward, the gel-out procedure was carried out 3.2.3. Isolated DNA was suspended in 50 μL water and added to the ligation mixture, according to the Tab. 24.

Tab. 24. Ligation mixture components.

Component	Volume [μL]
T4 DNA Ligase Buffer (10X) (Thermo Scientific)	19.5
DNA	5.0
T4 DNA Ligase (5U μL ⁻¹) (Thermo Scientific)	0.5

Ligation was carried out for 30 minutes at 22 °C. Obtained plasmids were later used for the transformation of *E. coli* TOP10F' competent cells according to the 3.2.7 procedure.

3.2.10. Polyacrylamide SDS-PAGE electrophoresis

Polyacrylamide SDS-PAGE electrophoresis was conducted according to the Laemmli method (Laemmli, 1970). Samples were loaded on the gel (5% stacking gel and 10% resolving gel) and electrophoresis was run at 180 V for 60 minutes in Tris-glycine (pH 8.3) running buffer. The resolving gel was stained in Coomassie Blue R-2500 solution for 15 minutes, followed by destaining for protein bands observation.

Solutions: Gel preparation buffers: A: acrylamide/Bis-acrylamide, 30% solution (Sigma-Aldrich); B: 2 M Tris-HCL pH 8.8, 4 mL SDS 10%; C: 1 M Tris-HCL pH 6.8, 4 mL SDS 10%; Ammonium persulfate 1% (per gel volume); TEMED 0.05 % (per gel volume) (Sigma-Aldrich). Running buffer: 25 mM Tris pH 8.3; 0.2 mM glycine; 0.1% SDS. Staining buffer: 112.5 mL methanol; 25 mL glacial acetic acid; 112.5 mL H₂O; 0.25 g Coomassie Blue R-2500 (Sigma-Aldrich). Destaining buffer: 20 mL methanol; 160 mL H₂O; 20 mL glacial acetic acid. 4x Sample loading buffer: 0.25 M TRIS-HCL pH 6.8, 30% (v/v) glycerol, 0.5 M DTT; 8% (m/m) SDS, 3.5 mM bromophenol blue (Sigma-Aldrich).

3.2.11. Western Blot analysis

Three layers of Whatman® qualitative filter paper (Sigma-Aldrich) was soaked in transfer buffer and placed at the anode of the apparatus. A nitrocellulose membrane was placed on top followed by gel after SDS-PAGE electrophoresis and another 3 layers of soaked Whatman® qualitative filter paper. The apparatus was closed with the cathode. Transfer of proteins from the gel to the nitrocellulose membrane was carried out for 1 hour at 40 mA. Afterward, the nitrocellulose membrane with transferred proteins was placed in a 5% solution of skim milk in a wash buffer and left overnight at 4 °C. The membrane was washed 3 times with a 1:10 wash buffer (rocking for 30 minutes) and then transferred to an antibodies solution and rocked for 1 hour. The membrane was again washed 3 times with 1:10 wash buffer (rocking for 60 minutes). The straining of bands containing 6xHisTags was made with 1 mL of 3,3',5,5'-tetramethylbenzidine (TMB) Liquid Substrate System for Membranes (Sigma-Aldrich).

Solutions: Transfer buffer: 25 mM Tris-HCL pH 8.3, 20% (v/v) methanol, 192 mM glycine; Wash buffer: 10 mM Tris-HCL pH 8.0, 30 mM NaCl; Antibody solution: 10 mM Tris-HCL pH 8.0; 30 mM NaCl; 1% (v/v) BSA; 0.05% (v/v) Tween20; 50 µL antibodies; 3, 3', 5, 5' – tetramethylbenzidine (Sigma-Aldrich). Antibodies: antyHis6 1:3000 [(Monoclonal Anti-polyhistidine-Peroxidase antibody A7 058-1VL(Sigma-Aldrich))]

3.2.12. Preparation of *E. coli* competent cells

To prepare TOP10F' competent cells 5 mL of LB medium supplemented with antibiotic (3.1.4) was inoculated with *E. coli* competent strains and incubated overnight at 37 °C, 180 rpm. 3 mL of overnight inoculum was added to 150 mL LB medium supplemented with antibiotics and incubated at 37 °C, 180 rpm until reaching cell optical density (OD₆₀₀) equal to 0.4. Cells were then placed on ice for 30 minutes followed by centrifugation at 4 °C for 10 minutes at 4 000 rpm. The formed cell pellet was suspended in 25 mL of cold CC buffer, incubated on ice for 30 minutes, and again centrifuged at 4 °C for 10 minutes at 4.000 rpm. Cell pellet was suspended in 5 mL of CC buffer, the solution was transferred into 100 µl aliquots and stored at -80 °C for later use.

Solutions: CC buffer: 2.5 M CaCl₂; 0.5 M PIPES pH 7.0; 15% (v/v) glycerol.

3.2.13. Optimization of overproduction of recombinant proteins in the Tabor-Studier system

For overproduction of recombinant proteins, 20 mL (or 5 mL for the screening experiments) of LB medium supplemented with ampicillin (100 µg mL⁻¹) was inoculated with the expression strain containing the gene encoding the protein. The cells were incubated overnight at 37 °C, 180 rpm. 10 mL of overnight inoculum was added to 800 mL (100 mL for the screening experiments) of LB medium supplemented with ampicillin (100 µg mL⁻¹) and optionally ethanol, glycerol, or sorbitol (3.1.4), and incubated at 37 °C, 180 rpm up to OD₆₀₀ reaching an appropriate value in the range of 0.5 – 1.

After reaching the optimal optical density, an inductor isopropyl- β -D-thiogalactoside (IPTG) was added up to the final concentration in the range of 0.05 - 2 mM and incubated at 37 °C, 30 °C or 15 °C for 6 h, 18 h and 24 h, respectively. After incubation, 1 mL of cell culture was used for polyacrylamide SDS-PAGE electrophoresis (3.2.10), while the remaining rest of the cell culture was transferred to 200 mL centrifuge tubes and centrifuged for 20 minutes at 4 000 rpm in 4 °C. The obtained cell pellet was stored for later use at -20 °C.

3.2.14. Preparation of cell-free extract

To prepare the cell-free extract (CFE), the cell pellet obtained after the expression of the protein (3.2.13) was suspended in 10 mL of optimal buffer for each protein supplemented with complete™ Protease Inhibitor Cocktail (CO-RO Roche). The mixture was sonicated on ice (30% amplitude vibration) 3 times for 30 seconds and then centrifuged for 20 min, 10 000 rpm at 4 °C.

Solutions: Optimal buffer for proteins: CaMet2NHp and CaMet2CHp: 20 mM sodium phosphate pH 8.0, 5 mM imidazole, 500 mM NaCl, 1 mM Tween20; CaMet2p: 20 mM sodium phosphate pH 7.0, 10 mM EDTA, 10 mM DTT; CaMet15NHp and CaMet15CHp: 20 mM Tris pH 8.0, 5 mM imidazole, 500 mM NaCl, 1 mM Tween20, 1 mM DTT; CaStr2NHp and CaStr2CHp: 20 mM Tris pH 8.0, 5 mM imidazole, 500 mM NaCl, 1 mM Tween20, 10% (v/v) glycerol, 1 mM DTT, 0.02 mM PLP.

3.2.15. Purification of recombinant oligoHis-tagged proteins using metal-affinity chromatography

Purification of recombinant proteins was performed with ÄKTA pure™ 25 Purification System (Cytiva). To purify recombinant His-tagged proteins, a cell-free extract protein solution was loaded onto a 5 mL HisTrap™ Fast Flow (Cytiva) column equilibrated with W5 buffer optimal for the given protein. After loading the column was washed with W5 buffer. Elution of proteins was carried out in a linear gradient with rising imidazole concentration from 0% to 100% W500 buffer (optimal for given protein) in 10 – 20 column volumes (CV). Linear flow rates from 0.5 mL min⁻¹ to 3 mL min⁻¹. Obtained fractions were subjected to SDS-PAGE gel electrophoresis (3.2.10).

Solutions: Optimal W5 buffers for proteins: CaMet2NHp and CaMet2CHp: 20 mM sodium phosphate pH 8.0, 5 mM imidazole, 500 mM NaCl, 1 mM Tween20; CaMet15NHp and CaMet15CHp: 20 mM Tris pH 8.0, 5 mM imidazole, 500 mM NaCl, 1 mM Tween20; CaStr2NHp and CaStr2CHp: 20 mM Tris pH 8.0, 5 mM imidazole, 500 mM NaCl, 1 mM Tween20, 10% (v/v) glycerol. Optimal W500 buffers for proteins: CaMet2NHp and CaMet2CHp: 20 mM sodium phosphate pH 8.0, 500 mM imidazole, 500 mM NaCl, 1 mM Tween20; CaMet15NHp and CaMet15CHp: 20 mM Tris pH 8.0, 500 mM imidazole, 500 mM NaCl, 1 mM Tween20; CaStr2NHp and CaStr2CHp: 20 mM Tris pH 8.0, 5 mM imidazole, 500 mM NaCl, 1 mM Tween20, 10% (v/v) glycerol.

3.2.16. Purification of native proteins using anion exchange chromatography

The obtained cell-free extract (3.2.14) was mixed with streptomycin sulfate of a final concentration of 1.1% to precipitate DNA. Solid streptomycin sulfate was added for 20 minutes to the cell extract placed in the ice bath and then stirred for 10 more

minutes. The mixture was centrifuged for 20 minutes at 12.000 rpm at 4 °C. To the obtained supernatant, saturated ammonium sulfate solution was added to the final concentration of 36.2%. The mixture was mixed in an ice bath for 20 minutes and then centrifuged for 20 minutes at 12 000 rpm at 4 °C. During this step, the protein mixture was initially purified, proteins dissolved in the supernatant were discarded, while the precipitate containing target proteins was dissolved in a buffer containing 40 mM NaCl and 10mM MgCl₂. Again, the mixture was centrifuged for 20 minutes at 12 000 rpm at 4 °C. To dispose of the excess salt in the mixture, a buffer was exchanged for buffer A according to procedure 3.2.21. Finally, 10 mL of the obtained protein solution was loaded on the Resource™ Q column (Cytiva). The elution of the proteins was carried out in a rising concentration of NaCl up to 1 M concentration in a phosphate buffer of pH 7 (Buffer B), in 10 column volumes. 2 mL fractions were collected and examined with the help of SDS-PAGE electrophoresis 3.2.10.

Solutions: Buffer A: 20 mM sodium phosphate buffer pH 7; Buffer B: 20 mM sodium phosphate buffer pH 7, 1 M NaCl.

3.2.17. Purification of proteins using size exclusion chromatography

Size exclusion chromatography (SEC) was performed as the last polishing step of protein purification to achieve a greater purity rate of protein samples for the determination of protein molecular mass and oligomeric structure (3.2.22) of crystallization trials (3.2.23). Collected target protein fractions after purification on His-Trap or Resource Q column were concentrated to a final volume of 5 mL and loaded onto Superdex™ 200 16/600 GL column (Cytiva). The isocratic elution was carried out in SEC1 buffer in 2 column volumes. 0.5 mL fractions were collected and examined with the help of SDS-PAGE and NATIVE-PAGE electrophoresis.

Solutions: SEC1 for proteins (crystallization trials): CaMet2NHp: 50 mM HEPES pH 7.5, 500 mM NaCl, 20 mM imidazole; CaMet15NHp: 25 mM Tris-HCl pH 8.0, 0.3M NaCl; CaStr2NHp: 25 mM Tris-HCl pH 8.0, 300 mM NaCl.

3.2.18. Determination of protein concentration using the Bradford method

To measure the concentration of proteins in the samples, a Bradford protein assay was used (Bradford, 1976). 1 mL of Bradford reagent (Sigma-Aldrich) was added to a 100 µL solution containing the purified protein. After 5 minutes, the absorbance was measured at 595 nm. A standard calibration curve was made using bovine serum albumin (Sigma-Aldrich) protein in a respectful manner (0 - 100 µg mL⁻¹).

To determine the concentration of the purified protein, the absorbance of the analyzed protein solution was compared to the standard values.

3.2.19. Densitometric analysis

The gel containing separated proteins after SDS-PAGE electrophoresis was used for the densitometric analysis of target proteins. Densitometric analysis was performed with the Gel analyzer software (Lazar Jr. and Lazar Sr.).

3.2.20. Concentration of recombinant protein solutions

Purified recombinant protein samples were concentrated with the help of Amicon™ Ultra Centrifugal Filter Units (Merck Millipore). The protein solution was placed into the filter and centrifuged at 4.500 rpm at 4 °C for 5 to 15 minutes, the cycle was repeated until the desired protein concentration.

3.2.21. Protein solution buffer exchange

The protein solution buffer was exchanged using a 5 mL HiTrap™ Desalting column (Cytiva) according to a given protocol.

3.2.22. Determination of the protein molecular mass and oligomeric structures

a) Bioinformatical analysis

With the help of the ProtParam (Gasteiger et al., 2005) and Translate (Gasteiger et al., 2003) programs (3.1.2) and the nucleotide sequence of the analyzed proteins retrieved from *Candida* genome database (Skrzypek et al., 2017) the amino acid sequence and the putative molecular weight of the recombinant proteins was determined.

b) SDS-PAGE electrophoresis

Separation of the mass marker (3.1.3) in SDS-PAGE electrophoresis was used to create a standard curve enabling calculation of the molecular mass of the analyzed proteins according to the equation:

$$\log MW = a \times R_f + b$$

where: *MW* - molecular weight of analyzed protein [kDa]

a, b - coefficients of the standard curve equation

R_f - relative migration distance of proteins

c) Size exclusion chromatography

To determine the molecular mass or oligomeric structure, size exclusion chromatography (SEC) of reference proteins was conducted using Superdex™ 200 10/300 Increase column (Cytiva) and Gel Filtration Markers Kit for Protein Molecular Weights 29.000-700.000 Da (Sigma-Aldrich) according to a given protocol. A standard curve showing the relationship between molecular mass and retention volume of eluted protein was made. A standard curve was used to determine the molecular mass of target proteins.

Collected fractions containing target protein after SEC with Superdex™ 200 16/600 GL column (Cytiva) were concentrated to 1 mg mL⁻¹ and 0.5 mL of obtained protein solution was loaded onto Superdex™ 200 10/300 Increase column (Cytiva). The isocratic elution was carried out in an SEC2 elution buffer in 2 column volumes. 0.5 mL fractions were collected and examined with the help of SDS-PAGE and NATIVE-PAGE electrophoresis.

Solutions: SEC2 for proteins: CaMet2p and CaMet2NHp: 50 mM sodium phosphate buffer pH 7.0, 150 mM NaCl; CaMet15p and CaMet15NHp: 25 mM Tris-HCl pH 8.0, 140 mM NaCl; CaStr2p and CaStr2NHp: 25 mM Tris-HCl pH 8.0, 300 mM NaCl.

d) Native PAGE electrophoresis

Native PAGE electrophoresis was carried out with the help of the NativePAGE™ Novex Bis-Tris Gel System kit (Invitrogen) according to the given manual. Staining of gels was made with NativePAGE™ Novex Bis-Tris Gel System kit (Invitrogen). Separation of the mass marker (3.1.3) in NATIVE-PAGE electrophoresis was used to create a standard curve enabling calculation of the molecular mass of the analyzed proteins according to the equation:

$$\log MW = a \times R_f + b$$

where: *MW* - molecular weight of analyzed protein [kDa]

a, b - coefficients of the standard curve equation

R_f - relative migration distance of proteins

3.2.23. Crystallization trials

Protein crystallization trials require a high purity rate (>95%) sample that was obtained with two-step chromatography. In the first step protein was purified with metal-affinity chromatography (3.2.15) followed by gel filtration (3.2.17) on Superdex™ 200 16/600 GL column (Cytiva). Collected fractions were next concentrated according to 3.2.20, to a concentration ranging from 2 mg mL⁻¹ to 20 mg mL⁻¹ and filtered with Ultrafree™-MC Centrifugal Filter Unit (Merck Millipore) for the removal of residual particles or precipitates. Screening of crystallization conditions was performed with a sitting-drop method on 96-well crystallization pLATEs with several crystallization screening kits from Hampton and Molecular dimensions. Additional optimization of obtained best-hit conditions was performed with a hanging-drop method on 24-well pLATEs.

Crystal formation was observed with polarised light microscopy. Several crystallization trials were performed in cooperation with the Institute of Bioorganic Chemistry of the Polish Academy of Sciences in Poznań using a Crystal Gryphon protein crystallography dispenser (Art Robbins Instruments).

3.2.24. Activity assay

a) Homoserine O-acetyltransferase (Met2p) activity assay

Homoserine O-acetyltransferase activity assay was conducted using the 5,5'-dithio-bis-(2-nitrobenzoic acid) (DTNB) method (Foyn et al., 2017). 300 nM of purified enzyme was added to L-homoserine, acetyl-CoA, Met2p buffer, and water up to a final volume of 50 μ L. The reaction was started by the addition of enzyme and carried out for 5 minutes at 37 °C then stopped by the addition of 100 μ L stop buffer. Next, 20 μ L of DTNB buffer was added, and 150 μ L of the mixture was transferred to a 96-well microplate and measured spectrophotometrically at 412 nm. Negative controls omitted the addition of the enzyme to the reaction mixture, enzyme was added only after stopping the reaction (after the stop buffer).

Solutions: Met2p buffer: 100 mM sodium phosphate buffer pH 8.0, 200 mM NaCl, 2 mM EDTA; Stop buffer: 3.2 M guanidinium-HCl, 100 mM sodium phosphate dibasic pH 6.8; DTNB Buffer: 100 mM sodium phosphate dibasic pH 6.8, 10 mM EDTA, 10 mg mL⁻¹ DTNB.

b) O-acetyl-L-homoserine sulphydrylase (Met15p) activity assay

O-Acetyl-L-homoserine sulphydrylase (Met15p) activity assay was performed with a HPLC-DAD-MS method with a pre-column derivatization of produced L-homocysteine (L-HCT) with a DTNB. The reaction mixture contained 10 nM of CaMet15p enzyme, Met15p buffer, O-acetyl-L-homoserine (L-OAH), Na₂S, 0.2 mM PLP, and water up to a final volume of 50 μ L. The reaction was started by the addition of enzyme and carried out for 10 minutes at 37 °C then stopped by the addition of 100 μ L of stop buffer. Next, 20 μ L of DTNB buffer was added, and 10 μ L of a sample was injected into the HPLC-DAD Zorbax Eclipse C18 column (5 μ m, 250 mm x 4.6 mm (Agilent)). A produced L-HCT-TNB complex was detected at λ =330 nm.

Solutions: Met15p buffer: 25 mM Tris-HCl pH 8.0; 100 mM NaCl pH 8.0, 200 mM NaCl, 2 mM EDTA; Stop buffer: 3.2 M guanidinium-HCl, 100 mM sodium phosphate dibasic pH 6.8; DTNB Buffer: 100 mM sodium phosphate dibasic pH 6.8, 10 mM EDTA, 10 mg mL⁻¹ DTNB; HPLC-DAD-MES mobile phase (A: 45% formic acid B: acetonitrile). The HPLC-DAD-MS analysis was performed using equipment funded by the Foster Foundation.

c) Cystathionine- γ -synthase (Str2p) activity assay

Cystathionine- γ -synthase (Str2p) activity assay was performed with a HPLC-DAD-MS method with a pre-column derivatization of a substrate L-cysteine (L-Cys) with a DTNB. The activity of an enzyme was measured by the decrease in substrate concentration during the reaction which corresponds to the equal amount of product L-cystathionine (L-CTT) produced. The reaction mixture contained 100 nM of CaStr2p enzyme, Str2p buffer, L-Cys, L-OAH, 0.2 mM PLP, and water up to a final volume of 50 μ L. The reaction was started by the addition of enzyme and carried out for 10 minutes at 37 °C then stopped by the addition of 100 μ L of stop buffer.

Next, 20 μL of DTNB buffer was added, and 10 μL of a sample was injected into the HPLC-DAD Zorbax Eclipse C18 column (5 μm , 250 mm x 4.6 mm (Agilent)). The amount of L-CYS-TNB complex was detected at $\lambda=330$ nm.

Solutions: Str2p buffer: 25 mM Tris-HCl pH 7.5, 100 mM NaCl pH 8.0, 200 mM NaCl, 2 mM EDTA; Stop buffer: 3.2 M guanidinium-HCl, 100 mM sodium phosphate dibasic pH 6.8; DTNB Buffer: 100 mM sodium phosphate dibasic pH 6.8, 10 mM EDTA, 10 mg mL^{-1} DTNB; HPLC-DAD-MES mobile phase (A: 45% formic acid B: acetonitrile). The HPLC-DAD-MS analysis was performed using equipment funded by the Foster Foundation.

3.2.25. Determination of enzyme inhibitory potential

Several commercial compounds and synthesized by the Department of Pharmaceutical Technology and Biochemistry (3.1.10) were tested for inhibitory potential on CaMet2NHp, CaStr2NHp, and CaMet15NHp. Inhibitory assay for individual protein was performed according to 3.2.24 with the addition of inhibitor compounds ranging from 1 to 15 mM concentration to the reaction mixture.

3.2.26. Determination of the Minimum Inhibitory Concentration

Most potent enzyme inhibitors were tested for the determination of minimum inhibitory concentration (MIC) inhibiting the growth of fungal strains (3.1.5) in various media (3.1.4). Determined MIC_{90} and MIC_{50} were defined as the lowest concentration of analyzed compound inhibiting cell growth by at least 90% or 50%, respectively. The assay was performed according to the modified M27-A3 protocol specified by the CLSI (Wayne, 2008). Fungal strains were first cultivated on YPG agar plates for 24 h at 30 °C. Overnight cultures were then suspended in phosphate-buffered saline to reach optical density of 0.1 measured at 660 nm. Serial dilutions of selected inhibitors and standard antibiotics (amphotericin B and fluconazole) (Sigma-Aldrich) were inoculated with culture of tested fungal strains obtaining a final concentration of 10^4 colony forming units (CFU) per mL medium in 96-well plates. Tested mediums include the RPMI-1640 medium and YNB medium with ammonium sulfate (AS) or sodium glutamate (SG) as a nitrogen source, and with or without supplementation of 10 mM L-methionine. The rate of fungal growth was assessed after 24 hours of incubation of plates at 30 °C, by the measurement of the optical density at 600 nm with a microplate reader (TECAN Spark 10M).

3.2.27. Checkerboard dilution test for determination of drug interaction

Potential interactions (synergistic, antagonistic, or indifferent) between selected compounds were determined using the checkerboard dilution test on 96-well plates in a YNB medium supplemented with sodium glutamate as a sole nitrogen source (3.1.4). The serially diluted first tested compound was spread along the y-axis of the plate and the serially diluted second tested compound was spread along the x-axis obtaining final concentrations ranging from at least 2 times MIC to 1/32 MIC.



Plates were next inoculated with tested fungal strains resulting in a final concentration of 10^4 colony forming units per mL medium. Cell growth was measured after 24-hour incubation of plates at 37 °C via the measurement of the optical density at 600 nm with a microplate reader (TECAN Spark 10M). The fractional inhibitory concentration index (FICI) was calculated according to the below formula:

$$FICI = \frac{MIC_{90} \text{ of A in combination}}{MIC_{90} \text{ of A alone}} + \frac{MIC_{90} \text{ of B in combination}}{MIC_{90} \text{ of B alone}}$$

MIC₉₀ - lowest concentration of tested compound inhibiting growth by at least 90%.

Obtained FICIs were assigned to the synergistic, antagonistic, or indifferent effect according to the instruction given by Odds (Odds, 2003): FICI ≤ 0.5 (synergy), FICI > 0.5 to ≤ 4 (indifferent effect), and FICI > 4 (antagonism). Obtained drug interactions were visualized and analyzed with the help of Combenefit software (version 2.021, Cancer Research UK Cambridge Institute (Di Veroli et al., 2016)) using the Loewe additivity model.

4. RESULTS AND DISCUSSION

4.1. Identification of genes encoding putative CaMet2p, CaMet15p and CaStr2p

4.1.1. Nucleotide sequences

In the initial step of the research, I conducted a bioinformatical analysis of the *Candida albicans* genome and identified *MET2* (orf19.2618), *MET15* (orf19.5645) and *STR2* (orf19.1033) genes that show high nucleotide sequence similarity to genes from other microorganism sources encoding enzymes exhibiting activities of the homoserine *O*-acetyltransferase EC 2.3.1.31 (Met2p), *O*-acetyl-L-homoserine sulphydrylase EC 2.5.1.49 (Met15p) and cystathionine- γ -synthase EC 2.5.1.48 (Str2p) enzymes, respectively.

Analysis of the nucleotide sequences enabled the design of specific starters for the amplification of the *MET2*, *MET15*, and *STR2* genes, and identification of possible codons requiring mutations. In several yeast species including *C. albicans* an universal leucine coding codon, CTG was found to be associated with translational deviations leading to recognition of the CTG codon by the serine-charged tRNAs and coding for serine as an effect. (White et al., 1995). The purpose of this project required heterologous expression of *C. albicans MET2*, *MET15*, and *STR2* genes in *Escherichia coli* host cells forcing an exchange of any CTG codons to those coding for leucine. I identified a CTG codon in the *MET2* nucleotide sequence at the position +490 to +493 (Tab. 25).

Tab. 25. *Candida albicans MET2* nucleotide sequence with CTG codon highlighted in red.

<i>MET2</i> Nucleotide sequence
ATGACATACAAAGACGTGACAGAAGAACAGTTACAAACTAATCCATATGTCAAGCTTGTGCCGGGACA AACCATAGTTGAAATCCCTGAATACACACTAGAGTGTGGCGAAACATTACATAATTTTCTGTGCTT ACAAGACCTGGGGTAAAGTTGAATGAGACCGCTGATAATGCATTAGTGATATGCCATGCTTTGAGTGGG TCTTCTGATGTTGACGATTGGTGGGGAGAATTACTTGGAACTGATAGAGCTTTTGATCCTTCTCGATA TCTCATCATTTGTATAAATTTTCTTGGATCGCCTTATGGGTCTTGTTCACCAGTCACAATTGACAAGA GCACTGGTAAGCCTTATGGTCCCTCATTTCCATTAGTAACATTCAAGGATGATGTTGGAATACAGAGA TTGATATTAGATTCATTGAATGTCAAACGGTTAGCTGCCGTTGTTGGAGGATCCATGGGGGGAATGTT GGCATTAGAATACCTGCAATTTACAACAATACCGGATACGTACAGAAAGTAGTCGCATTGGCTACTG CAGCCAGAACTTCAGCATGGTGCATATCTTGGAAATGAGACACAAAGACAATGCATTTTTCAGTGATCCT TTTTACGATGACGGGTATTACTACGAAACTGGAATAAACCTGATTCTGGATTAAGTGCCGCAAGAAT GGCCGCTTTGCTTACTTATCGTTCTAGAAACTCGTTTCAAAGTAGATTTGGCAGAAAATTGGGTCCGA GATCTCCTAATGATGGTGGTGGCAGTCCTAGAACCAACACGAAGAGCATTCTTTATTGCATAATGAC GGGTCAAAGCTTATCAATGGAGCTCCTGTAAATGAAAAATATCCACCAACTTATTTCTCGGCACAGTC ATATATGCGTTATAACGGTTCCAAATTTATCAATAGATTTGATGCAAATTGTTACATAGCCATTAGTC GAAAATTGGATACTAATGATCTTTCTCGAGGTCGAGTCAATGCACCCAACGACGCTAATGGTGATCCA TTGGTTCATGTTTTAAAGGATCTTTCAACCCCTACGTTGGTCATAGGAATTGAATCAGATCATCTTTT TACAATAACTGAACAAAACCTTTTGGCTGACAATATCCAAATGCTATATTTGAGACGTTGGACAGTG AAGAGGGACACGATGCATTTTGTAGAGTTTGGAAAATAAATAGTTTTCATCACTAGTTTTTTGAAT AATTGA

4.1.3. Amino acid sequences

Using *MET2*, *MET15*, and *STR2* nucleotide sequences retrieved from the *Candida* Genome Database (Skrzypek et al., 2017), ExPASy Translate Tool, and ProtParam Tool (Gasteiger et al., 2005), I obtained amino acid sequences and theoretical parameters characterizing putative *C. albicans* Met2p, Met15p and Str2p enzymes (Tab. 26). Established primary structures of researched proteins were used for the assessment of the probable molecular mass of the enzyme, which is crucial for the designation of protein overproduction.

Tab. 26. Theoretical parameters characterizing CaMet2p, CaMet15p, and CaStr2p enzymes obtained via *Candida* Genome Database (Skrzypek et al., 2017), ExPASy Translate Tool and ProtParam Tool (Gasteiger et al., 2005).

Protein	Assembly	Nucleotide sequence length	Amino acid sequence length	Isoelectric point	Molecular weight [kDa]
CaMet2p	orf19.2618	1230	409	5.20	45.4
CaMet15p	orf19.5645	1323	440	5.59	48.0
CaStr2p	orf19.1033	1788	595	5.66	67.2

To assess the amino acid sequence similarity of analyzed proteins to the amino acid sequences of homologous proteins I performed sequence alignment using BLAST and Esript program (Altschul et al., 1990; Robert and Gouet, 2014) (Tab. 27).

Tab. 27. Amino acid sequences identities between putative CaMet2p, CaMet15p, and CaStr2p and their identified counterparts from other sources.

Protein	CaMet2p		
Source	<i>Haemophilus influenzae</i>	<i>Staphylococcus aureus</i>	<i>Mycobacterium smegmatis</i>
PDB code	2B61	4QLO	6IOG
Identity [%]	34	28	32
Protein	CaMet15p		
Source	<i>Saccharomyces cerevisiae</i>	<i>Wolinella succinogenes</i>	<i>Mycobacterium marinum</i>
PDB code	8OVH	3R16	4KAM
Identity [%]	71	50	46
Protein	CaStr2p		
Source	<i>Escherichia coli</i>	<i>Helicobacter pylori</i>	<i>Nicotiana tabacum</i>
PDB code	1CS1	4L00	1I41
Identity [%]	27	29	25

All putative *C. albicans* Met2p, Met15p, and Str2p are homologous to their counterparts in other microorganisms with solved crystal structures (identity $\geq 25\%$) (Fig. S4 - Fig. S6). CaMet15p exhibits the highest sequence similarity, especially to the sequence encoding enzyme retrieved from *S. cerevisiae*. Both Met2p and Str2p sequence alignments resulted in an identity score of $\sim 30\%$ rate, which is relatively low, most probably because the only solved crystal structures of homologous enzymes are of bacterial or plant origin. However, amino acid sequence alignment of putative Met2p

and Str2p enzymes from *C. albicans* and *S. cerevisiae* showed 53% and 48% of sequence identity, respectively (Fig. S4 - Fig. S6).

4.2. Construction of expression systems and isolation of putative CaMet2p, CaMet15p and CaStr2p

The characterization of *C. albicans* putative Met2p, Met15p, and Str2p was one of the main goals of my project. To do this, I constructed plasmids containing genes encoding CaMet2p, CaMet15p and CaStr2p in appropriate systems and performed their heterologous expression in *E. coli* cells, followed by purification of proteins.

4.2.1. Construction of expression plasmids encoding CaMet2p, CaMet15p and CaStr2p

In the first step, I isolated genomic DNA from *C. albicans* SC5314 cells that was later used for the PCR reaction with specially designed starters (3.1.6). I designed starters in a way that enables amplification of the gene encoding given enzyme in 3 different forms. So finally, for each enzyme, 3 different plasmids were constructed: the one that contained the original gene encoding the wild-type protein, and two others with an added 6xHisTag domain, either to the C-end or the N-end of the polypeptide chain. Obtained PCR products were next cloned into pET101/D-TOPO vectors (Invitrogen). As mentioned above (4.1.1), because of differences in translation mechanisms between *E. coli* and *C. albicans* cells, plasmids containing the *MET2* gene required additional mutation of CTG (encoding L-leucine in *E. coli*) codon at a position of 490 to 493 to TCG (encoding serine in *E. coli*).

Because of the low protein production (CaMet15p) and incorrect folding of the protein (CaStr2p), I repeated the procedure with cloning into pLATE11, pLATE31, and pLATE52 vectors (Thermo Scientific). Final obtained plasmids were named as follows: pET101/D-TOPO + *MET2*, pET101/D-TOPO + *MET2CH*, pET101/D-TOPO + *MET2NH*, pLATE11 + *MET15*, pLATE31 + *MET15CH*, pLATE52 + *MET15NH*, pLATE11 + *STR2*, pLATE31 + *STR2CH*, pLATE52 + *STR2NH*. Plasmids maps are shown as supplementary figures (Fig. S1 - Fig. S3). I verified the correctness of plasmids by conducting a restriction digest analysis (Fig. 11) performed according to section 3.2.8. This was followed by DNA sequencing performed by an external service.



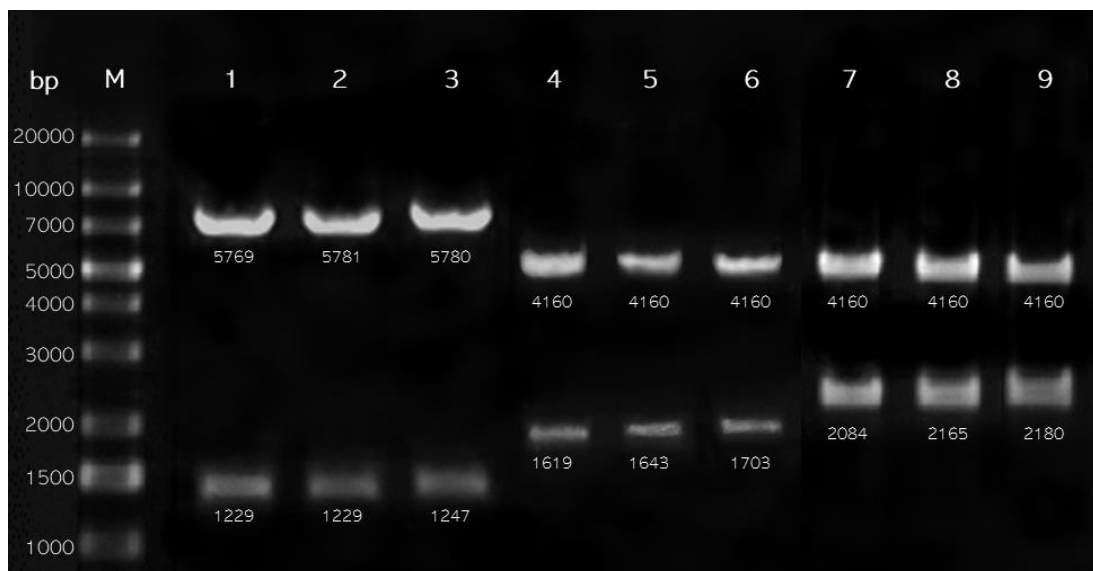


Fig. 11. Result of plasmids restriction digest analysis. Electrophoresis 80 V cm^{-1} , 1% agarose gel. Midori Green is used as a DNA stain. M, marker (Gene Ruler 1 kb PLUS DNA ladder (Invitrogen)); **1.** pET101/D-TOPO + *MET2*; **2.** pET101/D-TOPO + *MET2CH*; **3.** pET101/D-TOPO + *MET2NH*; **4.** pLATE11 + *MET15*; **5.** pLATE31 + *MET15CH*; **6.** pLATE52 + *MET15NH*; **7.** pLATE11 + *STR2*; **8.** pLATE31 + *STR2CH*; **9.** pLATE52 + *STR2NH*.

4.2.2. Production of recombinant proteins in *E. coli* host cells

To determine optimal conditions for efficient recombinant protein production in *E. coli* host cells, I performed a series of screening experiments leading to the selection of the most potent expression strain, medium composition as well as induction and production conditions. I tested several *E. coli* expression strains listed in 3.1.5. I performed screening experiments according to the scheme shown in the Fig. 12.



Fig. 12. Schematic representation of screening experiments for determination of optimal conditions to produce recombinant proteins.

I optimized the conditions of protein overproduction by manipulation of various factors such as concentration of inductor IPTG, optical density of cells at the time of induction, as well as temperature and time of cell incubation after induction (Fig. 12). At the same time, I checked how different media influence gene expression; I used LB medium, but also additionally supplemented with glycerol, glucose, ethanol, and sorbitol. It is said that glycerol or glucose supplementation inhibits the induction of lac operon, and gives more control over the expression system, by limiting the possible induction resulting from any possible presence of lactose particles in the medium, this is mostly important while using peptone-based media (Al-Samarrai et al., 2013). Sorbitol increases the osmotic pressure of the medium resulting in the accumulation of osmoprotectants inside the cell and thus stabilizes the native structure of the protein (Blackwell and Horgan, 1991). The exact influence of ethanol is unknown; however, it is known that ethanol influences the fluidity of the cell membrane by changing the composition of membrane lipids and thus influences transport through the membrane (Ingram and Buttke, 1985). Together, these changes can result in a change in DNA replication that can enhance DNA synthesis and at the same time enhance gene amplification and production of proteins (Basu and Poddar, 1994; Chhetri et al., 2015). During optimization experiments I observed that LB medium supplemented with ethanol facilitates the production rate of CaMet15NHp and CaMet15CHp, but not other

enzymes. Also, I did not notice any improvement in protein overproduction when culturing cells in LB medium supplemented with glucose, glycerol or sorbitol. All three versions of the CaMet2p enzyme were overproduced in 6 hours after induction at 37 °C, whereas CaStr2p and CaMet15p recombinant proteins required significantly lower temperature. A more detailed description of the recombinant proteins' overproduction is given below.

I determined the amount of protein produced via SDS-PAGE electrophoresis followed by Western blot in the case of His-tagged proteins. Given below in Fig. 13 are the results of recombinant protein production.

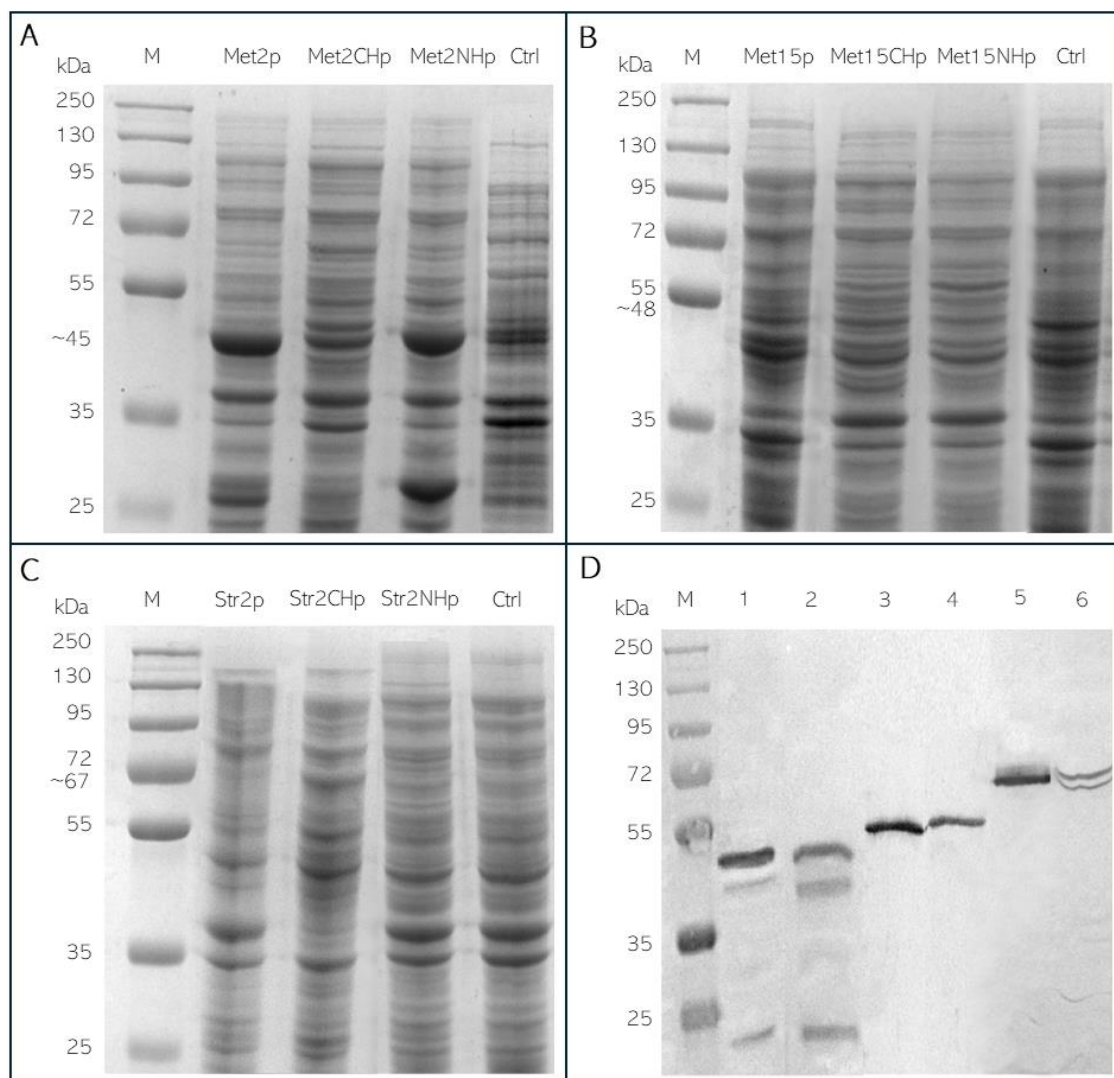


Fig. 13. A – C. Result of the SDS-PAGE analysis of recombinant protein overproduction, electrophoresis 18 V cm⁻¹ 10% gel; M, Marker (Page Ruler™ Plus Prestained Protein Ladder, Thermo Scientific). Ctrl, control (strain lacking expression plasmid). Expected molecular weights of proteins assuming monomeric structure: CaMet2p, CaMet2CHp, and CaMet2NHp 45 kDa; CaMet15p, CaMet15CHp, and CaMet15NHp 48 kDa; CaStr2p, CaStr2CHp and CaStr2NHp 67 kDa; **D.** Result of a Western blot analysis confirming production of His-tagged recombinant proteins. M, Marker (PageRuler™ Plus Prestained Protein Ladder, Thermo Scientific); 1, CaMet2NHp; 2, CaMet2CHp; 3, CaMet15NHp; 4, CaMet15CHp; 5, CaStr2NHp; 6, CaStr2CHp. Sample volumes: 1-2 3 μL; 3-6 20 μL.

I observed the highest level of target protein production in the case of CaMet2p, CaMet2NHp and CaMet2CHp, with contents of 23%, 19%, and 16% of total protein pool, respectively, (Tab. 28). All the above recombinant proteins were produced in *E. coli* strains that are lysogens of bacteriophage DE3 and therefore carry a chromosomal gene copy encoding T7 RNA polymerase under control of the lacUV5 promoter, facilitating high-level expression of target genes (Studier and Moffatt, 1986; Rosenberg et al., 1987; Studier et al., 1990).

The *STR2*-containing plasmids encoding recombinant proteins were initially produced in *E. coli* Rosetta (DE3) pLacI transformed with pET101/D-TOPO vector with relatively good rates of 25%, 21%, and 18% respectively, for CaStr2p, CaStr2NHp, and CaStr2CHp. However, these proteins were incorrectly folded, leading to their production in the form of insoluble aggregates that complicates and prolongs the purification of active enzymes. Similarly, the expression of the *MET15* gene in strains transformed with the pET101/D-TOPO vector resulted in meager protein production rates. Therefore, I took an attempt to reclone the *STR2* and *MET15* genes into other expression vectors in hope of a boost in protein production. I decided to use the pLATE family expression vectors operating in aLICator Ligation Independent Cloning and Expression System. This system is designed for the efficient production of target proteins in concern with tight regulation of gene expression, which enables the expression of proteins that are toxic for the host cells. Production of proteins encoded by the *STR2* gene using pLATE vectors significantly altered the production rate, however, obtained proteins were soluble, thus enabling their purification and activity assessment.

As shown in Fig. 13 C, the protein bands corresponding to putative CaStr2p, CaStr2CHp, and CaStr2NHp are not easily visible on the SDS-PAGE gel. In fact, the production of target proteins could only be confirmed for oligoHis-tagged versions by the Western blot analysis utilizing anti-oligoHis monoclonal antibodies that specifically recognize 6xHisTag domains (3.2.11). I performed optimization of conditions to produce the CaStr2CHp and CaStr2NHp using the immunodetection method as a tool for the determination of protein production rate and assessment of the leading conditions. CaStr2NHp and CaStr2CHp are produced with a 7% and 5% rate in *E. coli* Rosetta (DE3) pLacI and *E. coli* BL21 ER2566, respectively. Similarly to CaStr2p recombinant enzymes, CaMet15p, CaMet15CHp, and CaMet15NHp are produced at an extremely low level that could be determined only for His-tagged proteins with the help of immunodetection of Western blot, resulting in the production rate of 3% and 5% respectively for CaMet15NHp and CaMet15CHp. Without the immunodetection method, target proteins are indistinguishable from the SDS-PAGE gel. The Western blot analysis served also as a tool for the determination of optimal conditions for protein production that led to the selection of *E. coli* ER2655 strain cultured in LB medium at a lowered temperature of 15 °C and 24 h production time. *E. coli* ER2566 is an enhanced BL21 derivative with improved transformation of toxic clones and superior control of basal expression (Zhou et al., 2020). This strain was also found to be effective in the production of recombinant

proteins at lower temperatures (< 20°C) (Cieśliński et al., 2005; Zhou et al., 2023), which was also confirmed in my study results.

I performed optimizations of CaMet15p and CaStr2p native proteins production with not much success. The obtained production rate did not exceed that achieved for the oligoHis-tagged proteins (> 5%). For this reason, I did not take an attempt to purify CaMet15p and CaStr2p as the several-step method of purification of native proteins requires higher yields of protein samples. Given below in Tab. 28 are the optimal conditions for the production of proteins intended for the protein purification step.

Tab. 28. Conditions for recombinant protein production.

Protein	CaMet2p	CaMet2 NHp	CaMet2 CHp	CaMet15 NHp	CaMet15 CHp	CaStr2 NHp	CaStr2 CHp
Expression plasmid	pET101/D-TOPO + MET2	pET101/D-TOPO + MET2NH	pET101/D-TOPO + MET2CH	pLATE52 + MET15NH	pLATE31 + MET15CH	pLATE52 + STR2NH	pLATE31 + STR2CH
Host cell	<i>E. coli</i> One Shot™ BL21 Star™ (DE3)	<i>E. coli</i> Rosetta (DE3) pLysS	<i>E. coli</i> One Shot™ BL21 Star™ (DE3)	<i>E. coli</i> BL21 ER2566	<i>E. coli</i> BL21 ER2566	<i>E. coli</i> Rosetta (DE3) pLacI	<i>E. coli</i> BL21 ER2566
Medium	LB, amp	LB, amp, ch	LB, amp	LB, EtOH, amp	LB EtOH, amp	LB, amp	LB, amp
OD ₆₀₀	0.5	1.0	0.7	1.0	1.0	1.0	0.9
IPTG [mM]	0.05	1.0	0.5	1.0	1.0	1.0	1.0
Production conditions	37 °C, 6 h, 180 rpm	37 °C, 6 h, 180 rpm	37 °C, 6 h, 180 rpm	15 °C, 24 h, 220 rpm	15 °C, 24 h, 220 rpm	15 °C, 24 h, 180 rpm	15 °C, 24 h, 180 rpm
Production rate [%]	23	19	15	3	5	7	5

Solutions: LB medium supplemented with: ampicillin (amp) 100 µg mL⁻¹, chloramphenicol (ch) 34 µg mL⁻¹, ethanol (EtOH) 3%.

Analyzing the data presented in Tab. 28, I made several conclusions regarding optimization of the recombinant protein production:

- The introduction of 6xHisTag domains does not significantly affect the production rate.
- Low production of CaMet15CHp, CaMet15NHp, CaStr2NHp, and CaStr2CHp could result from several reasons, but probably not from the toxicity of cloned genes or their products as the growth of expression strains was comparable with the growth of the wild-type strain. Moreover, supplementation of the expression medium with glucose did not affect the production rate. Glucose addition ensures tighter control of gene expression by inhibition of the *lac* promoter induction caused by residual lactose presence in the medium
- Low production of CaMet15CHp, CaMet15NHp, CaStr2NHp, and CaStr2CHp might be a result of destabilization of produced proteins in host cells since lowering of the production temperature of application of strains lacking extracellular *ompT* or intracellular *lon* proteases increased the production rate.

Despite the low production rate of CaMet15CH, CaMet15NHp, CaStr2NHp, and CaStr2CHp, I decided to optimize the purification procedure of these enzymes versions, but I did not take an attempt to purify the native version especially since I have proved that the addition of 6xHisTag domain to either C- or N-terminus does not influence neither CaMet15p or CaStr2p enzymatic activity (described in detail in section 4.3.3 and 4.3.4). Moreover, purification of the native enzyme requires application of a multistep procedure characterized by a decreased recovery rate, which could significantly lower concentration of proteins in pool, disabling possibility for enzyme characterization analysis experiments.

4.2.3. Purification of recombinant proteins

I purified the 6xHis-tagged recombinant proteins using HisTrap™ Fast Flow columns (Cytiva), which are packed with Ni Sepharose High Performance resin designed for high-resolution purification of oligoHis-tagged proteins by immobilized metal ion affinity chromatography (3.2.15). HisTrap™ columns have a high binding capacity and low nickel ion leakage that ensures reliable capture of a target protein. The elution of proteins takes place in a linear gradient of increasing imidazole concentration, which competes with proteins for interaction with the Sepharose bead. The proteins that are not oligoHis-tagged poorly interact with the resin beads and are eluted at lower imidazole concentrations. This enables obtaining fast protein solutions of high purity. Optimization of the purification method involved the determination of buffer content and pH, a flow rate of protein loading and elution, and the duration of the selected chromatography phase (load, post-loading column wash, linear gradient elution).

Based on the literature data for each protein, initially, I used 20 mM Tris-HCl buffer of pH 7.0 supplemented with 5 mM imidazole as a binding buffer and 500 mM imidazole as an elution buffer, which was later altered depending on the protein needs. 20 mM sodium phosphate buffer of pH 8.0 facilitates CaMet2NHp and CaMet2CHp activity and stability. To obtain a purified protein solution ready for analysis I performed a purification of these two proteins in their optimal buffer. I did not observe a decrease in protein purification rate between the two buffer systems which enabled me to use sodium phosphate buffers for purification without the additional step of buffer exchange after protein elution from the column. CaMet15NHp and CaMet15CHp purification buffer required a slight adjustment of the pH to 8.0, to ensure optimal conditions for the activity, whereas CaStr2NHp and CaStr2CHp additionally required supplementation of 10% (v/v) glycerol to elution support enzyme stability. The addition of glycerol to buffers decreased the resolution of purification which was balanced by a decrease of flow rate from 2 mL min⁻¹ to 1 mL min⁻¹. I have also noticed a significant influence of the flow rate on the effectiveness of CaMet15NHp binding to the column resin; lowering the flow rate to 0.5 mL min⁻¹ during sample loading greatly increased the amount of target protein eluted from the column. Furthermore, a low production rate

of CaMet15NHp and CaMet15CHp by the host cell, imposed loading of 20 mL cell-free extract from 1.6 L harvest, in two steps of 10 mL sample loading with 10 column volumes washed with equilibration buffer in between.

Results of SDA-PAGE and densitometric analyses of protein purification can be seen in Fig. 14-16 and the summarized mass balance is given in Tab 29. Greatest recovery rates can be observed for CaMet15NHp and CaMet15CHp, followed by CaStr2NHp and CaStr2CHp, which might be related to increased loading or decreased flow rate which improve interaction between the protein and the resin promoting stronger binding.

With the help of ion-exchange chromatography on Resource Q™ column I purified wild-type CaMet2p (Fig. 14). Purification of the wild-type protein with ion-exchange chromatography involves more steps and time (section 3.2.16). For the anion exchange chromatography, pH of buffers used for protein purification should be at least 0.5 – 1 pH unit above the protein isoelectric point (pI), which ensures that the protein has a net negative charge and will bind to the positively charged anion exchange resin beads. To purify the CaMet2p, I used 20 mM sodium phosphate buffer of pH 7.0 as a binding buffer and 20 mM sodium phosphate buffer of pH 7.0 supplemented with 1M NaCl as an elution buffer. The speed of protein elution from the column turned out to be a relevant parameter of this approach. By lowering the flow of elution to 0.5 ml min⁻¹ I obtained improved resolution and purification rate of fractions containing CaMet2p protein leading to a protein sample of 44%. Several step procedures for the purification of the native proteins are burdened with decreased recovery rate, which in the case of the CaMet2p equaled 7 % (Tab. 29), however since the concentration of purified protein solution was sufficient for the analysis, there was no significant need for further optimization of the purification procedure.

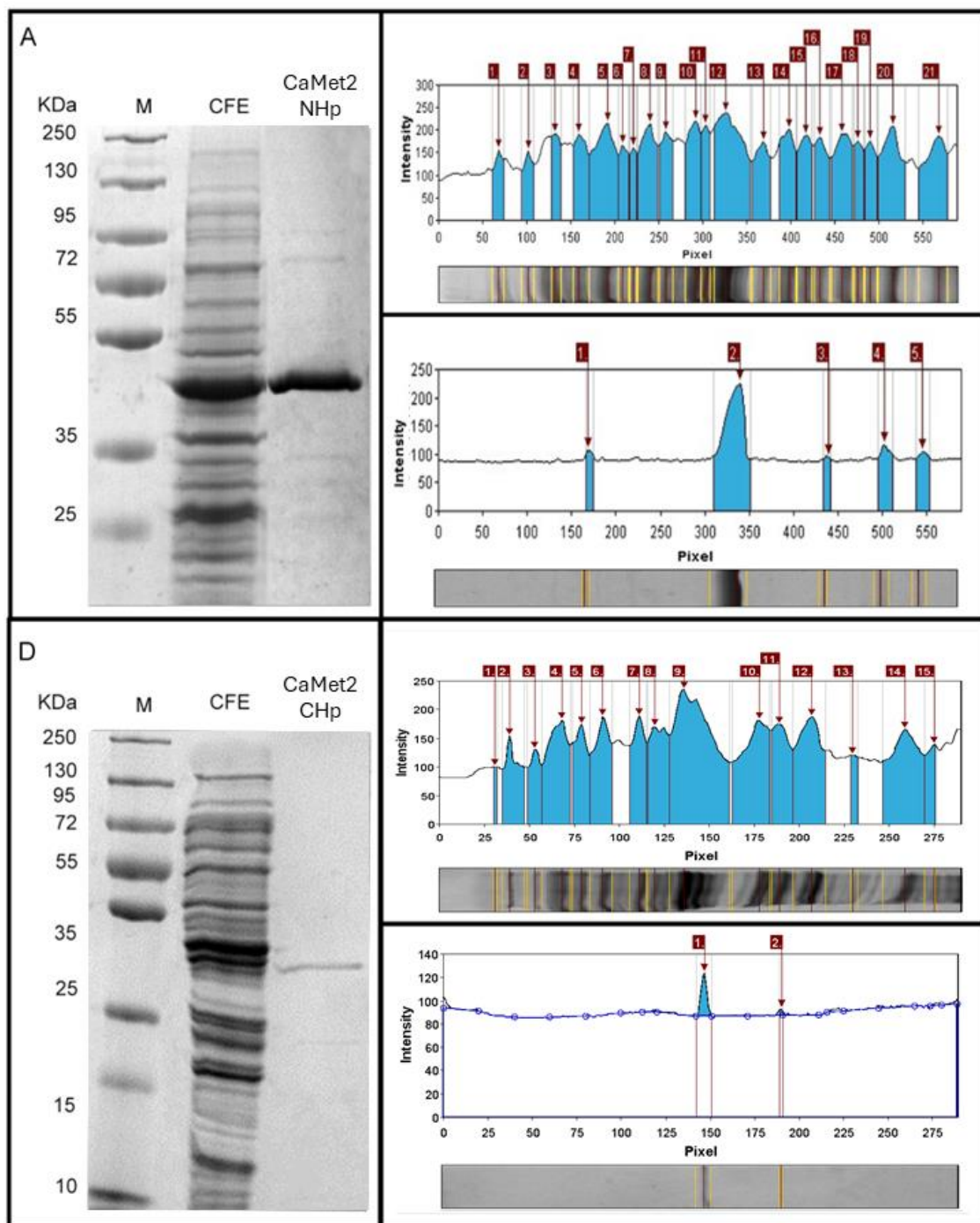


Fig. 14. Purification of CaMet2p, CaMet2NHp, and CaMet2Chp. **1A.** SDS-PAGE electrophoresis of cell-free extract (CFE) from *E. coli* One Shot™ BL21 Star™ (DE3) cells and purified CaMet2p; **1B.** Densitometric analysis of SDS-PAGE result of CFE; **1C.** Densitometric analysis of SDS-PAGE of CaMet2NHp; **2A.** SDS-PAGE electrophoresis of CFE from *E. coli* Rosetta (DE3) pLysS cells (CFE) and purified CaMet15NHp; **2B.** Densitometric analysis of SDS-PAGE of CFE; **2C.** Densitometric analysis of SDS-PAGE of CaMet2NHp; **3A.** SDS-PAGE electrophoresis of CFE from *E. coli* One Shot™ BL21 Star™ (DE3) (CFE) and purified CaMet2Chp; **3B.** Densitometric analysis of SDS-PAGE of CFE; **3C.** Densitometric analysis of SDS-PAGE of CaMet2Chp. Electrophoresis was performed at 18 V cm⁻¹ 10% gel. M, marker Thermo Scientific PageRuler™ Plus Prestained Protein Ladder. Densitometric analysis was performed with Gel Analyzer 19.1 software. Results were partly published (Kuplińska et al., 2022).

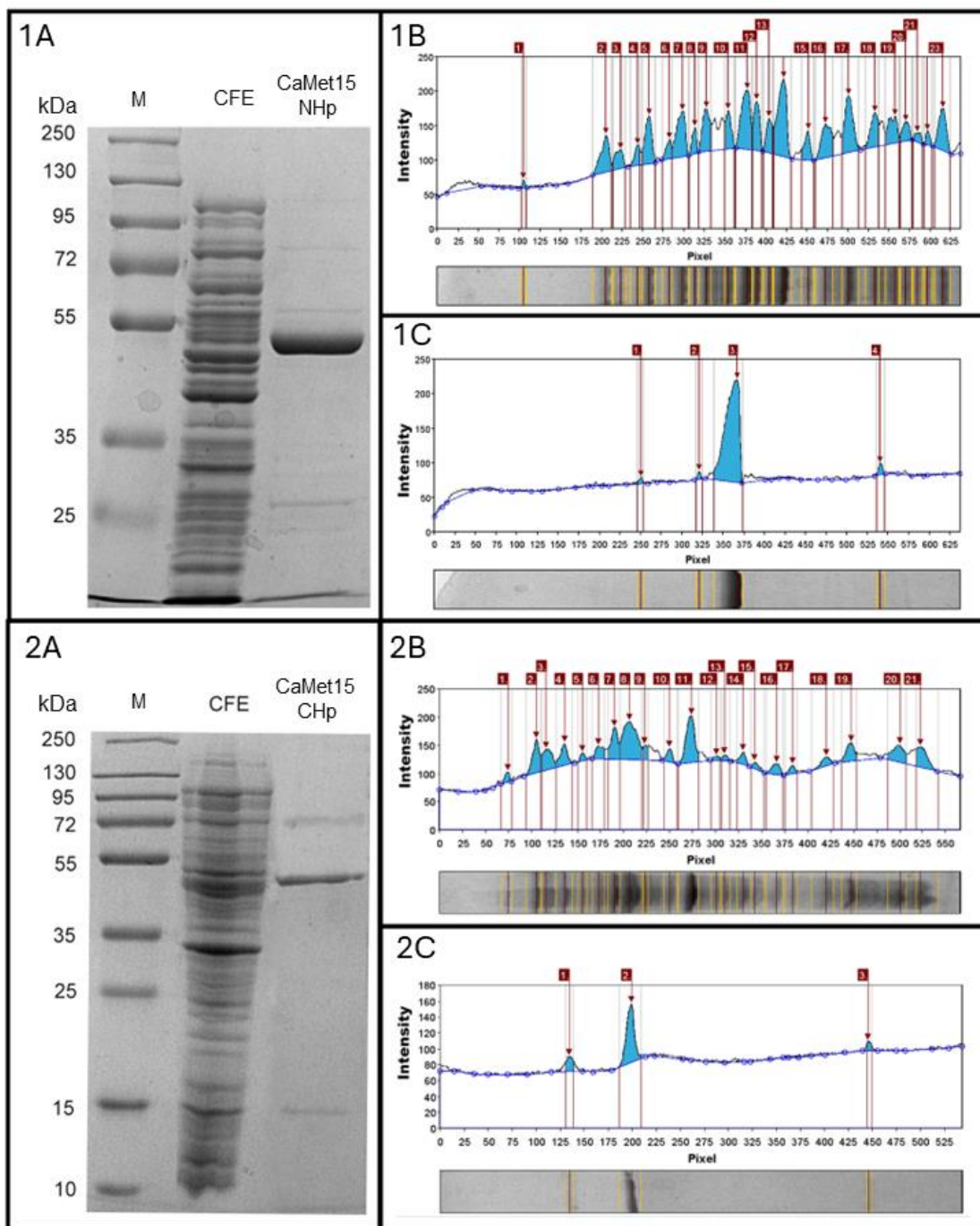


Fig. 15. Purification of CaMet15NHp and CaMet15CHp. **1A.** SDS-PAGE electrophoresis of cell-free extract (CFE) from *E. coli* ER2566 cells and purified CaMet15NHp; **1B.** Densitometric analysis of SDS-PAGE result of CFE; **1C.** Densitometric analysis of SDS-PAGE of CaMet15NHp. **2A.** SDS-PAGE electrophoresis of CFE from *E. coli* ER2566 cells (CFE) and purified CaMet15CHp; **2B.** Densitometric analysis of SDS-PAGE of CFE; **2C.** Densitometric analysis of SDS-PAGE of CaMet15CHp. Electrophoresis was performed at 18 V cm^{-1} 10% gel. M, marker Thermo Scientific PageRuler™ Plus Prestained Protein Ladder (Thermo Scientific). Densitometric analysis was performed with Gel Analyzer 19.1 software.

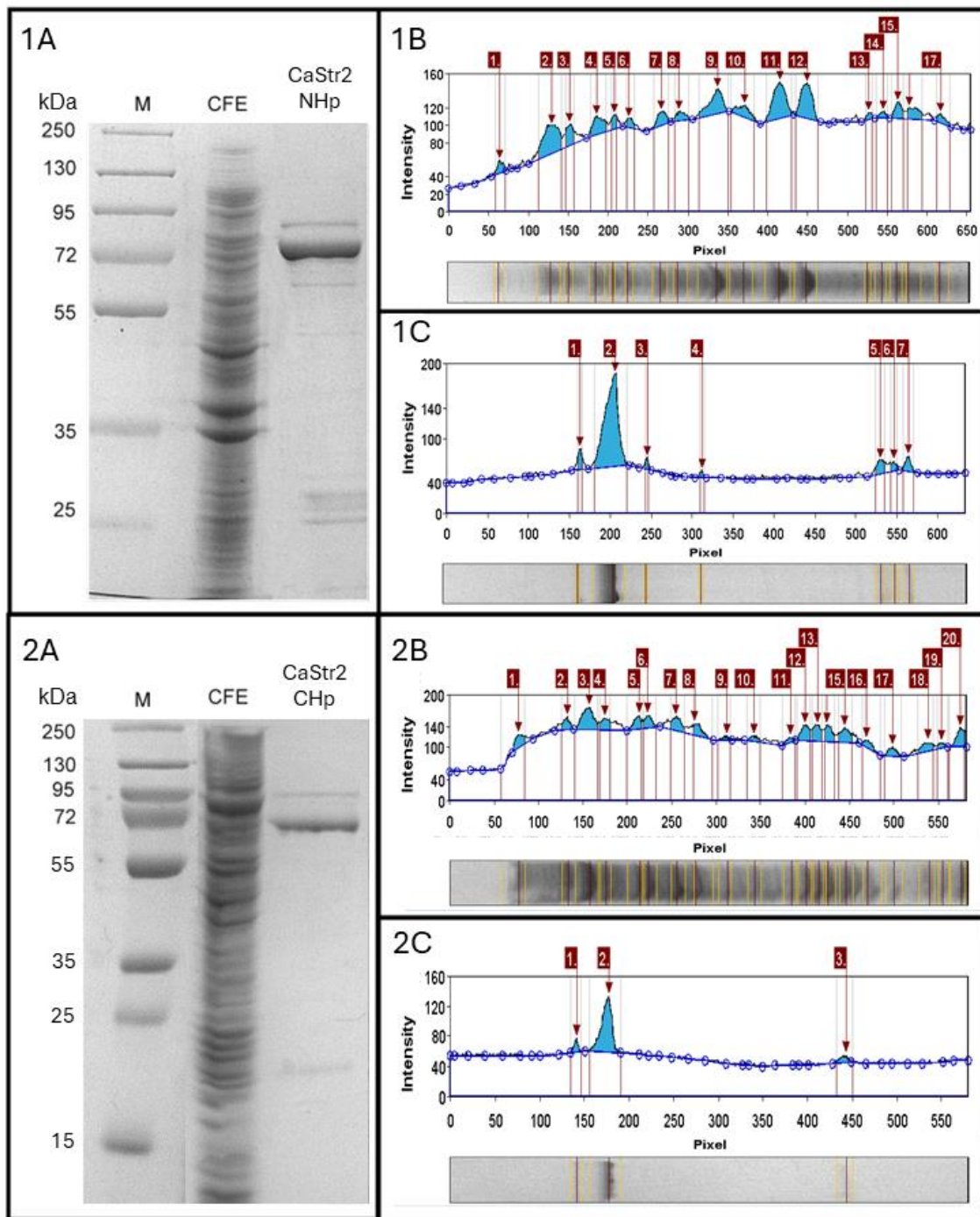


Fig. 16. Purification of CaStr2NHp and CaStr2CHp. **1A.** SDS-PAGE electrophoresis of cell-free extract (CFE) from *E. coli* ER2566 cells and purified CaStr2NHp; **1B.** Densitometric analysis of SDS-PAGE result of CFE; **1C.** Densitometric analysis of SDS-PAGE of CaStr2NHp; **2A.** SDS-PAGE electrophoresis of CFE from *E. coli* Rosetta (DE3) pLacI cells (CFE) and purified CaStr2CHp; **2B.** Densitometric analysis of SDS-PAGE of CFE; **2C.** Densitometric analysis of SDS-PAGE of CaStr2CHp. Electrophoresis was performed at 18 V cm^{-1} 10% gel. M, marker Thermo Scientific PageRuler™ Plus Prestained Protein Ladder (Thermo Scientific). Densitometric analysis was performed with Gel Analyzer 19.1 software.

Tab. 29. Mass balance of purified recombinant proteins. The purity rate was determined using SDS-PAGE analysis of protein samples and Gel Analyzer software.

Mass balance analysis of recombinant proteins							
Name	CaMet2p	CaMet2NHp	CaMet2CHp	CaMet15NHp	CaMet15CHp	CaStr2NHp	CaStr2CHp
Production rate [%]	23	19	15	3	5	7	5
Volume of loaded protein [mL]	10	10	10	20	20	10	10
CFE concentration [mg mL ⁻¹]	7.0	10.2	13.8	18.2	18.6	17.5	13.0
Volume of purified protein [mL]	10	10	10	14	10	14	12
Concentration of eluate pool [mg mL ⁻¹]	0.584	0.337	0.317	0.212	0.204	0.374	0.212
Purity rate [%]	44	86	92	90	93	79	83
Recovery [%]	16	17	15	27	22	43	39

4.3. Characterizations of recombinant CaMet2p, CaMet15p and CaStr2p

4.3.1. Determination of molecular mass and oligomeric structure

I determined the molecular masses of recombinant proteins using various methods (3.2.22): theoretical approach (bioinformatical analysis) and experimental using electrophoresis in both reducing and non-reducing conditions and size exclusion chromatography (SEC). To determine molecular mass from SDS-PAGE and NATIVE-PAGE electrophoresis I used GelAnalyzer software to calculate the retardation factor (R_f) for target proteins and protein molecular mass standards (PageRuler Plus Prestained Protein Ladder (SDS-PAGE) or Native MARK™ Unstained Protein Standard (NATIVE-PAGE) (section 3.1.3) that I used to plot a calibration curve: $\log MW = f(R_f)$. By plugging calculated R_f values of target proteins to obtain a linear equation I determined the log of the target proteins' molecular weight. To determine the molecular weight and oligomeric structure I also used SEC to plot a calibration curve by plotting a log of the molecular weight against the retention volume of standard proteins (Gel Filtration Markers Kit for Protein Molecular Weights (section 2.1.3)).

For CaMet2p, CaMet2CHp, and CaMet2NHp proteins, experimentally determined molecular masses of monomers are comparable to their theoretical molecular weight (Tab. 30). The quaternary structure of CaMet2p native protein assessed with SEC NATIVE-PAGE and SDS-PAGE electrophoresis suggests that CaMet2p forms a monomeric structure. On the other hand, the CaMet2NHp quaternary structure determined by SEC implies the presence of both monomer and dimer which was

confirmed by the NATIVE-PAGE showing a protein band representing a protein of 88 kDa corresponding to homodimer. It is possible that the native CaMet2p and CaMet2NHp enzyme versions are characterized by a heterogenic quaternary structure, however also, it is possible that there is only a single native form, but the enzyme dissociates or aggregates during migration through the column. In reference to study results characterizing Met2p protein structures, the bacterial enzyme forms a homodimer structure (Mirza et al., 2005; Sagong et al., 2019). There are no fungal Met2p structures for comparison. Based on the obtained results, it is not clear whether the *C. albicans* Met2p exists as a homodimer or a monomer. To clear these doubts, other techniques like mass spectrometry or X-ray crystallography should be applied. I made several attempts to obtain a crystal of CaMet2NHp, however with no success (section 4.5).

Tab. 30. Determination of molecular mass and oligomeric structure of CaMet2p and CaMet2NHp. Results were partially published (Kuplińska et al., 2022).

CaMet2p		
Method	Calculated mass [kDa]	Oligomeric structure
Bioinformatical analysis	45.4	Monomer
SDS-PAGE electrophoresis	45.0 ± 1.8	Monomer
SEC	42.0 ± 1.2	Monomer
Native-PAGE electrophoresis	38.7 ± 0.8	Monomer

Result of the CaMet2p SDS-PAGE and NATIVE-PAGE electrophoresis analysis						
SDS-PAGE			NATIVE-PAGE			
kDa	M	SEC	AEX	kDa	M	SEC
250				720		
130				480		
95				242		
72				146		
55				66		
35				20		
25						

M, marker;
AEX, CaMet2p purified with anion exchange chromatography;
SEC, CaMet2p purified with size exclusion chromatography.

Marker SDS-PAGE:
Thermo Scientific PageRuler™ Plus Prestained Protein Ladder (Thermo Scientific).

Marker NATIVE-PAGE:
NativePAGE™ Thermo Scientific Native MARK™ Unstained Protein Standard (Thermo Scientific).

CaMet2NHp		
Method	Calculated mass [kDa]	Oligomeric structure
Bioinformatical analysis	46.2	Monomer
SDS-PAGE electrophoresis	46.6 ± 1.5	Monomer
SEC	41.4 ± 2.3	Monomer
	85.1 ± 8.5	Dimer
Native-PAGE electrophoresis	88.0 ± 4.3	Dimer

Result of the CaMet2NHp SDS-PAGE and NATIVE-PAGE electrophoresis							
SDS-PAGE			NATIVE-PAGE			M, marker; AC, CaMet2NHp purified with affinity chromatography; SEC, CaMet2NHp purified with size exclusion chromatography	
kDa	M	AC	SEC	kDa	M		SEC
250				720			Marker SDS-PAGE: Thermo Scientific PageRuler™ Plus Prestained Protein Ladder (Thermo Scientific).
130				480			
95				242			Marker NATIVE-PAGE: NativePAGE™ Thermo Scientific Native MARK™ Unstained Protein Standard (Thermo Scientific).
72				146			
55				66			
35				20			
25							
15							

Experimentally determined single subunit molecular masses of CaMet15NHp and CaMet15CHp are both around 48 kDa and are comparable to the molecular weight calculated by the bioinformatical analysis (Tab. 31). The molecular mass estimated by SEC and NATIVE-PAGE was 188.4 kDa and 203.3 kDa, respectively. The quaternary structure of CaMet15NHp deduced due to comparison of data obtained by native PAGE and SEC analysis with that from SDS-PAGE is supposed to be homotetrameric. In the NATIVE-PAGE electrophoretogram, a faint band of 106.7 kDa can also be seen, which may be related to the dynamic dissociation or aggregation during protein migration. The obtained result is consistent with postulated quaternary structures of CaMet15p from *S. cerevisiae* (Mohr et al., 2023) (PDB code: 8OVH), *Wolinella succinogenes* (Tran et al., 2011) (PDB code: 3RI6) and *Mycobacterium marinum* (Baugh et al., 2015) (PDB code: 4KAM).

Tab. 31. Determination of molecular mass and oligomeric structure of CaMet15NHp.

CaMet15NHp		
Method	Calculated mass [kDa]	Oligomeric structure
Bioinformatical analysis	48.8	Monomer
SDS-PAGE electrophoresis	48.2 ± 1.7	Monomer
SEC	188.4 ± 4.6	Tetramer
Native-PAGE electrophoresis	203.3 ± 1.3	Tetramer
	106.7 ± 0.9	Dimer
Result of the CaMet15NHp SDS-PAGE and NATIVE-PAGE electrophoresis analysis		
		<p>M, marker; AC, CaMet15NHp purified with affinity chromatography; SEC, CaMet15NHp purified with size exclusion chromatography</p> <p>Marker SDS-PAGE: Thermo Scientific PageRuler™ Plus Prestained Protein Ladder (Thermo Scientific).</p> <p>Marker NATIVE-PAGE: NativePAGE™ Thermo Scientific Native MARK™ Unstained Protein Standard (Thermo Scientific).</p>

For CaStr2NHp and CaStr2CHp, molecular masses of monomers determined by SDS-PAGE are comparable to the theoretical molecular mass (Tab. 32). Molecular masses resulting from native Page and SEC analyses suggest monomeric and homodimeric structure of native proteins, The CaStr2p enzymes with solved crystal structures are characterized as homotetramers: *E. coli* (Clausen et al., 1998) (PDB code: 1CS1), *H. pylori* (Kramer et al., 2020) (PDB code: 4L00) and *N. tabacum* (Stegborn et al., 2001) (PDB code: 1I41). Results obtained in my analysis seem inconsistent with the above data, however the fungal version of Str2p may exist in different quaternary structures than its bacterial counterparts. In order to determine the oligomeric structure of the *C. albicans* Str2p with greater certainty, mass spectrometry or X-ray crystallography should be applied.



Tab. 32. Determination of molecular mass and oligomeric structure of CaStr2NHp.

CaStr2NHp		
Method	Calculated mass [kDa]	Quaternary structure
Bioinformatical analysis	67.2	Monomer
SDS-PAGE electrophoresis	67.5 ± 1.4	Monomer
SEC	74.3 ± 1.0	Monomer
	103.9 ± 7.5	Dimer
Native-PAGE electrophoresis	67.0 ± 4.3	Monomer
	131.0 ± 6.1	Dimer
Result of the CaStr2NHp SDS-PAGE and NATIVE-PAGE electrophoresis analysis		
		<p>M, marker; AC, CaStr2NHp purified with affinity chromatography; SEC, CaStr2NHp purified with size exclusion chromatography</p> <p>Marker SDS-PAGE: Thermo Scientific PageRuler™ Plus Prestained Protein Ladder (Thermo Scientific).</p> <p>Marker NATIVE-PAGE: NativePAGE™ Thermo Scientific Native MARK™ Unstained Protein Standard (Thermo Scientific).</p>

4.3.2. Enzymatic activity of CaMet2p, CaMet2Nhp, and CaMet2Chp.

To prove that the purified CaMet2p exhibits the activity of homoserine O-acetyltransferase, I conducted a series of experiments according to procedure 3.2.24a). A purified enzyme should be able to catalyze the reaction that utilizes L-homoserine (L-HOM) and acetyl-Coenzyme A (AcCoA), to produce O-acetyl-L-homoserine (L-OAH). I assessed CaMet2p enzymatic activity by measurement of the amount of produced Coenzyme A (CoA) throughout its reaction, using the 5,5-dithio-bis-(2-nitrobenzoic acid) (DTNB) reagent and a spectrophotometric detection (Fig. 17).

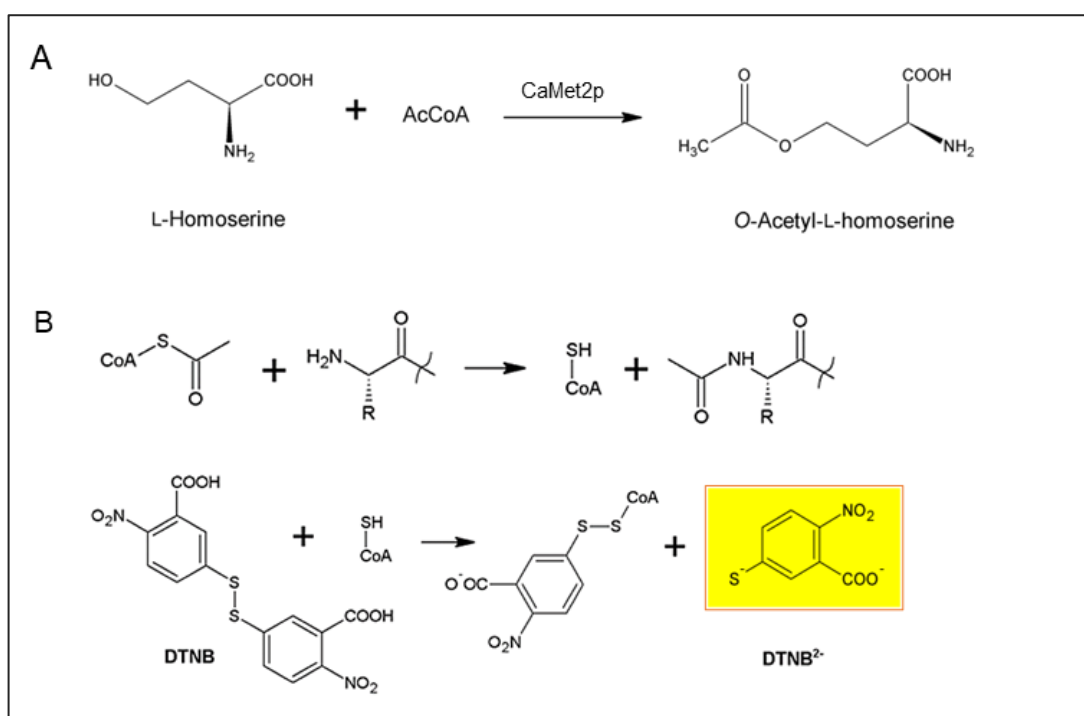


Fig. 17. A. The reaction catalyzed by CaMet2p; B. Detection of produced AcCoA with DTNB reagent.

All three purified enzyme versions: wild-type, and two 6xHisTagged, displayed catalytic activity that utilizes L-HOM and AcCoA as substrates to produce L-OAH. Moreover, activities of the CaMet2p and CaMet2Nhp were at a similar level and significantly higher than the activity of the CaMet2Chp (Fig. 18 D), which might be due to the effect of the 6xHisTag domain added to the C-terminus of the protein. The presence of the 6xHisTag domain could disturb the substrates' access to the active center, as one of the catalytic residues of CaMet2p, namely His389 is located near the C-terminus of the polypeptide chain of this protein.

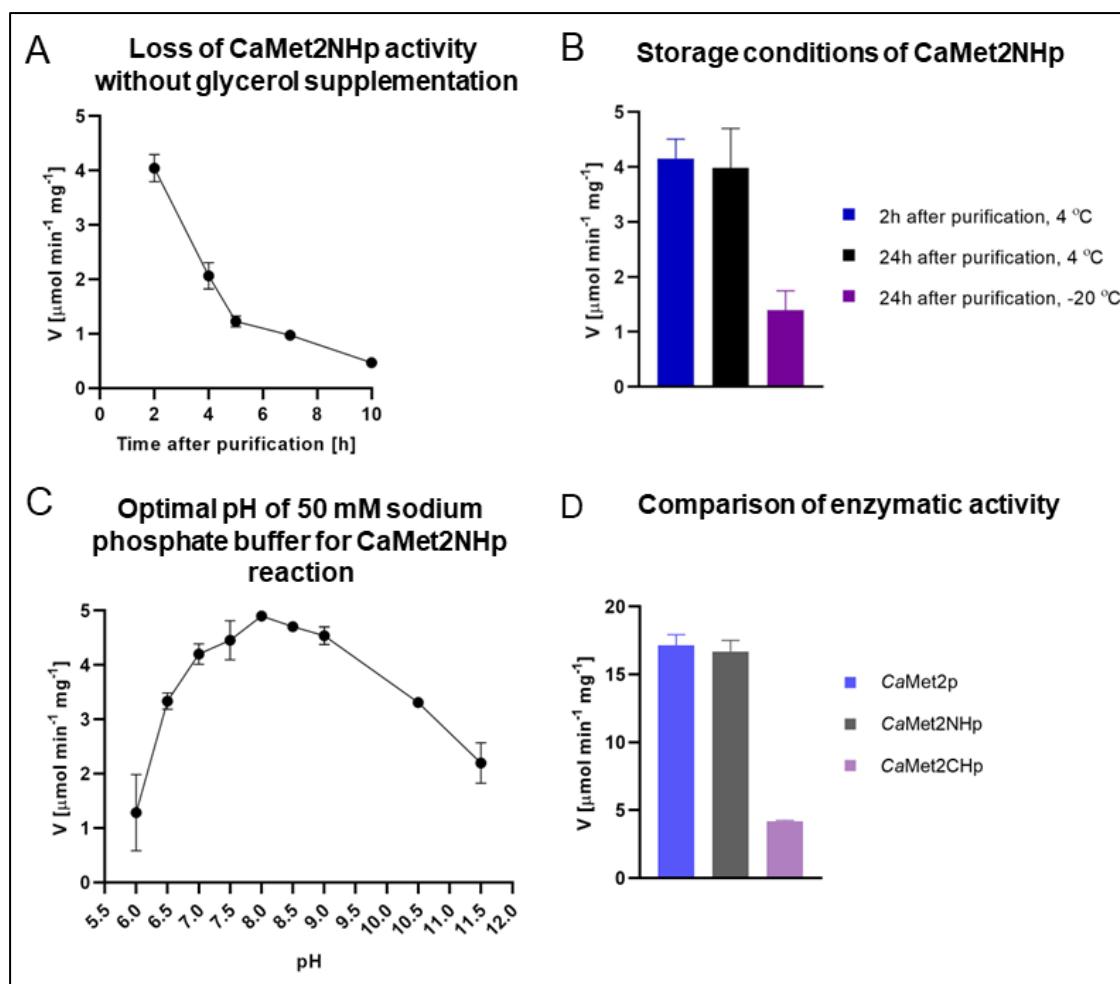


Fig. 18. Characterization of *s* CaMet2p, CaMet2NHp, and CaMet2CHp; **A.** Loss of activity of CaMet2NHp when stored in buffer not supplemented with glycerol; **B.** Determination of optimal storage conditions of CaMet2NHp; **C.** Effect of 50 mM phosphate buffer pH on CaMet2NHp activity; **D.** Comparison of CaMet2p, CaMet2NHp and CaMet2CHp activities. Results published by (Kuplińska et al., 2022).

Moreover, as can be seen in Fig. 18 A, purified CaMet2NHp dramatically lost its activity during the first 4 hours after isolation. The activity of the wild-type CaMet2p also decreased in time but approximately 30% within 24 hours. According to my study results, the activity of both CaMet2p and CaMet2NHp displayed greatest stability in 20 mM sodium phosphate buffer (pH 8.0) (Fig. 18 C) supplemented with 20% v/v glycerol and stored in 4 °C where it remained stable up to 2 weeks (Fig. 18 B). Consistent with obtained result, the highest enzymatic activity was also observed at pH 7.5 and 8.0 in the case of Met2p from *S. cerevisiae* and *S. pombe*, respectively (Yamagata, 1987b; Nazi and Wright, 2005). Additionally, a similar loss of activity was also reported for Met2p enzymes from *Bacillus polymyxa*, *Brevibacterium flavum*, and *Saccharomyces cerevisiae*, which could be rescued by the presence of a polyhydroxy agent (Wyman and Paulus, 1975; Shio and Ozaki, 1981; Yamagata, 1987b).

To characterize the enzymatic activity of *C. albicans* homoserine-*O*-acetyltransferase, I determined the kinetic parameters leading to the establishment of the Michaelis constant (K_M), the maximum velocity (V_{MAX}), the turnover

number (k_{CAT}) and kinetic efficiency ($k_{\text{CAT}}/K_{\text{M}}$). The kinetic parameters were assessed via measurement of the initial velocity of the reaction dependent on varying concentrations of one of the substrates and fixed concentration of the other (Fig. 19). I determined the kinetic parameters for both CaMet2p and CaMet2NHp versions of *C. albicans* enzyme. The obtained values are similar for both versions and almost identical in the case of the k_{CAT} parameter (Tab. 33). Comparable kinetic parameters indicate that the catalytic properties of the enzyme are not affected by the 6xHisTag domain at the N-terminus. However, the determination of K_{M} values gave quite ambiguous results comparing to ones determined for Met2p from *S. cerevisiae* and *S. pombe*, which are equal respectively to, 0.0270 mM and 0.0209 mM for AcCoA and 1.00 mM and 1.09 mM for L-HOM (Yamagata, 1987a; Nazi and Wright, 2005). On the other hand, the k_{CAT} parameters established for *S. pombe* enzyme, equivalent to 9.3 s^{-1} and 9.6 s^{-1} for AcCoA and L-HOM respectively, are comparable to k_{CAT} values determined in this work. Moreover, K_{M} values for both L-HOM and AcCoA in the case of bacterial *Mycobacterium smegmatis* derived Met2p enzyme were shown to be 0.06 mM and 0.158 mM, respectively (Sagong et al., 2019), which are closer to values obtained by me for the *C. albicans* enzyme. The above results indicate that the kinetic parameters of the same enzyme can differ greatly across species, even in the case of these belonging to the same family.

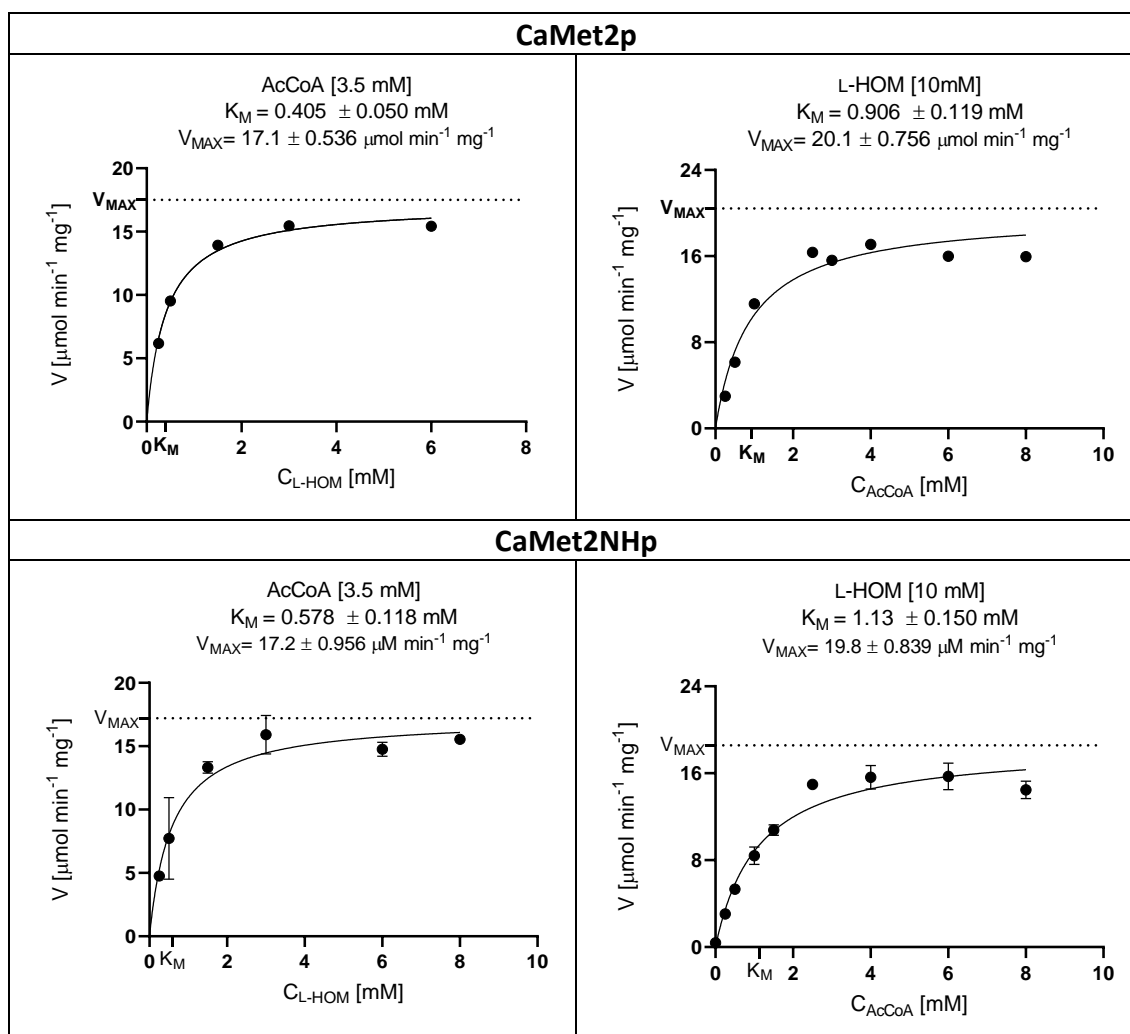


Fig. 19. Michaelis-Menten curves showing determination of K_M and V_{MAX} parameters for CaMet2p and CaMet2NHp. v , initial reaction velocity; $C_{Substrate}$, substrate concentration; AcCoA, acetyl coenzyme A; L-HOM, L-homoserine; K_M , Michaelis constant; V_{MAX} , maximum velocity of the reaction. Kinetic parameters were determined with GraphPad Prism software.

Tab. 33. Kinetic parameters determined for CaMet2p and CaMet2NHp. The value of the k_{CAT} parameter was calculated per monomer.

Substrate	K_M [mM]	k_{CAT} [s ⁻¹]	k_{CAT}/K_M [M ⁻¹ s ⁻¹]	V_{MAX} [μM min ⁻¹ mg ⁻¹]
CaMet2p				
L-HOM	0.405 ± 0.050	13.0 ± 0.405	32.1 × 10 ³	17.1 ± 0.536
AcCoA	0.906 ± 0.119	15.2 ± 0.572	16.8 × 10 ³	20.1 ± 0.756
CaMet2NHp				
L-HOM	0.578 ± 0.118	13.1 ± 0.723	22.7 × 10 ³	17.2 ± 0.956
AcCoA	1.13 ± 0.150	15.0 ± 0.635	13.3 × 10 ³	19.8 ± 0.839

4.3.3. Enzymatic activity of CaMet15NHp and CaMet15CHp

O-Acetyl-L-homoserine sulfhydrylase (Met15p) catalyzes the reaction that utilizes *O*-acetyl-L-homoserine (L-OAH) and sulfide ion as substrates and pyridoxal 5'-phosphate (PLP) as a cofactor to produce L-homocysteine (L-HCT) (Fig. 20). L-HCT reacts with DTNB, forming a yellow-colored complex, however, presence of S²⁻ ions in a buffer, which also reacts with DTNB, precludes application of DTNB-based method of enzyme activity determination.

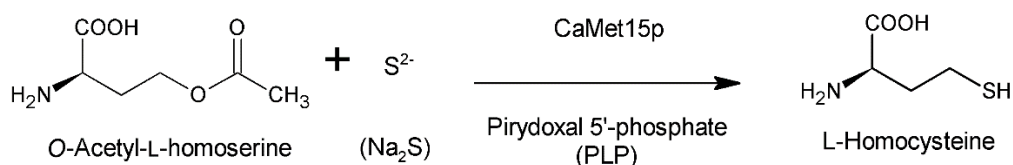


Fig. 20. Reaction catalyzed by CaMet15p

There are two approaches previously applied to assess Met15p enzymatic activity in a selective manner. These methods, proposed by Kredich and Tomkins, are based on determination of L-homocysteine with highly toxic mercury (II) chloride or use of a radioactive sulfide (³⁵S) (Kredich and Tomkins, 1966). For the above reasons, I decided to design and optimize a novel method of Met15p enzymatic activity assessment via the detection of the produced L-HCT by RP-HPLC-DAD employing pre-column derivatization of this product with DTNB. I performed the CaMe15NHp and CaMet15CHp activity assays according to procedure given in 3.2.24 b) (Fig. 21). Examples of chromatograms used to measure the reaction rate of CaMet15p are shown in Fig. S7, UV spectra of L-HCT-TNB peaks are given in Fig. S8.

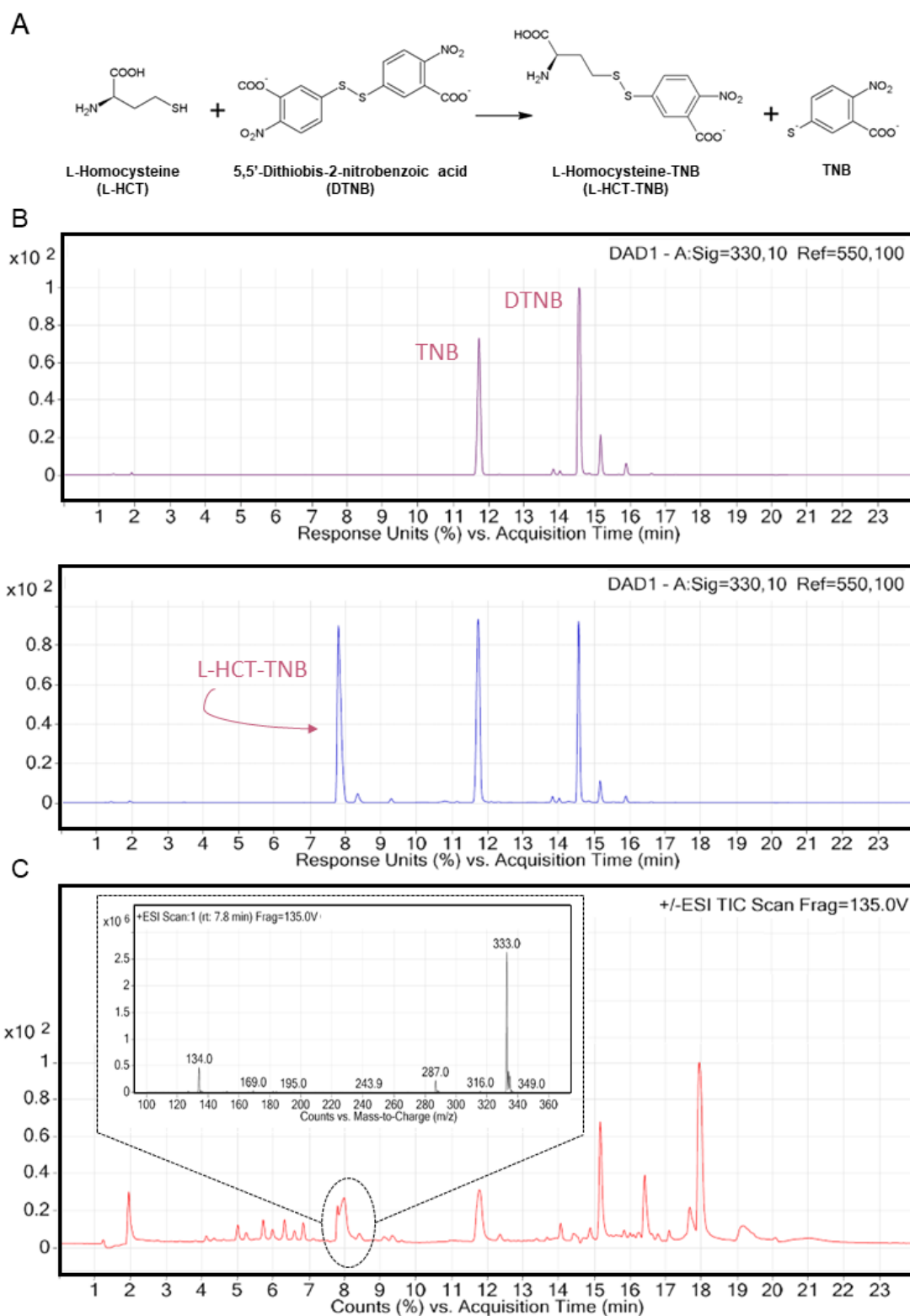


Fig. 21. Detection of L-homocysteine (L-HCT) with RP-HPLC-DAD combined with DTNB pre-column derivatization. **A.** Pre-column derivatization of L-HCT with DTNB; **B.** Chromatogram of the control reaction (top) and enzymatic (bottom) reaction mixture; **C.** Mass spectrometry analysis of the enzymatic reaction mixture (retention time 7.8 min). m/z : $[L-HCT-TNB+H]^+$ 333.0.

Both versions of the *C. albicans* enzyme, i.e. CaMet15CHp and CaMet15NHp, were found to exhibit the activity of *O*-acetyl-L-homoserine sulfhydrylase which converts L-OAH, a sulfide ion in the form of Na₂S with participation of the PLP cofactor, to produce L-HCT. The reaction rates catalyzed by CaMet15NHp and CaMet15CHp are comparable, what proves that addition of the 6xHisTag domain to either terminus of the enzyme does not influence enzyme activity (Fig. 22 A). Based on this result I decided to characterize only the N-terminus 6xHis-tagged version of the enzyme. Further studies showed that CaMet15NHp is partially associated with PLP cofactor, what can be seen by the enzyme's ability to catalyze the reaction without additional supplementation of the reaction buffer with PLP (Fig. 22 B). CaMet15NHp showed the highest activity in 50 mM Tris-HCl buffer of pH 8.0. Furthermore, CaMet15NHp turned out to be more stable than the wild type CaMet2p, as it was stable for 22 h post purification when stored at 4 °C, which could be increased to at least 2 days without significant activity loss when supplemented with glycerol (20% per volume) (Fig. 22 C-D).

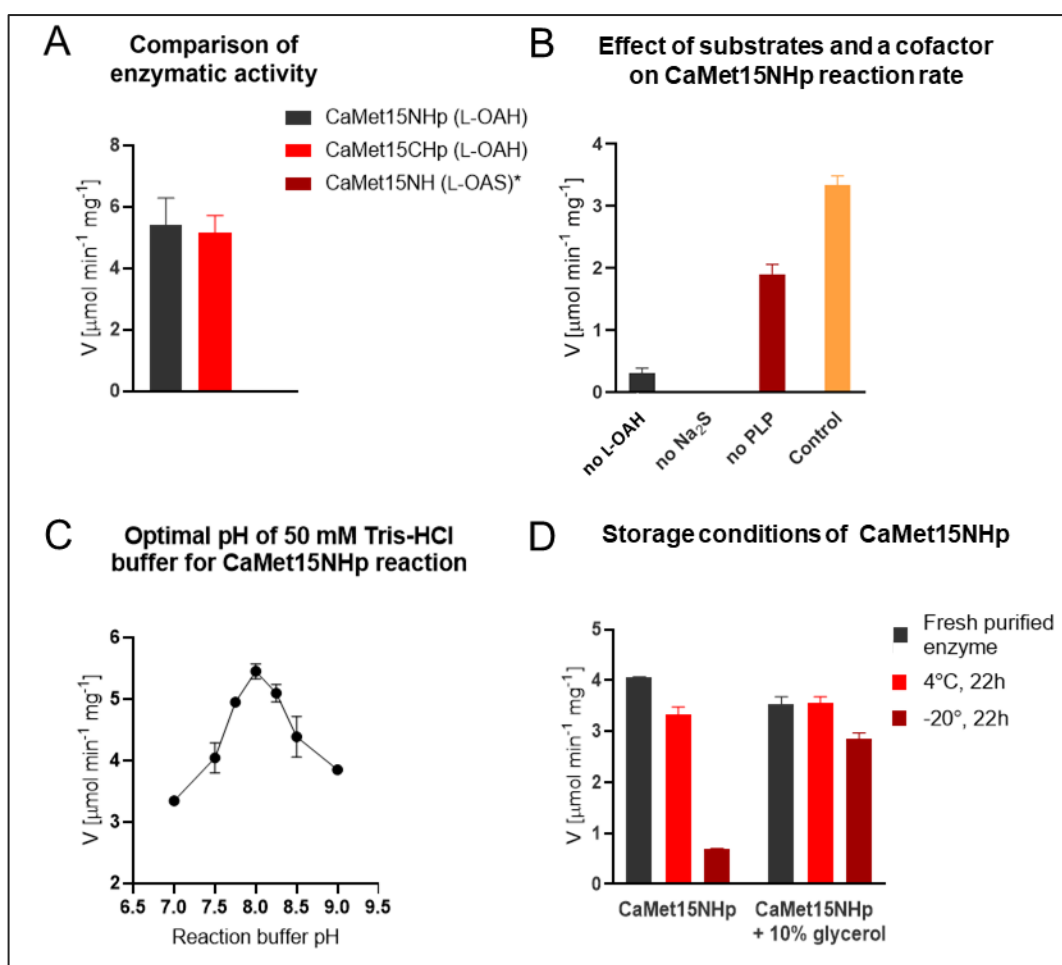


Fig. 22. Characterization of CaMet15NHp and CaMet15CHp. **A.** Comparison of sulfhydrylase activity of CaMet15CHp and CaMet15NHp, with L-OAH or L-OAS as a substrate; **B.** Influence of a substrate or PLP cofactor presence on CaMet15NHp activity, compared to the control reaction including all reaction components; **C.** Determination of optimal pH of the reaction catalyzed by CaMet15NHp; **D.** Optimal storage conditions preserving CaMet15NHp activity.

*No possible product (L-Cys) was detected in the postreaction mixture when L-OAS was used as a substrate.

To further characterize the CaMet15p, I conducted an experiment to verify the potential ability of this enzyme to utilize *O*-acetyl-L-serine (L-OAS) as a substrate. As shown in Fig. 22 A, CaMet15NHp does not exhibit the bifunctional *O*-acetyl-L-homoserine/*O*-acetyl-L-serine sulfhydrylase activity, as no L-Cys production was detected when *O*-acetyl-L-serine was present in the reaction mixture instead of L-OAH. This contrasts with the *S. cerevisiae* counterpart, which was found bifunctional (Yamagata et al., 1974). On the other hand, mono-functional *O*-acetyl-L-homoserine sulfhydrylase was demonstrated in *S. pombe*, containing two types of Met15p enzymes, one of which reacting only with L-OAH but not L-OAS (Yamagata, 1987a; Brzywczy et al., 1993). Other Met15p enzymes found in *B. flavum* and *T. thermophilus* displayed the bifunctional activities that were significantly shifted towards using L-OAH as preferred substrate, with a relative enzymatic activity of up to 5% observed when utilizing L-OAS (Ozaki and Shiio, 1982; Shimizu et al., 2001).

I characterized the kinetic parameters of CaMet15NHp leading to a determination of the Michaelis constant (K_M), the maximum velocity (V_{MAX}), the turnover number (k_{CAT}), and kinetic efficiency (k_{CAT}/K_M). The kinetic parameters were assessed via measurement of the initial velocity of the reaction dependent on altering the concentration of one of the substrates and a fixed concentration of the other at a constant concentration of the PLP cofactor (Fig. 23).

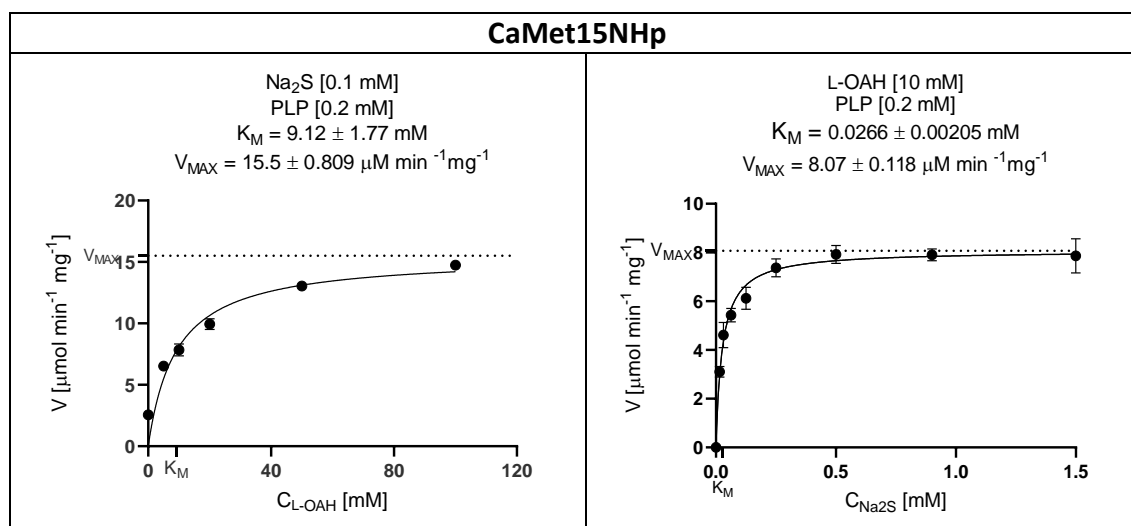


Fig. 23. Michaelis-Menten curves for determination of K_M and V_{MAX} parameters of CaMet15NHp. v , initial reaction velocity; $C_{L-OAH}/\text{Na}_2\text{S}$, substrate concentration; L-OAH, *O*-acetyl-L-homoserine; PLP, pyridoxal 5'-phosphate; K_M , Michaelis constant; V_{MAX} , maximum velocity of the reaction. Kinetic parameters were determined with GraphPad Prism software.

Determined K_M and V_{MAX} parameters are given in Tab. 34, and for Na_2S equal 0.0266 ± 0.00205 mM and $8.07 \pm 0.118 \mu\text{M min}^{-1} \text{mg}^{-1}$, respectively, and for L-OAH - 9.12 ± 1.77 mM and $15.50 \pm 0.81 \mu\text{M min}^{-1} \text{mg}^{-1}$, respectively. The K_M value for Na_2S is 350-fold lower than the value determined for L-OAH. Similar difference was previously reported for Met15p from *Schizosaccharomyces pombe*, where K_M was found



to be 0.0530 mM and 12.5 mM respectively for Na₂S and L-OAH (Yamagata, 1984). On the other hand, in the case of bacterial versions of Met15p the respective values were not as different. The K_M parameter value reported for *Thermus thermophilus* HB8 Met15p enzyme equals 1.30 mM for Na₂S and 6.80 mM for L-OAH (Shimizu et al., 2001).

Tab. 34. Kinetic parameters determined for CaMet15NHp. The value of the k_{CAT} parameter was calculated per monomer.

Substrate	K _M [mM]	k _{CAT} [s ⁻¹]	k _{CAT} /K _M [M ⁻¹ s ⁻¹]	V _{MAX} [μM min ⁻¹ mg ⁻¹]
CaMet15NHp				
L-OAH	9.12 ± 1.77	12.4 ± 0.647	1.36 × 10 ³	15.5 ± 0.809
Na₂S	0.0266 ± 0.00205	6.46 ± 0.0942	243 × 10 ³	8.07 ± 0.118

4.3.4. Enzymatic activity of CaStr2NHp and CaStr2CHp

Cystathionine-γ-synthase (Str2p) is a PLP-dependent enzyme catalyzing the γ-replacement reaction in which L-cystathionine (L-CTT) is formed from O-acetyl-L-homoserine (L-OAH) and L-cysteine (L-Cys) (Fig. 24).

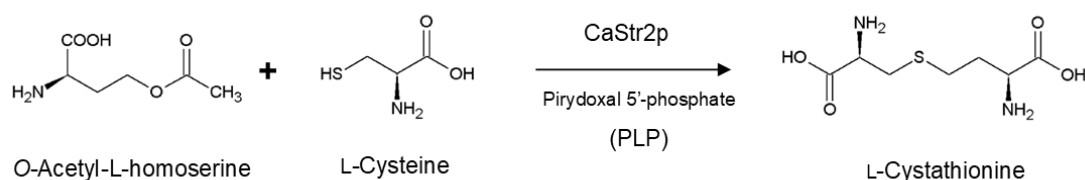


Fig. 24. Reaction catalyzed by CaStr2p.

Str2p is poorly described in microorganisms, in fact, only one fungal counterpart has been partially biochemically characterized but no fungal-derived enzyme crystal structure has been solved. Consequently, there is only one reported method for the assessment of fungal Str2p enzyme which involves the detection of ³⁵S-cysteine by a radio assay (Kerr and Flavin, 1970). The published method for determination of the activity of Str2p from aerobic crenarchaeon *Sulfolobus tokodaii*, relies on continuous coupled assay involving lactate dehydrogenase and cystathionine-β-lyase. This method is overly complicated and prone to variability related to the stability and efficiency of three enzymes (Sagong and Kim, 2017). The above reasons have encouraged me to introduce a novel method for assessment of Str2p enzymatic activity. The proposed method relies on indirect measurement of produced L-CTT via detection of a decrease in substrate, L-Cys concentration (Fig. 25). Examples of chromatograms used to measure the reaction rate of CaStr2p are shown in Fig. S9, UV spectra of L-Cys-TNB peaks are given in Fig. S10.

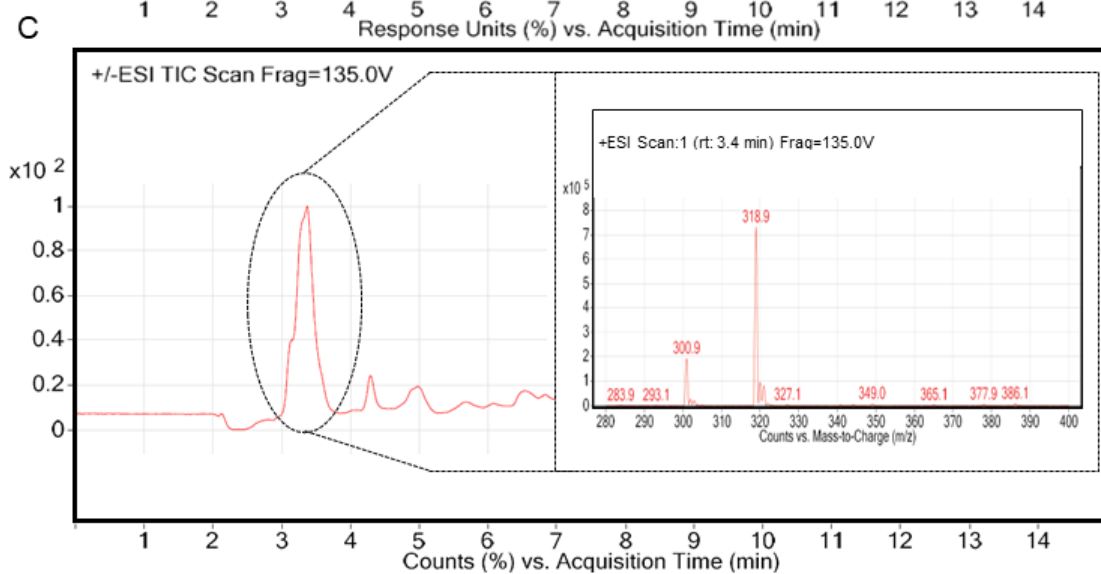
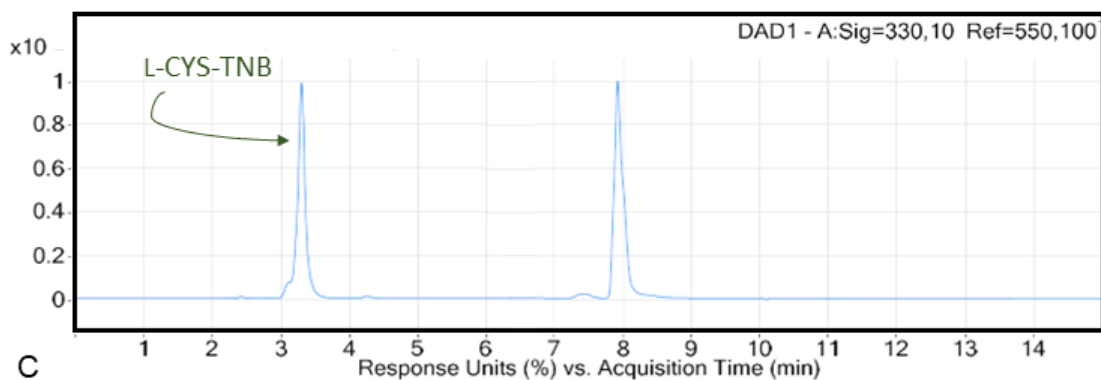
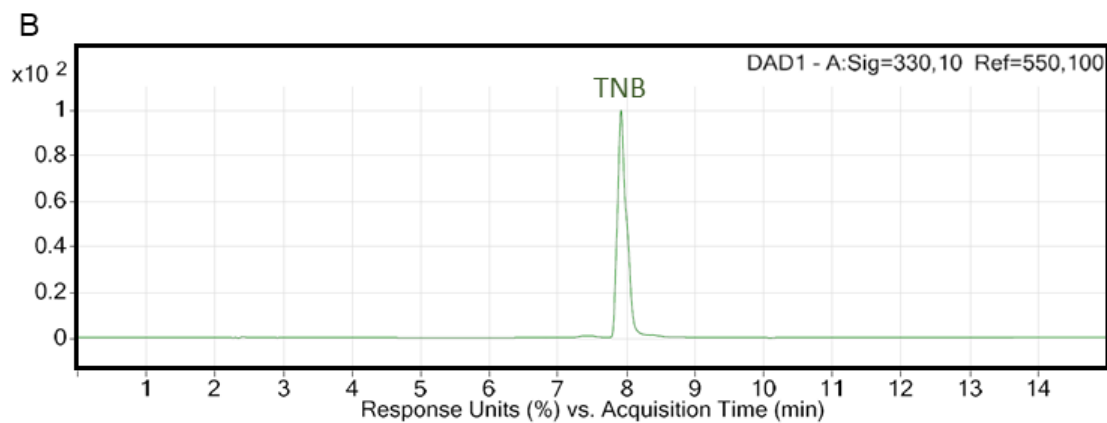
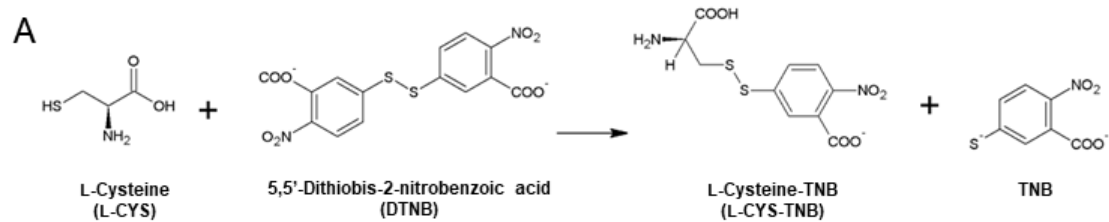


Fig. 25. Detection of L-cysteine (L-CYS) with RP-HPLC-DAD combined with DTNB pre-column derivatization. **A.** Pre-column derivatization of L-Cys with DTNB; **B.** Chromatogram of the control reaction (top) and enzymatic (bottom) reaction mixture; **C.** Mass spectrometry analysis of the enzymatic reaction mixture (retention time 7.8 min). m/z : [L-CYS-TNB+H]⁺ 319.



The novel method was used for determination of CaStr2CHp and CaStr2NHp activity. It was found that both recombinant enzyme versions exhibit a comparable activity of cystathionine- γ -synthase, utilizing L-Cys, L-OAH, and a PLP cofactor, to produce L-CTT (Fig. 26 A). Both substrates and a PLP cofactor are crucial for the reaction to occur. Since the added 6xHisTag domain had little effect on the activity of both enzyme versions, I decided to characterize only the N-terminally 6xHistagged enzyme version. Similarly to CaMet2NHp, CaStr2NHp quickly lost its activity when the buffer was not supplemented with glycerol. After 3.5 hours, the catalytic activity was completely lost. Temperature-dependent enzyme liability and instability were also observed in the case of *Neurospora crassa* Str2p, with a substantial decrease in enzyme activity within 1 hour after isolation (Kerr and Flavin, 1968). On the other hand, I observed that the addition of glycerol (20% per volume) helped to preserve CaStr2NHp activity at 4 °C and at -20 °C (Fig. 26 D), enabling storage of an active CaStr2NHp for at least 2 weeks, without a significant loss of activity. CaStr2NHp demonstrated the highest activity in 50 mM Tris-HCl buffer of pH 8.0 (Fig. 26 C).

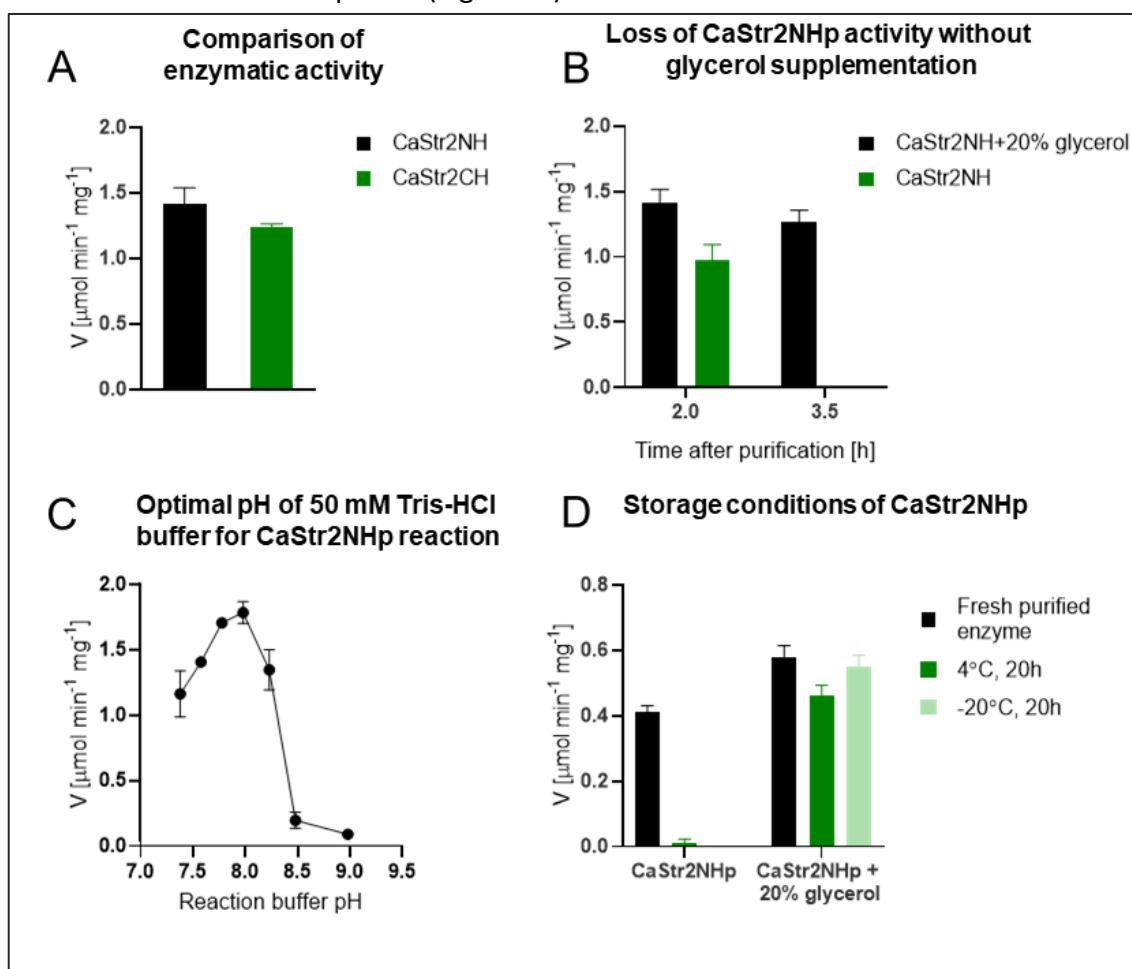


Fig. 26. Characterization of CaStr2NHp and CaStr2CHp. **A.** Comparison of CaStr2NHp and CaStr2CHp activity; **B.** Loss of activity in time by enzyme not supplemented with glycerol; **C.** Determination of optimal pH of the reaction catalyzed by CaStr2NHp; **D.** Optimal storage conditions to preserve enzyme activity.

I determined the kinetic parameters of CaStr2NHp, i.e. Michaelis constant (K_M), maximum velocity (V_{MAX}), turnover number (k_{CAT}), and kinetic efficiency (k_{CAT}/K_M). The kinetic parameters were assessed via measurement of the initial velocity of the reaction dependent on altering the concentration of one of the substrates and the fixed concentration of the other at a constant concentration of the PLP cofactor. Obtained results are presented in Fig. 27.

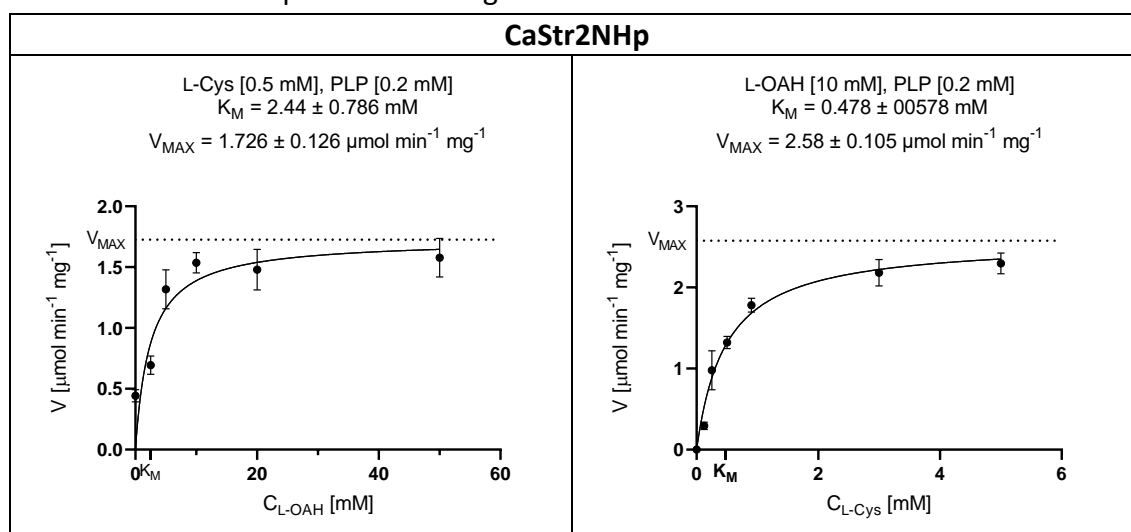


Fig. 27. Michaelis-Menten curves for determination of K_M and V_{MAX} parameters of CaStr2NHp. v , initial reaction velocity; $C_{L-OAH/L-CYS}$, substrate concentration; L-OAH, *O*-acetyl- L-homoserine; L-Cys, L-cysteine; K_M , Michaelis constant; V_{MAX} , maximum velocity of the reaction. Kinetic parameters were determined with GraphPad Prism software.

The obtained K_M and V_{MAX} parameters (Tab. 35) for L-OAH equal 2.44 ± 0.786 mM and $1.726 \pm 0.126 \mu\text{mol min}^{-1} \text{mg}^{-1}$, respectively, and for L-Cys - 0.478 ± 0.0578 mM and $2.58 \pm 0.105 \mu\text{mol min}^{-1} \text{mg}^{-1}$, respectively. For Str2p from *N. crassa*, V_{MAX} equal to $3.2 \mu\text{mol min}^{-1} \text{mg}^{-1}$ for *O*-acetyl-DL-homoserine was reported (Kerr and Flavin, 1968). That value is not very much different from the obtained value found for CaStr2NHp. Comparison with kinetic parameters with those of the bacterial Str2p is less justified, since these enzymes use a different substrate, namely *O*-succinyl-L-homoserine. However, the K_M values found for this substrate in the case of *Helicobacter pylori* and *E. coli* were 3.02 mM and 1.29 mM, respectively (Aitken et al., 2003; Kong et al., 2008).

Tab. 35. Kinetic parameters determined for CaStr2NHp. The value of k_{CAT} parameter was calculated per monomer.

Substrate	K_M [mM]	k_{CAT} [s ⁻¹]	k_{CAT}/K_M [M ⁻¹ s ⁻¹]	V_{MAX} [$\mu\text{mol min}^{-1} \text{mg}^{-1}$]
CaStr2NHp				
L-OAH	2.44 ± 0.786	1.93 ± 0.140	0.791×10^3	1.726 ± 0.126
L-Cys	0.478 ± 0.0578	2.87 ± 0.117	6.00×10^3	2.58 ± 0.105

4.4. Searching for inhibitors of CaMet2p, CaMet15p and CaStr2p

The most important objective of my research project was based on assumption that the three enzymes involved in L-Met biosynthesis pathway in *C. albicans*, i.e., CaMet2p, CaMet15p, and CaStr2p; can serve as novel molecular targets for antifungal chemotherapy. Thus, one of the particular aims of this research was searching for potential inhibitors of the above enzymes.

Selected compounds for the inhibitor screen were analogs of substrates utilized by the Met2p, Met15p, and Str2p, i.e. L-homoserine (L-HOM), O-acetyl-L-homoserine (L-OAH), L-homocysteine (L-HCT) and L-cysteine. Tested potential inhibitors were either commercially available compounds within which some were reported as inhibitors of enzymes involved in the amino acid biosynthetic pathways (Yamagata, 1987b; Jeitner and Cooper, 2014) and exhibiting antifungal activity (Vallejo et al., 2017), or structural analogs designed for specific inhibition of CaMet2p, CaMet15p or CaStr2p, synthesized in our research group (Fig. 28). L-methionine, i.e. the end-product of the MBP, was also included in the set of tested compounds, to check whether the investigated enzymes are the subject of a feedback regulation.

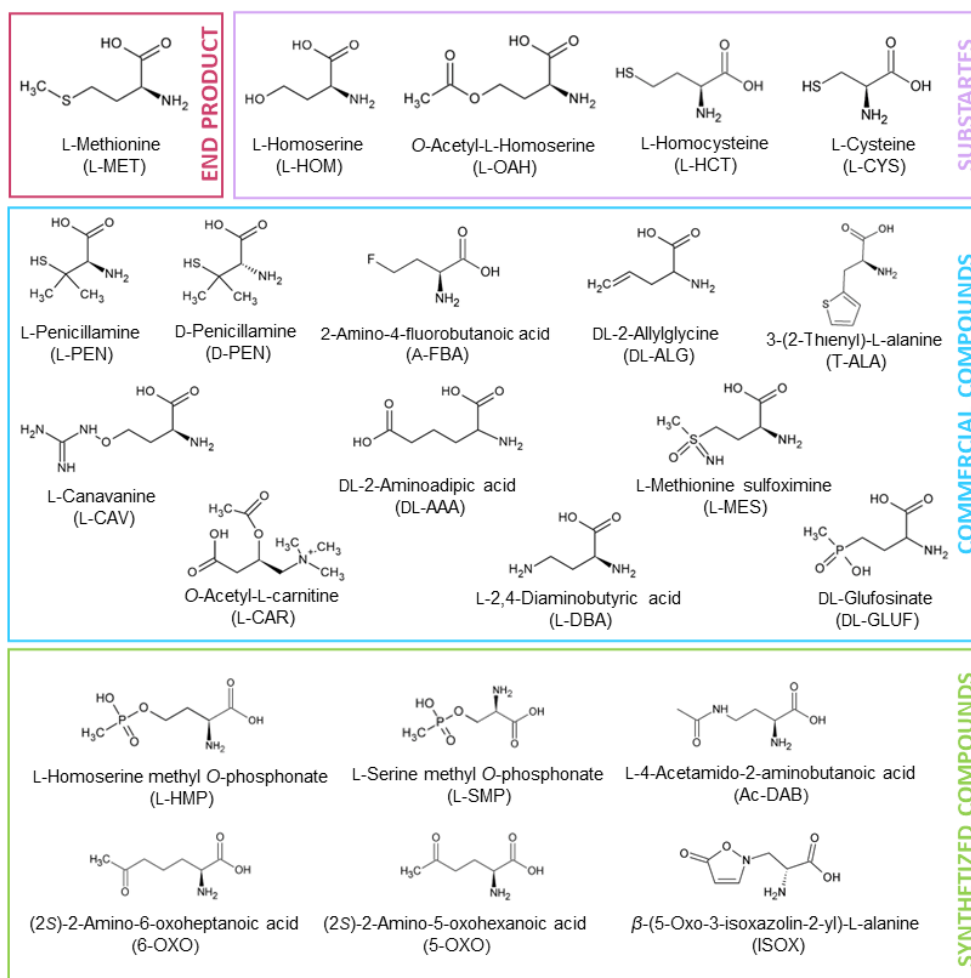


Fig. 28. Potential inhibitors of CaMet2p, CaMet15p, and CaStr2p. Compounds L-HMP, L-SMP, Ac-DAB, 6-OXO, 5-OXO and ISOX have been synthesized at the Department of Organic Chemistry, Gdańsk University of Technology. Other compounds are commercially available.

4.4.1. Inhibitory assay

All compounds specified above were tested for inhibition of respective enzymes under optimal conditions, using constant substrate concentration saturating the enzyme. For the assay, I decided to use enzymes' versions with an added 6xHisTag domain to the N-terminus.

Obtained results show that tested enzymes are sensitive to various inhibitors (Fig. 29). None of the three enzymes was particularly sensitive to inhibition by L-Met. CaMet2NHp appeared to be the least susceptible to the end product inhibition induced by 10 mM L-Met concentration (1.1 %), which is physiologically irrelevant and suggests that regulation of CaMet2p activity by feedback inhibition is unlikely. Similar results, showing no inhibitory effect caused by L-Met were reported for Met2p enzymes from *S. cerevisiae* and *Neurospora crassa*, in contrast to the evidence for a feedback inhibition found in the case of bacterial Met2p from *Bacillus subtilis*, *B. polymyxa*, and *Brevibacterium flavum* (Yamagata, 1987b). CaMet15NHp and CaStr2NHp appeared to be more susceptible to feedback inhibition evoked by 10 mM L-Met concentration resulting in 14.8 % and 24.1 %, respectively, yet still of no physiological relevance. However, inhibition of *C. albicans* Met15NHp by L-Met is weaker than that observed for Met15p of *Schizosaccharomyces pombe*, and *B. flavum* reporting 74% and 50%, respectively at 10 mM L-Met concentration, and *S. cerevisiae* 74% inhibition by 30 mM L-Met (Yamagata, 1984). On the other hand, the Str2p activity was not altered by 10 mM L-Met in *Corynebacterium glutamicum*, however, synthesis of the enzyme was strongly repressed by L-Met (60-70% with 100 $\mu\text{g mL}^{-1}$) (Kase and Nakayama, 1974), which was not supported by evidence given for *N. crassa* enzyme (Kerr and Flavin, 1968). This indicates that the feedback inhibition mechanism strongly varies between species. Nevertheless, the three *C. albicans* enzymes studied in this project do not seem to be regulated in this way.

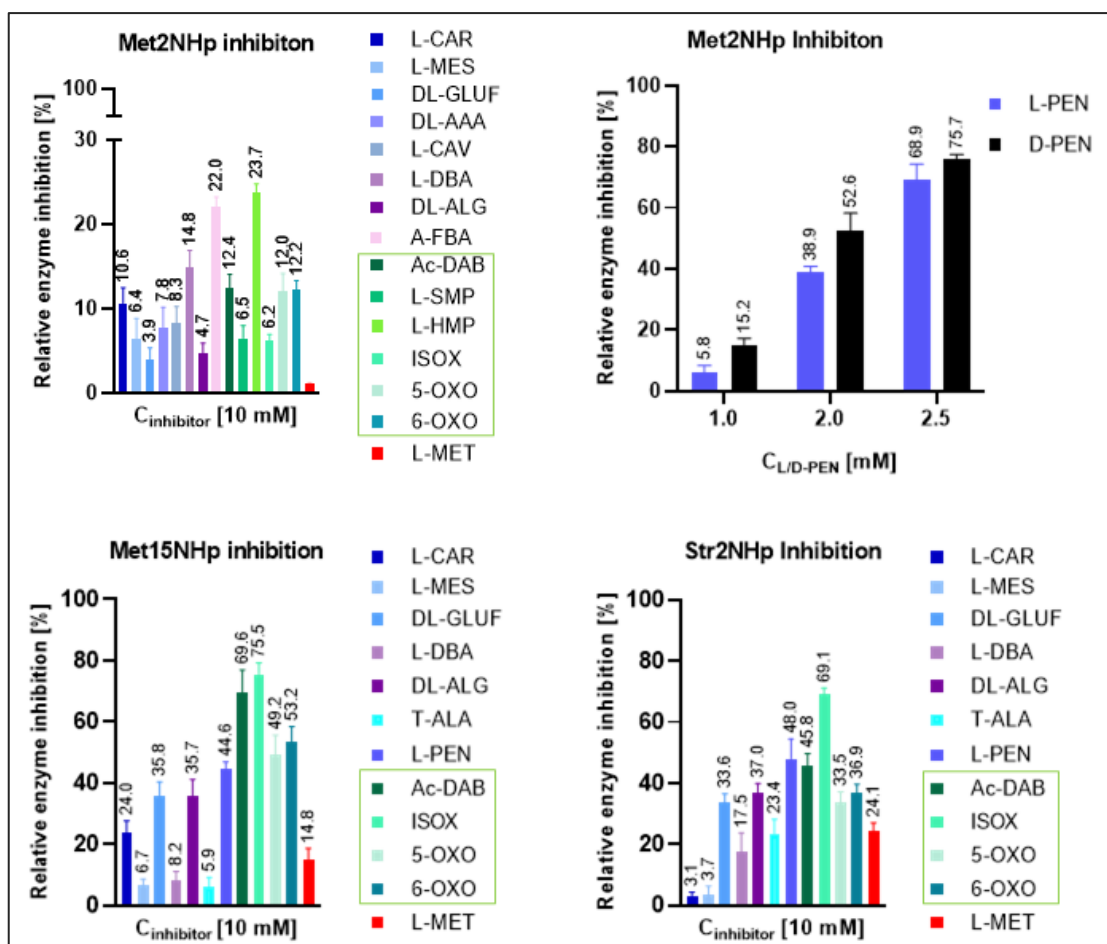


Fig. 29. Results of determination of inhibitory potency of tested inhibitors against CaMet2NHp, CaMet15NHp, and CaStr2NHp. Compounds synthesized in our group are shown in green boxes. Data shown are mean values of at least three independent experiments (\pm SD).

Two out of four compounds designed and synthesized in our group, namely ISOX and Ac-DAB, appeared to be the most potent, especially against CaMet15NHp and CaStr2NHp. This is not surprising, since these compounds seem to demonstrate the closest structural analogy to OAH i.e. the substrate of these enzymes (Fig. 29). ISOX at 10 mM inhibited both CaMet15NHp and CaStr2NHp at a similar level of \sim 70%. ISOX is an alanine derivative that was originally isolated from *Pisum sativum* (pea) and reported to exhibit a broad spectrum of growth inhibitory activity against several phytopathogenic fungi, that can be reversed by L-Met, L-Cys, and L-HCT (Lambein et al., 1969; Schenk et al., 1991). It was thus suggested that ISOX targets one of the enzymes of the MPB (Nowak et al., 2021). My research results confirm that enzymes of the MBP, specifically Met15p, and Str2p, are molecular targets for ISOX, which most probably is related to its antifungal activity.

Furthermore, comparable \sim 70% inhibition of CaMet15NHp can be observed for the 10 mM Ac-DAB, compound, which was a little less potent against CaStr2NHp (45.8%). This compound was previously reported as an inhibitor of bacterial Met15p (Kulikova et al., 2019). 6-OXO and 5-OXO differ from each other by one $-CH_2$ residue yet

display a similar inhibitory effect; ~50% (CaMet15NHp), ~30% (CaStr2NHp) and ~12% (CaMet2NHp).

The strongest inhibitory effect against CaMet2NHp was observed for L-PEN and D-PEN, resulting in ~70% inhibition of the enzyme activity at 2.5 mM concentration (Fig. 29). However, both L-PEN and D-PEN are less effective at inhibiting CaMet15NHp and CaStr2NHp, as their inhibitory potential was approximately 50% at a 10 mM concentration. Considering the stereospecificity, it is quite surprising that both penicillamine enantiomers display comparable inhibitory properties. Molecular docking analysis performed by Dr. Marek Wojciechowski, confirmed that both L-PEN and D-PEN are capable of binding to the *C. albicans* enzyme with similar affinities (Kuplińska et al., 2022). Penicillamine is a non-proteinogenic amino acid that was previously reported as an inhibitor of PLP-dependent enzymes (Lowther et al., 2012). Provided results of CaMet2NHp inhibition by penicillamine is in fact the first example of its inhibitory potency against PLP-independent enzyme.

Among other commercially available compounds tested, some inhibitory effect was also observed in the case of DL-ALG and DL-GLUF, which inhibited both CaMet15NHp and CaStr2NHp with ~35%, and insignificantly CaMet2NHp. DL-GLUF is a widely used herbicide, also known as D,L-phosphinothricin, a compound characterized as “a natural amino acid with unexpected herbicidal properties” (Hoerlein, 1994), shown to inhibit glutamine synthetase, found abundantly in plant leaves, and leading to internal amino acid starvation (Dayan et al., 2019). Glutamine synthetase catalyzes L-glutamine formation via ATP-dependent incorporation of ammonia into L-glutamate which is essential for nitrogen metabolism in plants (Takano and Dayan, 2020). DL-GLUF was also found to display an inhibitory effect towards glutamine synthetase from *S. cerevisiae* altering yeast physiology and in consequence its performance in industrial processes like winemaking (Vallejo et al., 2017). DL-ALG is a known inhibitor of the glutamate decarboxylase used in γ -aminobutyric acid (GABA) research (Bioulac et al., 1997). Glutamate decarboxylase is also present in yeast cells including *S. cerevisiae* (Coleman et al., 2001), and DL-ALG was found to significantly inhibit the growth of *S. cerevisiae* in minimal medium, that could be restored by the addition of L-Cys or L-Met (Dittmer et al., 1948; Dittmer, 1950). It may appear questionable whether pure enantiomers of DL-GLUF or DL-ALG could be more effective in inhibiting of tested enzymes, however taking into account comparable inhibitory effect caused by D-PEN and L-PEN, the type of enantiomer does not seem to play a key role.

For the determination of the potential mechanism of enzyme inhibition, I decided to examine the inhibition type of the most promising CaMet2NHp inhibitor, i.e. penicillamine. Considering the similar inhibitory potential of both enantiomers this study was performed only for L-PEN. The obtained Lineweaver-Burk plots are given in Fig. 30. The obtained results suggest that L-PEN acts as a noncompetitive inhibitor in respect to L-HOM, with a calculated K_i value of 1.62 mM. This surprising result is contradictory to the performed molecular docking analysis that implicated the binding

of L-PEN to the active site of the enzyme (Kuplińska et al., 2022). Admittedly, since there is no X-ray structure of *C. albicans* Met2p, an enzyme from *M. smegmatis* (PDBID: 6IOH) was used as the receptor for docking. Structural differences between bacterial and fungal models, and the fact that the 6IOH crystal structure is deprived of relatively large AcCoA, could result in divergent modes of L-PEN binding to the CaMet2NHp.

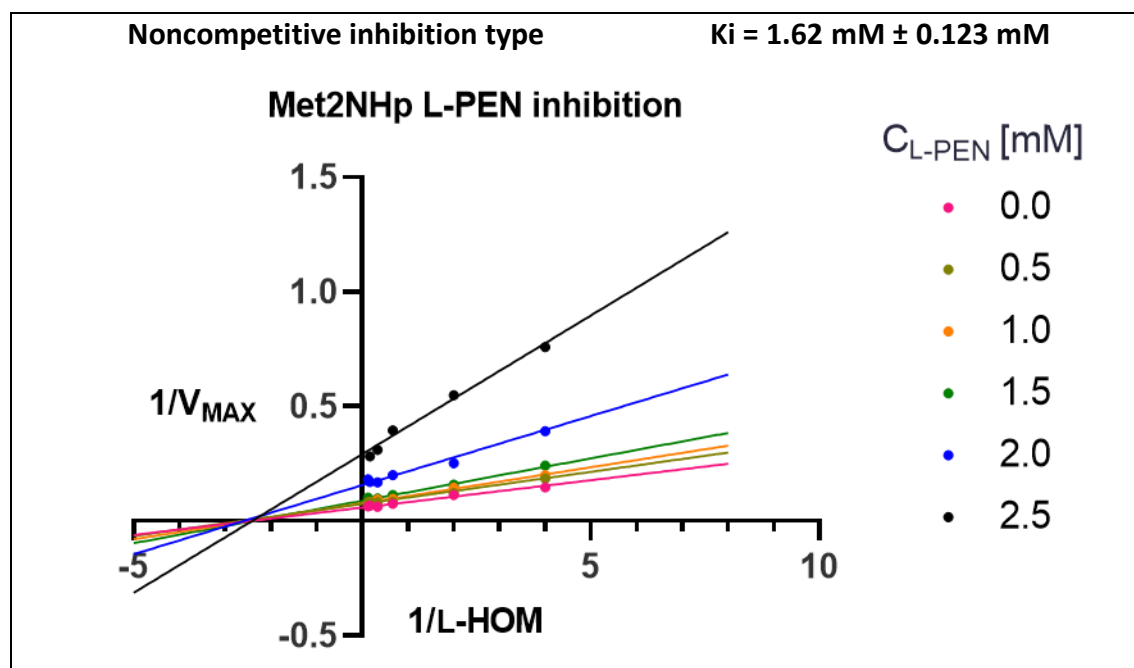


Fig. 30. Lineweaver-Burk plot of CaMet2NHp inhibition with L-PEN. K_i parameter was calculated using the GraphPad Prism software.

4.4.2. Antifungal activity of selected inhibitors

I selected the most potent inhibitors of CaMet2NHp, CaMet1NHp, and CaStr2NHp for the assessment of their antifungal activity against *C. albicans*, *C. glabrata* and *S. cerevisiae*. The chosen compounds were L-PEN, D-PEN, DL-GLUF, DL-ALG, Ac-DAB and ISOX. To evaluate antifungal activity, I determined minimal inhibitory concentrations of compounds that inhibit the cell growth at 90 % (MIC_{90}) or 50 % (MIC_{50}), in several different media (3.1.4); RPMI 1640, minimal YNB with ammonium sulfate (AS) or sodium glutamate (SG) as a sole nitrogen source, also in version additionally supplemented with 10 mM L-Met.

Tab. 36. Susceptibility of yeast strains to D-PEN, L-PEN, Ac-DAB, DL-ALG, DL-GLUF, ISOX, fluconazole (FLU), and Amphotericin B (AmB). No observable activity of a compound at measured concentrations is represented by (>1024). Growth media used: RPMI 1640, YNB without amino acids with ammonium sulfate (AS) or sodium glutamate (SG) as nitrogen source, with or without supplementation of 10 mM L-Met. The experiments were performed in triplicates. Results partially published in (Kuplińska et al., 2022).

Compound	Medium	MIC ₉₀ (MIC ₅₀) [$\mu\text{g}\cdot\text{mL}^{-1}$]		
		<i>C. albicans</i> ATCC 10231	<i>C. glabrata</i> ATCC 90030	<i>S. cerevisiae</i> ATCC 9763
D-PEN	YNB AS	>1024 (>1024)	>1024 (>1024)	>1024 (>1024)
	YNB AS L-MET	>1024 (>1024)	>1024 (>1024)	>1024 (>1024)
	YNB SG	>1024 (>1024)	>1024 (>1024)	>1024 (>1024)
	YNB SG L-MET	>1024 (>1024)	>1024 (>1024)	>1024 (>1024)
	RPMI	64 (32)	256 (128)	>1024 (>1024)
L-PEN	YNB AS	>1024 (>1024)	512 (256)	>1024 (128)
	YNB AS L-MET	>1024 (>1024)	>1024 (>1024)	>1024 (512)
	YNB SG	1024 (512)	512 (256)	>1024 (128)
	YNB SG L-MET	>1024 (1024)	>1024 (1024)	>1024 (512)
	RPMI 1640	64 (32)	128 (64)	1024 (128)
DL-GLUF	YNB AS	128 (16)	64 (16)	128 (8)
	YNB AS L-MET	>1024 (128/512)	1024 (128)	256 (32)
	YNB SG	256 (128)	128 (16)	128 (16)
	YNB SG L-MET	>1024 (1024)	1024 (32)	>1024
	RPMI 1640	>1024	>1024	>1024
DL-ALG	YNB AS	512 (16)	16 (4)	16 (4)
	YNB AS L-MET	>1024	>1024	512 (128)
	YNB SG	64 (8)	16 (4)	8 (4)
	YNB SG L-MET	>1024 (256)	512 (64)	256 (32)
	RPMI 1640	>1024 (1024)	>1024	16 (4)
Ac-DAB	YNB AS	>1024 (1024)	>1024 (>1024)	>1024 (>1024)
	YNB AS L-MET	>1024 (>1024)	>1024 (>1024)	>1024 (>1024)
	YNB SG	1024 (128)	>1024 (512)	>1024 (512)
	YNB SG L-MET	>1024 (>1024)	>1024 (>1024)	>1024 (>1024)
	RPMI 1640	>1024 (>1024)	>1024 (>1024)	>1024 (>1024)
ISOX	YNB AS	2 (1)	4 (1)	1024 (2)
	YNB AS L-MET	>64 (>64)	>64 (>64)	>1024 (>1024)
	YNB SG	2 (1)	2 (1)	512 (1)
	YNB SG L-MET	1024 (128)	>1024 (512)	>1024 (512)
	RPMI 1640	>64 (>64)	>64 (>64)	>64 (>64)
FLU	RPMI 1640	4	32	8
AmB	RPMI 1640	0.5	1	0.5

All tested compounds displayed an antifungal activity that could be restored with L-Met supplementation, indicating the L-Met biosynthetic pathway (MBP) as a target for these inhibitors (Tab. 36). Despite the relatively high enzyme inhibitory activity of Ac-DAB, its antifungal activity could only be observed in YNB SG medium. The observed MIC values were usually lower in YNB SG medium, which is related to the glutamine

effect and repression of *OPT* transporters gene expression in the presence of preferred and easily assimilated nitrogen sources like ammonium sulfate (Schielmann et al., 2017). On the other hand, ISOX displayed a comparable antifungal activity in both YNB AS and YNB SG mediums against *C. albicans* and *C. glabrata*. In fact, ISOX was the most effective compound against *C. albicans* and *C. glabrata* in YNB medium with a MIC₉₀ value of 2 µg mL⁻¹. The antifungal activity of ISOX was significantly lower against *S. cerevisiae* which might be due to selective targeting of *Candida spp.* enzymes. The MIC₉₀ parameter against *S. cerevisiae* could only be observed at a concentration of 1024 µg mL⁻¹ and 512 µg mL⁻¹ in YNB SA and YNB SG media, respectively, however cell growth not increasing 50% could be observed up to 2 µg mL⁻¹ and 1 µg mL⁻¹ in YNB SA and YNB SG media, respectively. Fungal growth inhibition caused by ISOX was surprisingly completely rescued in the RPMI 1640 medium. Antifungal activity of ISOX was previously reported for various fungal strains including *S. cerevisiae*, *C. utilis*, *C. lipolytica* (Schenk et al., 1991). Moreover, Schenk et al. assumed that antifungal activity of ISOX results from inhibition of L-Met, as fungal growth could be reversed by supplementation of the media with L-Met. These observations were repeated basing on the results presented in Tab. 36. Interestingly, despite the low inhibitory effect against CaMet2NHp, CaMet15NHp, and CaStr2NHp, DL-ALG and DL-GLUF displayed higher antifungal activity than Ac-DAB, with a clearer association with targeting MBP. Lower MIC₉₀ values could be observed for both compounds in all media not supplemented with L-Met. A decrease in growth of *S. cerevisiae* but not its complete abolishment caused by DL-ALG or DL-GLUF in media containing L-Met, what suggests that the MBP is not the only molecular target for these compounds. This is consistent with the results reporting DL-GLUF antifungal activity against *A. nidulans* and *Rhizoctonia solani*, which was akin to inhibition of glutamate synthase (Uchimiya et al., 1993; Tubajika and Damann, 2002; Takano and Dayan, 2020). DL-ALG is an inhibitor specifically designed and synthesized by Dittmer et al. as a metabolite antagonist of L-cysteine, that was found to inhibit the growth of *E. coli* and *S. cerevisiae* (Dittmer et al., 1948). The exact mechanism of the DL-ALG-induced microbial growth inhibition is unknown, although based on the results presented in Tab. 36, it can be suspected that it is related to targeting MBP. However, like DL-GLUF, DL-ALG leads to reduced cell growth, especially *S. cerevisiae*, even in media supplemented with L-Met, which suggests that MBP may not be the only molecular target of DL-ALG. Moreover, DL-ALG, together with L-PEN, was the only compound to exhibit antifungal activity in the RPMI medium. DL-ALG antifungal activity in RPMI medium is characterized by the lowest MIC₉₀ parameter achieved (in this medium, compared with other tested compounds) against *S. cerevisiae* at the level of 16 µg mL⁻¹.

I examined the antifungal potency of the two most potent inhibitors, L-PEN and ISOX, against other *Candida spp.* strains (Tab. 37). L-PEN was ineffective against all other tested *Candida spp.* strains, only *C. parapsilosis* and *C. dublinensis* was vulnerable to ISOX in a YNB AS with a MIC₉₀ of 4 and 0.5 µg mL⁻¹, respectively.

Tab. 37. Susceptibility of *Candida spp.* strains to L-PEN and ISOX. No observable activity of a compound at measured concentrations is represented by (>). The experiments were performed at least in three replicates. Results partially published in (Kuplińska et al., 2022).

MIC ₉₀ [µg mL ⁻¹]		
L-PEN		
Strain	YNB AS L-MET	YNB AS
<i>Candida parapsilosis</i> ATCC 22019	>1024	>1024
<i>Candida krusei</i> ATCC 6258	>1024	>1024
<i>Candida famata</i> DSM 3428	>1024	>1024
<i>Candida rugosa</i> DSM 2031	>1024	>1024
<i>Candida dublinensis</i> CBS 7987	>1024	>1024
ISOX		
Strain	YNB AS L-MET	YNB AS
<i>Candida parapsilosis</i> ATCC 22019	>64	4
<i>Candida krusei</i> ATCC 6258	>64	>64
<i>Candida famata</i> DSM 3428	>64	>64
<i>Candida rugosa</i> DSM 2031	>64	>64
<i>Candida dublinensis</i> CBS 7987	>64	0.5

D-PEN and L-PEN were the only compounds that exhibited antifungal activity in the RPMI 1640 medium against all tested strains, except for D-PEN against *S. cerevisiae*. On the other hand, DL-ALG displayed a high antifungal activity in RPMI 1640 only towards *S. cerevisiae* with MIC₉₀ parameter estimated as 16 µg mL⁻¹. RPMI 1640 provides human plasma physiological conditions concerning the content of the amino acids. Despite the antifungal effect of L-PEN against all strains, the relationship between L-Met concentration and antifungal activity could be observed at most in *C. glabrata* and *S. cerevisiae*.

The higher susceptibility of *C. glabrata* and *S. cerevisiae* strains to L-PEN could be related to different mechanisms of inorganic sulfur assimilation. Fungal organisms are capable of inorganic sulfur assimilation through an assimilatory mechanism leading to L-Cys biosynthesis in two separate ways (Marzluf, 1997; Hébert et al., 2011) (Fig. 3). The main route for L-Cys biosynthesis, found in most fungal cells, is the *O*-acetyl-L-serine (L-OAS) pathway, in which sulfide is condensed with L-OAS. The alternative route, the direct sulfhydrylation pathway, involves L-HOM formation throughout condensation of sulfide with L-OAH. L-HOM is next converted to L-CTT and L-Cys in two subsequent reactions via the reverse transulfuration pathway. Many fungi like *N. crassa*, *A. nidulans*, or *C. albicans* synthesize L-Cys via both the L-OAS pathway and the direct sulfhydrylation pathway, however, there are some organisms like *S. cerevisiae* and *C. glabrata* that lack the L-OAS pathway (Cherest and Surdin-Kerjan, 1992; Hébert et al., 2011).

I performed additional experiments on L-PEN influence on *C. glabrata* clinical isolates. Out of 8 examined isolates, 6 were characterized as fluconazole-resistant; all tested isolates appeared to be similarly susceptible to L-PEN as the wild *C. glabrata* ATCC 90030 strain in a YNB AS medium (Tab. 38).

Tab. 38. L-PEN and Flu susceptibility of *C. glabrata* clinical isolates. No observable activity of a compound at measured concentrations is represented by (>1024). R resistance to fluconazole, S sensitive to fluconazole. The experiments were performed at least in three replicates. Published in (Kuplińska et al., 2022)

Strain	Susceptibility	MIC ₉₀ (MIC ₅₀) [$\mu\text{g mL}^{-1}$]	
	Flu	Flu	L-PEN
<i>C. glabrata</i> CZD 6	S	32	512 (256)
<i>C. glabrata</i> CZD 209	R	>256	512
<i>C. glabrata</i> GD 211	R	256	512 (256)
<i>C. glabrata</i> GD 310	R	>256	512
<i>C. glabrata</i> CZD 342	S	16	512
<i>C. glabrata</i> CZD 373	R	256	512 (256)
<i>C. glabrata</i> CZD 377	R	>256	512
<i>C. glabrata</i> CZD 513	R	>256	512

L-PEN influenced *C. glabrata* and *S. cerevisiae* growth in YNB minimal medium not supplemented with L-Met. Inhibition of growth of *C. glabrata* at 50% could be achieved with 256 $\mu\text{g mL}^{-1}$ of L-PEN. The above confirms that *C. glabrata* is deprived of a functional L-OAS pathway leading to L-Cys biosynthesis, thus it can be only synthesized from L-Met through the reverse transsulfuration pathway. *S. cerevisiae*, also unable of L-Cys biosynthesis from L-OAS, was susceptible to L-PEN depending on the L-Met presence, represented by a 50 % cell growth decrease in YNB SA medium caused by 128 $\mu\text{g mL}^{-1}$ of L-PEN. The growth inhibition of cells by L-PEN could be restored by the addition of L-Met (Fig. 31).

On the other hand, despite possession of both L-OAS and transsulfuration pathways (Murillo et al., 2005), *C. albicans* is sensitive to L-PEN in RPMI 1640 medium. The RPMI medium is rich in amino acid content, thus the increased antifungal activity of L-PEN against *C. albicans* in this medium may be related to the amino acid permeases and transport of L-PEN into the cell. The likely role of the amino acid permease activity is also supported by the high antifungal activity of D-PEN in RPMI medium vs. no activity in YNB medium, regardless of L-Met supplementation. In fungal cells, the most abundant amino acid permease Gpa1p, is responsible for the uptake of the proteinogenic L-amino acids and some D-amino acids, as well as L-citrulline, L-ornithine and toxic analogs of amino acids (Jauniaux and Grenson, 1990).

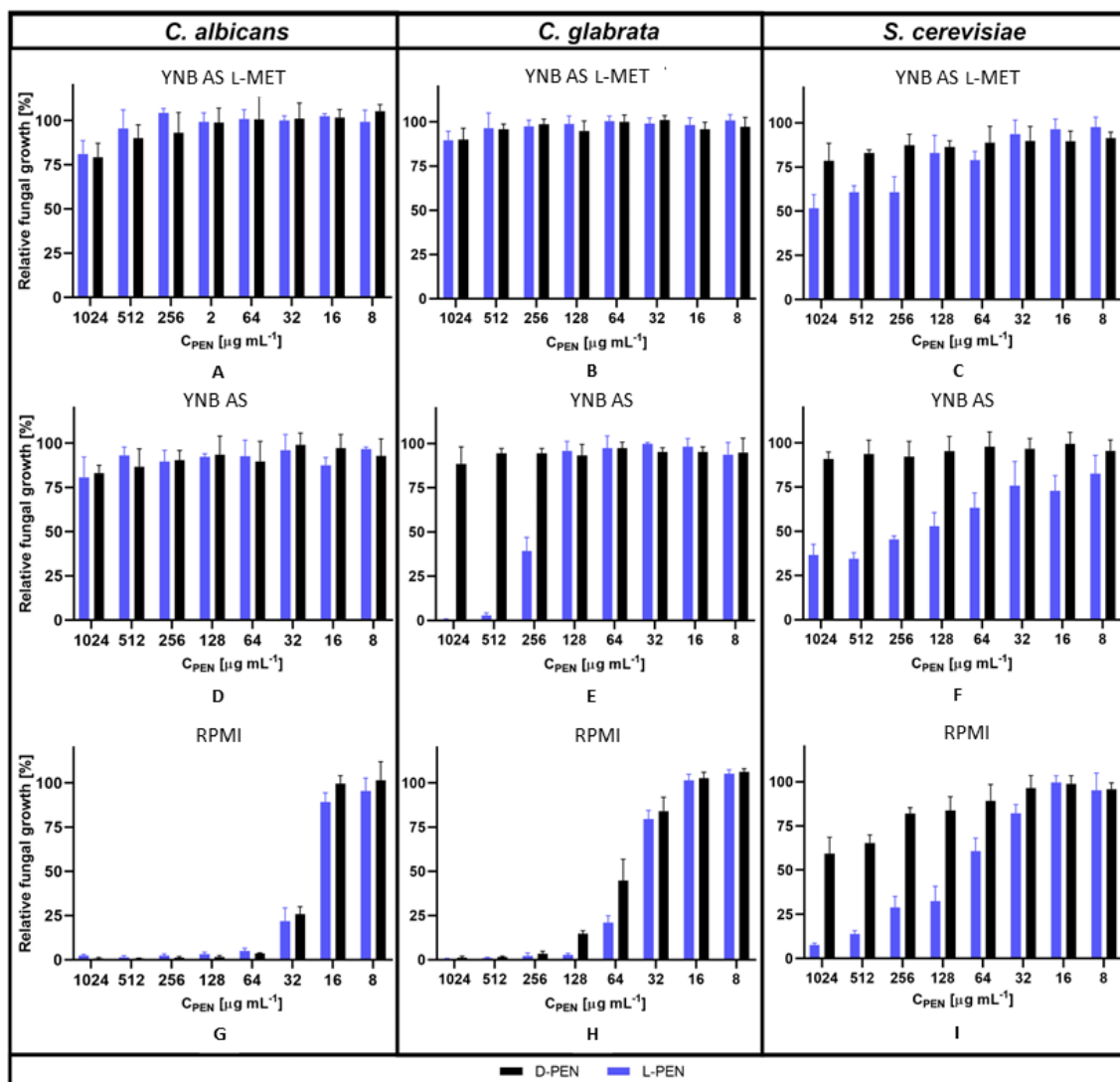


Fig. 31. Growth inhibition of *C. albicans*, *C. glabrata*, and *S. cerevisiae* by L-PEN and D-PEN in YNB AS medium with or without L-methionine (L-MET) (A-F), and RPMI 1640 medium (G-H). The error bars represent the standard deviation (SD). Results published in (Kuplińska et al., 2022).

For further studies, I determined the minimal L-Met concentration needed for *C. glabrata* growth rescue after treatment with L-PEN or ISOX in YNB AS medium (Fig. 32). Obtained results show that antifungal effect of ISOX could be easily restored with the addition of as little as 0.015 mM of L-Met, however the supplementation of medium with approximately 0.3 mM L-Met concentration restores the growth of *C. glabrata* cells treated with L-PEN. It is worth noticing, that the estimated L-Met concentration in human serum is about 10-fold lower (Corso et al., 2017). The concentration of L-Met in a healthy individual is reported to be at a stable level, in a range of 0.027 mM and 0.031 mM, depending on a habitual diet group (Schmidt et al., 2016). Abnormal levels of L-Met concentration reaching up to 0.6 mM were however observed in patients suffering from liver-related diseases such as hepatic encephalopathy (Sato et al., 2013). In a previously reported study, Schenk et al. suggested that restoration of growth of plant pathogenic fungi treated with ISOX in

media containing L-Met could result from the competition in the uptake of amino acids and their antimetabolites (Schenk et al., 1991). Thus, it might be possible that ISOX and L-Met could be transported into the cell via the same transmembrane carriers, which show higher affinity towards L-Met. This assumption could explain the rescue of fungal growth in medium containing as little as 0.015 mM of L-Met. Nevertheless, in this respect, the usefulness of ISOX as a potential antifungal drug candidate seems doubtful. Nevertheless, the above results prove that blocking of the fungal L-Met pathway with L-PEN could not be rescued by the external L-Met at its normal concentration found in human serum.

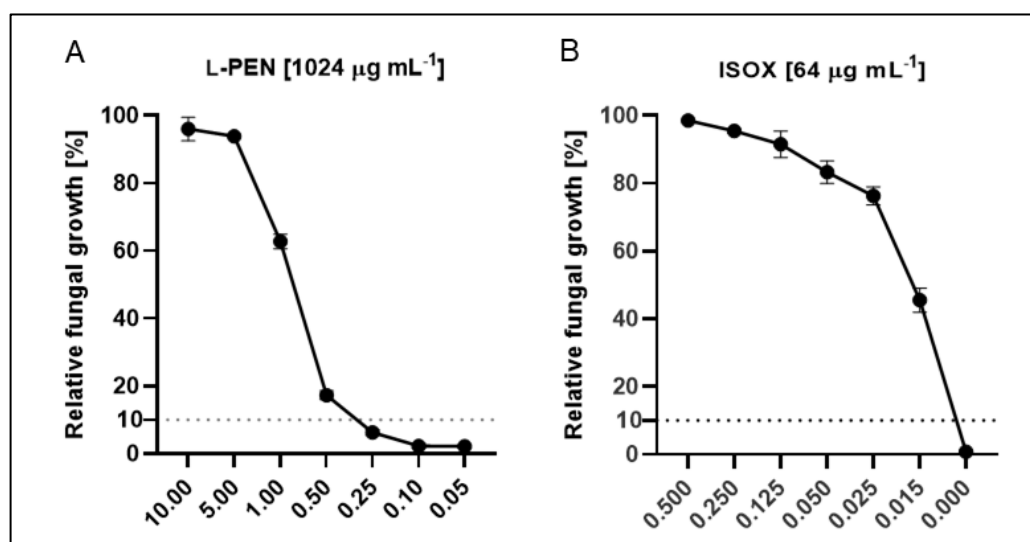


Fig. 32. *C. glabrata* growth inhibition by L-PEN (A) and ISOX (B) in YNB AS medium supplemented with L-Met in a concentration range from 0.00 mM to 10 mM. The 10% cell growth is represented by the dotted line, which serves as a borderline below which no growth is observed. The error bars represent \pm SD. Results partially published in (Kuplińska et al., 2022).

4.4.3. Assessment of the *CaMet2p*, *CaMet15p* and *CaStr2p* inhibitors interactions in combinations

Prior research has examined the antifungal effect of D-PEN in combination with fluconazole (FLU) against *C. albicans* (Li et al., 2019). The researchers found that D-PEN and FLU exhibited a synergistic effect against not only planktonic cells but also the biofilms of *C. albicans* strains that were resistant to and susceptible to FLU. The combined treatment reduced the fungal burden and raised the survival rate of *G. mellonella* larvae infected with *C. albicans*. It was found that the synergistic effect is linked to the prevention of morphological transformation, the disturbance of intracellular calcium homeostasis, and the activation of a metacaspase, which is intimately associated with cell apoptosis (Li et al., 2019).

One may expect that a synergistic growth inhibitory effect could be achieved for combination of inhibitors targeting two different enzymes of MBP. For the purpose of this study I performed a checkerboard dilution test for the assessment of interactions between L-PEN, i.e. inhibitor of *CaMet2p* and inhibitors of *CaMet15p* and *CaStr2p*,

related to the effect of L-PEN and FLU combination Data obtained are presented in Tab. 39. Determined MIC₉₀ values for individual compounds and in combination with L-PEN were used for the fractional inhibitory concentration index (FICI), that is broadly used for characterization of interaction type between two compounds; synergistic interaction (FICI ≤ 0.5), indifferent interaction (FICI > 0.5 do ≤ 4) or antagonistic interaction (FICI > 4).

The checkerboard dilution test results showed that the combination of AcDAB or DL-ALG with L-PEN demonstrated a synergistic antifungal effect against both tested *Candida* strains. Thus, it may be claimed that simultaneous inhibition of both fungal Met2p and Met15p, may lead to a more effective antifungal effect. Moreover, considering the differences between the two strains, in possessing only one, or both L-OAS pathway and transsulfuration pathway, respectively for *C. glabrata* and *C. albicans*, this combined antifungal effect is maintained. On the other hand, the combination of L-PEN with DL-GLUF was found to have an indifferent effect on fungal growth. This confirms that enzymes of the MBP are not the only ones affected by this compound, which is consistent with reports of DL-GLUF inhibitory effect against glutamine synthetase (Takano and Dayan, 2020). Indifferent effect could be also observed for the combination of L-PEN and ISOX, however some synergism is visible only in the lower concentration range of both compounds, but with no effect on the MIC₉₀ parameter (Fig. 33 G).

To better visualize the drug interactions, I used the Combenefit software to calculate the conjugation score according to the Loewe additivity model resulting in a heat map generation. I used the data from the *C. glabrata* checkerboard dilution test in the YNB GS medium. The drug interaction and growth percentage heat maps are shown in Fig. 33.

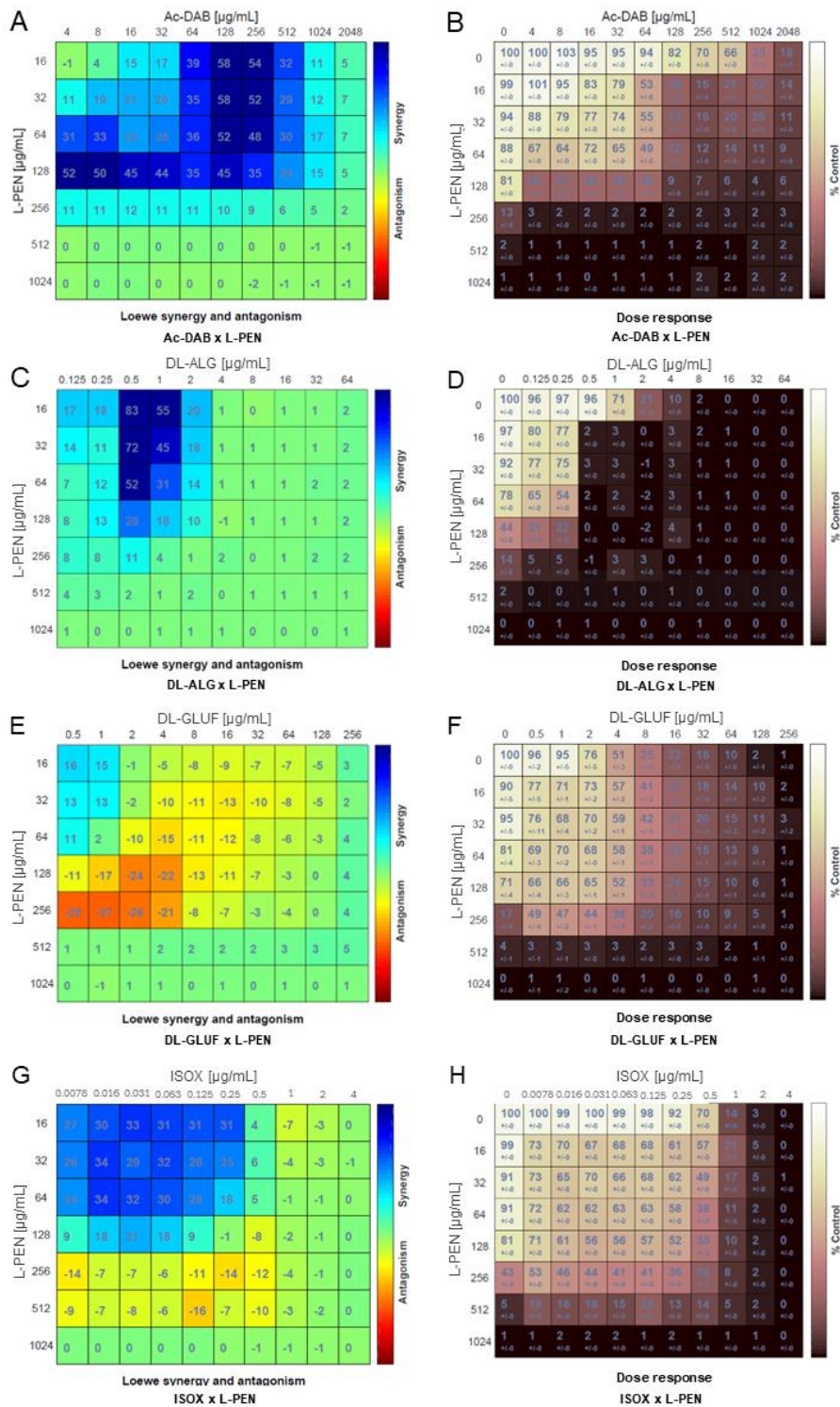


Fig. 33. Generated heat map of the checkerboard dilution test showing synergistic or antagonistic effect (A, C, E, G) between combination of L-PEN and Ac-DAB, DL-ALG, DL-GLUF or ISOX in YNB SG medium against *C. glabrata* ATCC 90030; blue color (synergistic effect); red color (antagonistic effect); green color (indifferent effect). Generated heat map of the checkerboard dilution test showing growth inhibition over an untreated control (B, D, F, H). Interaction effect scores were obtained using the Loewe additivity model via Combeneft software (Di Veroli et al., 2016).

Tab. 39. The checkerboard dilution test results of drug interaction between L-PEN and FLU, Ac-DAB, DL-ALG, or DL-GLUF against *C. glabrata* ATCC 90030 and *C. albicans* ATCC 10231. Test performed in a YNB GS medium without amino acids. Fractional Inhibitory Concentration Index (FICI). * Value used for FICI calculations, despite no MIC₉₀ observed at tested concentration. Synergistic effect (FICI ≤ 0.5), indifferent effect (FICI > 0.5 to ≤ 4), antagonistic effect (FICI > 4).

INHIBITOR	MIC ₉₀ [µg·mL ⁻¹]		FICI	EFFECT
	ALONE	COMBINATION		
<i>C. glabrata</i> ATCC 90030				
FLU	64	32	1.00	INDIFFERENT
L-PEN	512	256		
Ac-DAB	2048*	128	0.313	SYNERGY
L-PEN	512	128		
DL-ALG	8	0.5	0.0938	SYNERGY
L-PEN	512	16		
DL-GLUF	128	64	1.00	INDIFFERENT
L-PEN	512	256		
ISOX	2	1	1.50	INDIFFERENT
L-PEN	512	512		
<i>C. albicans</i> ATCC 10231				
Ac-DAB	1024	128	0.375	SYNERGY
L-PEN	1024	256		
DL-ALG	64	16	0.50	SYNERGY
L-PEN	1024	256		
DL-GLUF	256	512	1.50	INDIFFERENT
L-PEN	1024	1024		
ISOX	2	1	0.625	INDIFFERENT
L-PEN	1024	128		

4.5. Preliminary crystallization trials

Solving the protein crystal structure is the ultimate goal for the in-depth protein analysis. Determination of the atom coordinates and fitting them to the electron density of the crystal's asymmetric unit enables the building of the protein model (Rupp, 2009). A 3D-protein model provides a powerful tool for the determination of the relationship between the protein structure and the mechanism of reaction catalyzed by the enzyme leading to the assessment of the binding affinities of substrates and their analogues to the active site. This in consequence may lead to the design and development of an inhibitor that could become a long-awaited drug. For example, this structure-based design has been applied to yield Relenza (Zanamivir), an inhibitor of the neuraminidase enzyme used to treat the influenza virus (Mitrasinovic, 2010).

The spatial structure of proteins can be developed using three common methods; X-ray crystallography, nuclear magnetic resonance (NMR), or cryogenic electron microscopy (Cryo-EM), but approximately 90% of all protein models published in Protein Data Bank (PDB) were solved using the first method (Rupp, 2009). In fact, the method used for solving the crystal structure is not as important as crystal formation itself. Proteins are large and flexible macromolecules that in contrast to small molecules seldom assemble into regular repeating arrangements crucial for crystal formation, which makes obtaining a high-quality protein crystal challenging (Rupp, 2009). Moreover, proteins are vulnerable to shifts in temperature, pH, or hydration, thus variation in protein solution conditions comes with changes in protein properties such as charge or conformation. A single change of one of the parameters has an impact on the solubility of the protein, homogeneity of a sample, and as a result decrease in the crystal formation rate and crystal growth. Only a high-quality protein crystal will be suitable for X-ray crystallography; this includes a size preferably between 50 μm and 0.5 mm of an optimal shape and high internal order, allowing for a suitable X-ray diffraction pattern (Bergfors, 2009).

Optimization of conditions for protein crystal growth involves good planning, patience, and often a mysterious force called luck. One of the first steps requires a high-purity protein sample (>90%), that is then supersaturated, maintaining the equilibrium of the protein solubility (Wienczek, 1999). Prior determination of enzymes' optimal storage and those facilitating the activity is crucial for setting up crystallization trials since those should be performed immediately after protein purification to limit probability aggregation. Setting up a protein crystallization trial involves mixing a protein solution with versatile buffer solutions. A single screen experiment allows for testing of 96 different buffer solutions; however, this is usually not enough because the ratio between the protein solution and the buffer solution is also of high importance. Usually, one week after setting up the crystallization screen trials, if one is lucky, crystal candidates can be observed. Unfortunately, this does not mean the end of the crystallization journey, initial crystal candidates are usually small and of small resolution



not suitable for the diffraction analysis (Wiencek, 1999). Obtained best-hit conditions, must be then further optimized for a large high-quality crystal formation.

4.5.1. Bioinformatical prediction of crystallization success



Before performing crystallization trials, it is worth conducting bioinformatical analysis for the prediction of the crystallization success of a target protein. Based on the amino acid sequence of a protein, and crystallization data of its homologs, the XtalPred software (Slabinski et al., 2007) compares obtained data with the crystallization probability distribution calculated from TargetDB (Chen et al., 2004). Simply speaking, the XtalPred predicts biochemical and biophysical features that are used to assign the protein into one of five protein crystallization classes: optimal, suboptimal, average, difficult, and very difficult (Tab. 40) (Slabinski et al., 2007).

The software examines 10 parameters:

1. Amino acid sequence length
2. Grand average of hydropathy index (GRAVY), a measure of hydrophobicity or hydrophilicity of a protein, where a positive score means hydrophobicity and a negative score means hydrophilicity (Chang and Yang, 2013)
3. Instability index
4. Isoelectric point (pI)
5. Coiled-coil regions
6. Longest disorder of coil structure
7. Predicted percentage of coil structure presence in the secondary structure
8. Insertions score in multiple sequence alignment
9. Number of homologs in non-redundant (NR) database of protein sequence
10. Number of homologs in Protein Data Bank (PDB)

Prediction of crystallization success is made via a combination of individual probabilities of crystallization; however, individual features may indicate an unsuccessful probability of crystallization. A summary of the determination of crystallization success performed by XtalPred software is given in Tab. 40.

Tab. 40. Bioinformatic analysis of *C. albicans* Met2p, Str2p, and Met15p recombinant proteins probability of crystals formation. Analysis was performed with XtaPred software (Slabinski et al., 2007). Predicted crystallization classes were color-coded according to the scheme given by the program: EP, crystallization class prediction by Expert Pool method; RF, crystallization class prediction by Random Forest method. Calculated features indicated by the program as those indicating crystallization problems are highlighted in grey color.

Protein name	CaMet2p	CaMet2NHp	CaMet15p	CaMet15NHp	CaStr2p	CaStr2NHp
EP class	4	4	1	2	5	5
RF - class	9	10	3	4	8	8
Length	409	415	440	446	595	601
Gravy index	-0.32	-0.36	-0.22	-0.26	-0.37	-0.40
Instability index (II)	33.44	34.37	25.74	25.76	47.00	46.80
Isoelectric point (pI)	5.20	5.60	5.59	5.87	5.66	5.91
Coiled coils	0	0	0	0	21	21
Longest disorder of coil structure	15	29	3	13	42	39
% of coil structure	54	52	46	47	47	47
Insertions score	0.20	0.20	0.17	0.18	0.21	0.21
Homologs in NR (clustered to 60% sequence identity)	897	890	1057	1054	1139	1140
Homologs in PDB	21	21	152	161	120	120
EP crystallization classes ↓ Most promising  ↑ Least promising			RF crystallization classes ↓ Most promising  Least promising ↑			

The above results indicate that both CaMet15p and CaMet15NHp enzymes have the greatest probability of crystallization. CaMet15p was assigned to 1st and 3rd crystallization class prediction by Expert Pool method (EP) and crystallization class prediction by Random forest method (CR), respectively. CaMet15NHp was assigned to the 2nd and 4th of respectively, EP and CR crystallization class. On the other hand, scores for CaMet2p and CaMet2NHp as well as CaStr2p and CaStr2NHp indicate that these proteins have a low chance of forming crystals. CaMet2p and CaMet2NHp were assigned to the 4th EP crystallization class whereas CaStr2p and CaStrNHp were assigned to the 5th EP crystallization class. According to results generated via XtalPred, CaStr2p, and CaStr2NHp contain a high core of the longest disorder of coil structure (42 and 39 for CaStr2p and CaStr2NHp, respectively), which significantly reduces the probability of crystal formation by these proteins.

I have performed preliminary crystallization trials for CaMet15NHp and, despite the discouraged results, for CaMet2NHp and CaStr2NHp. I decided to perform trials on N-terminus 6xHistagged recombinant versions of all proteins, because of the reduced time needed for purification, very good purity parameters, and determined biochemical properties of all three enzymes.

4.5.2. Optimization of crystallization conditions

A high purity level, estimated to be >90% is crucial for protein crystal formation, since the presence of impurities influences homogeneity of a sample and decreases crystallization success (Wiencek, 1999). I performed a purification of proteins using affinity chromatography followed by size exclusion chromatography as described in 3.2.23. Obtained protein samples were next concentrated using Amicon Ultra Centrifugal Filter Units to obtain a protein solution of at least 2 mg mL⁻¹. The summary obtained protein samples ready for crystallization trials are given in Tab. 41. The CaMet15NHp was easily concentrated to at least 10 mg mL⁻¹ solution, in contrast to CaMet2NHp and CaStr2NHp. The latter two precipitated during concentration or displayed a tendency to bind to the surface of a cellulose membrane found on Amicon Ultra Centrifugal Filters units, which disabled high concentrations of CaMet2NHp and CaStr2NHp protein solutions. I attempted to dialyze CaMet2NHp against PEG 6.000 with no success. Exchange of buffer from 50 mM HEPES pH 7.5, 500 mM NaCl, 20 mM imidazole to 40 mM Tris-HCl pH8.0, 0.75M Trehalose facilitated CaMet2NHp stability and allowed for its concentration to 5.5 mg mL⁻¹.

Tab. 41. Summary of protein samples prepared for crystallization trials. Values are given for protein samples after SEC and concentration.

	CaMet2NHp	CaMet15NHp	CaStr2NHp
Purity level [%]	94.5%	96.0	92%
Concentration [mg mL ⁻¹]	5.5	15.0	2.5
Concentrated sample volume [μL]	150	500	100
Recovery [%]	70.5	97.8	53.4

I performed crystallization trials immediately after obtaining a concentrated protein solution or on the next day, with storage of a protein solution overnight at 4°C. I set up the crystallization screening plates at room temperature and one plate at 4°C (lower temperature decreases the process of protein crystallization allowing a more ordered structure formation) (Pusey and Gernert, 1988). I have also tried two methods for crystallization trials, a sitting and hanging drop vapor diffusion method. The sitting drop method is perfect for screening of many different conditions, it requires less volume of protein samples and buffers and can be automated. The hanging drop method is more time and volume-consuming but can result in a larger crystal formation; I used it only for optimization of the best hit conditions. Several sitting drop crystallization plates were performed in cooperation with the Institute of Bioorganic

Chemistry of the Polish Academy of Sciences in Poznań using a Crystal Gryphon protein crystallography dispenser (Art Robbins Instruments). Crystallization trials were set using a ranging protein solution concentration from 2 mg mL⁻¹ to 20 mg mL⁻¹, depending on the proteins' ability to concentrate. Various ratios (protein solution: crystallization buffer) were tested i.e. 1:1, 1:2, 2:1; 1:3; 3:1; 2:3; 3:2. Several screening kits from Hampton Research and Molecular Dimensions were used resulting in approximately 3,000 single droplet crystallization trials of CaMet15NHp, CaMet2NHp, and CaStr2NHp. The screening experiments did not result in protein crystal formation of CaMet2NHp or CaStr2NHp, therefore no best-hit condition was chosen for further optimization. However, the screening of best hit conditions for CaMet15NHp crystallization resulted in the establishment of four conditions: A) 0.2 M ammonium citrate tribasic pH 7.0, 20% w/v Polyethylene glycol 3,350; B) 0.1 M Tris pH 8.5, 0.3 M magnesium formate dihydrate; C) 0.2 M Potassium sodium tartrate tetrahydrate, 0.1 M Sodium citrate tribasic dihydrate pH 5.6, 2.0 M Ammonium sulfate; and D) 0.2 M lithium citrate tribasic tetrahydrate pH 8.4, 20% w/v Polyethylene glycol 3,350. In three conditions (A, B, D), the CaMet15NHp crystals were observed in the form of abundant in number long needles, whereas in condition C) it formed unregular cuboids (Fig. 34). To confirm the protein character of formed crystals I dyed the crystals with methylene blue, the crystals absorbed the dye and changed color to blue proving their origination from the CaMet15NHp (Fig. 34 A). The crystals that were formed in 0.1 M Tris pH 8.5, 0.3 M magnesium formate dihydrate buffer system, were highly abundant in number but were represented by long thin 2D needles, not suitable for diffraction analysis (Fig. 34 B). The two crystals, from conditions C and D, were sent via the Institute of Bioorganic Chemistry of the Polish Academy of Sciences in Poznań for a synchrotron diffraction analysis. Cuboid crystals obtained in condition 0.2 M potassium sodium tartrate tetrahydrate, 0.1 M Sodium citrate tribasic dihydrate pH 5.6, 2.0 M ammonium sulfate (Fig. 34 C) resulted in a blurred low diffraction of a low resolution (~20 Å). Thicker needles formed in condition D (0.2 M lithium citrate tribasic tetrahydrate pH 8.4, 20% w/v Polyethylene glycol 3,350) diffracted the X-rays to a resolution of 7 Å, which is still too low so that it could be used to solve the protein structure with a high degree detail. For the generation of a 3D protein model, a high-quality diffraction pattern of a resolution below 2 Å must be obtained (Su et al., 2015).

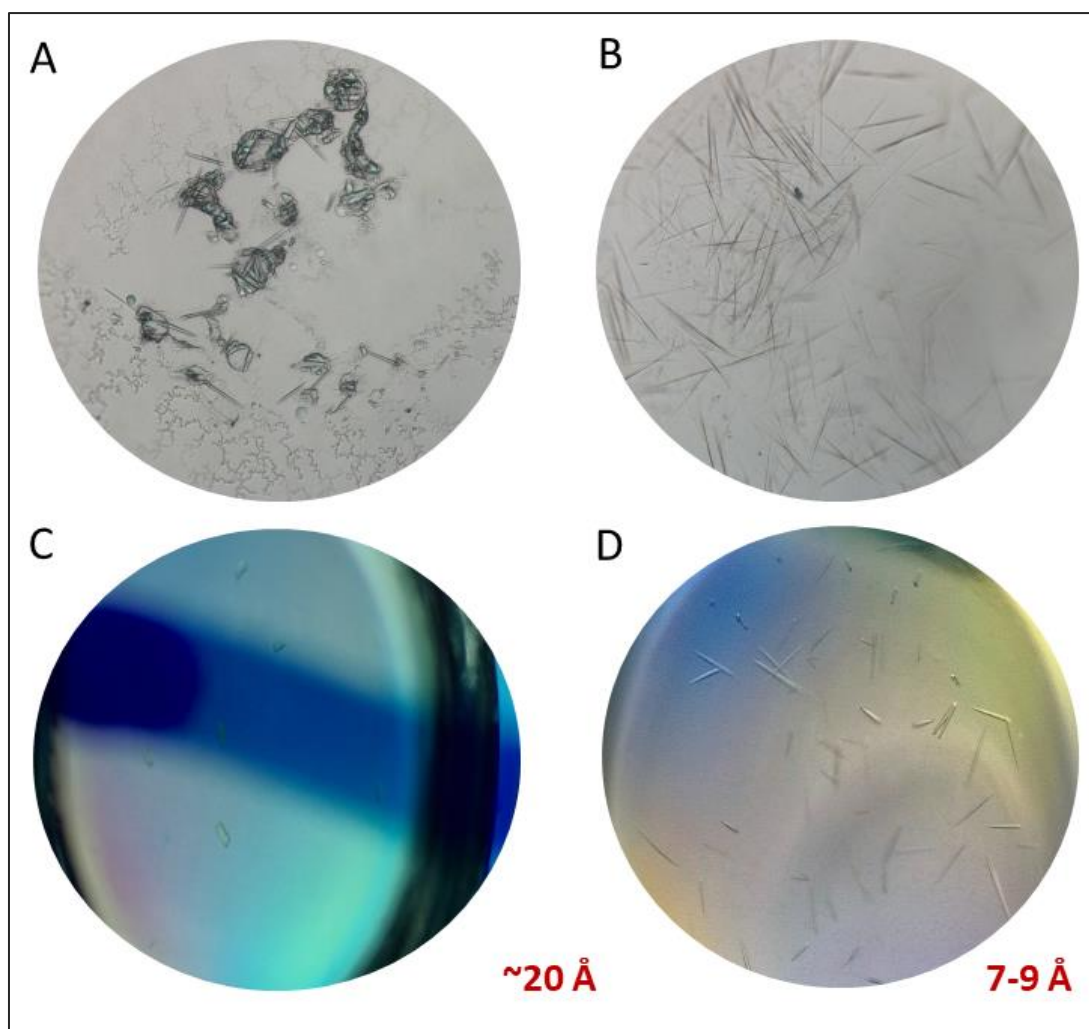


Fig. 34. Formed CaMet15NHp crystals in different buffer systems. **A.** 0.2 M ammonium citrate tribasic pH 7.0, 20% w/v polyethylene glycol 3,350 (dyed with methylene blue); **B.** 0.1 M Tris pH 8.5, 0.3 M magnesium formate dihydrate; **C.** 0.2 M Potassium sodium tartrate tetrahydrate, 0.1 M Sodium citrate tribasic dihydrate pH 5.6, 2.0 M ammonium sulfate (performed in cooperation with the Institute of Bioorganic Chemistry of the Polish Academy of Sciences in Poznań); **D.** 0.2 M lithium citrate tribasic tetrahydrate pH 8.4, 20% w/v Polyethylene glycol 3,350 (performed in cooperation with the Institute of Bioorganic Chemistry of the Polish Academy of Sciences in Poznań). Crystals were formed using a sitting-drop vapor diffusion method.

Several attempts can be made to improve the crystallization of CaMet15NHp and yield better-quality protein crystals:

1. Further optimization of best hit conditions, throughout the change in pH, protein concentration, and ratio. Setting up crystallization trials at 4°C.
2. Optimize the crystallization method. Change in the volume of the sitting drop method, setting up trials using the hanging drop method or by performing crystallization seeding.
3. Screen additives that could facilitate protein stability in crystallization buffer conditions.
4. Adding substrates, PLP, or an inhibitor to the crystallization sample to increase enzyme stability.

Despite the predicted by bioinformatical analysis of the low success of crystallization of CaMet2NHp and CaStr2NHp proteins, some ideas could be applied to yield crystal formation:

1. Production of highly concentrated protein samples, in the presence of stabilizing agents such as trehalose, substrates, or PLP.
2. Concentration of protein sample using milder methods e.g. dialysis against carboxymethyl cellulose, or Amicon Stirred Cell units, that do not require centrifugation.
3. Crystallization of the native CaMet2p enzyme, with prior optimization of the purification process for high-purity sample preparation.

Due to the limited time allocated for dissertation preparation, none of these attempts were pursued.

5. CONCLUSIONS

The research project, results of which are described in this dissertation has been aimed at characterization of three enzymes, Met2p, Met15p, and Str2p, involved in the *C. albicans* L-methionine biosynthesis pathway (MBP) in *C. albicans* as novel potential molecular targets for antifungal chemotherapy. Using thorough investigation and analysis, valuable insights have been gained into enhanced understanding of the *C. albicans*, *C. glabrata*, and *S. cerevisiae* MBP, as well as into the development of enzyme inhibitors exhibiting antifungal activity. As the result of extensive research and scholarly inquiry, this dissertation contributes to the existing body of knowledge in the field of fungal infection prevention, offering new perspectives and avenues for further investigation. Below I am providing key findings of the conducted research.

- Genes encoding three enzymes involved in the MBP, namely Met2p, Met15p, and Str2p have been identified in the *C. albicans* genome, cloned and expressed in *E. coli* host cells. Three versions of expression vectors were constructed, encoding a wild-type proteins and two recombinant versions with added 6xHisTag to either C- or N- terminus. Optimization of protein expression resulted in efficient protein production of a wild-type version of the CaMet2p and two recombinants, CaMet2CHp and CaMet2NHp, and a moderate level of CaMet15p and CaStr2p production in the form of both C- and N- terminus 6xHisTagged versions. Purification of expressed proteins enabled their further examination leading to characteristics of biochemical properties.
- Purified CaMet2p, CaMet2CHp, and CaMet2NHp exhibited the activity of homoserine *O*-acetyltransferase, catalyzing the reaction of *O*-acetyl-L-homoserine (L-OAH) formation from L-homoserine and acetyl-Coenzyme A. Introduction of 6xHistag domains did not influence enzymatic activity and kinetic parameters. Purified CaMet15CHp and CaMet15NHp displayed the activity of the *O*-acetylhomoserine sulfhydrylase converting L-OAH and a sulfide ion to yield L-homocysteine. Both recombinant enzyme versions were comparably active. CaMet15p reacts only with L-OAH but not L-OAS, thus it does not act as a bifunctional enzyme. Purified CaStr2CHp and CaStr2NHp presented cystathionine- γ -synthase activity utilizing L-OAH and L-cysteine to form L-cystathionine. Similarly, two recombinant 6xHisTagged versions displayed activity on a comparable level.
- Several commercially available compounds and 5 compounds designed and synthesized in our research group, structural analogs of enzymes' substrates were tested as potential inhibitors of CaMet2NHp, CaMet15NHp, and CaStr2NHp. Three compounds displayed ~70% inhibitory activity towards tested enzymes at 10 mM. L-4-acetamido-2-aminobutanoic acid (Ac-DAB) and β -(5-oxo-3-isoxazolin-2-yl)-L-alanine (ISOX) were effective against

CaMet15NHp and CaStr2NHp, but 2.5 mM of L-penicillamine (L-PEN) inhibited CaMet2NHp. All examined enzymes were insignificantly prone to feedback inhibition induced by L-Met.

- L-PEN was found to function as a noncompetitive inhibitor of CaMet2NHp enzyme with $K_i = 1.62$ mM
- Selected inhibitors were tested for antifungal activity in RPMI medium and minimal YNB medium conditionally supplemented with L-Met. Obtained results exposed the relationship between L-Met presence in the medium and the antifungal effect induced by L-PEN, Ac-DAB, and ISOX, thus confirming MBP targeting.
- *C. glabrata* and *S. cerevisiae* were more susceptible to L-PEN as they possess a single pathway leading to L-cysteine production, which could be then used as a precursor for L-Met biosynthesis.
- The growth inhibition of *C. glabrata* caused by L-PEN could be rescued by the addition of 0.3 mM L-Met concentration, which is 10-fold higher than the concentration of this amino acid in human serum. This is one of the far most important conclusions, as it proves the assumption that MBP can serve as a source of new molecular targets for antifungal chemotherapy.
- The lowest MIC₉₀ value against *C. albicans* in the RPMI medium, resembling human physiological plasma content, was found for L-PEN and was equal to 64 $\mu\text{g mL}^{-1}$.
- The combination of L-PEN and Ac-DAB or DL-2-allylglycine (DL-ALG) resulted in a synergistic effect and enhanced antifungal effect.
- Performed crystallization attempts of CaMet2NHp, CaMet15NHp, and CaStr2NHp resulted in observable CaMet15NHp crystal formation. Obtained crystals resulted in a low-resolution diffraction pattern of up to 7 Å, which is insufficient for solving a high degree of detailed protein structure.

To close, in my studies, results of which are described in this dissertation I have explored three enzymes of the MBP in *C. albicans*. Through the characterization of these enzymes, I have shed some more light on the usefulness of MBP as a source of molecular targets for novel antifungal agents, offering insights into the development of more effective inhibitors of enzymes involved in MBP. While this study has contributed to the understanding of *C. albicans* MBP, there remain possibilities for further investigation, particularly in the crystallization and solving structure of CaMet2p, CaMet15p, and CaStr2p. Overall, this work underscores the importance of searching for novel antifungal agents with a side effects-free mechanism of action. I hope that results and conclusions from this work should catalyze continued inquiry and further advancement in the field.



ACKNOWLEDGMENTS

The research presented in this dissertation was funded from the grant of the National Science Centre (OPUS 20) No. 2020/39/B/NZ7/01519 entitled 'Enzymes of the L-methionine biosynthetic pathway as novel molecular targets for antifungal chemotherapy'.

Project manager: Iwona Gabriel, PhD, DSc, Eng.

The LC-MS analysis was performed using equipment funded by the Foster Foundation (USA).

I would like to thank Piotr Szweda, PhD, DSc, Eng. from the Department of Pharmaceutical Technology and Biochemistry, Gdansk University of Technology for sharing the clinical isolates strains of *C. glabrata*.

SCIENTIFIC ACHIEVEMENTS

ARTICLES PUBLISHED IN SCIENTIFIC JOURNALS

1. **Kuplińska, A.**, & Rząd, K. (2021).
Molecular targets for antifungals in amino acid and protein biosynthetic pathways.
Amino Acids, 54, 961-991.
doi.org/10.1007/s00726-021-03007-6.
2. **Kuplińska, A.**, Rząd, K., Wojciechowski, M., Milewski, S., & Gabriel, I. (2022).
Antifungal Effect of Penicillamine Due to the Selective Targeting of L-Homoserine O-Acetyltransferase.
International Journal of Molecular Sciences, 23(14), 7763.
doi.org/10.3390/ijms23147763.
3. Rząd, K., Gabriel, I., Paluszkiwicz, E., **Kuplińska, A.**, Olszewski, M., Chylewska, A., Dąbrowska, A. M., & Kozłowska-Tylingo, K. (2024).
Targeting yeast topoisomerase II by imidazo and triazoloacridinone derivatives resulting in their antifungal activity.
Scientific Reports, 14(1), 3594.
doi.org/10.1038/s41598-024-54252-0.

SCIENTIFIC CONFERENCES

1. **Kuplińska, A.**, Rząd, K., Milewski, S.
6th International Conference of Cell Biology. 06th - 08th November 2020.
Cracow, Poland, on-line
Oral presentation: 'Construction of the recombinant cystathionine gamma synthase of L-methionine biosynthetic pathway from *Candida albicans*'.
2. **Kuplińska, A.**, Rząd, K., Milewski, S., Gabriel, I.
VI Pomorskie Spotkania z Mikrobiologią. 24th -25th June 2021.
Gdańsk, Poland, on-line.
Poster presentation: 'Konstrukcja rekombinantowej transacetylazy homoserynowej ze szlaku biosyntezy L-metioniny z *Candida albicans*'.
3. **Stefaniak, J.**, **Kuplińska, A.**, Gabriel, I., Milewska, M.
22nd Tetrahedron Symposium. 28th June - 1st July 2022.
Lisbon, Portugal.
Poster presentation: 'Synthesis and antifungal evaluation of potential inhibitors of the L-methionine biosynthesis pathway in pathogenic fungal cells'.



4. **Kuplińska, A.**, Rząd, K., Gabriel, I., Milewski, S.
25th IUBMB Congress, the 46th FEBS Congress the 15th PABMB Congress,
The Biochemistry Global Summit. 9th - 14th July 2022.
Lisbon, Portugal.
Poster presentation: 'Repression of L-methionine dependent fungal growth by L-penicillamine'.
5. **Kuplińska, A.**, Stefaniak, J., Rząd, K., Gabriel, I., Kozłowska-Tylingo, K., Milewski, S.
5th Congress of Polish Biosciences BIO 2023: 'Different faces of biosciences'
52nd Meeting of the Polish Biochemical Society. 13th - 16th September 2023.
Szczecin, Poland.
Poster presentation: '*Candida albicans* O-acetyl-L-homoserine sulfhydrylase (Met 15) characterisation with the use of a novel RP HPLC MS method'.
6. **Składanek, E., Kuplińska, A.**, Rząd, K.
TYGIEL 2024: 'Interdyscyplinarność kluczem do rozwoju'. 21st – 24th March 2024.
Lublin, Poland.
Poster presentation: 'Optymalizacja warunków krystalizacji enzymu reduktazy sacharopiny z *C. albicans*'.
7. **Gabriel, I., Kuplińska, A.**, Stefaniak-Skorupa, J., Rząd, K., Milewski, S.
24th Tetrahedron Symposium. 18th – 21st June 2024.
Montpellier, France
Poster presentation: '*O*-Acetyl-L-homoserine sulfhydrylase: molecular target for antifungals in methionine biosynthetic pathway'.

PARTICIPATION IN PROJECTS

1. **OPUS 20, National Science Centre.**
Participation in project: 2020/39/B/NZ7/0151, 'Enzymes of the L-methionine biosynthetic pathway as novel molecular targets for antifungal chemotherapy'.
Project manager: Iwona Gabriel, PhD, DSc, Eng.
2. **ARGENTUM - 'Excellence Initiative Research University' program Gdańsk University of Technology.**
Participation in project: DEC-24 2020 /IDUB/I.3.3, 'Pochodne akrydyny i akrydonu o aktywności inhibicyjnej wobec grzybowej topoizomerazy DNA jako potencjalne leki przeciwgrzybowe'.
Project manager: Kamila Rząd, PhD, DSc, Eng.



REFERENCES

- Aitken, S. M., Kim, D. H., and Kirsch, J. F. (2003). *Escherichia coli* cystathionine γ -synthase does not obey ping-pong kinetics. Novel continuous assays for the elimination and substitution reactions. *Biochemistry* 42, 11297–11306. doi:10.1021/bi035107o.
- Ajetunmobi, O. H., Badali, H., Romo, J. A., Ramage, G., and Lopez-Ribot, J. L. (2023). Antifungal therapy of *Candida* biofilms: Past, present and future. *Biofilm* 5, 100126. doi:10.1016/j.biofilm.2023.100126.
- Al-Samarrai, T. H., Jones, W. T., Harvey, D., Kirk, C. A., and Templton, M. (2013). Effect of 4% glycerol and low aeration on result of expression in *Escherichia coli* of Cin3 and three *Venturia inaequalis* EST's recombinant proteins. *Am. J. Mol. Biol.* 03, 1–9. doi:10.4236/ajmb.2013.31001.
- Alexander, F. W., Sandmeier, E., Mehta, P. K., and Christen, P. (1994). Evolutionary relationships among pyridoxal-5'-phosphate-dependent enzymes: Regio-specific α , β and γ families. *Eur. J. Biochem.* 219, 953–960. doi:10.1111/j.1432-1033.1994.tb18577.x.
- Altschul, S. F., Gish, W., Miller, W., Myers, E. W., and Lipman, D. J. (1990). Basic local alignment search tool. *J. Mol. Biol.* 215, 403–410. doi:10.1016/S0022-2836(05)80360-2.
- Amich, J., Dümig, M., O'Keeffe, G., Binder, J., Doyle, S., Beilhack, A., et al. (2016). Exploration of sulfur assimilation of *Aspergillus fumigatus* reveals biosynthesis of sulfur-containing amino acids as a virulence determinant. *Infect. Immun.* 84, 917–929. doi:10.1128/IAI.01124-15.
- Aoki, Y., Kamiyama, T., Fujii, T., Yamamoto, M., Ohwada, J., and Arisawa, M. (1995). Design of an antifungal methionine inhibitor not antagonized by methionine. *Biol. Pharm. Bull.* 18, 1267–1271. doi:10.1248/bpb.18.1267.
- Aoki, Y., Yamamoto, M., Hosseini-Mazinani, S. M., Koshikawa, N., Sugimoto, K., and Arisawa, M. (1996). Antifungal azoxybacilin exhibits activity by inhibiting gene expression of sulfite reductase. *Antimicrob. Agents Chemother.* 40, 127–132. doi:10.1128/aac.40.1.127.
- Azevedo, M. M., Faria-Ramos, I., Cruz, L. C., Pina-Vaz, C., and Gonçalves Rodrigues, A. (2015). Genesis of azole antifungal resistance from agriculture to clinical settings. *J. Agric. Food Chem.* 63, 7463–7468. doi:10.1021/acs.jafc.5b02728.
- Bae, N. S., Seberg, A. P., Carroll, L. P., and Swanson, M. J. (2017). Identification of genes in *Saccharomyces cerevisiae* that are haploinsufficient for overcoming amino acid starvation. *G3 Genes, Genomes, Genet.* 7, 1061–1084. doi:10.1534/g3.116.037416.
- Basu, T., and Poddar, R. K. (1994). Effect of ethanol on *Escherichia coli* cells. Enhancement of DNA synthesis due to ethanol treatment. *Folia Microbiol. Off. J. Inst. Microbiol. Acad. Sci. Czech Repub.* 39, 3–6. doi:10.1007/BF02814520.
- Baugh, L., Phan, I., Begley, D. W., Clifton, M. C., Armour, B., Dranow, D. M., et al. (2015).

Increasing the structural coverage of tuberculosis drug targets. *Tuberculosis* 95, 142–148. doi:10.1016/j.tube.2014.12.003.

Bergfors, T. M. (2009). *Protein Crystallization, Second Edition*. 2nd Edition. , ed. T. M. Bergfors California: International University Line.

Blackwell, J. R., and Horgan, R. (1991). A novel strategy for production of a highly expressed recombinant protein in an active form. *FEBS Lett.* 295, 10–12. doi:10.1016/0014-5793(91)81372-F.

Bongomin, F., Gago, S., Oladele, R. O., and Denning, D. W. (2017). Global and multi-national prevalence of fungal diseases—estimate precision. *J. Fungi* 3, 57. doi:10.3390/jof3040057.

Bradford, M. M. (1976). A rapid and sensitive method for the quantitation of microgram quantities of protein utilizing the principle of protein-dye binding. *Anal. Biochem.* 72, 248–254. doi:10.1016/0003-2697(76)90527-3.

Brown, G. D., Denning, D. W., Gow, N. A. R., Levitz, S. M., Netea, M. G., and White, T. C. (2012). Hidden killers: Human fungal infections. *Sci. Transl. Med.* 4, 1–10. doi:10.1126/scitranslmed.3004404.

Brzovic, P., Holbrook, E. L., Greene, R. C., Dunn, M. F., Brzovic, P., Holbrook, E. L., et al. (1990). Reaction Mechanism of Escherichia coli Cystathionine γ -Synthase: Direct Evidence for a Pyridoxamine Derivative of Vinylglyoxylate as a Key Intermediate in Pyridoxal Phosphate Dependent γ -Elimination and γ -Replacement Reactions. *Biochemistry* 29, 442–451. doi:10.1021/bi00454a020.

Brzywczy, J., and Paszewski, A. (1993). Role of *O*-acetylhomoserine sulfhydrylase in sulfur amino acid synthesis in various yeasts. *Yeast* 9, 1335–1342. doi:10.1002/yea.320091207.

Cavassin, F. B., Baú-Carneiro, J. L., Vilas-Boas, R. R., and Queiroz-Telles, F. (2021). Sixty years of Amphotericin B: An Overview of the Main Antifungal Agent Used to Treat Invasive Fungal Infections. *Infect. Dis. Ther.* 10, 115–147. doi:10.1007/s40121-020-00382-7.

Chang, K. Y., and Yang, J. R. (2013). Analysis and Prediction of Highly Effective Antiviral Peptides Based on Random Forests. *PLoS One* 8. doi:10.1371/journal.pone.0070166.

Chaton, C. T., Rodriguez, E. S., Reed, R. W., Li, J., Kenner, C. W., and Korotkov, K. V. (2019). Structural analysis of mycobacterial homoserine transacetylases central to methionine biosynthesis reveals druggable active site. *Sci. Rep.* 9, 1–11. doi:10.1038/s41598-019-56722-2.

Chen, L., Oughtred, R., Berman, H. M., and Westbrook, J. (2004). TargetDB: A target registration database for structural genomics projects. *Bioinformatics* 20, 2860–2862. doi:10.1093/bioinformatics/bth300.

Cherest, H., and Surdin-Kerjan, Y. (1992). Genetic analysis of a new mutation conferring

- cysteine auxotrophy in *Saccharomyces cerevisiae*: Updating of the sulfur metabolism pathway. *Genetics* 130, 51–58. doi:10.1093/genetics/130.1.51.
- Chhetri, G., Kalita, P., and Tripathi, T. (2015). An efficient protocol to enhance recombinant protein expression using ethanol in *Escherichia coli*. *MethodsX* 2, 385–391. doi:10.1016/j.mex.2015.09.005.
- Cieśliński, H., Kur, J., Białkowska, A., Baran, I., Makowski, K., and Turkiewicz, M. (2005). Cloning, expression, and purification of a recombinant cold-adapted β -galactosidase from antarctic bacterium *Pseudoalteromonas* sp. 22b. *Protein Expr. Purif.* 39, 27–34. doi:10.1016/j.pep.2004.09.002.
- Clark, T. A., and Hajjeh, R. A. (2002). Recent trends in the epidemiology of invasive mycoses. *Curr. Opin. Infect. Dis.* 15, 569–574. doi:10.1097/00001432-200212000-00003.
- Clausen, T., Huber, R., Prade, L., Wahl, M. C., and Messerschmidt, A. (1998). Crystal structure of *Escherichia coli* cystathionine γ -synthase at 1.5 Å resolution. *EMBO J.* 17, 6827–6838. doi:10.1093/emboj/17.23.6827.
- Corso, G., Cristofano, A., Sapere, N., La Marca, G., Angiolillo, A., Vitale, M., et al. (2017). Serum amino acid profiles in normal subjects and in patients with or at risk of Alzheimer dementia. *Dement. Geriatr. Cogn. Dis. Extra* 7, 143–159. doi:10.1159/000466688.
- Dayan, F. E., Barker, A., Bough, R., Ortiz, M., Takano, H., and Duke, S. O. (2019). Herbicide Mechanisms of Action and Resistance. *Compr. Biotechnol.*, 36–48. doi:10.1016/B978-0-444-64046-8.00211-1.
- De Pascale, G., Nazi, I., Harrison, P. H. M., and Wright, G. D. (2011). β -Lactone natural products and derivatives inactivate homoserine transacetylase, a target for antimicrobial agents. *J. Antibiot. (Tokyo)*. 64, 483–487. doi:10.1038/ja.2011.37.
- Denning, D. W. (2002). Echinocandins: A new class of antifungal. *J. Antimicrob. Chemother.* 49, 889–891. doi:10.1093/jac/dkf045.
- Denning, D. W. (2024). Global incidence and mortality of severe fungal disease. *Lancet Infect. Dis.* doi:10.1016/S1473-3099(23)00692-8.
- Di Veroli, G. Y., Fornari, C., Wang, D., Mollard, S., Bramhall, J. L., Richards, F. M., et al. (2016). Combenefit: An interactive platform for the analysis and visualization of drug combinations. *Bioinformatics* 32, 2866–2868. doi:10.1093/bioinformatics/btw230.
- Ding, N., Jiang, Y., Han, L., Chen, X., Ma, J., Qu, X., et al. (2016). Bafilomycins and odoriferous sesquiterpenoids from *Streptomyces albolongus* isolated from *Elephas maximus* feces. *J. Nat. Prod.* 79, 799–805. doi:10.1021/acs.jnatprod.5b00827.
- Dittmer, K., Goering, H. L., Goodman, I., and Cristol, S. J. (1948). The Inhibition of Microbiological Growth, by Allylglycine, Methallylglycine and Crotylglycine. *J. Am. Chem. Soc.* 70, 2499–2501. doi:10.1021/ja01187a057.

- Du, Y. L., and Ryan, K. S. (2019). Pyridoxal phosphate-dependent reactions in the biosynthesis of natural products. *Nat. Prod. Rep.* 36, 430–457. doi:10.1039/c8np00049b.
- Fisher, M. C., and Denning, D. W. (2023). The WHO fungal priority pathogens list as a game-changer. *Nat. Rev. Microbiol.* 21, 211–212. doi:10.1038/s41579-023-00861-x.
- Foyn, H., Thompson, P. R., and Arnesen, T. (2017). “DTNB-based quantification of in vitro enzymatic N-terminal acetyltransferase activity,” in *Methods in Molecular Biology*, ed. O. Schilling (New York: Humana Press Inc.), 9–15. doi:10.1007/978-1-4939-6850-3_2.
- Frändberg, E., Petersson, C., Lundgren, L. N., and Schnürer, J. (2000). *Streptomyces halstedii* K122 produces the antifungal compounds bafilomycin B1 and C1. *Can. J. Microbiol.* 46, 753–758. doi:10.1139/w00-050.
- Fujiu, M., Sawairi, S., Shimada, H., Takaya, H., Aoki, Y., Okuda, T., et al. (1994). Azoxybacilin, a Novel Antifungal Agent Produced by *Bacillus Cereus*: NR2991 Production, Isolation and Structure Elucidation. *J. Antibiot. (Tokyo)*. 47, 833–835. doi:10.7164/antibiotics.47.833.
- Gabriel, I., Kur, K., Laforce-Nesbitt, S. S., Pulickal, A. S., Bliss, J. M., and Milewski, S. (2014). Phenotypic consequences of *LYS4* gene disruption in *Candida albicans*. *Yeast* 31, 299–308. doi:10.1002/yea.3021.
- Gasteiger, E., Gattiker, A., Hoogland, C., Ivanyi, I., Appel, R. D., and Bairoch, A. (2003). ExPASy: The proteomics server for in-depth protein knowledge and analysis. *Nucleic Acids Res.* 31, 3784–3788. doi:10.1093/nar/gkg563.
- Gasteiger, E., Hoogland, C., Gattiker, A., Duvaud, S., Wilkins, M. R., Appel, R. D., et al. (2005). “Protein Identification and Analysis Tools on the ExPASy Server,” in *The Proteomics Protocols Handbook* (Humana Press), 571–607. doi:10.1385/1-59259-890-0:571.
- Gophna, U., Baptiste, E., Doolittle, W. F., Biran, D., and Ron, E. Z. (2005). Evolutionary plasticity of methionine biosynthesis. *Gene* 355, 48–57. doi:10.1016/j.gene.2005.05.028.
- Haidar, G., and Singh, N. (2018). How we approach combination antifungal therapy for invasive aspergillosis and mucormycosis in transplant recipients. *Transplantation* 102, 1815–1823. doi:10.1097/TP.0000000000002353.
- Han, M., Xie, M., Han, J., Yuan, D., Yang, T., and Xie, Y. (2018). Development and validation of a rapid, selective, and sensitive LC–MS/MS method for simultaneous determination of d- and l-amino acids in human serum: application to the study of hepatocellular carcinoma. *Anal. Bioanal. Chem.* 410, 2517–2531. doi:10.1007/s00216-018-0883-3.
- Hansen, J., and Johannesen, P. F. (2000). Cysteine is essential for transcriptional regulation of the sulfur assimilation genes in *Saccharomyces cerevisiae*. *Mol. Gen.*

- Genet.* 263, 535–542. doi:10.1007/s004380051199.
- Havlickova, B., Czaika, V. A., and Friedrich, M. (2008). Epidemiological trends in skin mycoses worldwide. *Mycoses* 51, 2–15. doi:10.1111/j.1439-0507.2008.01606.x.
- Hébert, A., Casaregola, S., and Beckerich, J. M. (2011). Biodiversity in sulfur metabolism in hemiascomycetous yeasts. *FEMS Yeast Res.* 11, 366–378. doi:10.1111/j.1567-1364.2011.00725.x.
- Ho, J., Camilli, G., Griffiths, J. S., Richardson, J. P., Kichik, N., and Naglik, J. R. (2021). *Candida albicans* and candidalysin in inflammatory disorders and cancer. *Immunology* 162, 11. doi:10.1111/IMM.13255.
- Hoenigl, M., Seidel, D., Sprute, R., Cunha, C., Oliverio, M., Goldman, G. H., et al. (2022). COVID-19-associated fungal infections. *Nat. Microbiol.* 7, 1127–1140. doi:10.1038/s41564-022-01172-2.
- Hoerlein, G. (1994). Glufosinate (phosphinothricin), a natural amino acid with unexpected herbicidal properties. *Rev. Environ. Contam. Toxicol.* 138, 73–145. doi:10.1007/978-1-4612-2672-7_4.
- Hou, Y. P., Mao, X. W., Qu, X. P., Wang, J. X., Chen, C. J., and Zhou, M. G. (2018). Molecular and biological characterization of *Sclerotinia sclerotiorum* resistant to the anilinopyrimidine fungicide cyprodinil. *Pestic. Biochem. Physiol.* 146, 80–89. doi:10.1016/j.pestbp.2018.03.001.
- Ingram, L. O. N., and Buttke, T. M. (1985). Effects of Alcohols on Micro-Organisms. *Adv. Microb. Physiol.* 25, 253–300. doi:10.1016/S0065-2911(08)60294-5.
- James, S. A., Phillips, S., Telatin, A., Baker, D., Ansorge, R., Clarke, P., et al. (2020). Preterm infants harbour a rapidly changing mycobiota that includes candida pathobionts. *J. Fungi* 6, 1–16. doi:10.3390/jof6040273.
- Jastrzębowska, K., and Gabriel, I. (2015). Inhibitors of amino acids biosynthesis as antifungal agents. *Amino Acids* 47, 227–249. doi:10.1007/s00726-014-1873-1.
- Jauniaux, J. -C, and Grenson, M. (1990). GAP1, the general amino acid permease gene of *Saccharomyces cerevisiae* Nucleotide sequence, protein similarity with the other bakers yeast amino acid permeases, and nitrogen catabolite repression. *Eur. J. Biochem.* 190, 39–44. doi:10.1111/j.1432-1033.1990.tb15542.x.
- Jeitner, T. M., and Cooper, A. J. L. (2014). Inhibition of human glutamine synthetase by L-methionine-S,R-sulfoximine—relevance to the treatment of neurological diseases. *Metab. Brain Dis.* 29, 983–989. doi:10.1007/s11011-013-9439-6.
- Johnson, M. D. (2021). Antifungals in Clinical Use and the Pipeline. *Infect. Dis. Clin. North Am.* 35, 341–371. doi:10.1016/j.idc.2021.03.005.
- Jones, P., Binns, D., Chang, H. Y., Fraser, M., Li, W., McAnulla, C., et al. (2014). InterProScan 5: Genome-scale protein function classification. *Bioinformatics* 30, 1236–1240. doi:10.1093/bioinformatics/btu031.



- Kase, H., and Nakayama, K. (1974). The regulation of L-methionine synthesis and the properties of cystathionine γ -synthase and β -cystathionase in *Corynebacterium glutamicum*. *Agric. Biol. Chem.* 38, 2235–2242. doi:10.1080/00021369.1974.10861488.
- Keighley, C., Garnham, & K., Harch, S. A. J., Robertson, & M., Chaw, & K., Teng, J. C., et al. *Candida auris*: Diagnostic Challenges and Emerging Opportunities for the Clinical Microbiology Laboratory. doi:10.1007/s12281-021-00420-y/Published.
- Kerr, D. S., and Flavin, M. (1968). Synthesis of cystathionine from O-acetylhomoserine in *Neurospora*: A step in methionine biosynthesis. *Biochem. Biophys. Res. Commun.* 31, 124–130. doi:10.1016/0006-291X(68)90041-7.
- Kerr, D. S., and Flavin, M. (1970). The regulation of methionine synthesis and the nature of cystathionine gamma-synthase in *Neurospora*. *J. Biol. Chem.* 245, 1842–1855. doi:10.1016/s0021-9258(19)77168-3.
- Kingsbury, J. M., and McCusker, J. H. (2010a). Cytocidal amino acid starvation of *Saccharomyces cerevisiae* and *Candida albicans* acetolactate synthase (*ilv2Δ*) mutants is influenced by the carbon source and rapamycin. *Microbiology* 156, 929–939. doi:10.1099/mic.0.034348-0.
- Kingsbury, J. M., and McCusker, J. H. (2010b). Fungal homoserine kinase (*thr1Δ*) mutants are attenuated in virulence and die rapidly upon threonine starvation and serum incubation. *Eukaryot. Cell* 9, 729–737. doi:10.1128/EC.00045-10.
- Kingsbury, J. M., and McCusker, J. H. (2010c). Homoserine toxicity in *Saccharomyces cerevisiae* and *Candida albicans* homoserine kinase (*thr1Δ*) mutants. *Eukaryot. Cell* 9, 717–728. doi:10.1128/EC.00044-10.
- Kondori, N., Nowrouzian, F., Ajdari, M., Hesselmar, B., Saalman, R., Wold, A. E., et al. (2021). *Candida* species as commensal gut colonizers: A study of 133 longitudinally followed Swedish infants. *Med. Mycol.* 58, 485–492. doi:10.1093/MMY/MYZ091.
- Kong, Y., Wu, D., Bai, H., Han, C., Chen, J., Chen, L., et al. (2008). Enzymatic characterization and inhibitor discovery of a new cystathionine γ -synthase from *Helicobacter pylori*. *J. Biochem.* 143, 59–68. doi:10.1093/jb/mvm194.
- Kramer, R. Z. ;, Bella, J. ;, Mayville, P. ;, Brodsky, B. ;, and Berman, H. M. (2020). Full wwPDB X-ray Structure Validation Report i O Title : COLLAGEN. Available at: <https://www.wwpdb.org/validation/2017/XrayValidationReportHelp> [Accessed April 5, 2024].
- Kredich, N. M., and Tomkins, G. M. (1966). The enzymic synthesis of L-cysteine in *Escherichia coli* and *Salmonella typhimurium*. *J. Biol. Chem.* 241, 4955–4965.
- Kreft, B. D., Townsend, A., Pohlenz, H. D., and Laber, B. (1994). Purification and Properties of Cystathionine [gamma]-Synthase from Wheat (*Triticum aestivum* L.). *Plant Physiol.* 104, 1215. doi:10.1104/PP.104.4.1215.
- Kuchi Bhotla, H., Balasubramanian, B., Meyyazhagan, A., Pushparaj, K., Easwaran, M.,

- Pappusamy, M., et al. (2021). Opportunistic mycoses in COVID-19 patients/survivors: Epidemic inside a pandemic. *J. Infect. Public Health* 14, 1720–1726. doi:10.1016/j.jiph.2021.10.010.
- Kulikova, V. V., Revtovich, S. V., Bazhulina, N. P., Anufrieva, N. V., Kotlov, M. I., Koval, V. S., et al. (2019). Identification of *O*-acetylhomoserine sulfhydrylase, a putative enzyme responsible for methionine biosynthesis in *Clostridioides difficile* : Gene cloning and biochemical characterizations. *IUBMB Life* 71, 1815–1823. doi:10.1002/iub.2139.
- Kumar, A., John, L., Alam, M. M., Gupta, A., Sharma, G., Pillai, B., et al. (2006). Homocysteine- and cysteine-mediated growth defect is not associated with induction of oxidative stress response genes in yeast. *Biochem. J.* 396, 61–69. doi:10.1042/BJ20051411.
- Kuplińska, A., and Rząd, K. (2021). Molecular targets for antifungals in amino acid and protein biosynthetic pathways. *Amino Acids* 1, 3. doi:10.1007/s00726-021-03007-6.
- Kuplińska, A., Rząd, K., Wojciechowski, M., Milewski, S., and Gabriel, I. (2022). Antifungal Effect of Penicillamine Due to the Selective Targeting of L-Homoserine *O*-Acetyltransferase. *Int. J. Mol. Sci.* 23. doi:10.3390/ijms23147763.
- Kur, K., Gabriel, I., Morschhäuser, J., Barchiesi, F., Spreghini, E., and Milewski, S. (2010). Disruption of homocitrate synthase genes in *Candida albicans* affects growth but not virulence. *Mycopathologia* 170, 397–402. doi:10.1007/s11046-010-9337-y.
- Laemmli, U. K. (1970). Cleavage of Structural Proteins during the Assembly of the Head of Bacteriophage T4. *Nature* 227, 680–685. doi:10.1038/227680a0.
- Lambein, F., Schamp, N., Vandendriessche, L., and Van Parijs, R. (1969). A new uv-sensitive heterocyclic amino acid frott pea seedlings : 2-alanyl-3-isoxazoliin-5-one. *Biochem. Biophys. Res. Commun.* 37, 375–382. doi:10.1016/0006-291X(69)90925-5.
- Lamoth, F., Lewis, R. E., and Kontoyiannis, D. P. (2022). Investigational Antifungal Agents for Invasive Mycoses: A Clinical Perspective. *Clin. Infect. Dis.* 75, 534–544. doi:10.1093/cid/ciab1070.
- Lazar Jr., I., and Lazar Sr., I. GelAnalyzer 19.1 (www.gelanalyzer.com). Available at: www.gelanalyzer.com.
- Li, Y. Y., Jiao, P., Li, Y. Y., Gong, Y., Chen, X., and Sun, S. (2019). The synergistic antifungal effect and potential mechanism of D-Penicillamine combined with fluconazole against *Candida albicans*. *Front. Microbiol.* 10, 1–10. doi:10.3389/fmicb.2019.02853.
- Liebmann, B., Mühleisen, T. W., Müller, M., Hecht, M., Weidner, G., Braun, A., et al. (2004). Deletion of the *Aspergillus fumigatus* lysine biosynthesis gene *lysF* encoding homoaconitase leads to attenuated virulence in a low-dose mouse infection model of invasive aspergillosis. *Arch. Microbiol.* 181, 378–383. doi:10.1007/s00203-004-

0667-3.

- Lowther, J., Beattie, A. E., Langridge-Smith, P. R. R., Clarke, D. J., and Campopiano, D. J. (2012). L-Penicillamine is a mechanism-based inhibitor of serine palmitoyltransferase by forming a pyridoxal-5'-phosphate-thiazolidine adduct. *Medchemcomm* 3, 1003–1008. doi:10.1039/c2md20020a.
- Lyman, M., Forsberg, K., Sexton, D. J., Chow, N. A., Lockhart, S. R., Jackson, B. R., et al. (2023). Worsening Spread of *Candida auris* in the United States, 2019 to 2021. *Ann. Intern. Med.* 176, 489–495. doi:10.7326/M22-3469.
- Marzluf, G. A. (1997). Molecular genetics of sulfur assimilation in filamentous fungi and yeast. *Annu. Rev. Microbiol.* 51, 73–96. doi:10.1146/annurev.micro.51.1.73.
- McCune, C. D., Chan, S. J., Beio, M. L., Shen, W., Chung, W. J., Szczesniak, L. M., et al. (2016). Zipped synthesis by cross-metathesis provides a cystathionine β -synthase inhibitor that attenuates cellular H₂S levels and reduces neuronal infarction in a rat ischemic stroke model. *ACS Cent. Sci.* 2, 242–252. doi:10.1021/acscentsci.6b00019.
- Mendonça, A., Santos, H., Franco-Duarte, R., and Sampaio, P. (2022). Fungal infections diagnosis – Past, present and future. *Res. Microbiol.* 173, 103915. doi:10.1016/j.resmic.2021.103915.
- Mindrebo, J. T., Nartey, C. M., Seto, Y., Burkart, M. D., and Noel, J. P. (2016). Unveiling the functional diversity of the alpha/beta hydrolase superfamily in the plant kingdom. *Curr. Opin. Struct. Biol.* 41, 233–246. doi:10.1016/j.sbi.2016.08.005.
- Mirza, I. A., Nazi, I., Korczynska, M., Wright, G. D., and Berghuis, A. M. (2005). Crystal structure of homoserine transacetylase from *Haemophilus influenzae* reveals a new family of α/β -hydrolases. *Biochemistry* 44, 15768–15773. doi:10.1021/bi051951y.
- Mitrasinovic, P. (2010). Advances in the Structure-Based Design of the Influenza A Neuraminidase Inhibitors. *Curr. Drug Targets* 11, 315–326. doi:10.2174/138945010790711932.
- Mohr, M. K. F., Saleem-Batcha, R., Cornelissen, N. V, and Andexer, J. N. (2023). Enzymatic Synthesis of L-Methionine Analogues and Application in a Methyltransferase Catalysed Alkylation Cascade. *Chem. – A Eur. J.* doi:10.1002/chem.202301503.
- Morad, H. O. J., Wild, A. M., Wiehr, S., Davies, G., Maurer, A., Pichler, B. J., et al. (2018). pre-clinical imaging of invasive candidiasis using immunoPET/MR. *Front. Microbiol.* 9. doi:10.3389/fmicb.2018.01996.
- Morgan, J., Meltzer, M. I., Plikaytis, B. D., Sofair, A. N., Huie-White, S., Wilcox, S., et al. (2005). Excess Mortality, Hospital Stay, and Cost Due to Candidemia: A Case-Control Study Using Data From Population-Based Candidemia Surveillance. *Infect. Control Hosp. Epidemiol.* 26, 540–547. doi:10.1086/502581.
- Morzycka, E., and Paszewski, A. (1982). Cysteine and homocysteine synthesis in *Saccharomyces lipolytica*; identification and characterization of two cysteine

synthases. *Acta Biochim. Pol.* 29, 81–93. Available at: <http://www.ncbi.nlm.nih.gov/pubmed/7180327>.

- Munro, H. N. (1970). "Free Amino Acid Pools and Their Role in Regulation," in *Mammalian Protein Metabolism* (Academic Press), 299–386. doi:10.1016/b978-0-12-510604-7.50012-8.
- Murillo, L. A., Newport, G., Lan, C. Y., Habelitz, S., Dungan, J., and Agabian, N. M. (2005). Genome-wide transcription profiling of the early phase of biofilm formation by *Candida albicans*. *Eukaryot. Cell* 4, 1562–1573. doi:10.1128/EC.4.9.1562-1573.2005.
- Musumeci, S., Coen, M., Leidi, A., and Schrenzel, J. (2022). The human gut mycobiome and the specific role of *Candida albicans*: where do we stand, as clinicians? *Clin. Microbiol. Infect.* 28, 58–63. doi:10.1016/j.cmi.2021.07.034.
- Nazi, I., Scott, A., Sham, A., Rossi, L., Williamson, P. R., Kronstad, J. W., et al. (2007). Role of homoserine transacetylase as a new target for antifungal agents. *Antimicrob. Agents Chemother.* 51, 1731–1736. doi:10.1128/AAC.01400-06.
- Nazi, I., and Wright, G. D. (2005). Catalytic mechanism of fungal homoserine transacetylase. *Biochemistry* 44, 13560–13566. doi:10.1021/bi0514764.
- Newell, S. Y., Arsuffi, T. L., and Fallon, R. D. (1988). Fundamental Procedures for Determining Ergosterol Content of Decaying Plant Material by Liquid Chromatography. *Appl. Environ. Microbiol.* 54, 1876–1879. doi:10.1128/aem.54.7.1876-1879.1988.
- Nowak, M. G., Skwarecki, A. S., and Milewska, M. J. (2021). Amino Acid Based Antimicrobial Agents – Synthesis and Properties. *ChemMedChem* 16, 3513–3544. doi:10.1002/cmdc.202100503.
- Obando Montoya, E. J., Mélin, C., Blanc, N., Lanoue, A., Foureau, E., Boudesocque, L., et al. (2014). Disrupting the methionine biosynthetic pathway in *Candida guilliermondii*: Characterization of the *MET2* gene as counter-selectable marker. *Yeast* 31, 243–251. doi:10.1002/yea.3012.
- Odds, F. C. (2003). Synergy, antagonism, and what the checkerboard puts between them. *J. Antimicrob. Chemother.* 52, 1. doi:10.1093/jac/dkg301.
- Pascon, R. C., Ganous, T. M., Kingsbury, J. M., Cox, G. M., and McCusker, J. H. (2004). *Cryptococcus neoformans* methionine synthase: Expression analysis and requirement for virulence. *Microbiology* 150, 3013–3023. doi:10.1099/mic.0.27235-0.
- Patterson, T. F. (2005). Advances and challenges in management of invasive mycoses. *Lancet* 366, 1013–1025. doi:10.1016/S0140-6736(05)67381-3.
- Perfect, J. R. (2017). The antifungal pipeline: A reality check. *Nat. Rev. Drug Discov.* 16, 603–616. doi:10.1038/nrd.2017.46.

- Pflughoef, K. J., and Versalovic, J. (2012). *Human microbiome in health and disease*. doi:10.1146/annurev-pathol-011811-132421.
- Pianalto, K. M., and Alspaugh, J. A. (2016). New horizons in antifungal therapy. *J. Fungi* 2. doi:10.3390/jof2040026.
- Pusey, M. L., and Gernert, K. (1988). A method for rapid liquid-solid phase solubility measurements using the protein lysozyme. *J. Cryst. Growth* 88, 419–424. doi:10.1016/0022-0248(88)90017-6.
- Rajasingham, R., Smith, R. M., Park, B. J., Jarvis, J. N., Govender, N. P., Chiller, T. M., et al. (2017). Global burden of disease of HIV-associated cryptococcal meningitis: an updated analysis. *Lancet Infect. Dis.* 17, 873–881. doi:10.1016/S1473-3099(17)30243-8.
- Raut, A., and Huy, N. T. (2021). Rising incidence of mucormycosis in patients with COVID-19: another challenge for India amidst the second wave? *Lancet Respir. Med.* 9, e77. doi:10.1016/S2213-2600(21)00265-4.
- Rayens, E., Norris, K. A., and Cordero, J. F. (2022). Mortality Trends in Risk Conditions and Invasive Mycotic Disease in the United States, 1999–2018. *Clin. Infect. Dis.* 74, 309–318. doi:10.1093/cid/ciab336.
- Robert, X., and Gouet, P. (2014). Deciphering key features in protein structures with the new ENDscript server. *Nucleic Acids Res.* 42, W320–W324. doi:10.1093/nar/gku316.
- Robinson, S. L., Christenson, J. K., and Wackett, L. P. (2019). Biosynthesis and chemical diversity of β -lactone natural products. *Nat. Prod. Rep.* 36, 458–475. doi:10.1039/c8np00052b.
- Rodrigues, M. L., and Nosanchuk, J. D. (2020). Fungal diseases as neglected pathogens: A wake-up call to public health officials. *PLoS Negl. Trop. Dis.* 14, e0007964. doi:10.1371/journal.pntd.0007964.
- Rosenberg, A. H., Lade, B. N., Dao-shan, C., Lin, S. W., Dunn, J. J., and Studier, F. W. (1987). Vectors for selective expression of cloned DNAs by T7 RNA polymerase. *Gene* 56, 125–135. doi:10.1016/0378-1119(87)90165-X.
- Rupp, B. (2009). *Biomolecular Crystallography Principles, Practice, and Application to Structural Biology*. 1st Editio. , eds. S. Scholl, A. Engels, and S. Hill New York: Garland Science, Taylor & Francis Group, LLC.
- Sagong, H. Y., Hong, J., and Kim, K. J. (2019). Crystal structure and biochemical characterization of O-acetylhomoserine acetyltransferase from *Mycobacterium smegmatis* ATCC 19420. *Biochem. Biophys. Res. Commun.* 517, 399–406. doi:10.1016/j.bbrc.2019.07.117.
- Sagong, H. Y., and Kim, K. J. (2017). Structural insights into substrate specificity of cystathionine γ -synthase from *Corynebacterium glutamicum*. *J. Agric. Food Chem.* 65, 6002–6008. doi:10.1021/acs.jafc.7b02391.

- Sahu, U., Rajendra, V. K. H., Kapnoor, S. S., Bhagavat, R., Chandra, N., and Rangarajan, P. N. (2017). Methionine synthase is localized to the nucleus in *Pichia pastoris* and *Candida albicans* and to the cytoplasm in *Saccharomyces cerevisiae*. *J. Biol. Chem.* 292, 14730–14746. doi:10.1074/jbc.M117.783019.
- Sato, K., Fukushima, D., Doi, H., and Satomi, S. (2013). Higher serum methionine levels as a predictive factor in patients with irreversible fulminant hepatic failure. *Transplant. Proc.* 45, 1904–1906. doi:10.1016/j.transproceed.2012.11.028.
- Schenk, S. U., Lambein, F., and Werner, D. (1991). Broad antifungal activity of β -isoxazolinonyl-alanine, a non-protein amino acid from roots of pea (*Pisum sativum* L.) seedlings. *Biol. Fertil. Soils* 11, 203–209. doi:10.1007/BF00335768.
- Schiemann, M., Szweda, P., Gucwa, K., Kawczynski, M., Milewska, M. J., Martynow, D., et al. (2017). Transport deficiency is the molecular basis of *Candida albicans* resistance to antifungal oligopeptides. *Front. Microbiol.* 8, 1–12. doi:10.3389/fmicb.2017.02154.
- Schmidt, J. A., Rinaldi, S., Scalbert, A., Ferrari, P., Achaintre, D., Gunter, M. J., et al. (2016). Plasma concentrations and intakes of amino acids in male meat-eaters, fish-eaters, vegetarians and vegans: A cross-sectional analysis in the EPIC-Oxford cohort. *Eur. J. Clin. Nutr.* 70, 306–312. doi:10.1038/ejcn.2015.144.
- Schöbel, F., Jacobsen, I. D., and Brock, M. (2010). Evaluation of lysine biosynthesis as an antifungal drug target: Biochemical characterization of *Aspergillus fumigatus* homocitrate synthase and virulence studies. *Eukaryot. Cell* 9, 878–893. doi:10.1128/EC.00020-10.
- Scorzoni, L., de Paula e Silva, A. C. A., Marcos, C. M., Assato, P. A., de Melo, W. C. M. A., de Oliveira, H. C., et al. (2017). Antifungal therapy: New advances in the understanding and treatment of mycosis. *Front. Microbiol.* 8. doi:10.3389/fmicb.2017.00036.
- Shao, W., Yang, Y., Zhang, Y., Lv, C., Ren, W., and Chen, C. (2016). Involvement of *BcStr2* in methionine biosynthesis, vegetative differentiation, multiple stress tolerance and virulence in *Botrytis cinerea*. *Mol. Plant Pathol.* 17, 438–447. doi:10.1111/mpp.12292.
- Shiio, I., and Ozaki, H. (1981). Feedback inhibition by methionine and S-adenosylmethionine, and desensitization of homoserine O-acetyltransferase in *Brevibacterium flavum*. *J. Biochem.* 89, 1493–1500. doi:10.1093/oxfordjournals.jbchem.a133342.
- Shimizu, H., Yamagata, S., Masui, R., Inoue, Y., Shibata, T., Yokoyama, S., et al. (2001). Cloning and overexpression of the *oah1* gene encoding O-acetyl-L-homoserine sulfhydrylase of *Thermus thermophilus* HB8 and characterization of the gene product. *Biochim. Biophys. Acta - Protein Struct. Mol. Enzymol.* 1549, 61–72. doi:10.1016/S0167-4838(01)00245-X.
- Singh, A., and Sherman, F. (1974). Characteristics and relationships of mercury resistant

mutants and methionine auxotrophs of yeast. *J. Bacteriol.* 118, 911–918. doi:10.1128/jb.118.3.911-918.1974.

Skrzypek, M. S., Binkley, J., Binkley, G., Miyasato, S. R., Simison, M., and Sherlock, G. (2017). The Candida Genome Database (CGD): Incorporation of Assembly 22, systematic identifiers and visualization of high throughput sequencing data. *Nucleic Acids Res.* 45, D592–D596. doi:10.1093/nar/gkw924.

Slabinski, L., Jaroszewski, L., Rychlewski, L., Wilson, I. A., Lesley, S. A., and Godzik, A. (2007). XtalPred: A web server for prediction of protein crystallizability. *Bioinformatics* 23, 3403–3405. doi:10.1093/bioinformatics/btm477.

Steegborn, C., Laber, B., Messerschmidt, A., Huber, R., and Clausen, T. (2001). Crystal structures of cystathionine γ -synthase inhibitor complexes rationalize the increased affinity of a novel inhibitor. *J. Mol. Biol.* 311, 789–801. doi:10.1006/jmbi.2001.4880.

Steegborn, C., Messerschmidt, A., Laber, B., Streber, W., Huber, R., and Clausen, T. (1999). The crystal structure of cystathionine γ -synthase from *Nicotiana tabacum* reveals its substrate and reaction specificity. *J. Mol. Biol.* 290, 983–996. doi:10.1006/jmbi.1999.2935.

Stop neglecting fungi (2017). *Nat. Microbiol.* 2, 17120. doi:10.1038/nmicrobiol.2017.120.

Studier, F., Rosenberg, A. H., Dunn, J. J., and Dubendorff, J. W. (1990). Use of T7 RNA polymerase to direct expression of cloned genes. *Methods Enzymol.* 185, 60–89. doi:10.1016/0076-6879(90)85008-C.

Studier, F. W. (1991). Use of bacteriophage T7 lysozyme to improve an inducible T7 expression system. *J. Mol. Biol.* 219, 37–44. doi:10.1016/0022-2836(91)90855-Z.

Studier, F. W., and Moffatt, B. A. (1986). Use of bacteriophage T7 RNA polymerase to direct selective high-level expression of cloned genes. *J. Mol. Biol.* 189, 113–130. doi:10.1016/0022-2836(86)90385-2.

Su, H., Han, L., Ding, N., Guan, P., Hu, C., and Huang, X. (2018). Bafilomycin C1 exert antifungal effect through disturbing sterol biosynthesis in *Candida albicans*. *J. Antibiot. (Tokyo)*. 71, 467–476. doi:10.1038/s41429-017-0009-8.

Su, X. D., Zhang, H., Terwilliger, T. C., Liljas, A., Xiao, J., and Dong, Y. (2015). Protein crystallography from the perspective of technology developments. *Crystallogr. Rev.* 21, 122–153. doi:10.1080/0889311X.2014.973868.

Suliman, H. S., Appling, D. R., and Robertus, J. D. (2007). The gene for cobalamin-independent methionine synthase is essential in *Candida albicans*: A potential antifungal target. *Arch. Biochem. Biophys.* 467, 218–226. doi:10.1016/j.abb.2007.09.003.

Tabor, S. (1990). Expression Using the T7 RNA Polymerase/Promoter System. *Curr. Protoc. Mol. Biol.* 11, 16.2.1-16.2.11. doi:10.1002/0471142727.mb1602s11.

- Takano, H. K., and Dayan, F. E. (2020). Glufosinate-ammonium: a review of the current state of knowledge. *Pest Manag. Sci.* 76, 3911–3925. doi:10.1002/ps.5965.
- Tran, T. H., Krishnamoorthy, K., Begley, T. P., and Ealick, S. E. (2011). A novel mechanism of sulfur transfer catalyzed by O-acetylhomoserine sulfhydrylase in the methionine-biosynthetic pathway of *Wolinella succinogenes*. *Acta Crystallogr. Sect. D Biol. Crystallogr.* 67, 831–838. doi:10.1107/S0907444911028010.
- Tu, Y., Kreinbring, C. A., Hill, M., Liu, C., Petsko, G. A., McCune, C. D., et al. (2018). Crystal structures of cystathionine β -synthase from *Saccharomyces cerevisiae*: One enzymatic step at a time. *Biochemistry* 57, 3134–3145. doi:10.1021/acs.biochem.8b00092.
- Tubajika, K. M., and Damann, K. E. (2002). Glufosinate-ammonium reduces growth and aflatoxin B1 production by *Aspergillus flavus*. *J. Food Prot.* 65, 1483–1487. doi:10.4315/0362-028X-65.9.1483.
- Ubhi, D., Kago, G., Monzingo, A. F., and Robertus, J. D. (2014). Structural analysis of a fungal methionine synthase with substrates and inhibitors. *J. Mol. Biol.* 426, 1839–1847. doi:10.1016/j.jmb.2014.02.006.
- Uchimiya, H., Iwata, M., Nojiri, C., Samarajeewa, P. K., Takamatsu, S., Ooba, S., et al. (1993). Bialaphos treatment of transgenic rice plants expressing a bar gene prevents infection by the sheath blight pathogen (*Rhizoctonia solani*). *Bio/Technology* 11, 835. doi:10.1038/nbt0793-835.
- Vallejo, B., Picazo, C., Orozco, H., Matallana, E., and Aranda, A. (2017). Herbicide glufosinate inhibits yeast growth and extends longevity during wine fermentation. *Sci. Rep.* 7. doi:10.1038/s41598-017-12794-6.
- Verweij, P. E., Chowdhary, A., Melchers, W. J. G., and Meis, J. F. (2016). Azole resistance in *Aspergillus fumigatus*: Can we retain the clinical use of mold-active antifungal azoles? *Clin. Infect. Dis.* 62, 362–368. doi:10.1093/cid/civ885.
- Viaene, J., Tiels, P., Logghe, M., Dewaele, S., Martinet, W., and Contreras, R. (2000). *MET15* as a visual selection marker for *Candida albicans*. *Yeast* 16, 1205–1215. doi:10.1002/1097-0061(20000930)16:13<1205::AID-YEA615>3.0.CO;2-C.
- Wahl, M. C., Huber, R., Prade, L., Marinkovic, S., Messerschmidt, A., and Clausen, T. (1997). Cloning, purification, crystallization, and preliminary X-ray diffraction analysis of cystathionine γ -synthase from *E. coli*. *FEBS Lett.* 414, 492–496. doi:10.1016/S0014-5793(97)01057-0.
- Wayne, P. (2008). Reference method for broth dilution antifungal susceptibility testing of yeasts; Approved standard - Third Edition. *CLSI Doc. M27-A3*. Available at: https://clsi.org/media/1461/m27a3_sample.pdf.
- White, T. C., Andrews, L. E., Maltby, D., and Agabian, N. (1995). The ““Universal”” Leucine Codon CTG in the Secreted Aspartyl Proteinase 1 (SAP1) Gene of *Candida albicans* Encodes a Serine In Vivo. *J. Bacteriol.* 177, 2953–2955.



- Wiederhold, N. P. (2017). Antifungal resistance: current trends and future strategies to combat. *Infect. Drug Resist.* 10, 249–259. doi:10.2147/IDR.S124918.
- Wiederhold, N. P. (2022). Pharmacodynamics, Mechanisms of Action and Resistance, and Spectrum of Activity of New Antifungal Agents. *J. Fungi* 2022, Vol. 8, Page 857 8, 857. doi:10.3390/JOF8080857.
- Wiencek, J. M. (1999). New strategies for protein crystal growth. *Annu. Rev. Biomed. Eng.*, 505–534. doi:10.1146/annurev.bioeng.1.1.505.
- World Health Organization (2022). WHO fungal priority pathogens list to guide research, development and public health action. *Licence CC BY-NC-SA 3.0 IGO* 1, 1–48. Available at: <https://www.who.int/publications/i/item/9789240060241> [Accessed June 5, 2023].
- Wyman, A., and Paulus, H. (1975). Purification and properties of homoserine transacetylase from *Bacillus polymyxa*. *J. Biol. Chem.* 250, 3897–3903. doi:10.1016/s0021-9258(19)41483-x.
- Yadav, A. K., Desai, P. R., Rai, M. N., Kaur, R., Ganesan, K., and Bachhawat, A. K. (2011). Glutathione biosynthesis in the yeast pathogens *Candida glabrata* and *Candida albicans*: Essential in *C. glabrata*, and essential for virulence in *C. albicans*. *Microbiology* 157, 484–495. doi:10.1099/mic.0.045054-0.
- Yamagata, S. (1984). O-acetylhomoserine sulfhydrylase of the fission yeast *Schizosaccharomyces pombe*: Partial purification, characterization, and its probable role in homocysteine biosynthesis. *J. Biochem.* 96, 1511–1523. doi:10.1093/oxfordjournals.jbchem.a134980.
- Yamagata, S. (1987a). O-Acetyl-L-serine-O-acetyl-L-homoserine sulfhydrylase from *Saccharomyces cerevisiae*. *Methods Enzymol.* 143, 478–483. doi:10.1016/0076-6879(87)43085-1.
- Yamagata, S. (1987b). Partial purification and some properties of homoserine O-acetyltransferase of a methionine auxotroph of *Saccharomyces cerevisiae*. *J. Bacteriol.* 169, 3458–3463. doi:10.1128/jb.169.8.3458-3463.1987.
- Yamagata, S. (1989). Roles of O-acetyl-L-homoserine sulfhydrylases in microorganisms. *Biochimie* 71, 1125–1143. doi:10.1016/0300-9084(89)90016-3.
- Zhou, L., Ma, Y., Wang, K., Chen, T., Huang, Y., Liu, L., et al. (2023). Omics-guided bacterial engineering of *Escherichia coli* ER2566 for recombinant protein expression. *Appl. Microbiol. Biotechnol.* 107, 853–865. doi:10.1007/s00253-022-12339-6.
- Zhou, L., Yu, H., Wang, K., Chen, T., Ma, Y., Huang, Y., et al. (2020). Genome re-sequencing and reannotation of the *Escherichia coli* ER2566 strain and transcriptome sequencing under overexpression conditions. *BMC Genomics* 21. doi:10.1186/s12864-020-06818-1.





LIST OF FIGURES

- Fig. 1. The WHO fungal priority pathogens list. Adapted from (World Health Organization, 2022). _____ 15
- Fig. 2. Examples of essential amino acid food sources. Created on the base of (Munro, 1970). _____ 20
- Fig. 3. The putative *C. albicans* MBP. Enzymes explored in this dissertation are marked with yellow circles i.e. Met2p EC 2.3.1.31 homoserine *O*-acetyltransferase; Met15p EC 2.5.1.49 *O*-acetyl-L-homoserine sulfhydrylase; Str2p EC 2.5.1.48 cystathionine- γ -synthase. Other enzymes: Cys3p EC 4.4.1.1 cystathionine- γ -lyase; Cys4p EC 4.2.1.22 cystathionine- β -synthase; Met6p EC 2.1.1.13 methionine synthase; Sah1p EC 3.3.1.1 adenosylhomocysteinase; Sam1p, Sam2p EC 2.5.1.6 methionine adenosyltransferase; Str3p EC 4.4.1.8 cystathionine- β -lyase; CYSK orf 19.7152 putative *O*-acetyl-L-serine sulfhydrylase homolog from *Aspergillus*; CYSA orf 19.1159 putative L-serine *O*-transacetylase analog of *Aspergillus nidulans*. Figure adapted from (Kuplińska et al., 2022). _____ 21
- Fig. 4. Reaction catalyzed by *C. albicans* Met2p. _____ 24
- Fig. 5. Model of a putative structure of the *C. albicans* Met2p, built on the template of *M. smegmatis* Met2p (PDB: 6IOH) and AlphaFold. L-HOM placed in the center of the active site, neighboring catalytic residues are presented as sticks and labeled according to the *C. albicans* amino acid sequence (residue number for *M. smegmatis* is given in parentheses). Figure generated by Marek Wojciechowski (Kuplińska et al., 2022). _____ 25
- Fig. 6. Reaction catalyzed by fungal Met15p. _____ 25
- Fig. 7. Structure of *W. succinogenes* Met15p. A. Structure of the biological tetramer with PLP represented as spheres; B. Superposition of homologous Met15p enzymes with PLP in the center (cyan): PDB codes: 2cb1 (green), 1n8p (blue), 2o7c (gray). Adapted from (Tran et al., 2011). _____ 26
- Fig. 8. Reaction catalyzed by fungal Str2p. _____ 27
- Fig. 9. Structure of *C. glutamicum* Str2p. A. Single monomer with bound PLP cofactor; B. Tetrameric structure with bound PLP cofactor, one of the active dimers is highlighted, with separate color coding for distinct monomers, the N-terminal loop domain of two monomers is shown with arrows. Color coding of domains found in single monomer: the large PLP-binding domain (cyan/blue), the small C-terminal domain (pink/orange), and an extended N-terminal loop domain (green/yellow). Adapted from (Sagong et al., 2019). _____ 28
- Fig. 10. Inhibitors of enzymes from the L-methionine biosynthetic pathway. A. CTCQC; B. Azoxybacillin; C. Ebelactone A; D. Cyprodinil; E. (L, L)-2,7-Bis-(hydrazino)-1,8-octanedioic acid; F. Bafilomycin C1. Adapted from (Jastrzębowska and Gabriel, 2015; Kuplińska and Rząd, 2021). _____ 29

- Fig. 11. Result of plasmids restriction digest analysis. Electrophoresis 80 V cm^{-1} , 1% agarose gel. Midori Green is used as a DNA stain. M, marker (Gene Ruler 1 kb PLUS DNA ladder (Invitrogen)); 1. pET101/D-TOPO + *MET2*; 2. pET101/D-TOPO + *MET2CH*; 3. pET101/D-TOPO + *MET2NH*; 4. pLATE11 + *MET15*; 5. pLATE31 + *MET15CH*; 6. pLATE52 + *MET15NH*; 7. pLATE11 + *STR2*; 8. pLATE31 + *STR2CH*; 9. pLATE52 + *STR2NH*. _____ 56
- Fig. 12. Schematic representation of screening experiments for determination of optimal conditions to produce recombinant proteins. _____ 57
- Fig. 13. A – C. Result of the SDS-PAGE analysis of recombinant protein overproduction, electrophoresis 18 V cm^{-1} 10% gel; M, Marker (Page Ruler™ Plus Prestained Protein Ladder, Thermo Scientific). Ctrl, control (strain lacking expression plasmid). Expected molecular weights of proteins assuming monomeric structure: CaMet2p, CaMet2CHp, and CaMet2NHp 45 kDa; CaMet15p, CaMet15CHp, and CaMet15NHp 48 kDa; CaStr2p, CaStr2CHp and CaStr2NHp 67 kDa; D. Result of a Western blot analysis confirming production of His-tagged recombinant proteins. M, Marker (PageRuler™ Plus Prestained Protein Ladder, Thermo Scientific); 1, CaMet2NHp; 2, CaMet2CHp; 3, CaMet15NHp; 4, CaMet15CHp; 5, CaStr2NHp; 6, CaStr2CHp. Sample volumes: 1-2 3 μL ; 3-6 20 μL . _____ 58
- Fig. 14. Purification of CaMet2p, CaMet2NHp, and CaMet2CHp. 1A. SDS-PAGE electrophoresis of cell-free extract (CFE) from *E. coli* One Shot™ BL21 Star™ (DE3) cells and purified CaMet2p; 1B. Densitometric analysis of SDS-PAGE result of CFE; 1C. Densitometric analysis of SDS-PAGE of CaMet2NHp; 2A. SDS-PAGE electrophoresis of CFE from *E. coli* Rosetta (DE3) pLysS cells (CFE) and purified CaMet15NHp; 2B. Densitometric analysis of SDS-PAGE of CFE; 2C. Densitometric analysis of SDS-PAGE of CaMet2NHp; 3A. SDS-PAGE electrophoresis of CFE from *E. coli* One Shot™ BL21 Star™ (DE3) (CFE) and purified CaMet2CHp; 3B. Densitometric analysis of SDS-PAGE of CFE; 3C. Densitometric analysis of SDS-PAGE of CaMet2CHp. Electrophoresis was performed at 18 V cm^{-1} 10% gel. M, marker Thermo Scientific PageRuler™ Plus Prestained Protein Ladder. Densitometric analysis was performed with Gel Analyzer 19.1 software. Results were partly published (Kuplińska et al., 2022). _____ 63
- Fig. 15. Purification of CaMet15NHp and CaMet15CHp. 1A. SDS-PAGE electrophoresis of cell-free extract (CFE) from *E. coli* ER2566 cells and purified CaMet15NHp; 1B. Densitometric analysis of SDS-PAGE result of CFE; 1C. Densitometric analysis of SDS-PAGE of CaMet15NHp. 2A. SDS-PAGE electrophoresis of CFE from *E. coli* ER2566 cells (CFE) and purified CaMet15CHp; 2B. Densitometric analysis of SDS-PAGE of CFE; 2C. Densitometric analysis of SDS-PAGE of CaMet15CHp. Electrophoresis was performed at 18 V cm^{-1} 10% gel. M, marker Thermo Scientific PageRuler™ Plus Prestained Protein Ladder (Thermo Scientific). Densitometric analysis was performed with Gel Analyzer 19.1 software. _____ 64

- Fig. 16. Purification of CaStr2NHp and CaStr2CHp. 1A. SDS-PAGE electrophoresis of cell-free extract (CFE) from *E. coli* ER2566 cells and purified CaStr2NHp; 1B. Densitometric analysis of SDS-PAGE result of CFE; 1C. Densitometric analysis of SDS-PAGE of CaStr2NHp; 2A. SDS-PAGE electrophoresis of CFE from *E. coli* Rosetta (DE3) pLacI cells (CFE) and purified CaStr2CHp; 2B. Densitometric analysis of SDS-PAGE of CFE; 2C. Densitometric analysis of SDS-PAGE of CaStr2CHp. Electrophoresis was performed at 18 V cm^{-1} 10% gel. M, marker Thermo Scientific PageRuler™ Plus Prestained Protein Ladder (Thermo Scientific). Densitometric analysis was performed with Gel Analyzer 19.1 software. _____ 65
- Fig. 17. A. The reaction catalyzed by CaMet2p; B. Detection of produced AcCoA with DTNB reagent. _____ 71
- Fig. 18. Characterization of s CaMet2p, CaMet2NHp, and CaMet2CHp; A. Loss of activity of CaMet2NHp when stored in buffer not supplemented with glycerol; B. Determination of optimal storage conditions of CaMet2NHp; C. Effect of 50 mM phosphate buffer pH on CaMet2NHp activity; D. Comparison of CaMet2p, CaMet2NHp and CaMet2CHp activities. Results published by (Kuplińska et al., 2022). _____ 72
- Fig. 19. Michaelis-Menten curves showing determination of K_M and V_{MAX} parameters for CaMet2p and CaMet2NHp. v , initial reaction velocity; $C_{\text{substrate}}$, substrate concentration; AcCoA, acetyl coenzyme A; L-HOM, L-homoserine; K_M , Michaelis constant; V_{MAX} , maximum velocity of the reaction. Kinetic parameters were determined with GraphPad Prism software. _____ 74
- Fig. 20. Reaction catalyzed by CaMet15p _____ 75
- Fig. 21. Detection of L-homocysteine (L-HCT) with RP-HPLC-DAD combined with DTNB pre-column derivatization. A. Pre-column derivatization of L-HCT with DTNB; B. Chromatogram of the control reaction (top) and enzymatic (bottom) reaction mixture; C. Mass spectrometry analysis of the enzymatic reaction mixture (retention time 7.8 min). m/z : [L-HCT-TNB+H]⁺ 333.0. _____ 76
- Fig. 22. Characterization of CaMet15NHp and CaMet15CHp. A. Comparison of CaMet15NHp, CaMet15CHp activity and CaMet15NHp activity when L-OAS was used as a substrate instead of L-OAH *no possible product (L-Cys) was detected in the postreaction mixture when L-OAS was used as a substrate; B. Influence of a substrate or PLP cofactor presence on the CaMet15NHp activity, compared to the control reaction including all reaction components; C. Determination of optimal pH of the reaction catalyzed by CaMet15NHp; D. Optimal storage conditions preserving CaMet15NHp activity. _____ 77
- Fig. 23. Michaelis-Menten curves for determination of K_M and V_{MAX} parameters of CaMet15NHp. v , initial reaction velocity; $C_{\text{L-OAH/Na}_2\text{S}}$, substrate concentration; L-OAH, *O*-acetyl-L-homoserine; PLP, pyridoxal 5'-phosphate; K_M , Michaelis constant; V_{MAX} , maximum velocity of the reaction. Kinetic parameters were determined with GraphPad Prism software. _____ 78

- Fig. 24. Reaction catalyzed by CaStr2p. _____ 79
- Fig. 25. Detection of L-cysteine (L-CYS) with RP-HPLC-DAD combined with DTNB pre-column derivatization. A. Pre-column derivatization of L-Cys with DTNB; B. Chromatogram of the control reaction (top) and enzymatic (bottom) reaction mixture; C. Mass spectrometry analysis of the enzymatic reaction mixture (retention time 7.8 min). m/z : [L-CYS-TNB+H]⁺ 319. _____ 80
- Fig. 26. Characterization of CaStr2NHp and CaStr2CHp. A. Comparison of CaStr2NHp and CaStr2CHp activity; B. Loss of activity in time by enzyme not supplemented with glycerol; C. Determination of optimal pH of the reaction catalyzed by CaStr2NHp; D. Optimal storage conditions to preserve enzyme activity. _____ 81
- Fig. 27. Michaelis-Menten curves for determination of K_M and V_{MAX} parameters of CaStr2NHp. v , initial reaction velocity; $C_{L-OAH/L-CYS}$, substrate concentration; L-OAH, *O*-acetyl- L-homoserine; L-Cys, L-cysteine; K_M , Michaelis constant; V_{MAX} , maximum velocity of the reaction. Kinetic parameters were determined with GraphPad Prism software. _____ 82
- Fig. 28. Potential inhibitors of CaMet2p, CaMet15p, and CaStr2p. Compounds L-HMP, L-SMP, Ac-DAB, 6-OXO, 5-OXO and ISOX have been synthesized at the Department of Organic Chemistry, Gdańsk University of Technology. Other compounds are commercially available. _____ 83
- Fig. 29. Results of determination of inhibitory potency of tested inhibitors against CaMet2NHp, CaMet15NHp, and CaStr2NHp. Compounds synthesized in our group are shown in green boxes. Data shown are mean values of at least three independent experiments (\pm SD). _____ 85
- Fig. 30. Lineweaver-Burk plot of CaMet2NHp inhibition with L-PEN. K_i parameter was calculated using the GraphPad Prism software. _____ 87
- Fig. 31. Growth inhibition of *C. albicans*, *C. glabrata*, and *S. cerevisiae* by L-PEN and D-PEN in YNB AS medium with or without L-methionine (L-MET) (A-F), and RPMI 1640 medium (G-H). The error bars represent the standard deviation (SD). Results published in (Kuplińska et al., 2022). _____ 92
- Fig. 32. *C. glabrata* growth inhibition by L-PEN (A) and ISOX (B) in YNB AS medium supplemented with L-Met in a concentration range from 0.00 mM to 10 mM. The 10% cell growth is represented by the dotted line, which serves as a borderline below which no growth is observed. The error bars represent \pm SD. Results partially published in (Kuplińska et al., 2022). _____ 93
- Fig. 33. Generated heat map of the checkerboard dilution test showing synergistic or antagonistic effect (A, C, E, G) between combination of L-PEN and Ac-DAB, DL-ALG, DL-GLUF or ISOX in YNB SG medium against *C. glabrata* ATCC 90030; blue color (synergistic effect); red color (antagonistic effect); green color (indifferent effect). Generated heat map of the checkerboard dilution test showing growth inhibition over an untreated control (B, D, F, H). Interaction effect scores were obtained using the Loewe additivity model via Combeneft software (Di Veroli et al., 2016). ____ 95

Fig. 34. Formed CaMet15NHp crystals in different buffer systems. A. 0.2 M ammonium citrate tribasic pH 7.0, 20% w/v polyethylene glycol 3,350 (dyed with methylene blue); B. 0.1 M Tris pH 8.5, 0.3 M magnesium formate dihydrate; C. 0.2 M Potassium sodium tartrate tetrahydrate, 0.1 M Sodium citrate tribasic dihydrate pH 5.6, 2.0 M ammonium sulfate (performed in cooperation with the Institute of Bioorganic Chemistry of the Polish Academy of Sciences in Poznań); D. 0.2 M lithium citrate tribasic tetrahydrate pH 8.4, 20% w/v Polyethylene glycol 3,350 (performed in cooperation with the Institute of Bioorganic Chemistry of the Polish Academy of Sciences in Poznań). Crystals were formed using a sitting-drop vapor diffusion method. _____ 102

LIST OF TABLES

Tab. 1. Clinically applied antifungal drugs for the treatment of invasive fungal infections. Created on the base of (Pianalto and Alspaugh, 2016; Johnson, 2021)	18
Tab. 2. Laboratory equipment used in research.	32
Tab. 3. Software used in research.	33
Tab. 4. Mass markers used in research.	33
Tab. 5. Solid media for bacterial and yeast cultures.	33
Tab. 6. Liquid media for bacteria and yeast culture.	33
Tab. 7. Liquid media for MIC and synergism assay.	34
Tab. 8. Bacterial and yeast strains used in research.	34
Tab. 9. Maps of plasmids used for cloning experiments.	35
Tab. 10. Oligonucleotides used in research for PCR reaction.	37
Tab. 11. Restriction enzymes used in research.	38
Tab. 12. Substrates and a cofactor of CaMet2p, CaMe15p, and CaStr2p enzymes.	38
Tab. 13. Potential inhibitors of CaMet2p, CaStr2p, and CaMe15p enzymes.	39
Tab. 14. Programs used in bioinformatical analysis.	39
Tab. 15. Reaction mixture components for the PCR reaction	41
Tab. 16. The temperature-time profile of the PCR reaction.	41
Tab. 17. Components of the pET101/D-TOPO vector cloning mixture.	41
Tab. 18. Components of the pLATE vectors LIC cloning mixture.	42
Tab. 19. Components of the annealing reaction.	42
Tab. 20. Restriction digest reaction mixture components.	43
Tab. 21. Mutagenesis reaction mixture components.	43
Tab. 22. Mutagenesis PCR temperature gradient profile.	43
Tab. 23. <i>DpnI</i> restriction enzyme digestion reaction mixture components.	44
Tab. 24. Ligation mixture components.	44
Tab. 25. <i>Candida albicans</i> MET2 nucleotide sequence with CTG codon highlighted in red.	53
Tab. 26. Theoretical parameters characterizing CaMet2p, CaMet15p, and CaStr2p enzymes obtained via Candida Genome Database (Skrzypek et al., 2017), ExPASy Translate Tool and ProtParam Tool (Gasteiger et al., 2005).	54
Tab. 27. Amino acid sequences identities between putative CaMet2p, CaMet15p, and CaStr2p and their identified counterparts from other sources.	54
Tab. 28. Conditions for recombinant protein production.	60
Tab. 29. Mass balance of purified recombinant proteins. The purity rate was determined using SDS-PAGE analysis of protein samples and Gel Analyzer software.	66
Tab. 30. Determination of molecular mass and oligomeric structure of CaMet2p and CaMet2NHp. Results were partially published (Kuplińska et al., 2022).	67
Tab. 31. Determination of molecular mass and oligomeric structure of CaMet15NHp.	69
Tab. 32. Determination of molecular mass and oligomeric structure of CaStr2NHp.	70
Tab. 33. Kinetic parameters determined for CaMet2p and CaMet2NHp. The value of the k_{CAT} parameter was calculated per monomer.	74
Tab. 34. Kinetic parameters determined for CaMet15NHp. The value of the k_{CAT} parameter was calculated per monomer.	79



- Tab. 35. Kinetic parameters determined for CaStr2NHp. The value of k_{CAT} parameter was calculated per monomer. _____ 82
- Tab. 36. Susceptibility of yeast strains to D-PEN, L-PEN, Ac-DAB, DL-ALG, DL-GLUF, ISOX, fluconazole (FLU), and Amphotericin B (AmB). No observable activity of a compound at measured concentrations is represented by (>1024). Growth media used: RPMI 1640, YNB without amino acids with ammonium sulfate (AS) or sodium glutamate (SG) as nitrogen source, with or without supplementation of 10 mM L-Met. The experiments were performed in triplicates. Results partially published in (Kuplińska et al., 2022). _____ 88
- Tab. 37. Susceptibility of *Candida spp.* strains to L-PEN and ISOX. No observable activity of a compound at measured concentrations is represented by (>). The experiments were performed at least in three replicates. Results partially published in (Kuplińska et al., 2022). _____ 90
- Tab. 38. L-PEN and Flu susceptibility of *C. glabrata* clinical isolates. No observable activity of a compound at measured concentrations is represented by (>1024). R resistance to fluconazole, S sensitive to fluconazole. The experiments were performed at least in three replicates. Published in (Kuplińska et al., 2022) ____ 91
- Tab. 39. The checkerboard dilution test results of drug interaction between L-PEN and FLU, Ac-DAB, DL-ALG, or DL-GLUF against *C. glabrata* ATCC 90030 and *C. albicans* ATCC 10231. Test performed in a YNB GS medium without amino acids. Fractional Inhibitory Concentration Index (FICI). * Value used for FICI calculations, despite no MIC₉₀ observed at tested concentration. Synergistic effect (FICI ≤ 0.5), indifferent effect (FICI > 0.5 to ≤ 4), antagonistic effect (FICI > 4). _____ 96
- Tab. 40. Bioinformatic analysis of *C. albicans* Met2p, Str2p, and Met15p recombinant proteins probability of crystals formation. Analysis was performed with XtaPred software (Slabinski et al., 2007). Predicted crystallization classes were color-coded according to the scheme given by the program: EP, crystallization class prediction by Expert Pool method; RF, crystallization class prediction by Random Forest method. Calculated features indicated by the program as those indicating crystallization problems are highlighted in grey color. _____ 99
- Tab. 41. Summary of protein samples prepared for crystallization trials. Values are given for protein samples after SEC and concentration. _____ 100

LIST OF SUPPLEMENTARY FIGURES

- Fig. S1. Maps of constructed expression plasmids: pET101/D-TOPO + *MET2*, pET101/D-TOPO + *MET2CH*, pET101/D-TOPO + *MET2NH*. Created in Snap Gene software. 132
- Fig. S2. Maps of constructed expression plasmids: pLATE11 + *MET15*, pLATE31 + *MET15CH*, pLATE52 + *MET15NH*. Created in Snap Gene software. _____ 133
- Fig. S3. Maps of constructed expression plasmids: pLATE11 + *STR2*, pLATE31 + *STR2CH*, pLATE52 + *STR2NH*. Created in Snap Gene software. _____ 134
- Fig. S4. Multiple sequence alignment of *C. albicans* Met2p amino acid sequence with characterized enzymes from other microorganisms. CA *C. albicans*; SC *S. cerevisiae*; HI *H. influenzae*; MS *M. smegmatis*; SA *S. aureus*. PDB codes: 2B61, 4QLO; 6IOG. Conserved regions marked in red boxes; similarities marked in red font; catalytic residues marked with asterisk. Analysis performed using the ENDscript program (Robert and Gouet, 2014). _____ 135
- Fig. S5. Multiple sequence alignment of *C. albicans* Met15p amino acid sequence with characterized enzymes from other microorganisms. CA *C. albicans*; SC *S. cerevisiae*; WS *W. succinogenes*; MM *M. marinum*; PDB codes: 8OVH, 3RI6; 4KAM. Conserved regions marked in red boxes; similarities marked in red font; catalytic residues marked with asterisk. Analysis performed using the ENDscript program (Robert and Gouet, 2014). _____ 136
- Fig. S6. Multiple sequence alignment of *C. albicans* Str2p amino acid sequence with homologous enzymes from other organisms. CA *C. albicans*; SC *S. cerevisiae*; HP *H. pylori*; EC *E. coli*; NT *N. tabacum* PDB codes: 1CS1, 4L00, 1I41. Conserved regions marked in red boxes; similarities marked in red font; catalytic residues marked with asterisk. Catalytic non-conserved residues marked with black circle. Analysis performed using the ENDscript program (Robert and Gouet, 2014). _____ 137
- Fig. S7. Examples of chromatograms showing peak area of L-HCT-TNB (marked with an arrow); L-HCT produced in the reaction catalyzed by CaMet15NHp. The reaction mixture consists of 10 nM of enzyme, 0.2 mM PLP, 0.1 mM Na₂S, and varying concentrations of L-OAH: A. 0 mM; B. 20 mM; C. 50 mM; D. 100 mM. At void time (approximately 2 minutes), elution of peaks resulting from sample matrix can be observed. Analysis performed via Agilent 1200 Quaternary DAD HPLC System. 138
- Fig. S8. A. UV spectrum of the L-HCT-TNB peak of samples containing 10 nM of CaMet15NHp, 0.2 mM PLP, 0.1 mM Na₂S, and varying concentrations of L-OAH. B. Purity of the L-HCT-TNB peak. Analysis performed via Agilent 1200 Quaternary DAD HPLC System. _____ 139
- Fig. S9. Examples of chromatograms showing peak area of L-Cys-TNB (marked with an arrow) and L-Cys decrease in the reaction catalyzed by CaStr2NHp. The reaction mixture consists of 100 nM of enzyme, 0.2 mM PLP, 5 mM L-Cys, and varying concentrations of L-OAH: A. 0 mM; B. 5 mM; C. 10 mM; D. 20 mM. At void time (approximately 2 minutes), elution of peaks resulting from sample matrix can be observed. Analysis performed via Agilent 1200 Quaternary DAD HPLC System. 140
- Fig. S10. UV spectrum of the L-Cys-TNB peak of samples containing 100 nM of CaStr2NHp, 0.2 mM PLP, 5 mM L-Cys, and varying concentrations of L-OAH. B. Purity of the L-Cys-TNB peak. Analysis performed via Agilent 1200 Quaternary DAD HPLC System. _____ 141

SUPPLEMENTARY FIGURES

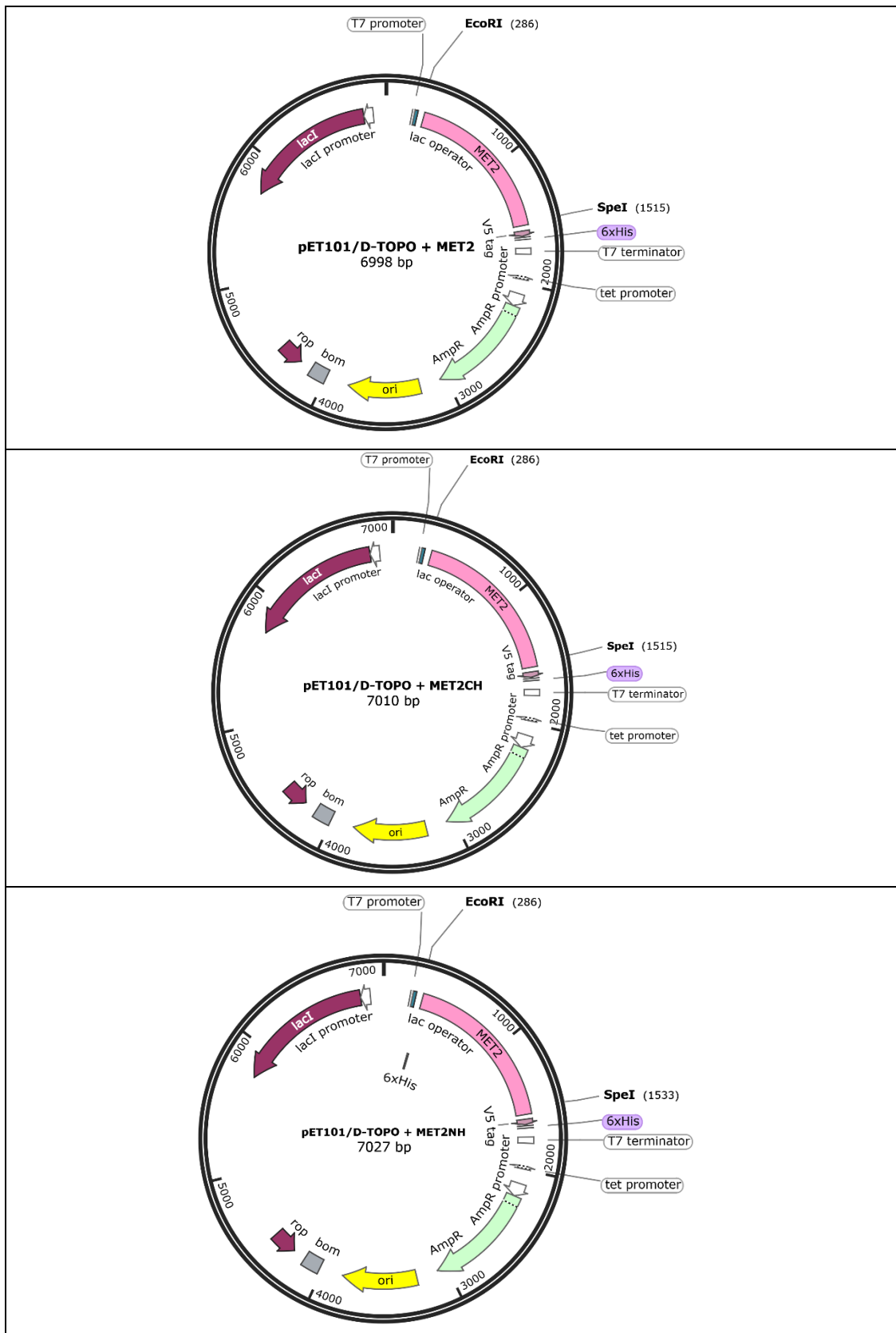


Fig. S1. Maps of constructed expression plasmids: pET101/D-TOPO + MET2, pET101/D-TOPO + MET2CH, pET101/D-TOPO + MET2NH. Created in Snap Gene software.

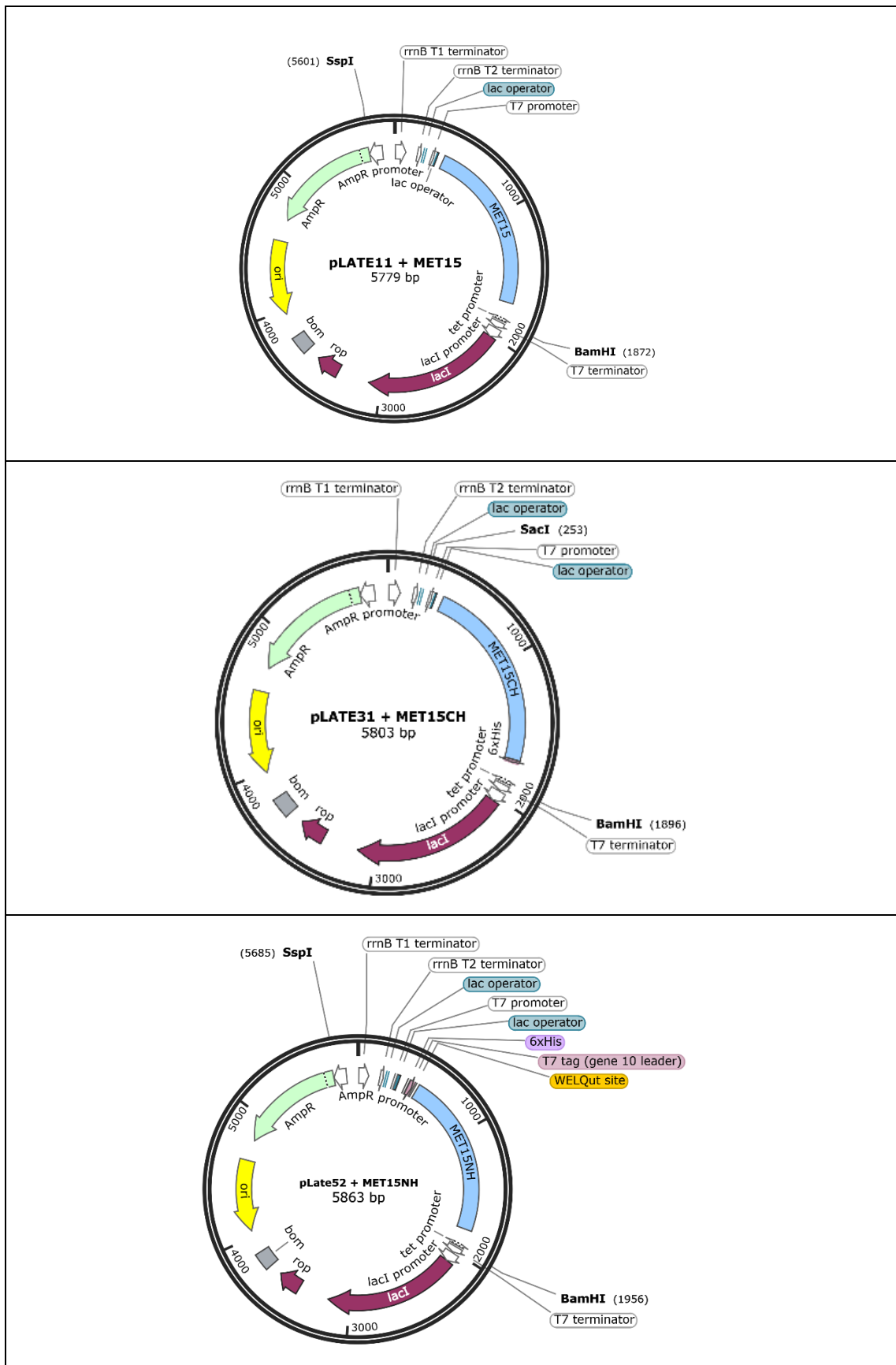


Fig. S2. Maps of constructed expression plasmids: pLATE11 + *MET15*, pLATE31 + *MET15CH*, pLATE52 + *MET15NH*. Created in Snap Gene software.

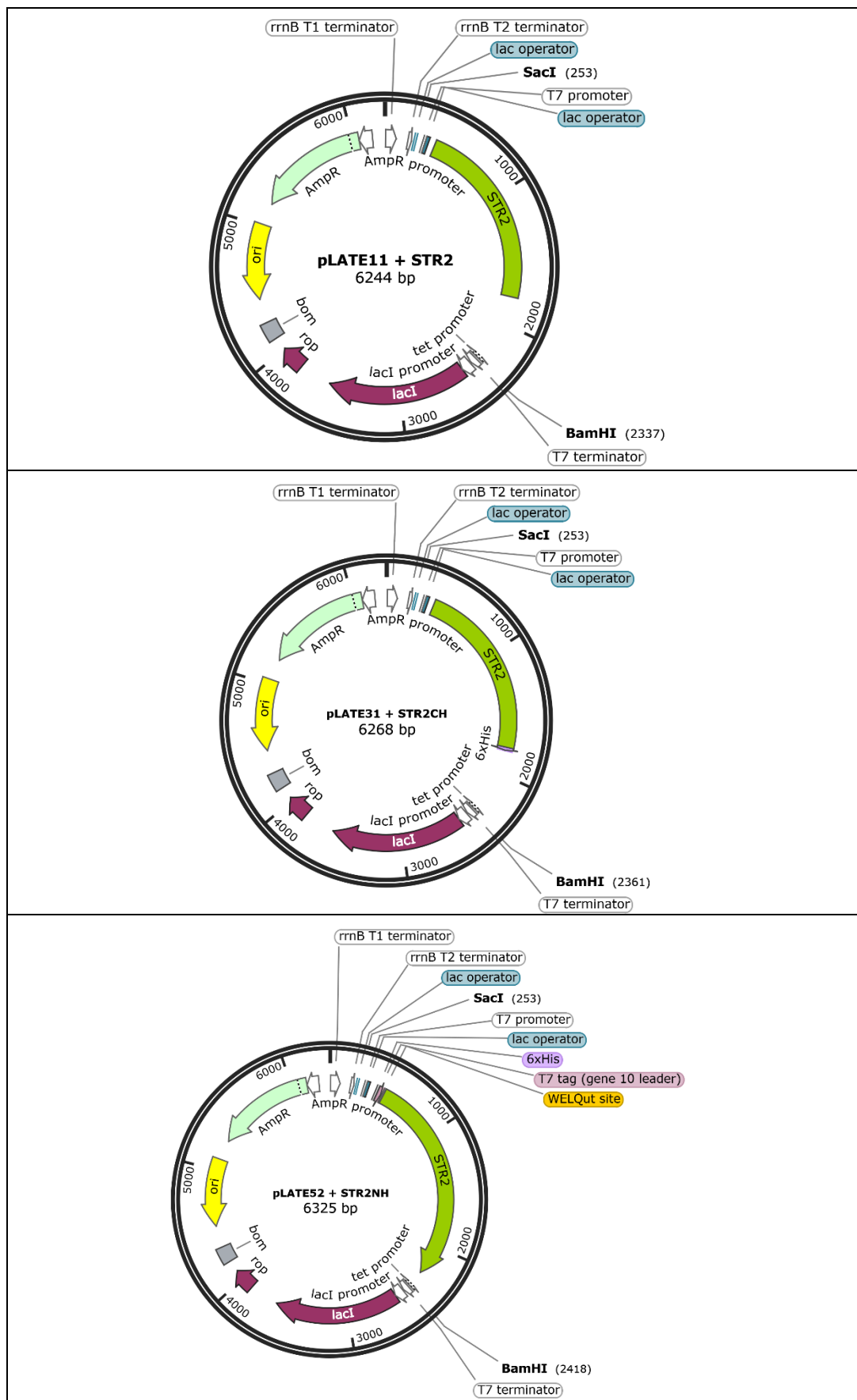


Fig. S3. Maps of constructed expression plasmids: pLATE11 + STR2, pLATE31 + STR2CH, pLATE52 + STR2NH. Created in Snap Gene software.

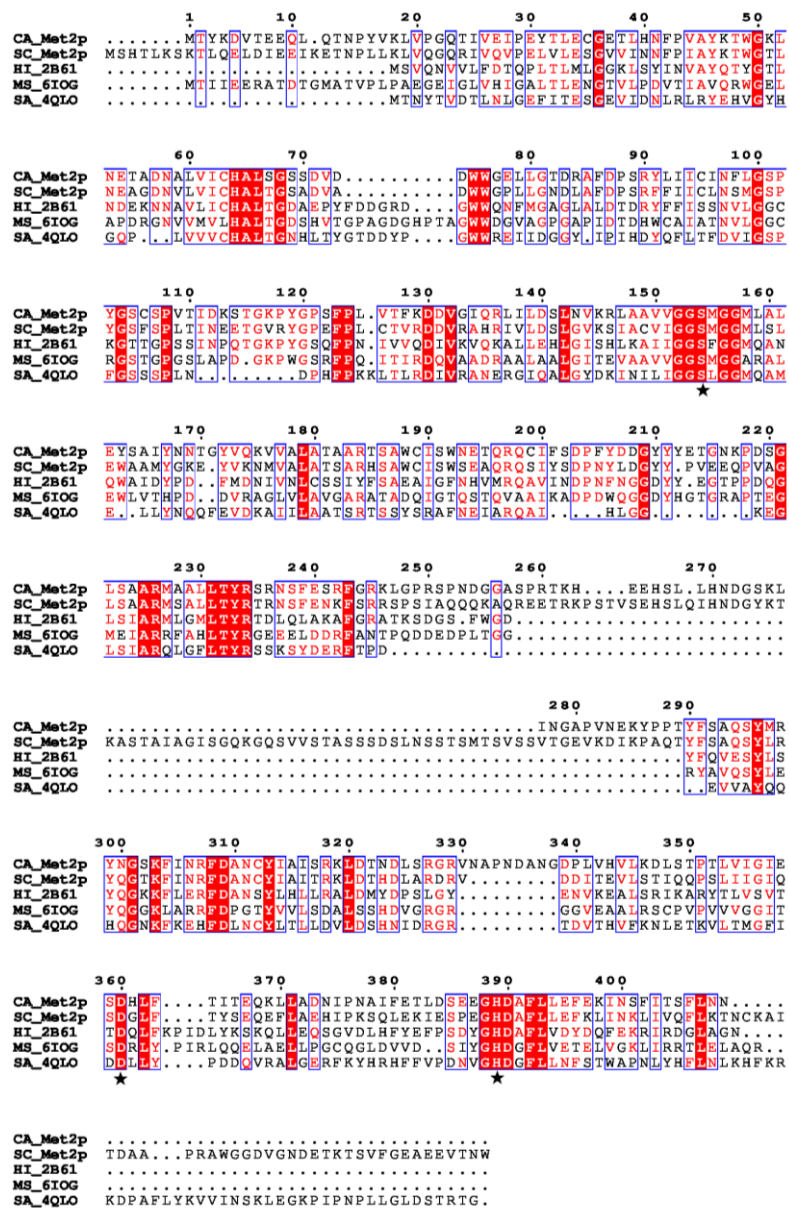


Fig. S4. Multiple sequence alignment of *C. albicans* Met2p amino acid sequence with characterized enzymes from other microorganisms. CA *C. albicans*; SC *S. cerevisiae*; HI *H. influenzae*; MS *M. smegmatis*; SA *S. aureus*. PDB codes: 2B61, 4QLO; 6IOG. Conserved regions marked in red boxes; similarities marked in red font; catalytic residues marked with asterisk. Analysis performed using the ENDscript program (Robert and Guet, 2014).

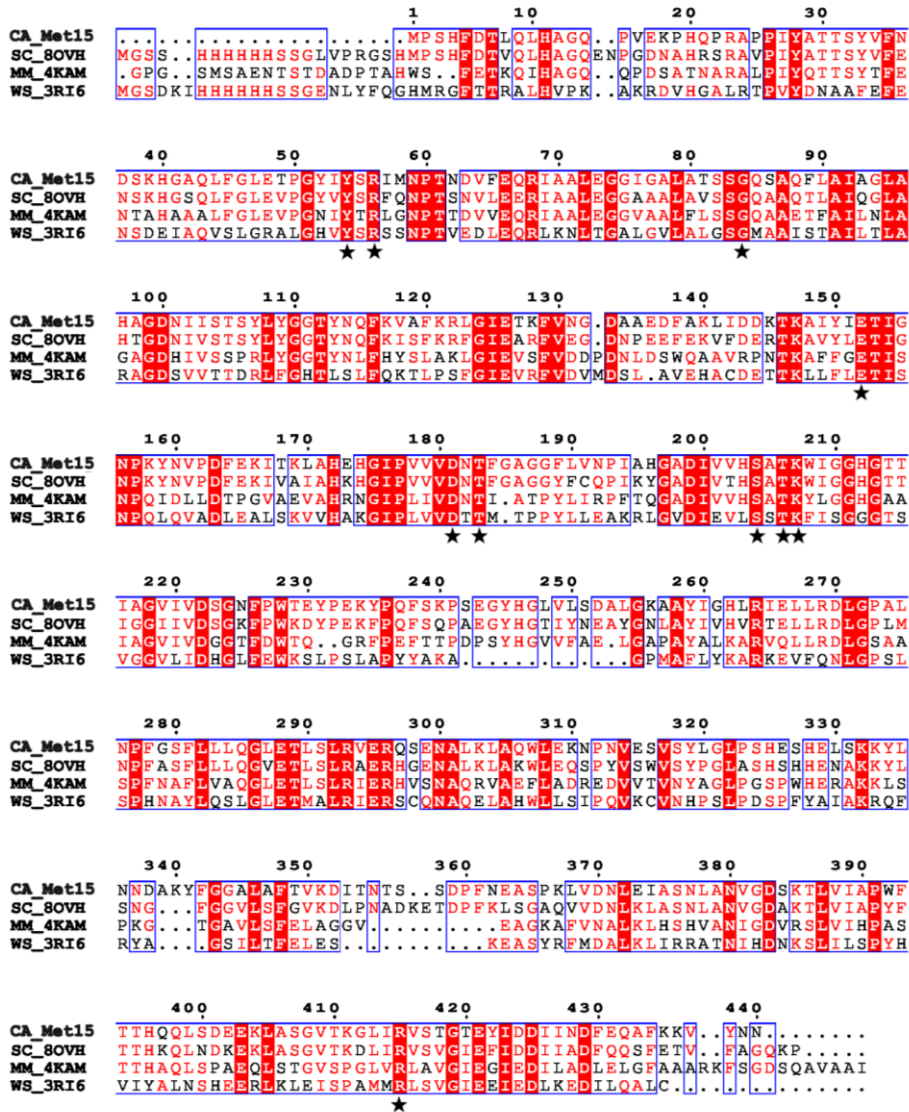


Fig. S5. Multiple sequence alignment of *C. albicans* Met15p amino acid sequence with characterized enzymes from other microorganisms. CA *C. albicans*; SC *S. cerevisiae*; WS *W. succinogenes*; MM *M. marinum*; PDB codes: 8OVH, 3RI6; 4KAM. Conserved regions marked in red boxes; similarities marked in red font; catalytic residues marked with asterisk. Analysis performed using the ENDscript program (Robert and Gouet, 2014).

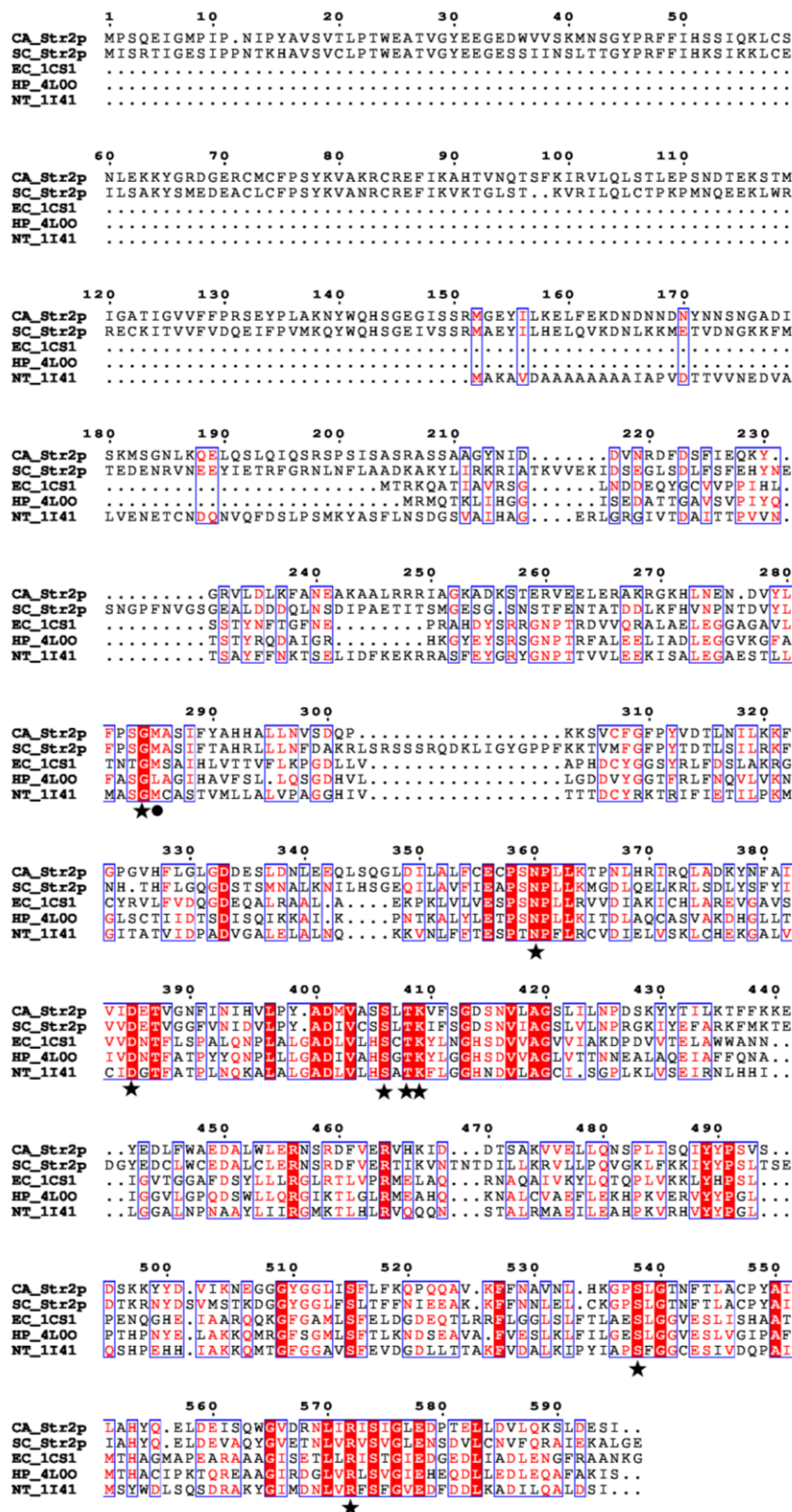


Fig. S6. Multiple sequence alignment of *C. albicans* Str2p amino acid sequence with homologous enzymes from other organisms. CA *C. albicans*; SC *S. cerevisiae*; HP *H. pylori*; EC *E. coli*; NT *N. tabacum* PDB codes: 1CS1, 4L00, 1I41. Conserved regions marked in red boxes; similarities marked in red font; catalytic residues marked with asterisk. Catalytic non-conserved residues marked with black circle. Analysis performed using the ENDscript program (Robert and Gouet, 2014).

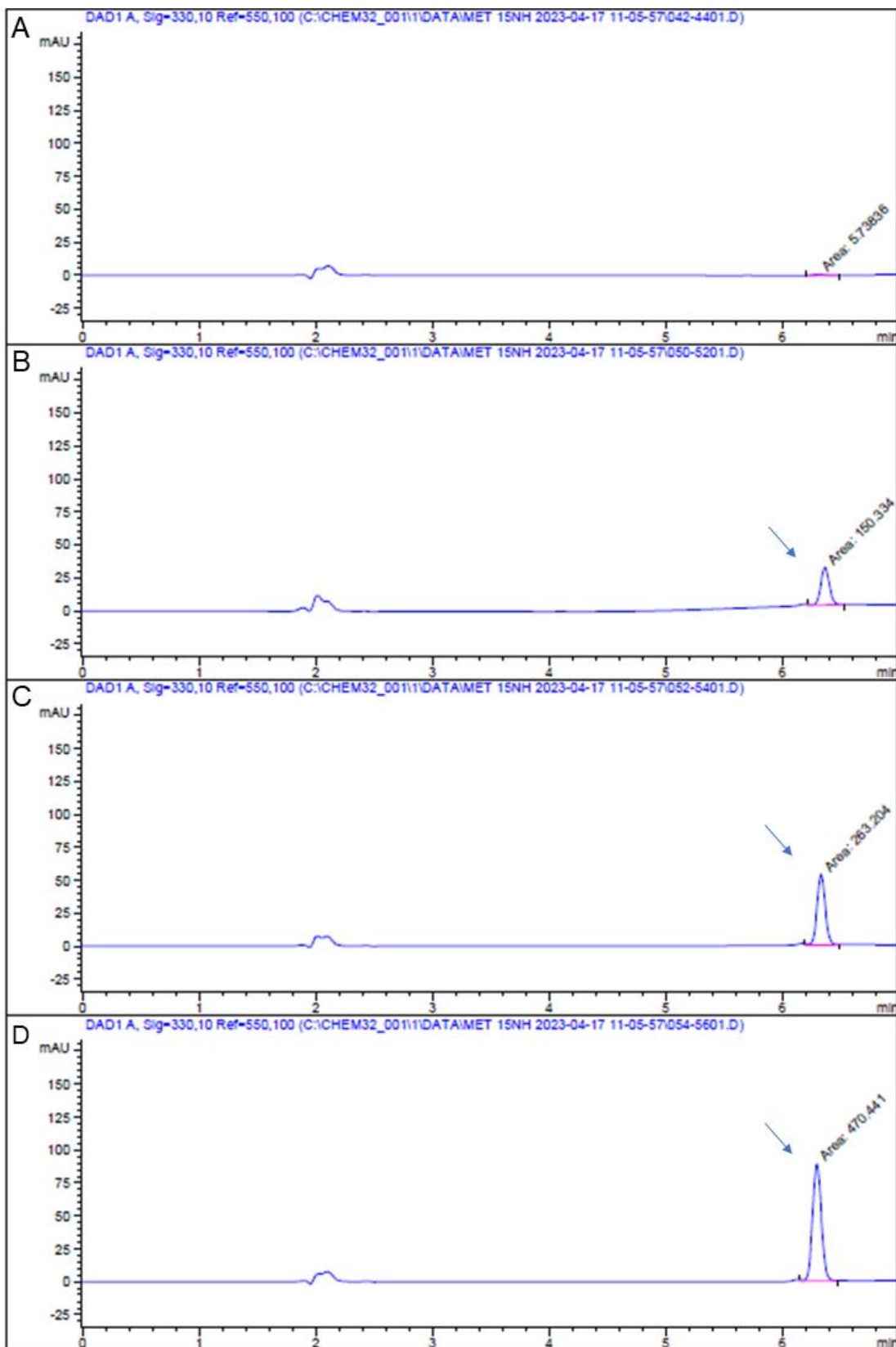


Fig. S7. Examples of chromatograms showing peak area of L-HCT-TNB (marked with an arrow); L-HCT produced in the reaction catalyzed by CaMet15NHp. The reaction mixture consists of 10 nM of enzyme, 0.2 mM PLP, 0.1 mM Na₂S, and varying concentrations of L-OAH: **A.** 0 mM; **B.** 20 mM; **C.** 50 mM; **D.** 100 mM. At void time (approximately 2 minutes), elution of peaks resulting from sample matrix can be observed. Analysis performed via Agilent 1200 Quaternary DAD HPLC System.

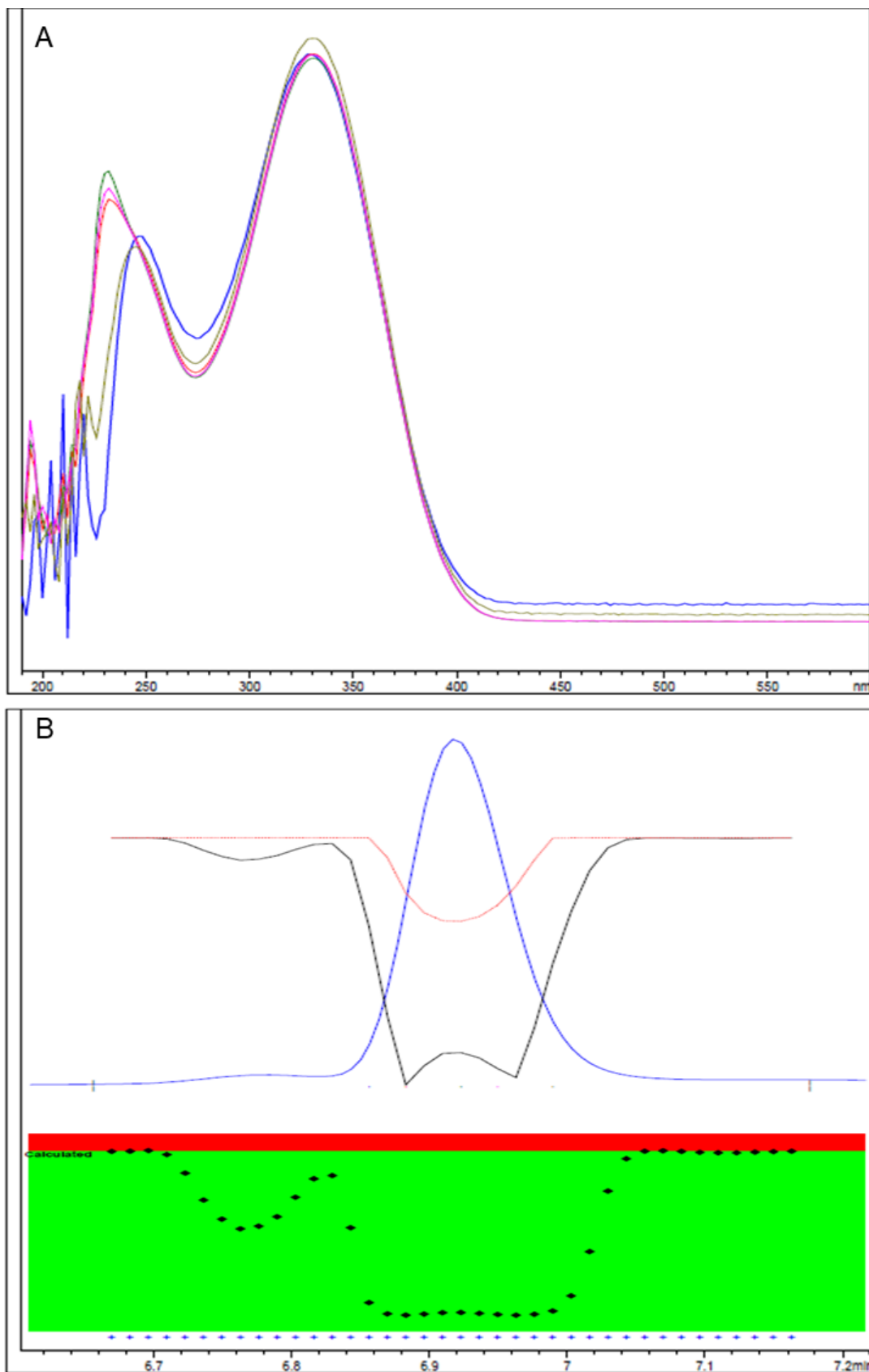


Fig. S8. **A.** UV spectrum of the L-HCT-TNB peak of samples containing 10 nM of CaMet15NHp, 0.2 mM PLP, 0.1 mM Na₂S, and varying concentrations of L-OAH. **B.** Purity of the L-HCT-TNB peak. Analysis performed via Agilent 1200 Quaternary DAD HPLC System.

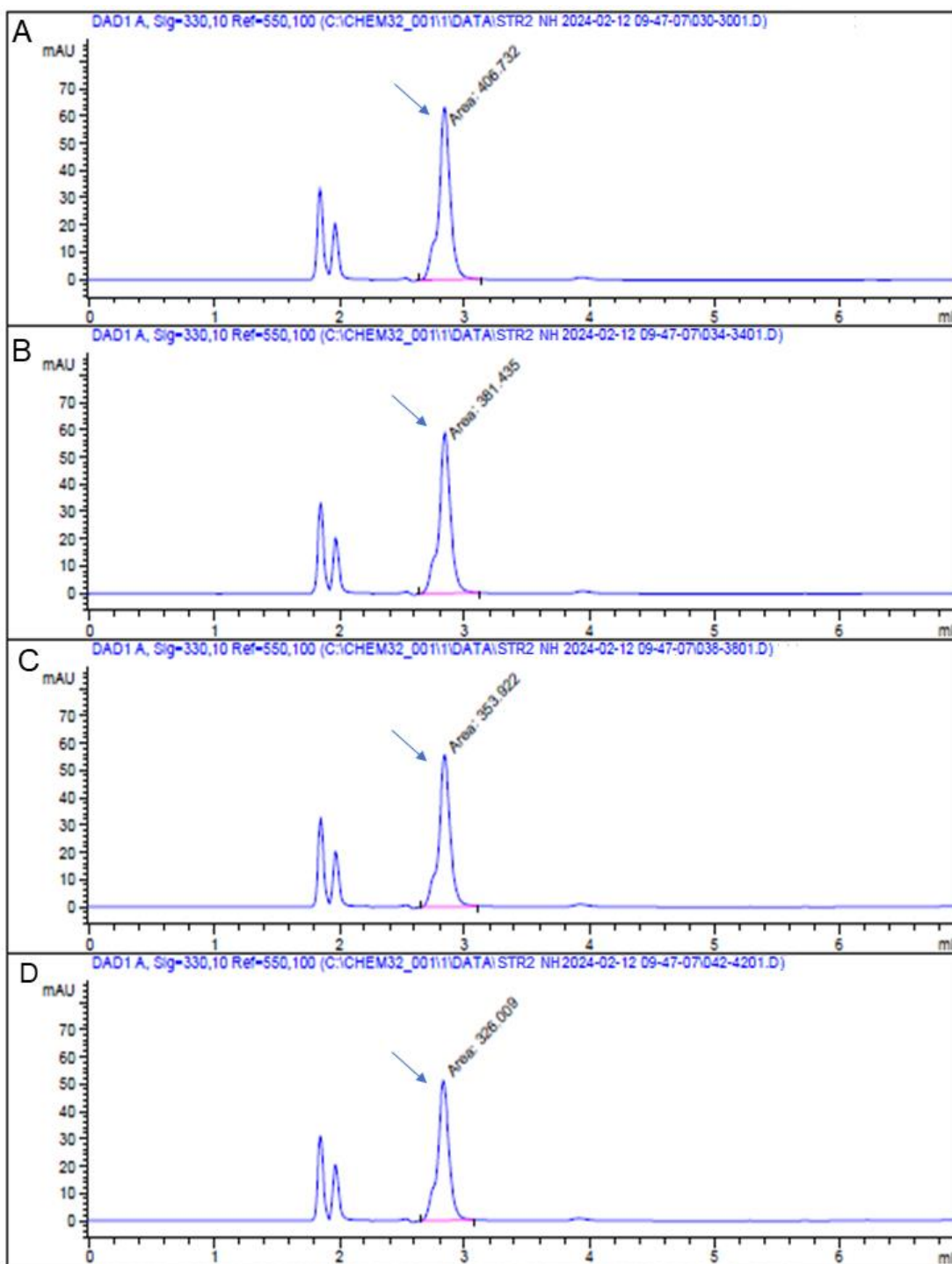


Fig. S9. Examples of chromatograms showing peak area of L-Cys-TNB (marked with an arrow) and L-Cys decrease in the reaction catalyzed by CaStr2NHp. The reaction mixture consists of 100 nM of enzyme, 0.2 mM PLP, 5 mM L-Cys, and varying concentrations of L-OAH: **A.** 0 mM; **B.** 5 mM; **C.** 10 mM; **D.** 20 mM. At void time (approximately 2 minutes), elution of peaks resulting from sample matrix can be observed. Analysis performed via Agilent 1200 Quaternary DAD HPLC System.

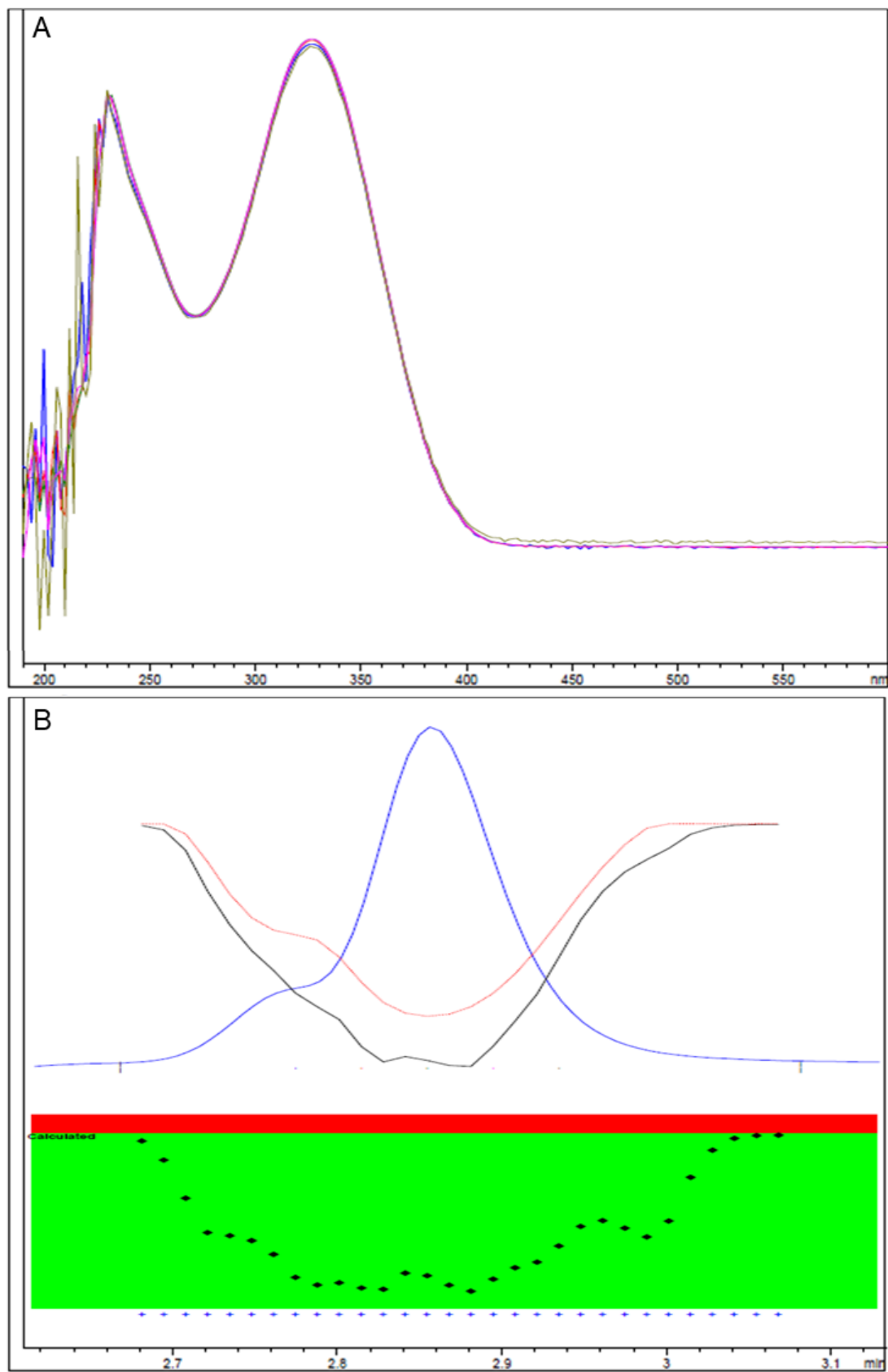


Fig. S10. UV spectrum of the L-Cys-TNB peak of samples containing 100 nM of CaStr2NHp, 0.2 mM PLP, 5 mM L-Cys, and varying concentrations of L-OAH. **B.** Purity of the L-Cys-TNB peak. Analysis performed via Agilent 1200 Quaternary DAD HPLC System.

